



# **Numerical Analysis and Material Selection of Functionally Graded Pipes Based on Metals and Ceramics for Deep Offshore Oil and Gas Operations in Gulf of Guinea**

A thesis submitted to the University of Strathclyde  
In partial fulfilment of the requirement for the award of a degree of Doctor of  
Philosophy (PhD)

By

SIMON OLUSHOLA AMOS

**Department of Mechanical & Aerospace Engineering  
University of Strathclyde  
Glasgow, UK**

## ABSTRACT

The environmentally challenged conditions of deep offshore oil and gas operations has necessitated the demand for unique materials that could withstand both the loading conditions of the operations and the corrosion resistance. The work presented herein has explored the use of Functionally Graded Material (FGM) to validate its ability to proffer solutions to deep offshore oil and gas operations and their components, particularly in the Gulf of Guinea.

FGM was specifically used in the present work due to its unique property exhibition that changes continuously throughout its thickness with no discontinuities within the material. This unique feature was utilized in this research to derive a combination of FGM's that could meet the required strength, fracture toughness, specific stiffness and corrosion rate for oil and gas operations in Gulf of Guinea.

An assessment of currently available material combinations was investigated to determine feasible FGM combinations (metal and ceramics) that could meet the unique operating requirements. In tandem, the Analytic Hierarchy Process (AHP) technique was further used to rank the materials identified and a sensitivity analysis was carried out on weight, price and density variations in the final ranking the material. The four (4) most highly ranked Metal/Ceramic combinations were used for all the finite element thermal and structural analyses undertaken in this work.

Four (4) distinct FGM pipe were modelled by finite element analysis (FEA) using the Abaqus Finite Element system based on the key Metal/Ceramics materials selected, to reasonably mimic the physical behaviour of a series of offshore piping systems configurations. In practice, three piping configurations were considered; Straight, Elbow and T- Piece pipe components, all these were modelled for a range of pressure and temperature conditions.. From the reviewed literature, only a few benchmarks were available to validate the computational models, this is as a result of the evolving nature of the usage of FGM for piping in oil and gas industry. Using work by Ghannad *et al.* on "2D thermo-elastic model of an axisymmetric FGM hollow cylinder", the FGM parameters used for the validation were axial stress, circumferential stress and von-mises stress. The comparison of results obtained from Ghannad's Paper showed excellent agreement with deviations of most of the variables used for the within 5% with both the numerical and analytical results from the literature.

As an FGM cannot have a single yield point by definition, an equation for the determination of effective yield strength for FGM's was developed which depends on the yield strength of the

FGM constituents and the non-homogeneity factor of the FGM. This equation was validated using the conventional averaging approach of the FGM yield strengths and it showed excellent agreement with less than 1% for FGM's with higher numbers of layers.

Further to the determination of an ideal approach to calculate the effective yield strength of the FGM's, the Finite Element Analysis (FEA) of the four FGM combinations were modelled using the approach in the validated model with the main intent of predicting the design limits for each of the FGM material combinations. This was repeated for the three piping components considered (Straight, Elbow and T-Piece Pipe configurations).

The normalized stress approach was used for the determination of the design limit, this approach compared the effective yield strength of the FGM to the effective Von-mises stress for each of the configurations to determine the FGM failure tendencies due to yielding. The FGM design limit was determined when any of the layer in the FGM normalized stress was closest to one (1), above this limit the material begins to yield (Fail). The design limit was determined using the normalized stress between the ranges of  $0.99 < \text{normalized stress} < 1.01$ . The FEA of the FGM's considered was limited to thermal and pressure loading, hence only thermal and pressure design limits were determined for all the FGM's considered in all the configurations and non-homogeneity factors.

From the typical oil and gas operating conditions considered in Gulf of Guinea, the design limit results for the **Straight pipes** reveals that all the 20 FGM's could be deployed for the operations being considered. The results from this study allowed straight FGM's to be ranked based on thermal and pressure loading conditions.

On the same note, the design limit results for the **Elbow Pipes** reveals that only 10 FGM's from the 20 modelled FGM's could be adequately deployed for the operations being considered. The results from this study allowed elbow FGM's to be ranked based on thermal and pressure loading conditions. .

Furthermore, the design limit results for the **T-Pieces Pipes** reveals that all the FGM's modelled could be adequately deployed for the operations being considered. The results from this study allowed T-piece FGM's to be ranked based on thermal and pressure loading conditions. .

Finally, it is worth noting that the work undertaken herein concludes the development of a matrix of internal pressure and thermal loading for Straight, Elbow and T-Piece FGM Pipe

configurations that could serve as guide for FGM material selection for oil and gas service conditions similar to that in Gulf of Guinea.

## **ACKNOWLEDGEMENTS**

My profound appreciation goes to the Almighty God for giving me the opportunity, enablement, and resources needed to complete this program. I would like to express my sincere gratitude to my supervisor, Professor David Nash for his exceptional supervision, guidance, encouragement and friendliness through my research period at the University of Strathclyde, Glasgow. His vast knowledge and steer made it possible for all my ideas to be implemented for the successful completion of this research.

I would equally like to specially thank Dr M.D Asraf Uzzaman his coaching and support in terms of resources and tools needed made this research successful. My sincere appreciation to the Interns; Guillaume Gilli, Mathieu Vilattea and Nicolas Corlay, their support with the tools used for this research at its initial phase made this research successful.

I would like to acknowledge my wife Adeola Susan Amos for her love, support and understanding towards the successful completion of this study, her words of encouragement and support served as motivation for me to put in my best. Special thanks to my beautiful children (Jemimah, Jeremiah, Josiah and Joshua), I cannot thank you all enough for your understanding of the busy times I had during the research.

I am very much grateful to my Dad and Mum for the love and encouragement they have shown to me throughout my life. I will like to also appreciate my Sister, Gloria Godiya Amos-Metulukuro, Engr. Abba Yakubu and Mr Mascot Ogunjemiyo for their moral support through the research period. I will equally like to appreciate Dr Olaoluwa Popoola for all the kind gestures showered on me when in Glasgow through the research period.

Finally, many thanks to family and friends for your prayers and words of encouragement, they kept me going.

## DECLARATION

I hereby declare that this thesis represents my own work conducted under the guidance of my supervisors, except where due acknowledgement is made, and that it has not been previously included in a thesis, dissertation or report submitted to this University or to any other institution for a degree, diploma or other qualifications.

A handwritten signature in blue ink, appearing to read 'Simon Olushola Amos', with a large initial 'S' and 'O'.

*Signed,*

**SIMON OLUSHOLA AMOS**

# Table of Contents

ABSTRACT .....	ii
ACKNOWLEDGEMENTS .....	v
DECLARATION.....	vi
CHAPTER 1: INTRODUCTION.....	2
1.1. BACKGROUND .....	2
1.2. CONVENTIONAL ENGINEERING MATERIAL BEHAVIOUR .....	5
1.2.1 Metals.....	5
1.2.2 Ceramics .....	5
1.2.3 Polymers.....	7
1.2.4 Fibre Reinforced Composites.....	8
1.3. ENVIRONMENTAL DEGRADATION OF CONVENTIONAL ENGINEERING MATERIALS .....	9
1.3.1 Corrosion of Metals .....	10
1.3.2 Environmental Degradation of Ceramic Materials .....	13
1.3.3 Environmental Degradation of Composites.....	14
1.4. STATEMENT OF THE PROBLEM .....	15
1.5. AIM AND OBJECTIVES .....	17
1.6. SIGNIFICANCE OF THE STUDY.....	18
1.7. SCOPE OF STUDY .....	19
CHAPTER 2: LITERATURE REVIEW.....	21
2.1 INTRODUCTORY REMARKS.....	21
2.2 RESEARCH ON FUNCTIONALLY GRADED MATERIALS.....	21
2.3 RESEARCH ON FGM USING FINITE ELEMENT ANALYSIS ON VARIOUS LOADING CONDITIONS.....	22
2.4 RESEARCH ON MATERIAL SELECTION FOR ENGINEERING APPLICATIONS	26
2.5 RESEARCH ON PRESSURE SYSTEMS PIPING COMPONENTS USING FGM DESIGN .....	28
2.6 CONCLUDING REMARKS .....	41
CHAPTER 3: MATERIAL SELECTION .....	43
3.1. INTRODUCTION.....	43
3.2. MATERIAL CLASSIFICATION AND RANKING .....	44
3.2.1 Candidate Ceramic Materials.....	45
3.2.2 Candidate Metallic Materials.....	47

3.2.3	Ranking of Candidates Materials through MADM.....	50
3.3.	CONCLUDING REMARKS .....	66
CHAPTER 4: DEVELOPMENT OF NUMERICAL MODEL FOR FGM PIPES.....		67
4.1.	INTRODUCTORY REMARKS.....	67
4.2.	FGM MODEL DEVELOPMENT FOR A STRAIGHT PIPE.....	67
4.2.1	Problem Formulation .....	67
4.2.2	Model Focus and Developments .....	69
4.2.3	Geometry and material properties .....	71
4.2.4	Element type and mesh sensitivity.....	72
4.2.1	Loading and boundary conditions.....	72
4.3.	RESULTS VALIDATION .....	73
4.4.	PARAMETRIC STUDY.....	76
4.4.1	The effect of number of layers .....	76
4.4.2	The effect of non-homogeneity factor (n).....	78
4.5.	CONCLUDING REMARKS .....	80
CHAPTER 5 DESIGN LIMIT PREDICTION FOR FGM .....		82
5.1.	DETERMINATION OF EFFECTIVE YIELD STRENGTH OF FGM.....	82
5.2.	FEA OF THE IDENTIFIED CANDIDATE MATERIALS-USING STRAIGHT PIPE CONFIGURATION AS CASE STUDY .....	87
5.2.1	Description of the model.....	87
5.2.2	Part Module .....	87
5.2.3	Property Module .....	87
5.2.4	Step Module .....	90
5.2.5	Load Module.....	90
5.2.6	Mesh Module .....	90
5.3.	ESTABLISHING THE DESIGN LIMIT FOR THE FGM'S.....	91
5.4.	CONCLUDING REMARKS .....	95
CHAPTER 6: ELBOW PIPE CONFIGURATION FGM DESIGN LIMITS AND ITS IMPACT ON THE FGM BEHAVIOUR .....		97
6.1.	INTRODUCTION.....	97
6.2.	MODELLING OF ELBOW PIPES .....	97
6.2.1	Model Geometry.....	98
6.2.2	Materials .....	99
6.2.3	Step Module.....	101
6.2.4	Load Module.....	101



6.2.5	Mesh Module .....	102
6.2.6	Results: Establishing the Design Limits for the Elbow FGM's .....	103
6.2.7	Detailed Result Comparison for Straight and Elbow FGM Pipe .....	108
6.3.	CONCLUDING REMARKS .....	109
<b>CHAPTER 7: T-PIECE PIPE CONFIGURATION FGM DESIGN LIMITS AND ITS IMPACT ON FGM BEHAVIOUR.....</b>		<b>111</b>
7.1.	INTRODUCTORY REMARKS.....	111
7.2.	MODELLING OF T-PIECE PIPE .....	111
7.3.	MODEL GEOMETRY.....	112
7.4.	T-PIECE NUMERICAL RESULT VALIDATION .....	112
7.5.	MATERIALS .....	115
7.5.1.	FGM Material Composition.....	115
7.5.2.	FGM Materials Properties .....	115
7.6.	STEP MODULE.....	117
7.7.	LOAD MODULE.....	117
7.8.	MESH MODULE.....	118
7.9.	RESULTS .....	119
7.10.	CONCLUDING REMARKS .....	123
<b>CHAPTER EIGHT: DESIGN RECOMMENDATIONS.....</b>		<b>125</b>
8.1.	INTRODUCTORY REMARKS.....	125
8.2.	IDEAL FGM MATERIALS FOR DEEP OFFSHORE OIL AND GAS OPERATIONS 125	
8.3.	FGM BEHAVIOURAL DEPENDENCE NUMBER OF LAYERS AND NON-HOMOGENEITY FACTOR (n) .....	125
8.4.	EFFECTIVE YIELD STRENGTH OF FGM COMPONENTS .....	129
8.5.	DESIGN LIMIT FOR STRAIGHT FGM PIPE .....	129
8.6.	DETERMINATION OF DESIGN LIMIT FOR ELBOW FGM PIPE.....	130
8.7.	DETERMINATION OF DESIGN LIMIT FOR T-PIECE FGM PIPE.....	131
8.8.	CONCLUDING REMARKS .....	133
<b>CHAPTER NINE: CONCLUSIONS AND FURTHER WORK .....</b>		<b>134</b>
9.1.	INTRODUCTION.....	134
9.2.	MATERIAL SELECTION AND RANKING .....	134
9.3.	NUMERICAL INVESTIGATION OF FGM AND DESIGN LIMIT PREDICTION	134
9.4.	SUGGESTION FOR FURTHER WORK .....	138
<b>REFERENCES.....</b>		<b>139</b>

<b>APPENDIX A: TEMPERATURE AND PRESSURE DESIGN LIMIT FOR ELBOW PIPES</b>	<b>148</b>
<b>DESIGN LIMITS FOR FGM 1</b> .....	<b>148</b>
<b>DESIGN LIMITS FOR FGM 2</b> .....	<b>149</b>
<b>DESIGN LIMITS FOR FGM 3</b> .....	<b>151</b>
<b>DESIGN LIMITS FOR FGM 4</b> .....	<b>152</b>
<b>APPENDIX A: TEMPERATURE AND PRESSURE DESIGN LIMIT FOR T-PIECE FGM PIPES</b> .....	<b>155</b>
<b>DESIGN LIMITS FOR FGM 1</b> .....	<b>155</b>
<b>DESIGN LIMITS FOR FGM 2</b> .....	<b>156</b>
<b>DESIGN LIMITS FOR FGM 3</b> .....	<b>157</b>
<b>DESIGN LIMITS FOR FGM 4</b> .....	<b>159</b>





# CHAPTER 1: INTRODUCTION

## 1.1. BACKGROUND

A functionally graded material (FGM) is a specialized type of material which is characterized by gradual changes of its composition and microstructure through the whole volume of the component. This gradual variation in the microstructure gives rise to a variation in the material properties in specific directions through the thickness of the material. A group of Japanese Scientists made the idea of functionally graded materials (FGMs) pronounced in 1984, while in search of a material that can be used as thermal barriers during a space plane project. The materials was considered as a novel idea and they described the FGM as “inhomogeneous composite that has all its properties (mechanical, physical and chemical) changing continuously with no discontinuities within the material” (Encyclopedia of Materials Vol. 1-11). The changes in the material properties through the volume of the component in FGM are accomplished by the combination of two dissimilar materials (e.g. mixing a metal with a ceramic), in which the ratio of mixture varies from layer to layer through the entire FGM. For example, metal and ceramic FGM could be accomplished by placing the metal layer in one side and ceramic layer in other side of the FGM having numerous interlayers between them. With each interlayer having a distinct volume fraction when compared with the main constituents of the FGM, the composition variation through the layers of the FGM results in a smooth and gradual transition from metal phase to ceramic phase (see figure 1.1).

The unique property variation exhibited by FGM through the layers is the main reason FGM is being manufactured to take advantage of the properties trend. For instance, in a graded metal/ceramic components, unique properties like strength, toughness and machinability of metal, coupled with heat, wear and corrosion resistance of ceramic is being realized from a single component. This advantage makes FGMs very applicable in various applications (Arash, 2000). This has resulted in a quest to research more on FGMs so as to develop and utilize FGM in different industrial applications.

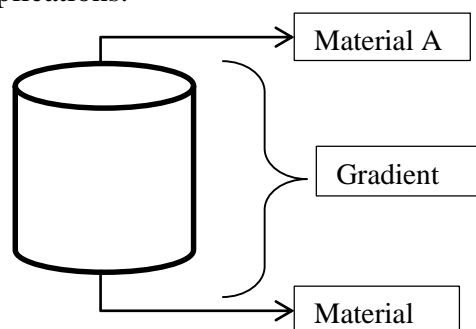


Fig.1.1: Schematic image of FGM

The excellent uniqueness with the FGM is the awareness that gradients can be designed at a micro-structure level to tailor specific materials to specialized functional performance in particular applications. The continuous variation in material properties is actually the distinction between FGM and conventional composite that has stepped material properties without continuity. This continuous gradation of properties in FGM reduces the effect of thermal stresses, residual stresses and stress concentration that is usually prevalent with conventional composite. This now has given rise to FGM being considered in application where extreme thermal loading is required (e.g. structural engineering design) (Mine, 2013). FGM materials also reduce the interface problem as a result of proficient and continuous change of material properties from one surface to another (Mine, 2013).

The behavior of FGM structures when subjected to mechanical loading have been focused on by many researchers from different engineering background in recent years, this is not limited to engineering applications as nuclear power plants, heat engine components, subsea components and aerospace structure etc.

As earlier stated, FGMs are specialized composites in which the volume fraction of particles varies in one or numerous directions. A vital benefit of a repetitive variation of volume fraction of constituent phases in the FGM is the eradication of stress discontinuity that is a norm with laminated composites and hence, problems that could arise due to delamination. (Victor & Larry, 2007).

With the advent of improved manufacturing techniques such as three-dimensional printing, centrifugal casting, powder metallurgy, chemical vapor deposition and spray forming, bulk FGMs are becoming a commercial reality as evident in its application in the aerospace and structural industries (Victor & Larry, 2007). Researchers and engineers must now find ways to determine the best method by which to tailor constituent materials according to a particular application. This endeavor involves three main parts; 1) generating models to accurately determine the material properties for a specific material composition, 2) creating efficient methods by which to analyze such components in response to certain loads, and 3) finding methodologies to efficiently determine the optimal distribution of material composition such that performance goals are maximized. Other effects such as constituent material chemistry, and residual stresses imposed on the structure due to the manufacturing process are also important criteria to consider.

In the first case, there are several homogenization methods for estimating the effective properties of two phase functionally graded materials. Most methods can be separated into two

main groups, namely, rigorous elasticity based approaches, and simplified strength of materials based estimates. The main reason for use of a homogenization scheme is due to the fact that modern computational techniques are ill-suited to tackling a complete three dimensional solution to the governing elasticity equations for large scale structures that are microscopically-heterogeneous. Thus, it is possible to replace an FGM's heterogeneous microstructure with an idealized microstructure that is easier to analyze. The homogenization scheme in tandem with the idealized microstructure provides an effective representation of the material properties based on the relative volume fractions of constituent materials. In this manner the analysis of FGMs can be simplified using theory of elasticity, with homogenized macroscopic material properties that vary spatially. Secondly, modern numerical techniques are currently under development for the analysis of FGMs. These include mesh free methods such as the element-free Galerkin Method, as well as the more traditional Finite Element Method (Ueda & Gasik, 2000). However, each of the aforementioned numerical techniques is only an approximate method; they only weakly satisfy the governing thermo-elasticity theory in an integral sense or through the principal of virtual work.

Advanced, materials have played a crucial role in the development of our society and culture. The development of advanced polymers, the engineering alloys, and advanced structural ceramics was made from basic exploitation of base elements from the periodic table into various inorganic and organic compounds (see Figure 1.2). Furthermore, FGMs have been developed by combining advanced engineering materials in the form of particulates, fibers, whiskers, or platelets. In the continuous drive to improve structural performance, there is a current initiative to tailor the material architecture at microscopic scales to optimize certain functional properties of a structure.

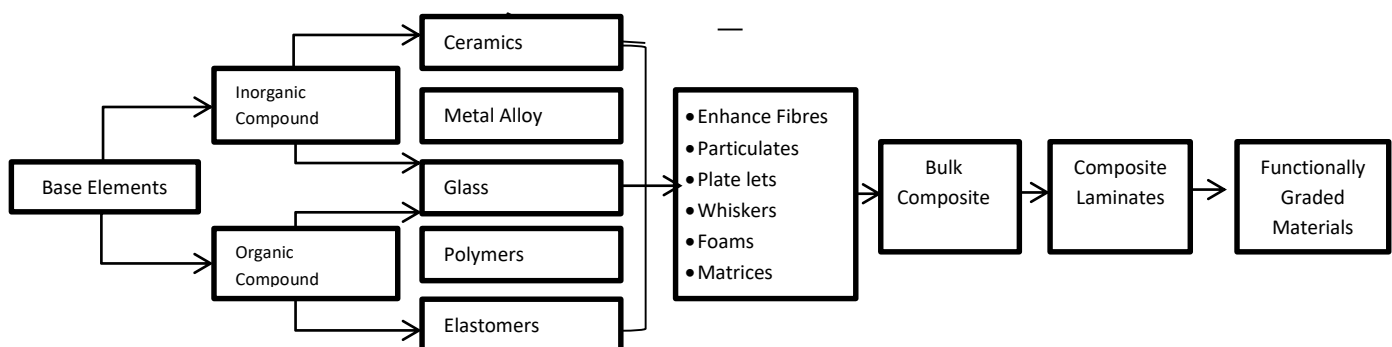


Fig. 1.2 Illustration of modern material hierarchy [5]

## **1.2. CONVENTIONAL ENGINEERING MATERIAL BEHAVIOUR**

There are numerous type of materials with highly distinct properties. The availability of numerous materials gives an engineer the advantage to select the material that will be most-suited for any component been designed. Consequently, it is vital to understand the mechanical properties of the materials and the physical phenomena causing them. The atomic structure of materials determines their mechanical properties. To probe further into these properties, it is vital to have knowledge of the materials structure.

### **1.2.1 Metals**

Metals are special class of materials with numerous important applications. They are well-known for their numerous advantageous properties, not limited to high thermal and electrical conductivity, ductility (i.e. their capability to undergo necking without breaking) and the luster exhibited on their surfaces. Metals ductility coupled with the special strength achieved through alloying makes appealing to be used for various engineering applications. They possess a high tendency for oxidation. Hence, they are transformed into metallic alloy as many elements are soluble in them in their solid state. For example, the alloying iron and carbon produce steel. This is possible with a large number of metallic elements to produce a wide range of alloys. Many of which have numerous technical value, of note are the following: alloys based on iron (steels and cast irons), aluminum, copper (bronzes and brasses), nickel, titanium, and magnesium (Joachim et.al.). Atoms in metals are arranged in such a way that their electrons are spread over many atoms. This is mostly achieved in atoms arranged in a dense and regular manner. This makes metals to form crystals that are illustrious by the well-ordered structure exhibited.

### **1.2.2 Ceramics**

Ceramics are classified as all non-metallic and non-organic materials (Hornbogen et. al., 1994). The Physical distinction between metals and ceramics is in the type on bonding, ceramics possess a bonding type that results in the outer shell being completely filled and does not consist of metallic bonding. They sometimes exist as one element in different forms (e.g. as diamond or graphite) and may also be in a compounds of different elements. Notable amongst ceramics are silicate ceramics, containing silicon oxide, oxide ceramics example; aluminium oxide  $Al_2O_3$ , zirconium oxide  $ZrO_2$ , or magnesium oxide and ceramics without oxide example; silicon nitride and silicon carbide. Ceramics are bonded chemically in different forms, it could exist with ionic, covalent, van der Waals, hydrogen and dipole bonds.



More often the ceramics crystal structure is complex when compared with that of metals. For instance, basic ceramics like diamond does not form cubic or hexagonal structures like metals when it crystallize. Diamond lattice structure is cubical in nature, however, it doesn't form a Bravais lattice due to the fact that each atomic site has its uniqueness. This type of lattices are known as *lattices with a basis*. Notable example of such lattice is also the hexagonal close-packed structure, which is achieved by insertion a diatomic basis by each location of the Bravais lattice (Joachim et.al.).

Most times, ceramics are not being used in the crystalline form, they are mostly used in their amorphous state. When used in this state, they are known as glasses. In most cases, glasses are transparent due to fact that they do not possess the grain boundaries required for light refraction. They are mostly based on silicon oxide, SiO<sub>2</sub> mostly used for window glass. Enamel is another glassy material that is worthy of note, is used for coating metals. It has high impact strength and it is a good corrosion resistance material.

Ceramics exhibits high strength and elastic stiffness when subjected to compressive load, they have appreciable resistance against many chemicals and also shows stability at elevated temperature (applicable to only crystalline ceramics), most glasses (Amorphous Ceramics) have no high melting point, they becomes less hardened at elevated temperatures and exhibits the characteristics of a viscous fluid. The temperature at which the Amorphous Ceramics softens is reasonably below crystalline ceramics melting point.

Besides all the benefits of ceramics properties as stated above, they also exhibits distinct disadvantage: Their brittleness is a great challenge during service and manufacturing process. They normally fail by brittle fracture, hence the initial crack existing in the material is a key factor in the determination of their strength.

Ceramics do not deform plastically. Failure mostly occurs through *cleavage fracture*, through an existing crack that keeps growing and propagating. The compaction of ceramics generates pores which act like cracks and thus leading to failure through crack propagation. Ceramics are unable of eliminate the effect of the crack propagation due to lack of plastic deformation. This make the fracture toughness of ceramics to be low in comparison with metals, ceramics usually contain cracks with different sizes and orientations. Ceramics strength is determined by the cracks that have the lowest failure strength and its fracture toughness is mainly determined by its chemical bonding strength as it informs the energy required to create fresh surface.

The concept known as *modulus interaction* is one of the ways to detect cracks in ceramics, the stress required to progress with a crack is reduced when the Young's modulus of the particle is larger than that of the matrix due to the matrix being partly unloaded within the particles.

However, if the Young's modulus of the particles is lesser than that of the matrix, the crack is shifted away from the particles, hence the stress is elevated with the particles and cracks are attracted by the particle. In addition, if the particles cannot be penetrated by the crack, the crack will have to progress along its boundary. It is worthy of note that in all these cases the crack path becomes enlarged (Joachim et.al.).

### 1.2.3 Polymers

Polymers contains macromolecules, they are mostly bonded together with covalent bonding, through a large molecular chains. For this reason, chain molecules can be considered as the basic building units of a polymer. Unlike metals and Ceramics which are made up of atoms, polymers are made of linear components which in return makes their structure more intricate than other classes of materials (Joachim et.al.).

The individual chain molecules (which is made up of several identical units, called monomers) contained in a polymer are normally organic compound. The number of monomers in a molecular chain is usually of the order  $10^3$  to  $10^5$  which causes a total molecular length of up to a few micrometers. The average number of monomers in the chain molecules of a polymer is called the degree of polymerization. Every molecule which can link in such a chain reaction can be used to produce polymers. Along these lines, there exists a wide range of polymers with emphatically changing synthetic and physical properties and in between the molecular chains, there are no strong chemical bonds. Contingent upon the molecular structure, the firmly temperature dependent dipole, hydrogen, or van der Waals bonds are shaped. Polymers could be formed by *addition polymerization* and *condensation polymerization* (Jastrzebski, 1976).

The mechanical properties of polymers are principally determined by the portability of the chain molecules. The portability relies upon the chemical structure of the polymer. For example, a polymer which contains a carbon chain (single bond) is pliable at each of the carbon atoms because a single bond between two carbon atoms is free to rotate freely. Alternatively, double bonds are rigid and this is because the mobility or portability is also affected by the presence of side groups. Ethylene is a typical example of a monomer that can form a polymer. The resulting polymer consists of a chain with a carbon atom back bone. Symbolically, this is written as  $[C_2H_4]_n$ , with the index 'n' denoting the number of repeat units, the degree of polymerization. As clarified above, straight chains are the establishing units of polymers. Though, it is conceivable to covalently cross-link the chains, shaping a molecular system. These cross-links are vital in deciding the mechanical properties of the polymer since they fix the chains in respect to one another and consequently render it difficult to draw out single chain

molecules. Because of this, a difference can be drawn between *thermoplastics* with no cross-linkage, *elastomers (or rubbers)* with few cross-links and *duromers* (additionally called *thermosetting polymers, thermosets, or resins*, the last name being because of the way that they are shaped by solidifying a resin component) with numerous crosslinks. Elastomers and duromers, unlike thermoplastics which can be semi-crystalline (made up of a mixture of crystalline and amorphous regions), both have chemical bonds that make a regular arrangement of the chain molecules impossible which in return makes them almost completely amorphous. The volume fraction of the crystalline regions in a semi-crystalline thermoplastic is called its *crystallinity*. In a semi-crystalline thermoplastic, the crystalline regions consist of only regularly folded molecules. Usually, The crystalline regions have a thickness of approximately 10nm and also a length between 1µm and 10µm and In between them are amorphous regions. The crystalline regions are regularly arranged radially with gaps filled using amorphous material, forming *spherulites* which are similar to the crystallites in a metal. Their extension is about 0.01mm to 0.1mm.

#### **1.2.4 Fibre Reinforced Composites**

There are different materials (composites) which can be consolidated to exploit positive properties of each material used. The result of this mix might be alluring for molecule or particle reinforcing of metals and for dispersion-strengthened ceramics. Composites, being fairly difficult to precisely define can be thought about as a material that includes two physically distinct phases. Composites used today are characterized by the following properties:

- A strengthening second phase is embedded in a continuous matrix.
- The strengthening second phase and the matrix are initially separate materials and are joined during processing – internal processes like precipitation do thus not produce the second phase.
- The particles of the second phase have a size of several micrometres at least.
- The strengthening effect of the second phase is at least partially caused by load transfer.
- The volume fraction of the strengthening second phase is at least approximately 10%.

(Joachim et.al.).

Fibre reinforced composites, or fibre composites (for short) in which the particles of the second phase are long fibres, surrounded by a matrix of the other component is what is emphasized on. One model is glass-fibre fortified polymer (GFRP) in which a polymer network is reinforced by including glass fibres As at first expressed, the target of shaping composites is to consolidate

wanted properties of the constituents. Focusing on glass-fibre reinforced polymers, the glass fibres increment the stiffness and strength, and the encompassing lattice makes the material increasingly bendable and shields the fibres from concentrated loads. There are a numerous number of possible combinations due to the fact that different materials are joined in composites. Metal, ceramic, or polymer matrix composites can be strengthened with different kinds of particles or fibres. Composites may be classified either by the geometry of the strengthening particles (fibres, fabrics, etc.) or by the matrix material used.

### **1.3. ENVIRONMENTAL DEGRADATION OF CONVENTIONAL ENGINEERING MATERIALS**

There are various differences in the level or degree of reactivity of the major group of conventional materials (metals, polymers and ceramics) even though all materials will react to some degree with certain environmental constituents. Metals are by a wide margin the most reactive of these groups and this is a reason why metals are found in nature in form of compounds. The metals compounds in the ores, oxides, sulfides, nitrides and the likes are very stable compounds. At the point when metals are expelled from these components, they want to return to where they originated from. Metals are taken from their ore and refined with the goal that they are formable and effectively manufactured into numerous desirable structures where they can be utilized. While returning to where they originated from, they may mix and react with many elements that exist in whatever environment to which they may become exposed, including those that are not normally found in ambient atmospheres, these could include the oxygen, gaseous hydrogen, nitrogen atmospheres, etc.

Billions of dollars is been spent for extracting metals from their compounds as found in nature, and then billions more to protect them from reactions that occur in their new environment. Estimates of loses in US industries due to corrosion of steel fall in the range \$70Billion to \$80Billion per year (Rogers, et. al. 1995). In the same vein an estimated amount of above \$50Million is spent per year in Deep Offshore Gulf of Guinea in Nigeria for maintaining corrosion related issue.

Metals are responsive due to the fact that they have free electrons meandering around searching for something to which they can end up appended, and in this manner bring down the general energy of the matrix. Polymers are considerably more exposed to natural debasement than ceramics. In polymers, light inside the scope of the bright wavelength area can break the C-C bonds between molecules, causing what is known as *charring [carbonization]*. One of the greatest effects of environment on polymers is caused by organic solvents.

In polymers, the solvents of electro-chemical reactions in polymers diffuses into the polymer body without breaking bonds and then causes plastization and swelling effects, which is commonly known as physical erosions. Natural fluids additionally lead to the decay of polymer properties. A few synthetic chemicals cause crazing and modification of mechanical properties of polymers. When all is said in done, polymers are influenced by daylight, atomic response, heat, oxygen, stickiness and natural solvent.

Some chemicals can attack ceramics which leads to their degradation and loss of quality but after all of these, ceramics are still the materials that are least affected by environment. Some ceramics are used to etch glasses and this is so because these ceramics have their silicates attacked by hydrofluoric acid. Strongly bond ceramics are very stable and inert to attack be attack by most aqueous solutions including acids and alkaline solutions.

### **1.3.1 Corrosion of Metals**

Generally, metals reacts with the earth and its environment and this can be classified into two noteworthy groups: That with the fluid condition (through a galvanic cell) that is otherwise called electrochemical consumption, and that with different reactants, for example, oxygen (oxidation), acids and a large group of other media. The most noticeable degradation system for metals is galvanic corrosion and it is describes as the loss of metal by a galvanic response. This is accomplished by evacuation of either iron particles or the electrons.

Taking into consideration a real iron sample which consists of grain boundaries, displacements and impurity atoms mostly in the form of precipitates such as iron carbides or oxide inclusions left as a residue of the refining process. Any of these can wind up being anodic or cathodic in line with the main body of the iron. The atoms in the grain boundary are more disordered and not as rigidly stuck together as those in the perfect lattice and this is the reason why the atoms in the grain boundary can go into solutions simpler than the atoms with the grain proper. A boundary is anodic if more atoms go into solutions at the grain boundary than from the former lattice causing more electrons to be generated there and these electrons will be expended in the inside of the grain not minding the fact that the region itself may be producing its electrons by the dissolution of the iron atoms.

The term '*Passivation*' describes a process that affects the corrosion rates of metals very considerably and always in an advantageous direction. High passivity metals form tight adherent proactive oxide, stainless steel is passive because of its chromium content Nickel and Iron show some degree of passivity but not to the extent of stainless steel. Polarization curves

are used to visualize Passivation. This curve shows the plot of electrode potential against log of the current density [as shown in figure 1.3]. The active region of the polarization curve has the current and electrode disintegration rate of a typical active metal increment exponentially with expanding positive potential on the electrode otherwise called the metal active state. In the case of metals with passive capacity, a marked decrease exists in the rate of corrosion which has a factor of  $10^3$  to  $10^6$  when the potential exceeds some critical value denoted as  $E_p$  on the polarization curve. The corresponding critical current is known as  $I_c$  (Rogers, et. al. 1995).

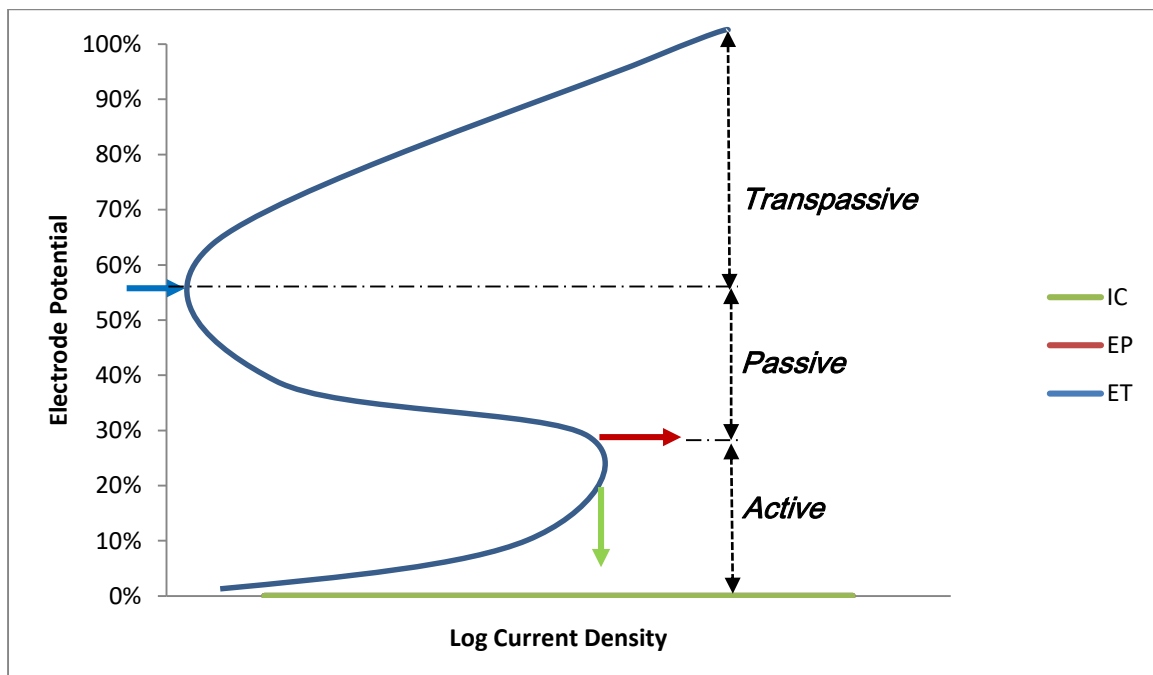


Fig 1.3: Schematic polarization curve for a metal that displays an active- passive transition. Source: (Rogers, et. al. 1995).

The current density speedily reduces to a constant value which does not change with expanding electrode potential once the  $E_p$  value is lower than the electrode potential. This is the passive state of the metal as noted on the above polarization curve as the passive region. But when the electrode potential attained is sufficiently high [ $E_T$ ] the metal again becomes active. The part of the curve is termed the *trans-passive region*.

Nature can change the condition of passivity. Most oxide films are affected negatively by chlorine ions, particularly that of aluminium. Confined erosion can occur because of breaks in the film. Different sorts of corrosion can be experienced by metals.

**Uniform Corrosion** as the term suggests is defined as a type of corrosion attack (deterioration) that is more or less uniformly distributed over the entire exposed surface of a metal. Uniform corrosion also refers to the corrosion that proceeds at approximately the same rate over the exposed metal surface. Cast irons and steels corrode uniformly when exposed to open atmospheres, soils and natural waters, leading to the rusty appearance.

**Localized Corrosion:** or known as **pitting corrosion** when the depth is more than the diameter of the pit. At certain depths the pits may branch out into several directions. A small, narrow pit with minimal overall metal loss can lead to the failure of an entire engineering system. In pitting corrosion, the anodic sites do not shift but become fixed at certain points on the surface. Pitting often requires a certain amount of initiation time but the pits grows faster with time as conditions within the pit becomes more aggressive. Oxygen fixation cells can start a pit and the distinction in oxygen concentration between the pit and the surface will quicken pit development rates.

**Crevice Corrosion:** This refers to the localized attack on a metal surface at, or immediately adjacent to, the gap or crevice between two joining surfaces. The gap or crevice can be formed between two metals or a metal and non-metallic material. Outside the gap or without the gap, both metals are resistant to corrosion. Relating to the non-metallic material scenario, the second material may be debris, such as grease or mud, gaskets and parking materials and as a result this type of crevice corrosion has been called **deposit or gasket corrosion**. Relating to the 'metal-metal' scenario, cracks and seams may be the point of corrosion initiation even between two regions of the same metals. The mechanism varies from material to material and with environment, but what is common in all crevice corrosion is the presence of a crevice where stagnant fluids collect.

**Stray-Current Corrosion:** This refers to corrosion resulting from stray current - the current flowing through paths other than the intended circuit most commonly encountered in soils containing water. It is more common in underground structures. Protective coating and insulation are two possible preventive methods that may be used for this type of corrosion.

**Intergranular Corrosion:** Sometimes called "*intercrystalline corrosion*" or "*interdendritic corrosion*", Consists of selective attack at the grain boundaries. The fact that chemical etchants reveals grain boundaries is evidence of the susceptibility to chemical attack and dissolution at these boundaries. It occurs in austenitic stainless steels, some super alloys, and possibly in other high-chromium alloys that have been heated into certain temperature ranges.

***Selective Leaching Corrosion:*** refers to the selective removal of one element (minor) from an alloy by corrosion processes. A common example is the dezincification of unstabilized brass, whereby a weakened, porous copper structure is produced.

***Erosion-Corrosion:*** Erosion Corrosion refers to the combined action involving erosion and corrosion in the presence of a moving corrosive fluid or a metal component moving through the fluid, leading to accelerated loss of metal. Grooves and gullies normally appear.

***Corrosion fatigue*** Corrosion Fatigue refers to the process in which a metal fractures prematurely under conditions of simultaneous corrosion and repeated cyclic loading at lower stress levels or fewer cycles than would be required to cause fatigue of that metal in the absence of the corrosive environment. One primary role of corrosion in the corrosion fatigue process is that of providing surface defects for crack formation and propagation. Crack propagation can also be enhanced by a corrosive process in some alloys whereby the energy required to break atom bonds and provide two new surfaces is reduced by the corrosive media.

### **1.3.2 Environmental Degradation of Ceramic Materials**

Ceramics materials are basically insulators, the type of uniform corrosion experienced in metals cannot happen on account of absence of conductor. This does not mean that other forms of chemical attacks are not conceivable. Hydrofluoric acid is used to etch glass and other ceramics materials. The degradation of ceramics by the environment is less as compared to that of metals and polymers. Numerous ceramics materials will decompose at high temperatures, and most times, the environment can fasten or change the decomposition rate.

***Dissolution corrosion*** describes the impact which corrosion and other environmental influence has on ceramics material and some of the same metallic behavior of grain boundary or stress corrosion may be included. There are many parts which can provide a conductive path for electrons to flow in galvanic cell reaction and some examples of these components are bonding agents, grain growth and mineralizer. Thus, corrosive attack is often centered on minute quantities of such components. Processes like reaction sintering, vapors deposition and hot pressing have eliminated the effects of this minor constituents and hence less concern for corrosive effects in ceramics.

***Weathering*** describes the corrosion of glasses by atmospheric conditions. Weathering occurs due to the presence of water vapor and is believed to be related to tensile stress set up by an



ion exchange of the alkali by hydrogen ions. Soda-lime silica glasses lose considerable strength due to atmospheric corrosion by water vapor. Glass corrosion by liquids occurs more frequently than that by vapors. Glasses are soluble in liquids over a wide range of PH values from acids to bases, including water to a slight extent. The high-silicate glasses such as the borosilicates and alumina silicates of about 98%  $\text{SiO}_2$  content have excellent corrosion resistance compared to the water-soluble sodium silicates. Glasses fibres are much more subject to corrosion than are the bulk glasses due to the higher surface/volume ration. Humid environments lower the strength of the glass fibres which is why most glass fibres are produced with a polymer coating.

Ceramics are relatively resistant when they are chemically attacked and this can be easily related to bond strength. Though weakly bonded ionic salts, nitrates, oxalates, chlorides and sulfates are dissolved in water and weak acids, while the more strongly bonded  $\text{Al}_2\text{O}_3$ ,  $\text{Si}_3\text{N}_4$  and  $\text{ZrSiO}_4$  are resistant to many types of chemicals, including aqueous solutions, strong acids, bases and liquid metals and hence can be used as crucible materials. These oxides are also acid and base resistant and are used either to replace metals or as a coating for metals.

Ceramic materials are used in applications like gas turbine and because of this; very high temperatures are not desired. Oxides and silicates are more stable in high-temperature oxide environment are the carbides, nitrides and borides. Porosity is also a factor since oxidation can occur along interconnected pore channels. For heat engines,  $\text{Si}_3\text{N}_4$  and  $\text{SiC}$  appear to be the leading candidate materials since they possess good stability, thermal conductivity, low thermal expansion and good high temperature strength.

### **1.3.3 Environmental Degradation of Composites**

The responses of metals [steels], polymers and ceramics to ecological degradation have been portrayed in discussions above. It won't be strange to state that the ecological impacts would kind of pursue the rule of mixtures since the properties of composites are an element of their constituents and this is somewhat true. Any of the ecological impacts referenced already on the individual constituent would be relied upon to effectively affect these particular constituents; given that there exist a way whereby the harming fixings can arrive at the individual constituents.

In increasingly modern composites, for example, organic matrix fiber composites, different issues emerge. The most generally dreaded is the disintegration and breaking of interfacial bonds. Swelling and plastization of tars can be caused by water and in this way allows the entrance of water or different fluids by capillarity activity along the fiber-matrix interface.

Weakening of PMC [Polymer Matrix Composites] by dampness or chemical assimilation is of incredible concern. The quality of these composites can be decreased if the compound species in the environment attack the polymer, the support material or the interface between the two materials. MMC [Metal Matrix Composites] are not as susceptible to moisture as susceptible to moisture deterioration as are PMC's. The major concern with for MMC applications is the temperature stability of the matrix and reinforcement constituents in the environment of interest. Damage from external environment can be minimized if the reinforcement material is not exposed. Galvanic corrosion has been observed in some MMC's (Joachim et. al.).

This section explored the properties and degradation of basic Engineering Materials; Metals, Ceramics and Composites, this is vital to this study as it gives a premise upon which the proposed FGM solution could be benchmarked based on properties and behavior.

#### **1.4. STATEMENT OF THE PROBLEM**

Recent challenging Engineering Operations in the Gulf of Guinea has increased the demand for unique structural materials due to the severe working conditions, specifically in Offshores Oil and Gas facilities where the challenge posed by corrosion is really alarming. Hence, a need for research into a specialized material that meet the challenges strength, fracture toughness, specific stiffness and corrosion experience in most Deep Offshore Operations including the Gulf of Guinea where all deep water operation in Nigeria are located. In clear perspectives, this research was necessitated as a result of the lingering operational challenges faced with Sea Water Processing Line on most Deep Offshore Production Facilities in the Gulf of Guinea.

This research focused on a specific facility with a profound exposure in terms of these challenges on its Sea Water Processing Line during operation. The line was originally designed with steel pipes and later replaced with a conventional composite material of FRP (Fiber Reinforced Polymer) to reduce the effect of corrosion on the line due to the corrosive nature of sea water as shown in the pictures below:



Fig. 1.4: Application of Fiber Reinforced Plastic (FRP) on an Offshore Facilities at Gulf of Guinea.

The stopgap solution of replacing the sea water processing system with FRP on the facility has yielded favorable outcome as most of the challenges faced with the steel piping were greatly eliminated, particularly that of the corrosion.

Despite all the benefits derived from FRP, some salient challenges are being experienced while using the FRP on the sea water processing system as a result of stresses. These include:

- Limitation to operating conditions.
- Frequent cracking of the FRP.
- Frequent failure at the flange.

Consequently, the above mentioned challenges result in a huge maintenance cost for the FRP annually, running into about 2 million USD per operating facility.

Hence, the justification for a research on a material that will have all the advantages of FRP (in terms of specific stiffness and corrosion resistance) and equally have wide range of operating temperature with the fracture toughness required to withstand crack and flange failure during operations.

Although the highlighted challenges were experienced in the Gulf of Guinea. The findings from the research could be applicable to all Oil and Gas Operations, most especially Offshore Operations.

The class of materials proposed to meet these increased demands is Functionally Graded Materials (FGMs). The uniqueness of FGM's properties makes it suitable to be tailored to specific service/operations such as the huge temperature gradient and corrosive environment in the oil and gas industry.

The applications of functionally graded materials (FGMs) are increasing because of their capability to control the thermo-mechanical stresses in structures under thermal and mechanical loadings. FGMs are a new kind of composite materials whose thermo-mechanical properties vary continuously along certain directions. There have been few analytical solutions from numerous researchers in recent years to determine the stress distribution in structures, especially in cylindrical structures.

This research work focuses on the stress analysis of functionally graded pipe components, with the main purpose of making it an ideal replacement for the conventional materials used in extreme service condition in offshore Oil and Gas operation.

## **1.5. AIM AND OBJECTIVES**

The aim of the work contained in this thesis is to analyze the stresses on a Functionally Graded Pipe components subjected to thermal and mechanical loading numerically with the purpose of

using the material as a replacement to current composite material (FRP) used on the Sea Water Processing Line of most FPSO in deep offshore operations in Gulf of Guinea.

This is achieved through the following specific objectives:

- To perform stress analysis of FGM as a finite pipe under a range of different thermal and mechanical loadings – that replicates the real-life operating scenarios.
- To determine and optimize the material constituent to be used for the FGM modelling.
- Predicts the design limit of the FGM based on Von Mises failure criteria.
- Carry out parametric studies of other FGM pipe configurations and material combinations, this will give insight on the most optimal configuration and material combination. The configurations under consideration are:
  - Straight FGM pipe Configuration
  - Elbow FGM pipe configuration.
  - T-Piece FGM pipe configuration.

All these FGM configurations and material combinations were subjected to mechanical and thermal loading conditions only.

## **1.6. SIGNIFICANCE OF THE STUDY**

The reviewed literature for this research revealed that there is little information available on FGM as applied to pipe components. Nevertheless, the benefits of FGMs as used in other service conditions such as structural support shows that there is much potential for their application to the oil and gas sector. The outcome from the research explored FGM Pipe application in the oil and gas industry and also revealed the piping configurations (straight pipe, elbow pipe and T-piece pipe) that is suitable for different pressure and temperature limits. In addition, the research also proffered the optimum FGM material combination to be considered for oil and gas operations within the conditions below:

- Ability to withstand the operating temperature range of 0 to 150°C.
- Excellent Corrosion Resistance
- Excellent interaction with salt water.
- Availability.
- Excellent fracture toughness
- Excellent specific stiffness due to offshore application
- Fatigue and tensile strength
- Economic considerations

The outcome of the research is a benchmark for future studies on FGM utilization for oil and gas piping operation. In addition, it will also guide in the decision making for all the prevailing challenges faced by the operators of deep offshore Oil and Gas Assets on the Sea Water Processing Line of their facilities.

### **1.7. SCOPE OF STUDY**

The study is to analyze the effect of stress on a Functionally Graded Pipe subjected to different thermal and mechanical loading. The focus will be as follows:

- To perform a finite element analysis on the FGM and to also perform a detailed simulation on the FGM through various loading conditions.
- Select the most optimum materials for the FGM combinations.
- Develop and predict the design limit for the FGM's
- Perform an elbow FGM pipe configuration FEA and determine its design limits.
- Perform a T-piece FGM pipe configuration FEA and determine its design limits.



## **CHAPTER 2: LITERATURE REVIEW**

### **2.1 INTRODUCTORY REMARKS**

There have been numerous studies performed to analyze the response of Functionally Graded Materials subjected to mechanical and thermal loading and other variables, most of these investigations are based on analytical or numerical approaches. This chapter delves into some of these literatures related and relevant to the problem under consideration.

Furthermore, some literatures on material selection were also reviewed; this was to give insight on the material selection approach that was considered in the present study while determining the most suitable material constituent for the FGM that will meet the desired service conditions. In addition, literatures on FGM Pipe configurations were also reviewed with more attention on the Elbow Pipe configuration being one of the configurations considered in this study. These literatures as reviewed provided in-depth understanding of literatures relating to the structural behavior of different aspects of elbow (bend) pipes. These ranges from the determination of the ultimate loading conditions that the elbow pipe will fail (Internal Pressure, Bending Moment, etc.) and some parametric studies on the pipe bend to understand the failure mode under different ranges of design.

In summary, the review focuses on, literatures on generic FGM study, Finite Element Analysis of FGM's, Material Selection approach of FGM's and Analysis on Elbow Pipe configuration. They are as detailed in the following subsection.

### **2.2 RESEARCH ON FUNCTIONALLY GRADED MATERIALS**

Several key papers in the literature were reviewed to give an insight on the present state of knowledge on Finite Element Analysis of FGM's in general within the past five years. The detailed summary of all the contributions from the literatures reviewed within this section are detailed in table 2.1.

1. Abotula et. al. 2012, undertook research on dynamic curving cracks in functionally graded materials under thermo-mechanical loading. The study focused on the crack growth along the path of an FGM, Basic Material properties such as thermal conductivity, mass density, shear-modulus and coefficient of thermal expansion were varied along the gradation direction of the FGM. The stress field of the crack propagation in the FGM was developed using the asymptotic analysis in conjunction with displacement potentials. Asymptotic temperature fields was developed for both the exponential variation of thermal conductivity and for temperature fields which was used to derive thermo-mechanical stress fields for the



curving crack in FGMs. The derived thermo-mechanical stress fields was used to develop components of the stresses and the effect of curvature parameters, temperature and gradation on these stresses are discussed. Finally, the minimum strain energy density criterion was used to determine the effect of curvature parameters, crack-tip speeds, non-homogeneity values. The finding from this study revealed that the thermo-mechanical stress at the crack-tip is affected significantly by non-homogeneity parameters. It was also determined that the FGM's mechanical properties gradation affects the contours of the maximum shear stress considerably, on the other hand thermal properties gradations as no significant effect on the stresses. The main conclusion from this study is that, non-homogeneity factor has high influence on thermo-mechanical stress and that for stress consideration; emphasis should be more on mechanical property gradation of the FGM rather than the thermal property gradation.

2. Shariyat et.al, 2013, researched on low-velocity impact analysis of the functionally graded plates using commercial finite element software and discrete models for variations of the material properties. The study focused on the analysis of two directionally- graded circular plates using the nonlinear approach when subjected to preloads that is radial. Some unique features of this research are: (a) the study modelled a precise variation of material properties, (b) it focused on FGM's with property variation in both radial and transverse directions, (c) it takes into account the initial compressive/extensional radial loads, (d) it evaluated the influence of radial pre-load with the nonlinear von Karman-type strain-displacement relations, (e) it used the refined contact law account for the material heterogeneity along the plate thickness. The study performed a detailed sensitivity analysis including effects of various material heterogeneity, geometric, and motion parameters are accomplished. The study by Shariyat et.al guided the approach used in the present research to account for the material properties heterogeneity along the pipe thickness.

### **2.3 RESEARCH ON FGM USING FINITE ELEMENT ANALYSIS ON VARIOUS LOADING CONDITIONS**

This section focuses on the review of literatures that were tailored specifically toward the study of Finite Element Analysis of FGM's subjected to various loading conditions. The review delineated on those studies performed within the past five years. A detailed review of some literatures that were within the scope of reference are detailed below, while all reviewed literatures within this confines are summarized in table 2.2

2.3.1. Jing-Hua Zhanga, Guang-Ze Lia and Shi-Rong Lib (2015)

Jing-Hua Zhanga, et. al (2015) researched on the transient displacements of a ceramic–metal Functionally Graded Material (FGM) cylindrical shell subjected to dynamic thermal loading are investigated using the differential quadrature method (DQM). The grading of metal–ceramic properties along the thickness direction was determined by the simple power law distribution that accounted for the volume fractions of the constituents as shown in equation and figure 2.1 below. Laplace transform and power series approach was used to determine the transient temperature field of both the ceramic–metal. Furthermore, the transient displacements of the axisymmetric deformed shell were obtained by solving governing equations using the DQM. The study also analyzed the effects of the shape geometry and the material constitutions on the transient central deflection. The study discovered that the transient deformations of the FGM cylindrical shell under dynamic thermal loading could be controlled by changing the volume fractions of the ceramics.

$$V_e(z) = \left(h - 2z/2h\right)^N, V_i(z) = 1 - V_e \quad 2.1$$

$N$  = Power law index

$i$  = Constituent of inner surface

$e$  = Constituent of outer surface

$h$  = Thickness

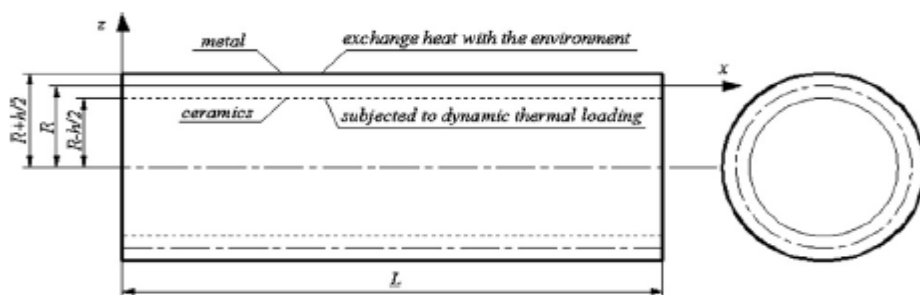


**Fig 2.1:** The sketch of the ceramic–metal FGM cylindrical shell subjected to dynamic thermal loading. (Jing-Hua, et. al, 2015)

According to this model, the effective material properties (Young's modulus  $E$ , coefficient of thermal expansion  $\alpha$ , the specific heat capacity  $C$ , coefficient of thermal conductivity  $K$  and mass density ( $\rho$ ) can be expressed as:

$$P(z) = (P_i - P_e)V_i(z) + P_e \quad 2.2$$

Poisson's ratio  $\mu$  does not vary considerably with the material constituents so it is assumed to be a constant, i.e.  $\mu(z) = \mu$ :

The research by Jing-Hua Zhanga et. al. was based on the classical shell theory with boundary conditions at both edges simply supported. Through study, the following conclusion was drawn:

- The thermal membrane force and the temperature field tends to be stable with as time increases, while the thermal bending moment reaches a peak at first from zero and then tends to be zero with time goes by.
- Considering thickness, radius and length effect on the FGM shell transient deflection. The thicker shell responds slower to deflection and tends have a smaller stable value, while the bigger radius responds faster and tends to have bigger stable value. On the contrary, the effect on the transient deflection is negligible considering the bigger length. On the same note, the thermal membrane force in the circumferential direction increases gradually and tends to be stable over time.
- The properties of FGM due to its gradation have significant effects on the deformation of the FGM shells. The central deflections of the metal/ceramic FGM shells are in-between those of the metal and the ceramic shells and increase monotonously as power law index increases. Hence, the deflections of the FGM cylindrical shell could be altered by changing the volume fractions of the constituent materials. The research guided the approach used in FGM Material gradation in the present research by the use of the Power Law Equation, it also shed more light on the relevance of FGM property gradation on the FGM deformation.

### 2.3.2. Mine Uslu Uysal (2013)

Uysal investigated the thermal and mechanical loading on functional graded plates. The research was based on the mechanical deformation behavior of shear deformable functionally graded ceramic-metal (FGM) plates. The buildup of the FGM was based on power law theory. In addition, the mechanical properties of the plate are graded in the thickness direction according to a power-law, displacement and stress is obtained using finite element method (FEM). The load is uniformly distributed over the plate surface but varied in the thickness direction only. The FGM modelled by Uysal is defined to be a material which has a continuous gradation through the- thickness ( $h$ ), with either side being fully metal or ceramic respectively. A mixture of the two materials composes the through-the thickness characteristics. This material gradation along the thickness ( $h$ ) is determined by a parameter, “ $n$ ” known as non-homogeneity factor. At  $n = 0$ , the plate is a fully ceramic plate while at  $n = \infty$  the plate is fully

metal. The non-homogeneity factor and the position in the plate determine the material properties of the whole FGM and varies according to a power law.

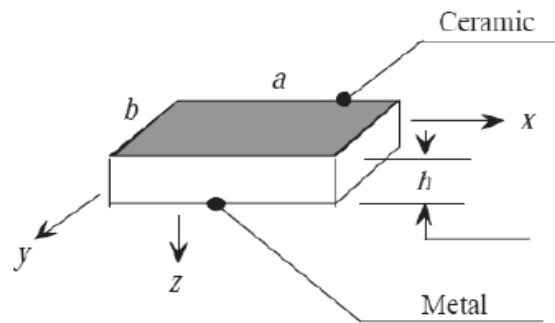


**Fig.2.2:** Schematic diagram and dimension of plate

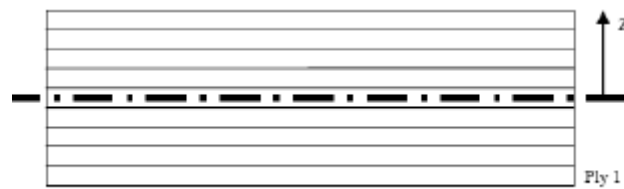


**Fig. 2.3:** Schematic of the FGM gradation

The typical material properties  $P$ ,  $\nu$ ,  $E$  etc., are varied through the plate thickness according to the expressions (a power law) as shown below:

$$E(z) = (E_t - E_b) \left( \frac{2z+h}{2h} \right)^n + E_b \quad 2.4$$

$$\nu(z) = (\nu_t - \nu_b) \left( \frac{2z+h}{2h} \right)^n + \nu_b \quad 2.5$$

$$p(z) = (p_t - p_b) \left( \frac{2z+h}{2h} \right)^n + p_b \quad 2.6$$

The value “ $n$ ” in the above equation is significant as it influences the volume fraction of the FGM constituent. It essentially determines the amount and distribution of ceramic/metal in the plate. Higher values of “ $n$ ” makes the plate to tend toward metal (lower plate surface), on the other hand, lower values of “ $n$ ” make the plate tend toward ceramic (upper plate surface). The “ $n$ ” value could be varied to tailor the FGM to specific applications. Uysal characterizes “ $n$ ” for each of the models studied.

The approach used study by Uysal et al. to determine the material gradation of FGM was used in the present research. The use of ply and technique of dividing the FGM into two to determine material variation through the non-homogeneity factor as utilized by Uysal et al. was also explored in the present research. In addition, the power law was also used to derive the FGM constituent proper as used by the study being reviewed.

## **2.4 RESEARCH ON MATERIAL SELECTION FOR ENGINEERING APPLICATIONS**

Optimising the material selection/combination for FGM is one of the research objectives for this work, and to effectively achieve this objective, some past literatures that on FGM material combination and applications were reviewed. This section of the literature review focused on the review of past literatures on FGM Modelling with emphasis on the materials combination/application of the FGM. Some of literatures reviewed that considered the FGM materials similar to the materials of this study are presented below. The detailed literatures reviewed on FGM material selection/application is as summarized in in table 2.3.

### **2.4.1 Douglas E. Burkes and John J. Moore (2006)**

Burkes and Moore studied the microstructure and kinetics of a functionally graded NiTi–TiC<sub>x</sub> composite produced by combustion synthesis (Douglas & John, 2006)

They were able to produce Nickel Titanium alloy or Nitinol (NiTi) and Titanium Carbide (TiC<sub>x</sub>) functionally graded material (FGM) through use of a combustion synthesis (CS) reaction utilizing the propagating mode (SHS). The produced FGM takes advantage of the unique superelastic and shape memory capabilities of Nitinol with the high hardness, wear and corrosion resistance of Titanium Carbide Ceramics. The produced FGM was considered the graded in both its porosity and composition with excellent material interaction. The X-Ray diffraction (XRD) of the FGM conducted shows presence of Titanium Carbide with equi-atomic Nitinol and minor NiTi<sub>2</sub> and NiTi<sub>3</sub> phases. The TiC<sub>x</sub> content in the FGM decreased with increasing Nitinol content. A detail study conducted over the length of the FGM shows a decrease in hardness as the Nitinol content increased.

### **2.4.2 N. H. Faisal et al. (2017)**

Faisal et al. researched on the Cyclic Nanoindentation and Nano-Impact Fatigue Mechanisms of Functionally Graded TiN/TiNi Film (Faisal et al., 2017).

Faisal et al. studied the fatigue mechanisms of functionally graded Titanium Nitride (TiN) and Titanium Nickel alloy (TiNi) films under the effect of several loading cycle and impact investigations. The functionally graded film has the unique properties of quasi-elasticity and

shape memory behavior of TiNi film combined with the tribological and anti-corrosion properties of the Titanium Nitride (TiN) Ceramics. The nanomechanical investigation was conducted on the FGM to study the modes of failure employing both conical and Berkovich indenters with varied loads within a particular range. The study reveals that the results change profoundly to the load applied, mode of loading and geometry of probe. The study concludes that the induced localised indentation stress, film failure, and generation of pseudo-elasticity at a lower load range is critically dependent on the shape of the indenter.

#### 2.4.3 Xing-Hong Zhang et al. 2000

Zhang et al. researched on the microstructure and mechanical properties of TiC-Ni functionally graded materials by simultaneous combustion synthesis and compaction (Xing-Hong et al. 2000).

The study by Zhang et al. was able to fabricate Titanium Carbide (TiC) and Nickel (Ni) FGM through the instantaneous combustion fusion and hot compaction of Titanium, Carbon and Nickel powders under a hydrostatic pressure. The grading of the composition was enhanced by FEA and achieved through the piling diverse powder mixtures of preferred compositions. X-ray diffraction and microprobe analysis investigation of the FGM reveals that the combustion reaction was complete and the final products have phases of TiC and Ni only. The FGM physical and mechanical properties measurements reveal that these properties were mainly dependent on Nickel content and apparently get to its peak values of density, flexural strength and hardness at standard temperature when the Nickel content was increased to 20 wt%. The maximum in fracture toughness value was found to be with FGM Combination of TiC-30 wt% Ni material.

#### 2.4.4 In-Jin Shon and Zuhair A. Munir (2005)

Shon and Munir worked on Synthesis of TiC, TiC-Cu Composites, and TiC-Cu Functionally Graded Materials by Electrothermal Combustion (In-Jin & Munir, 2005).

The study synthesized Titanium carbide and its composites and FGMs of TiC-xCu through an electrothermal combustion (ETC) method. The titanium carbide synthesized through ETC showed minimal porosity as compared to those synthesized by ordinary ignition with the aid of radiative heating. The study revealed that composites and FGMs with higher copper content can be synthesized effectively by electrothermal combustion. It also revealed that in the Functionally Graded Material product the variation in composition in the graded region was seen to be almost linear for samples with  $0 \leq x \text{ (wt \%)} \leq 75$ .

#### 2.4.5 Zhaohui Zhang et al. (2012)

Zhang et al researched on the new rapid route to in-situ synthesize TiB–Ti system functionally graded materials using spark plasma sintering method (Zhaohui et al., 2012)

The research was on a four-layer Titanium Boride and Titanium system FGM that was synthesized speedily through a sintering procedure that uses spark plasma with the aid of graphite die that changes in its cross sectional area. The configuration and microstructure the FGN layers were categorized by X-ray diffraction (XRD) and scanning electron microscopy. The mechanical properties of individual layer were analyzed with the aid of three point bending procedure and a single-edge notched beam method. The results from the research reveals that a steady graded temperature field can be achieved while utilizing the Spark Plasma Sintering (SPS) process. The synthesized FGM displays fine and dense microstructure that is continuous and free from crack at the interfaces. The relatively high hardness observed at the interfaces signifies that the interfaces between the FGM are well-bonded. The study also reveals that the bending strength and the fracture toughness of the FGM layers are high when the material is synthesized with a pre-designed die than when it is synthesized with a common cylindrical die.

## **2.5 RESEARCH ON PRESSURE SYSTEMS PIPING COMPONENTS USING FGM DESIGN**

Over the years, there have been numerous studies on different aspect of elbow (bend) pipes, this studies ranges from the determination of the ultimate loading conditions to which the pipe will fail (Internal Pressure, Bending Moment, etc.) to some parametric studies on the pipe bend to understand the failure mode under difference ranges of design. Most of the studies presently in literatures focuses on elbow (bend) pipe made of conventional engineering materials, based on the available literatures, studies on the Finite Element Analysis (FEA) of Elbow (bend) FGM Pipes are limited or unavailable, hence the present study will give a fair understanding of how bend FGM pipe behave under combine loading conditions. The review of literature reveals the following researches and findings as regards to FEA of elbow pipes made from conventional engineering materials (As summarized in table 2.4).

#### 2.5.1 Christo Michael T., Veerappan A. R., and Shanmugam S. (2012)

Michael et. al. researched on the Comparison of plastic limit and collapse loads in pipe bends with shape imperfections under in-plane bending and an internal pressure (Christo et. al. 2012). The research by Michael et al. was premised on the fact that when Elbow (bend) pipes are subjected to closing bending moment, there is a significant deformation (ovalization) in the

cross section this tends to make the geometry deteriorated, as shown in figure 2., below it results in the thinning of the extrados and thickening of the Intrados (Christo et. al. 2012).

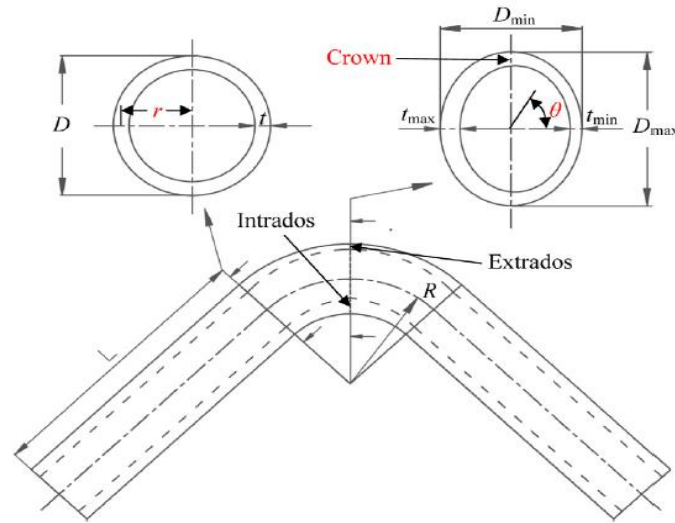


Figure 2.4: Pipe bend geometry with attached straight pipe (Christo et. al. 2012).

The degree to which ovalization occurs is dependent on the variance of major and minor diameters divided by the pipe nominal diameter. This is expressed in percentage form as percentage ovality;

$$C_o = \frac{(D_{Max}-D_{Min})}{D} * 100 \quad 2.7$$

Where

$$D = \frac{(D_{Max} + D_{Min})}{2}$$

Based on the study, thinning occurs at pipe bend extrados, and it is illustrated as the ratio of the variance of the pipe bend nominal thickness and the minimum thickness divide by the pipes nominal thickness, this is equally expressed in percentage term as;

$$C_t = \frac{(t-t_{Min})}{t} * 100 \quad 2.8$$

On the other hand, thickening occurs at pipes intrados and it is illustrated as the variance pipe bend maximum thickness and the nominal thickness divided by the pipes nominal thickness, this is expressed in percentage terms as;

$$C_{th} = \frac{(t_{Max}-t)}{t} * 100 \quad 2.9$$



The study by Michael et al. compared the limit load on the basis of minimal displacement limit analysis and failure load on the basis of extreme displacement analysis for pipe elbow (bend) with imperfect-shapes, the study was carried out with finite element method using ABAQUS software. The failure and limit moments were determined from the drawn moment-rotation curves for each of the model. The failure load was obtained using the twice-elastic-slope method. The study reveals that the effect of thinning on limit and failure moments are negligible and consequently thinning need not to be examined when analysing pipe bends. It also reveals that ovality plays significant role in both limit and failure loads for most cases examined. Furthermore, it was revealed that ovality plays a significant role in the determination of failure loads. Despite the difference in the loading condition between the present research and the research being reviewed, the reviewed study guided in the modelling of the FGM Elbow pipe on Abaqus.

2.5.1 Shun-Jie Li, Chang-Yu Zhou, Jian Li, Xiang-Ming Pan and Xiao-Hua He (2017)  
Li et. al. worked on the effect of bend angle on plastic limit loads of pipe bends under different load conditions (Shun-Jie, et. al. 2017).

The research by Li et. al. was based on the following assumptions:

- The research sample is a pipe bend with thin wall having equal thickness, while residual stresses from the forming stages is not been considered.
- Seamlessly plastic and elastic material was assumed that is adapted to non-hardening J 2 flow theory.
- Huge displacement analysis is being considered, due to the large deformation envisaged as a result of bending moment and pressure.

Based on these assumptions, Li et. al. modelled pipe bend with thin wall (with ratio of pipe external diameter to internal diameter  $K \leq 1.2$ ) having equal thickness. Various parametric studies were modelled ranging from  $t = 2, 5 \& 10$  mm,  $R = 200, 400 \& 600$  mm and bend angle values as  $30^\circ, 60^\circ, 90^\circ, 120^\circ, 150^\circ$  and  $180^\circ$  respectively. A total of 270 models were used in this study to give insight on the effect of bend angle on pipe bend plastic limit loads.

The research utilized non-linear three dimensional analyses to study the effect of angles (bend) on plastic limit loads of pipe bends. Base on the FEA carried out, which focuses on the features of deformation, stress and strain and the influence of bend angle on the limit load. From the results, it shows that bend angle has higher effect between  $0^\circ \sim 120^\circ$  when subjected to internal pressure, in-plane bending moment and torsion moment, and at angles between  $0^\circ \sim 90^\circ$  under out-of-plane moment. The reviewed study has a similar loading condition that is common with

the present research; that is Internal Pressure in the pipe. Although, the present study did not consider bending and torsion moment, the reviewed research provided clarity on multi-point constraint (MPC) application on Abaqus.

#### 2.5.2 Yun-Jae Kim and Chang-Sik Oh (2007).

Kim and Oh researched on the Effects of attached straight pipes on finite element limit analysis for pipe bends (Yun-Jae and Chang-Sik, 2007).

The study by Kim and Oh explored the effects of attached straight pipes on pipe bends under internal pressure loading and bending moment. The research estimated size and influence of the length of the straight pipe attached to pipe bends (90°). This was based on Finite Element Analysis seamlessly plastic elastic materials having minimal geometry change option. One of the vital point of this research is the application of bending moment at the piping end devoid of end effects. This was achieved by the use of a subroutine for multi-point constraint (MPC) in the ABAQUS software. The research considered a 90° bend pipes, with average radius and pipe thickness as  $r$  and  $t$  respectively, with  $R$  as the bend radius. This is as shown in Figure 2.  $R/r$  and  $r/t$  are vital variables that are associated with the bend configuration, this is inclusive of the bend characteristic  $\lambda$ , and their relationship is as stated in the equation below:

$$\left(\lambda = \frac{Rt}{r^2} = \frac{R/r}{R/t}\right) \quad 2.10$$

The values of these variables were tactically used at different ranges to be able to determine the effect of pipe bend configuration on plastic limit loads, a range of within the range of  $\lambda$  from 0.1 to 0.5 was used. Based on the research objective, the length of the attached straight pipe was also varied,  $L$  (Fig. 1), was also systematically varied, with the inclusion of a limit scenario when  $L=0$  (90° pipe bend with no pipe attached).

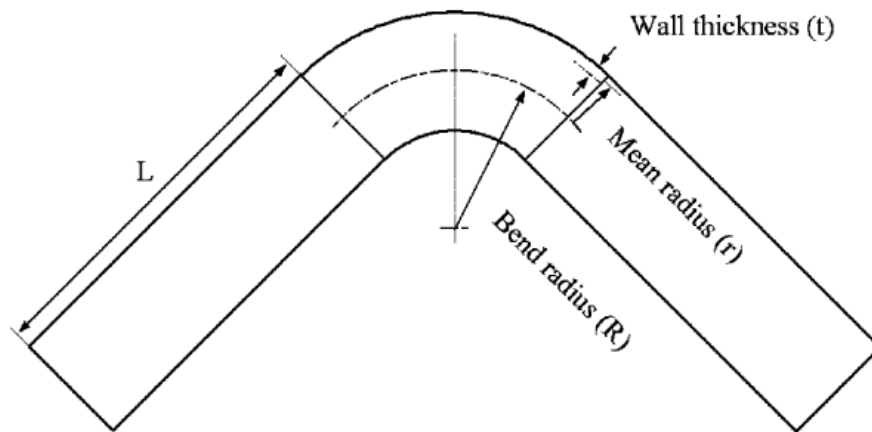


Figure 2.5: Schematic illustration of 90° pipe bend with the attached Pipe (Yun-Jae and Chang-Sik, 2007).

The study reveals that the effect of the length of the attached straight pipe on plastic limit loads is significant, the load limits tend to reduce with reduction in the length of the attached straight pipe. While in the scenario where there was no attachment to the pipe bend (Limiting Case), the load limits were found to be almost same as current analytical solutions. The reviewed study guided the modelling of the elbow FGM pipe in the present study. It guided the length of the straight FGM pipes attached to the elbow ends that will not alter the ideal limiting loads for each considered elbow FGM pipe.

### 2.5.3 Jian Li, Chang-Yu Zhou, Ji-Lin Xue, Xiao-Hua He (2014)

Li et. al. researched on Limit loads for pipe bends under combined pressure and out-of-plane bending moment based on finite element analysis (Jian et. al. 2014).

Li et. al. analyzed the effect of minimal displacement, huge displacement with configuration and material that are not linear were considered in the study, the focus of the analysis was on limit load of pipe elbows (bends) subjected to both internal pressure and out-of-plane bending moment, this was studied with the aid of a non-linear finite element simulations that has three-dimensions with the intention of giving more insight to limit load of pipe elbows under complex loading conditions.

Sixteen (16) models were used for this research, these models have four (4) different radiuses and four (4) different pipe wall thickness and an elbow bend angle of 90° was considered. The attached straight pipe to the elbow has a length that is adequate ( $L > 3r$ ) to negate the proven end effect on the limit load, the bend characteristics was also define from equation (4) as stated above.

The FEA was performed with ABAQUS code, the left elbow pipe end left plane end had fixed constraint boundary condition, while on the right plane end of the pipe, a Multi-Point Constraint (MPC) was applied to all the nodes at the plane (as shown in Figure 3). These resulted to a single node at the middle of the plane and a firm beam was designed by connecting the node at the middle of the plane to the other node on the plane. This made is easier to apply a bending moment on the plane through the node at the center, Internal pressure and axial tension stress were applied also applied to the right plane end of the elbow pipe (Jian et. al. 2014).

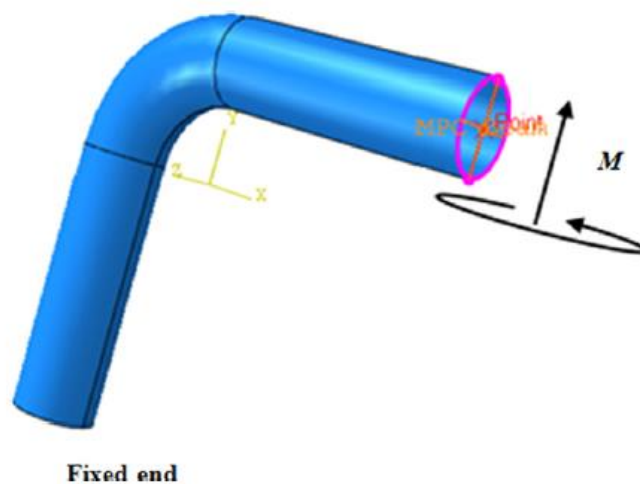


Figure 2.6: Finite element model with boundary conditions (Jian et. al. 2014).

Their research revealed through normalized methods that the relative thickness of the pipe bend ( $r/t$ ) is the major factor influencing bending moment limits. It was also found that yield strain has significant effect on limit load when considering large displacement is considered. This literature provided clarity on the minimum ratio of the Length of the attached straight Pipe ( $L$ ) to the radius of the elbow pipe ( $r$ ) that will negate the end effect on the limiting load. This same approach was used in the present study.

#### 2.5.4 Andrew Robertson, Hongjun Li and Donald Mackenzie (2005)

Robertson et. al. worked on plastic collapse of pipe bends under combined internal pressure and in-plane bending (Andrew et. al. 2005).

This study made use of ANSYS code to model three (3) piping systems with 90°elbow bend and attached with straight pipe at each ends of the bend, the straight pipes were terminated with rigid flanges, this is as shown in Figure 4. The chosen length of the straight pipe was to ensure that the response of the bend to applied load was not influenced by the stiff flanges at pipes

end. This condition was proven to have been met for all the three piping system considered when  $L > 10r$  through a sensitivity analysis conducted.

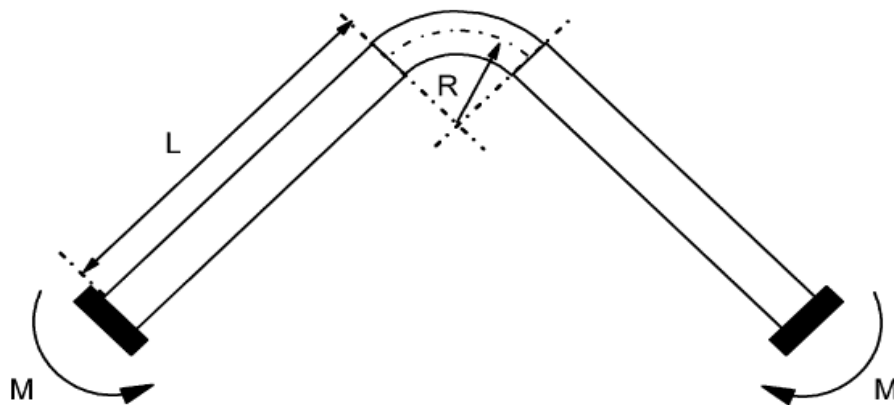


Figure 2.7: Pipe bend attached to two straight runs subject to in-plane bending (Andrew et. al. 2005).

This study considered three load cases; proportional loading, successive pressure–moment loading and successive moment–pressure loading (Andrew et. al. 2005). The outcome of the study reveals that results show that hypothetical limit analysis is not conventional for all the blends of loading considered. It equally revealed that analytical plastic load is reliant on the criteria of the collapse considered. The effect of significant deformation is better accounted for through plastic variability load. It was also observed that the comparative and pressure–moment load cases displays reasonable geometric strengthening, while on the other hand, moment–pressure load case displays reasonable geometric weakening.

#### 2.5.5 Sumesh S, AR. Veerappan, S Shanmugam (2017).

Sumesh et. al. worked on the Structural Deformations on Critical Cracked Pressurised Pipe Bends: Implication on the Von mises Stresses (Sumesh et. al. 2017).

This study used ABAQUS code to perform the FEA of elbow pipe with distorted configuration and having acute circumferential cracks through its wall and the limit analysis considered. Also, the length of the straight pipe (L) attached to the elbow pipe was chosen to be 10 times the radius of the pipe, that means  $L=10r$ . The research focuses on mainly circumferential cracks through the wall and it's crucial effect on pipe bends and collapse moment when compared with axial and surface cracks. The study assumes the crack to be located at in the elbow centre by the extrados. The comparative lengths of crack proportional to crack threshold angles were also examined.

The research provided the variation in Von mises stresses gotten along the bends of elbows with through wall critical cracks under internal pressure as a result of configuration anomalies.

The study considered two extremely cracked 90° elbow pipe models with pipe ratios of 5 and 10, have bend ratios of 2 and 3 for the 3D FEA. The outcome of the FEA shows a disparity in stress observed in the intrados, crown, extrados and crack tip area, this was attributed to the effect of bend radius and ovality (Sumesh et. al. 2017).

**Table 2.1: Summary of research on Functionally Graded Materials**

Researcher	Load Case	Type of Specimen	Mode of Analysis	Description
Gu and Asaro (1996)	Stress intensity factor	an isotropic and FGM strip.	Orthotropy rescaling and analytical solution	Studied the relationship between driving force, the energy release rate and toughness of the material and direction of crack propagation.
Reddy (2000)	shear deformation	Functionally graded rectangular plate	third-order shear deformation plate theory	analyzed the static behavior of functionally graded rectangular plates
Nakamura, T et. al 2000	indented Load	Functionally graded rectangular plate	Inverse Analysis and Kalman filter technique	Determination of properties of Graded Materials by Inverse Analysis and Instrumented Indentation
Cheng and Batra (2000)	three-dimensional elastic deformations	thermos-functionally graded elliptic	asymptotic expansion	
Jackson (2000)		FGM Object	Representation Method	The study establishes a clear separation between design of FGM objects, their processing, and their fabrication
Reddy and Cheng (2001)	three-dimensional elastic deformations	thermos-functionally graded rectangular plate	asymptotic expansion	
J.H. Kim and G.H. Paulino (2002)	Fracture analysis	FGM	Numerical Techniques	Investigated the effects of boundary conditions, material properties and crack tip mesh generation
Vel and Batra (2002,2003a, 2003b)	steady-state and quasi-static transient thermos-elastic	Functionally graded thick plate	Power series	steady-state and transient thermos-elastic response of functionally graded plates
Swaminathan, K. et. al 2014	Static and Dynamic	Functionally graded material	Both analytical and numerical methods	The research presents a comprehensive review of the various methods employed to study the static, dynamic and stability behavior of Functionally Graded Material (FGM) plates
Qian and Batra (2004)	steady-state and quasi-static transient thermos-elastic	Functionally graded thick plate	meshless local Petrov-Galerkin method	steady-state and transient thermos-elastic response of functionally graded plates
Setoodeh, A. R & Afrahim, S. 2014		Functionally Graded Pipe	Euler–Bernoulli model, Von Karman and Galerkin method	this research presents an analytical solution for the size dependent nonlinear vibration behavior of micro-pipes conveying fluid made of functionally graded materials'
Dağ et al. (2004)	Bending and stress intensity factor	graded orthotropic coating	Analytical and Finite element method	studied on the effects of material gradation on fracture mechanics parameters for cracks lying along the interface
Hiroyuki Matsunaga, 2008	thermal and mechanical loading conditions	Plates	two-dimensional (2D) higher-order deformation theory	Stress analysis of functionally graded plates subjected to thermal and mechanical loadings. Composite Structures
Hoang V. T. and Nguyen D. D., 2010	Compressive, thermal and combined loads.	functionally graded plates	Galerkin procedure	Analytical approach to investigate the stability of functionally graded plates under in-plane compressive, thermal and combined loads.
Alibeigloo, A., 2010	thermo-mechanical load	functionally graded (FG) rectangular plates	Fourier series and state-space method	Response of functionally graded (FG) rectangular plates with simply supported edges subjected to thermo-mechanical loads using three-dimensional thermo-elastic analysis.
Golmakani, M. E & Kadkhodayan, M. 2011	thermo-mechanical load	Functionally Graded Plates	first-order shear deformation plate theory (FSDT) and large deflection von Karman equations	Large deflection analysis of shear deformable functionally graded plates subjected to thermo-mechanical loads and under various boundary conditions
Singha M. K et. al. 2011	Transverse load	Functionally graded plate	Finite element procedure and Newton–Raphson iteration technique	Nonlinear behaviors of functionally graded material (FGM) plates under transverse distributed load are investigated using a high precision plate bending finite element
Ismail Mechab et. al 2012		Functionally graded plate	Four-variable refined plate theory	analytical solutions of static and dynamic analysis of functionally graded plates using Four-variable refined plate theory

Fallah, F. and Nosier, A., 2012.	asymmetric transverse loading and heat conduction	Functionally Graded (FG) circular plates	A two parameter perturbation technique, in conjunction with Fourier series	Nonlinear behavior of functionally graded circular plates with various boundary supports under asymmetric thermo-mechanical loading. Composite Structures
Sandeep Abotula et. al. 2012	Thermo-Mechanical Loading	FGM	Asymptotic analysis	Mixed-mode dynamic crack growth along an arbitrarily smoothly varying path in functionally graded materials (FGMs) under thermo-mechanical loading was studied.
Da-Guang Zhang, 2013	Thermal, Bucking and Bending	FGM Plates	physical neutral surface and high-order shear deformation theory	Modeling and Analysis of FGM rectangular plates based on physical neutral surface and high order shear deformation theory
Salehi, M. et. al 2013	rotating bending fatigue	functionally graded steel (FGS)	Vickers micro-hardness test and scanning electron microscopy (SEM)	Fatigue behavior of functionally graded steel produced by electro-slag re-melting.
Loc V. Tran et. al, 2013	static, dynamic and buckling	rectangular and circular plate (FGM)	Iso-geometric approach (IGA) and higher order deformation plate theory (HSDT)	Iso-geometric approach (IGA) and higher order deformation plate theory (HSDT) to study the behavior of functionally graded material (FGM) plates.
Bateni M, et. al 2013	thermal and mechanical loading conditions	Functionally Graded Rectangular Plate	multi-term Galerkin method and four-variable refined plate theory	A comprehensive study on stability of FGM plates
Shariyat M., Jafari R. 2013	Velocity impact analysis	Functionally graded plates		Researched on nonlinear low-velocity impact analysis of two directionally- graded circular plates under radial preloads
Won-Hong Lee et. al 2014	Bending Analysis	functionally graded material (FGM) plates	refined higher order shear and normal deformation theory	Refined higher order shear and normal deformation theory for E-, P-, and S-FGM plates on Pasternak elastic foundation
Zhong-Min Wang & Yan-Zhuang Liu, 2015	transverse vibration	Functionally Graded Pipes	Hamilton's principle	the research addressed problems related to the transverse vibration of pipe conveying fluid made of functionally graded material
Gagandeep Bhardwaj et. al, 2015	transverse and moment	functionally graded material (FGM) plates	extended iso-geometric analysis (XIGA)	Numerical simulation of functionally graded cracked plates using NURBS based XIGA under different loads and boundary conditions
Huu-Tai Thai & Seung-Eock Kim, 2015	mechanical and thermal	functionally graded plates and shells	theoretical models	A review of theories for the modeling and analysis of functionally graded plates and shells
Haizhu Pan , Tianshu Song and Zhihai Wang 2015		functionally graded material (FGM) plates	Numerical Techniques	Analyzed the influences of the non-homogeneity constants and geometric parameters on the stress intensity factors (SIFs)
Zhanqi Cheng et. al 2015	Mixed-mode loading	Functionally Graded Plate	peridynamic model	Peri-dynamic model for dynamic fracture in functionally graded materials.
Sator, L et. al 2016.	Transversal dynamic loading.	Thick/Thin Functionally Graded Plate	classical Kirchhoff–Love theory, 1st and 3rd order shear deformations plate theories	Transient analysis of homogeneous as well as FGM (functionally graded material) thin and/or thick plates subjected to transversal dynamic loading.
Tieliang Yang et. al 2016	Thermal environment	functionally graded materials (FGM) plates	Analytical Technique	Investigated Analytically the vibration and sound radiation characteristics of functionally graded materials (FGM) plates subjected to thermal environment

**Table 2.2: Summary of research on FGM using Finite Element Analysis on various loading conditions**

Researcher	Load Case	Type of Specimen	Mode of Analysis	Description
Praveen, G, N and Reddy, J. N. (1997)	Thermal Loading	functionally graded ceramic-metal plates	finite element	Investigated the response of functionally graded ceramic-metal plates using finite element that accounts for the transverse shear strains, rotary inertia and moderately large rotations in the von Karman sense.
Yildirim and Erdoğan (2004)	Fracture and thermal analysis	FGM Coatings	Finite Element Method	Studied to determine the effect of temperature dependence of the material properties.
Yildirim et al. (2005).	mechanical and transient thermal loads		Finite Element Method	Compared the SIF of FGM and that of homogeneous ceramics coating
L. Banks-Sills et al. (2005)	Linear Elastic Fracture	anisotropic and monoclinic material	Finite Element Method	Derived stress intensity factors for various problems by employing Displacement Extrapolation, M-Integral and J-Integral methods.
R. Afshar , M. Bayat, R.K. Lalwani and Y.H. Yau , 2010	Mechanical	Glass-like (viscoelastic) functionally graded cylinder	Finite Element Method	Investigated the elastic behavior of glass-like functionally graded infinite hollow cylinder under hydrostatic loads using finite element method
Hosseini, S. S. et. al 2012	mechanical and steady state thermal loading	isotropic and orthotropic functionally graded materials (FGMs)	extended finite element method (XFEM)	Thermo-mechanical XFEM crack propagation analysis of functionally graded materials.
Malekzadeh,P & Monajjemzadeh S.M 2012	Thermal Loading	Functionally graded plate	finite element method (FEM) with Newmark's time integration scheme	Investigated the dynamic response of functionally graded (FG) plates in thermal environment under a moving load
Malekzadeh,P & Shojaee, S. A 2012	Thermal Loading	Functionally graded plate	three-dimensional finite element method (FEM)	Investigated the dynamic response of functionally graded (FG) plates under a moving heat source
Woo-Young Jung and Sung-Cheon Han 2013.	Vibration Analysis	functionally graded material (FGM) and laminated composite structures	finite element, based on a first-order shear deformation theory	Transient analysis of FGM and laminated composite structures using a refined 8-node ANS shell element
Asemi et.al. (2013).	three dimensional static analyses	Functionally graded plate	Finite Element Method	Studied the effects of power law exponents on static behavior of a fully clamped 2D-FGM plate
Navid Valizadeh et. at, 2013	Static bending, mechanical and thermal buckling, linear free flexural vibration and supersonic flutter	Functionally graded material (FGM) plates.	based iso-geometric finite element method	NURBS-based finite element analysis of functionally graded plates: Static bending, vibration, buckling and flutter
Uysal (2013)	mechanical and thermal loads	Metal-ceramics FGM Plates	FEA Using Abaqus	research explored analysis of FGM flat plates and shell panels, and their applications to structural problems
Bhattacharya, S. et. al 2013	Cyclic Thermal Loading	Functionally graded plates	XFEM	The fatigue lives of aluminum alloy, FGM and an equivalent composite plates are evaluated using Paris law in the presence of multiple discontinuities, and are compared with each other
Nguyen-Xuan, H. et. al, 2014	static, free vibration and buckling analysis	Functionally graded plates	Iso-geometric finite element analysis (IGA) with a refined plate theory (RPT)	Iso-geometric finite element analysis (IGA) with a refined plate theory (RPT) for static, free vibration and buckling analysis of functionally graded material (FGM) plates
Kamran Asemi, Manouchehr Salehi and Mehdi Akhlaghi, 2014	Thermal Loading	an axisymmetric thick truncated cone made of functionally graded materials	Finite Element Method	Transient thermal stresses in functionally graded thick truncated cones by graded finite element method.



**Table 2.3: Summary of FGM Literatures reviewed on material composition**

S/N	PAPERS REVIEWED	METALS	CERAMICS	FGM PRODUCTION METHOD	FGM PROPERTIES	OBSERVATIONS
1	Douglas E. Burkes and John J. Moore (2006)	Nickel Titanium alloy (Nitinol)	Titanium Carbide	Combustion synthesis (CS) reaction utilizing the propagating mode (SHS)	1 Unique superplastic 2 Shape memory capabilities 3 High hardness, wear and corrosion resistance	1 Minor NiTi2 and NiTi3 Produced 2 Hardness reduces with increase in Nitinol.
2	N. H. Faisal et al. (2017)	Nickel Titanium alloy (Nitinol)	Titanium Nitrite	Not Provided	1 Quasi-elasticity and shape memory behavior. 2 Tribological and anti-corrosion properties	Localized indentation stress, film failure, and pseudo-elasticity is dependent on the shape of the indenter
3	Xing-Hong Zhang et al. 2000	Nickel	Titanium Carbide	Simultaneous combustion fusion and hot compaction	Maximum fracture toughness was found to be with FGM Combination of TiC-30 wt% Ni material	1 FGM properties mainly dependent on Nickel content 2 Properties get to its peak values of density, flexural strength and hardness at standard temperature
4	In-Jin Shon and Zuhair A. Munir (2005)	Copper	Titanium Carbide	Electro thermal combustion (ETC) method	Not Provided	Titanium carbide synthesized through ETC showed minimal porosity as compared to those synthesized by ordinary ignition
5	Zhaohui Zhang et al. (2012)	Titanium	Titanium Boride	sintering procedure that uses spark plasma with the aid of graphite die	1 Fine and dense microstructure that is continuous and free from crack at the interfaces 2 Bending strength and the fracture toughness are high	steady graded temperature field can be achieved while utilizing the Spark Plasma Sintering (SPS) process
6	Yoshimi Watanabe et al. (2009)	1 Copper 2 Aluminum	1 Silicon Carbide (SiC) Titanium Oxide (TiO2)	Centrifugal Mixed-Powder Method	Not Provide	Improved hardness on the surface of the Al/TiO2 FGM as a result of TiO2 nano-particles.
7	Clémentine Madeca et al. (2017)	Titanium (Ti)	Alumina (AL2O3)	Spark plasma sintering	1 High toughness and hardness 2 Resistant to crack than pure Alumina	FGM has invariably absent ductile property, which was attributed to the formation of oxides and carbides from the sintered FGM materials
8	Sabine Decker & Lutz Krüger (2016)	High-alloy metastable austenitic steels (CrMnNi steel)	Magnesia Partially Stabilized Zirconia (Mg-PSZ)	Asymmetric Spark Plasma Sintering (SPS)	Reduced the initiation of cracks	Temperature difference between the two constituent makes it had to densify the FGM Part
9	Yongjin Wang et al. (2015)	9Cr18 steel	Not Provided	Thixoforging Process	Exhibited high wear resistant	1 Thixotropic sample performance was influenced by deformation time at low strain rate 2 Thixotropic process reduce barrier and acute distortion associated with the formation of FGM structure
10	Muhammad Akmal et al. (2015)	stainless steel (316L)	hydroxyapatite (HA)	Sintering and compaction	Increased the hardness	1 FGMs with nano-sized HA (nHA) shows improved densification as compared to the the FGMs with micro-sized HA (mHA) 2 Chromium was seen to be diffusing through the 316L and HA interfaces
11	Lourdes D. Bobbio et al. (2018)	304L stainless steel	Titanium alloy (Ti-6Al-4V)	Additive manufacturing technique	Not Provided	Cracks observed was due to the creation of brittle $\delta$ -Fe-Ti-6Al-4V
12	J.A. Escribano et al. (2014)	stainless steel	Titanium carbon-nitride Ti(C,N)	Colloidal processing	1 Fine and dense microstructure that is continuous and free from crack at the interfaces 2 Bending strength and the fracture toughness are high	1 The fabrication process can be used for FGM micro-architectures that are complex 2 Fabrication process good for processing of fine powders that has lower flow ability and compressibility.
13	Justyna Zygmuntowicz et al. (2016)	Nickel	Aluminium Oxide	centrifugal-slip casting method	Not provided	Nickel particles effectively spread in a gradient path of the FGM.
14	John J. Moore (2006)	Nickel Titanium alloy (Nitinol, NiTi)	Titanium Carbide (TiCx)	Combustion Synthesis	1 Extremely elastic and shape memory capabilities 2 Extreme hardness, corrosion and wear resistance	1 Cooling rate, burning velocity and combustion temperature at each layer of the FGM declined with increasing Nitinol content. 2 Presence of blowholes were in the FGM layer with high Nitinol content.

15	Muhammad Ihsan Abdul Latiff et al. (2014)	Nickel	Alumina Plate	Sintering process	Not Provided	Sintering temperature has no influence on the sintering behaviors of the FGM, inclusive of its radial dimensions and microstructures
16	Liping Wang et al. (2006)	Nickel-Cobalt alloy (Ni-Co)	Cobalt-oxide (Wurtzite, CoO)	Electro-deposition and subsequent cyclic thermal oxidation and quenching	1 Superior corrosion resistance in solutions of NaCl and NaOH. 2 Exhibited extraordinary improvement of wear resistance and dry self-lubricating performance	Nickel-Cobalt alloy gradient deposits show graded structure alteration from face-centred cubic to hexagonal close packed
17	E, Yarraparredy et al. (2006)	Nickel	Tungsten Carbide	Laser Based Direct Metal Deposition (LBDMD) Process	High erosion resistance	1 LBDMD process can effectively use to fabricate FGM's that are defect free 2 FGM's erosion resistance is better than that of Nickel-Tungsten alloy and that of Steel (grade 4140)
18	XinXing Ma et al. (2018)	Copper	Tungsten*	Intensified electrical current influence and density that is quite high	1- Macro-hardness of the FGM rises in a gradual manner for the surface at the inner layer to the core layer. 2-Thermal conductivity of the FGM decreases as the temperature increases	1-Technique is highly adequate for the W/Cu FGMs fabrication 2- FGM fabricated at higher temperature and over a long period of time has tendency to absorb higher copper content
19	Wilfredo Montealegre Rubio (2012)	copper (Cu)	Nickel (Ni)*	Sintering technique with the aid of spark plasma.	Not Provided	Resonance frequency results of the simulated solution and the experimental solution were almost same.
20	Yun-Han Ling et al. (2002)	Copper (Cu)	Silicon Carbide (SiC)	Sintering Process under extremely high pressure	Fatigue cracks was observed on the FGM's surface at about 300 cyclic impacts	1- FGM has lower CD4 production as compared SMF800 nuclear graphite 2- Minor impairment was observed on the FGM's surface after in situ plasma irradiation.
21	Guoqiang Luo et al. (2014)	Copper	Tungsten*	Non-aqueous tape-casting method in combination with the space hot-pressing sintering technique	1- Increases in the FGM's electrical and thermal conductivity as compared to that of standardized composite.	Smooth and Parallel FGM's boundaries
22	Takahiro Kunimine et al. (2014).	Copper	Diamond*	centrifugal sintered-casting methods	Not Provided	FGM was successfully fabricated with the proposed technique in improved conditions
23	Mustafa Ubeyli et al. (2014)	Aluminum Alloy (AA) 7075	Silicon Carbide (SiC)	powder metallurgy	High strength	1-Major cracks at the macro-level 2-Micro-cracks were observed in the samples in region near to the deformation zone
24	El-Galy, I. H. et al. (2017)	Aluminium (Al)	Silicon Carbide Particles (SiCp)	centrifugal casting	1- Higher hardness value at the outer zone as compared to the inner zones. 2-Hardness value increased with increase in SiCp weight fraction	1-Tensile strength of the FGM was found to be related to Silicon Carbide Particle percentage increase. 2-Wear resistance not related to Silicon Carbide Particle percentage increase
25	Fatih Erdemir et al. (2015)	Aluminium alloy (Al2024)	Silicon Carbide (SiC)	hot pressing and consolidation technique	1-Good corrosion resistance 2-Lower wear rate	The FGM's main wear mechanisms were identified as abrasive and adhesive wear mechanisms
26	R. Rodriguez-Castro et al. (2002)	Aluminium alloy (Al-A359)	Silicon Carbide Particles (SiCp)	centrifugal casting	Not Provided	1-Increase in tensile and yield strength of the FGM as the volume fraction of SiC particle increases between 0.20–0.30 2-deduction in tensile and yield strength was observed within SiC concentration of 0.30–0.40 3-Rate of crack propagation is inversely proportional to SiC content.
27	Jayakumar, E et al. (2016)	Aluminum (A319)	Silicon Carbide Particles (SiCp)	Centrifugal Casting Technique	Relatively high hardness	1-Higher hardness value (94.4 HRB) was obtained at the zone that is rich in SiC particles. 2-Resistance to wear was

observed at the FGMMC particle-rich zone

**Table 2.4: Summary of Literatures reviewed on Finite Element Analysis of Bend Pipes under various loading conditions.**

S/N	Papers Reviewed	Material Used	Loading Condition	FE Tool used	Pipe bend configurations considered	Observations
1	Christo Michael T. et. al. (2012)	Stainless Steel	Combination of in-plane closing bending and an internal pressure,	ABAQUS Version 6.9.	90° Pipe bend only	1-The effect of thinning on limit and failure moments are negligible. 2-Ovality plays significant role in both limit and failure loads determination.
2	Shun-Jie Li et. al (2017).	Not stated but has Young's Modulus of $2 \times 10^5$ MPa	Internal pressure, torsion moment, in-Plane bending moment and out-of-plane moment.	ABAQUS	Considered pipe bend with angle of 30°, 60°, 90°, 120°, 150° and 180	1- bend angle has higher effect between 0°~120° when subjected to internal pressure, in-plane bending moment and torsion moment, and at angles between 0°~90° under out-of-plane moment
3	Yun-Jae Ki and Chang-Sik Oh (2007)	Not stated	Internal Pressure and in-plane bending	ABAQUS Version 6.2-1	90° Pipe bend with variation of attached straight pipe length	1-The effect of the length of the attached straight pipe on plastic limit loads is significant. 2-Load limits tend to reduce with reduction in the length of the attached straight pipe.
4	Jian Li et. al. (2014)	Not stated but has Young's modulus of 210,000MPa	Internal pressure and out-of-plane bending	ABAQUS Version 6.9.	90° Pipe bend only	1-The relative thickness of the pipe bend ( $r/t$ ) is the major factor influencing bending moment limits. 2-It was also found that yield strain has significant effect on limit load when considering large displacement
5	Andrew Robertson, Hongjun Li and Donald Mackenzie (2005)	Not stated but has Elastic Modulus of 200 GN/m <sup>2</sup> ,	Internal pressure and in-plane closing moment)	ANSYS V6.1 & V7.1	90° Pipe bend only, with sensitivity analysis on the length of attached straight pipe	1-The hypothetical limit analysis is not conventional for all the blends of loading considered. 2-The analytical plastic load is reliant on the criteria of the collapse considered.
6	Jian Li et. al. (2015)	Not stated but has Young's Modulus of 200GPa	Torsion moment and in-Plane bending	ABAQUS	90° Pipe bend only	1-The major factor affecting the limit load is $r/t$ . 2-Plastic load limits is not affected by loading path and material constants. 3-The Results show that the estimate from circular interaction is very vital for elbow pipe analysis subjected to both torsion and bending moment.
7	Sumesh S. et. al. (2017)	Stainless steel	Internal Pressure and Axial Tension	ABAQUS Version 6.10	90° Pipe bend only	Analysis shows disparity in stress observed in the intrados, crown, extrados and crack tip area, this was attributed to the effect of bend radius and ovality.

## 2.6 CONCLUDING REMARKS

There have been numerous researches on Functionally Graded Materials (FGM) of various configurations ranging from; Plates, Shell, Cylinder, Cone etc. subjected to different forms of loading as stated in the above reviews. The research was tailored towards understanding the behavior of FGM under various loading conditions.

From the above review, it clearly shows that there is currently no research on FGM that is tailored towards developing an FGM piping structure that is aimed at deploying the FGM to proffer solution to any operational challenges being faced with the Oil and Gas Industry. In addition, the out of some of the reviewed literatures provided an informed steer on how to proceed with some of the challenges faced in the present study.

Firstly, the literature reviewed on FGM material combinations provided good understanding on the material combinations that have been deployed for the FGM fabrications, it equally sheds light on the available FGM fabrication technologies with all their advantages and drawbacks.

Secondly, the literatures reviewed on FEA of elbow pipes revealed that there are limited researches on elbow FGM pipes. However, the review guided the approach used to model the FGM elbow pipe in the present research. This guidance is not limited to end effect of the attached straight pipe on elbow pipe limiting load and clarity on multi-point constraint (MPC) application on Abaqus.

Lastly, the reviewed literatures on straight FGM FEA provided clarity in the present research on issues around material gradation of FGM, determination of FGM material variation through the non-homogeneity factor and the power law application to derive FGM material properties through the thickness.

On the same note, the present research explored the unique characteristics of the FGM to proffer solution to the challenges being faced with the piping system of deep offshore operations of the oil and gas industry, particularly the Gulf of Guinea and examined the possibility of utilizing different pipe configurations for these services in the oil and gas industry. To achieve this, the research modelled a Straight, Elbow and T-Piece Pipe configurations and subjected it to Thermal and Mechanical loading. This provided better appreciation of the different FGM pipe configurations' behavior and possibility of their usage for various services in the nearest future.

To achieve this, the study considered into the vast Engineering Material availability and properties with the aid of the CES EduPark Software so as to determine the candidate materials

that will be suitable for the proposed FGM combination. All these are as detailed in the succeeding chapter.

## CHAPTER 3: MATERIAL SELECTION

### 3.1. INTRODUCTION

The most significant reason for Facilities Degradation and equipment failure in the oil and gas industry is largely attributed to corrosion. The selection of materials that are completely resistant to all corrosive agents (process fluid) is possible for most applications; however the drawback is the associated cost of such approach. Hence, in practice, cost effective materials of known corrosion rates are selected, provision is mostly made through the material thickness to compensate for the gradual effect of corrosion over the life of the material. It is equally vital not to neglect the effect of atmospheric corrosion when selecting materials, as it often leads to many instances of facilities failure and at times does greater damage to facilities than the internal corrosion. Consequently, all facets of corrosion traits must be addressed, from both project and operation phase of the facilities.

Corrosion in oil and gas industry is mostly to be propagated only in the liquid phase (water and sour crude), the oil phase (if sweet crude) is been considered not to be corrosive. Hence, it is necessary for water to be present for corrosion to be propagated; this means water vapor with temperature above dew point is not corrosive in behavior (Alireza, 2014).

Furthermore, in a three phase flow (oil, gas and water), for corrosion to propagate there must be evidence of the materials been wetted by water. This invariable means that if water in a three phase flow is trapped by the oil, it is most likely that corrosion will not be propagated.

The main factors controlling corrosion in the oil and gas industry are as follows [96]:

- CO<sub>2</sub> partial pressure
- H<sub>2</sub>S partial pressure
- Fluid temperature
- Water salinity
- Water cut
- Fluidynamics
- PH.

Engineers in the 21<sup>st</sup> century are exposed wide ranges of materials that will enable them meet all challenges that are corrosion related.

In addition to the advent of newer and improved materials such as GFRP, FGM, etc., there have been giant stride in materials processing and advanced techniques for molding ceramics,

polymers, and composites. The technique for material selection in recent time has greatly improved due to the availability of the required knowledge of materials that enable them to be used more efficiently and effectively to reduce cost. Unlike in early days were material selection was basically a trial and error process. This chapter, therefore, focuses mainly on the material selection for a Functionally Graded Materials Pipe for the oil and gas application.

A functionally graded material (FGM) is a newly improved material which is characterized by stepwise variation of microstructure and composition of the material over a volume of the component. This gradual variation results in varying of material properties in special coordinates through the thickness of the material. In an FGM, the variation of material properties through the volume of the component is mostly accomplished by the combination of metal and ceramic mixture, the mixing ratio varies from layer to layer in the material.

The main purpose of FGMs, such as metal ceramic FGMs, is to take advantage of different properties of metal and ceramic. In graded metal/ceramic components, incompatible properties like strength, toughness and machinability of metal are coupled with heat, wear and corrosion resistance of ceramic in a single part. The combination of these unique properties from each of the FGM constituent makes FGMs very applicable in various applications and to be tailored to specific applications were the conventional engineering material will not be suitable.

### **3.2. MATERIAL CLASSIFICATION AND RANKING**

Classification and ranking all available engineering material is vital to this study, which will ensure that the most suitable material combination is identified for the Functional Graded Material that will meet the required need as detailed in the Problem Definition Section of the study. The material selection and ranking process was achieved through the use of CES Edupack 2017 software.

The aim is to be able to rank and identify candidate materials, both metallic and ceramics that could be explored further on their possibility of been used in the proposed FGM solution. The first check on the candidate material is its ability to be deployed to the specified service condition.

The candidate material is required to possess the following properties from an industrial perspective for NNPC:

- Ability to withstand the operating temperature range of 0 to 150°C
- Withstand maximum operate pressure of 21BarG.
- Excellent Corrosion Resistance
- Excellent interaction with salt water.

- Readily available.
- Ability to be machined.
- Excellent tensile strength.
- Excellent Fracture Toughness
- Excellent specific stiffness due to offshore application.

### 3.2.1 Candidate Ceramic Materials

The ceramic material to be considered for the FGM must have properties that are compatible with that of the ideal candidate material for the FGM as highlighted above. To achieve this, a hypothetical technical ceramics material was created having properties that are required for the service condition as proposed in the FGM solution. Properties considered in developing the hypothetical materials are as highlighted above.

This was used as a benchmark to adequately select from the 326 technical ceramic materials that are on CES Edupack 2017 software.

Specific stiffness of the material is vital as it determines the total weight of the pipe on the offshore facilities where the proposed design is intended to be deployed, offshore operations has weight constraints hence ceramics material with high specific stiffness will be ideal for the FGM material. A test of this property on all technical ceramics in the software reveals that only 126 technical ceramics materials met the minimum criteria set for specific stiffness of above  $0.11\text{GPa}/(\text{kg}/\text{m}^3)$  and that of the hypothetical ceramics. This is as shown in the table 3.1 below:

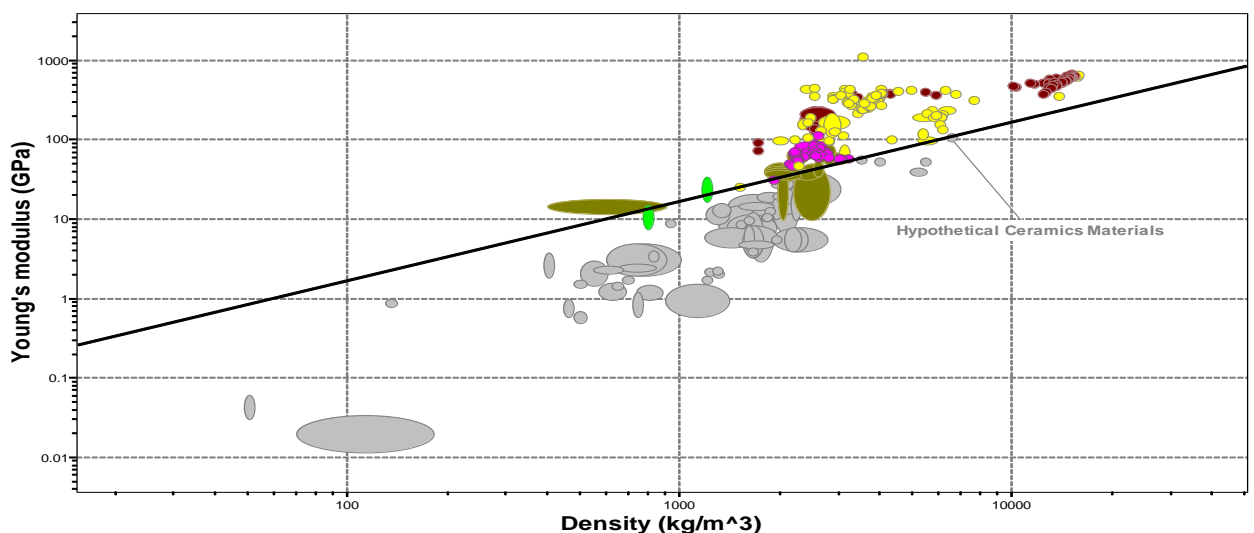


**Figure 3.1: Comparison of Specific Stiffness of Ceramic Materials with reference to the Hypothetical Material.**



As stated in the problem definition, one of the main challenges with the existing solution deployed is the high rate of crack propagation. Therefore, to mitigate against this identified challenge, ceramics material with high fracture toughness will be recommended as a candidate material for the FGM. Fracture toughness is a property that defines material ability to withstand fracture, it is actually one the most important properties that is considered for many design applications. Hence, the fracture toughness of the 126 ceramics materials that passed the initial test was compared concurrently with the cost per unit volume of each of the materials. This approach will guide in identifying materials with high fracture toughness as well as the cost and benefit derived from the materials.

The chart below shows that only 53 of the 126 met the minimum criteria required when the fracture toughness ( $1.25\text{MPa}\cdot\text{m}^{0.5}$  minimum was used) was compared with the cost per unit weight of the materials (Considered only cost below 70USD/Kg). They are broadly classified into the ranges of the following:

*Alumina, Aluminium-nitrate, Beryllia, Boron Carbide, Molybdenum, Sialons, Silicon-carbide, Silicon-nitride, Titanium-carbide, Titanium-diboride, Titanium-dioxide, Tungsten-carbide, Zirconia, Zirconium-carbide*

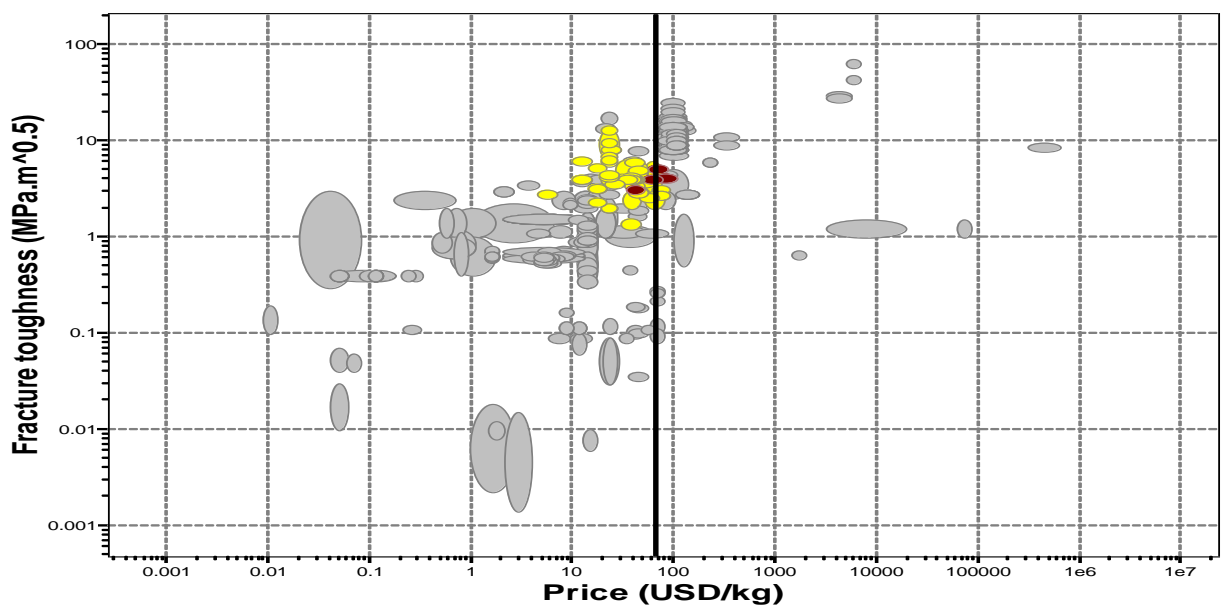


**Figure 3.2: Comparison of Fracture Toughness with Unit Price of identified Ceramic Materials.**

From the review of the literature, several FGM production technique has been deployed in the past for divers operations and applications, they includes; *Centrifugal Casting, Hot Pressing, Powder Metallurgy, Sintering Process, Laser Based Direct Deposit, Combustion Synthesis and Colloidal Processing*. The Sintering process of metals and ceramics was the

most common technique used in FGM fabrication as revealed from the literature review, this informed the decision to use the process as the basis for selecting the most appropriate ceramics to be used for the FGM considering the fact that the proposed FGM is a metal-ceramics FGM, the results from this evaluation shows that only *Alumina, Aluminum Nitrite, Boron Carbide, Silicon Carbide, Silicon Nitride, Tungsten Carbide and Zirconia* scaled through the test of the possibility of being fabricated as FGM through the conventional Sintering Process. Hence, the seven identified ceramics materials can potentially be used as candidate material for the proposed FGM.

The seven (7) identified ceramics materials were further streamlined into four (4) based on the availability of literatures that have used the materials in the past for FGM fabrication, this proves material availability and also demonstrates that the technology for fabricating the FGM's from the materials has been proven. The four identified ceramics materials were Silicon Carbide (HIP), Tungsten Carbide (Hot Press) Alumina and Zirconia (MgO stabilized). These were further ranked based on their suitability to be used for the proposed service condition. The ranking is as shown in the table 3.3 below.

**Table 3.3: Detailed attributes of candidate ceramics materials.**

	Price per unit volume (USD/Kg)	Fracture toughness (Mpa. m <sup>0.5</sup> )	Fatigue strength at 10 <sup>7</sup> Cycles (Mpa)	Tensile strength (Mpa)	Salt water application	Fresh water application	Density Kg/m <sup>3</sup> )	Young Modulus (GPa)
Silicon Carbide (HIP)	17.6	3.25	439	500.5	3	3	3145	400
Tungsten Carbide (Hot Press)	23.85	8.2	309	352.5	4	4	15700	669
Alumina 94 (SGM)	5.6	6.2	219.5	250.5	2	2	3650	330
Zirconia (Transformation toughened) L	22.85	13	363	414	1	1	5740	246.5

### 3.2.2 Candidate Metallic Materials

The Metallic Material to be considered for the FGM must have properties that are compatible with that of the ideal candidate material for the FGM to be used in offshore oil and gas operations. To achieve this, a hypothetical technical metallic material was created having properties as required for the service condition proposed for the FGM. Properties considered for the hypothetical materials are as highlighted:

- Ability to withstand the operating temperature range of 0 to 150°C.

- Excellent Corrosion Resistance
- Excellent interaction with salt water.
- Readily available.
- Excellent tensile strength.
- Excellent specific stiffness due to offshore application
- Fatigue and tensile strength
- Excellent Fracture toughness

The Hypothetical material was used as a benchmark to adequately select from the 1832 Metallic materials that are on the database of CES Edupack 2017 software.

The role played by specific stiffness of the material is vital as it determine to total weight of the pipe on the offshore facilities, the constraint posed by weight in all deep offshore designs is key and worth considering. To mitigate against this, metallic materials with high specific stiffness (Above  $0.11 \text{GPa}/(\text{kg}/\text{m}^3)$ ) would be ideal for the FGM material. About 159 Metallic materials from the database closely met the minimum criteria set for specific stiffness and that of the hypothetical material. This is as shown in the table below:

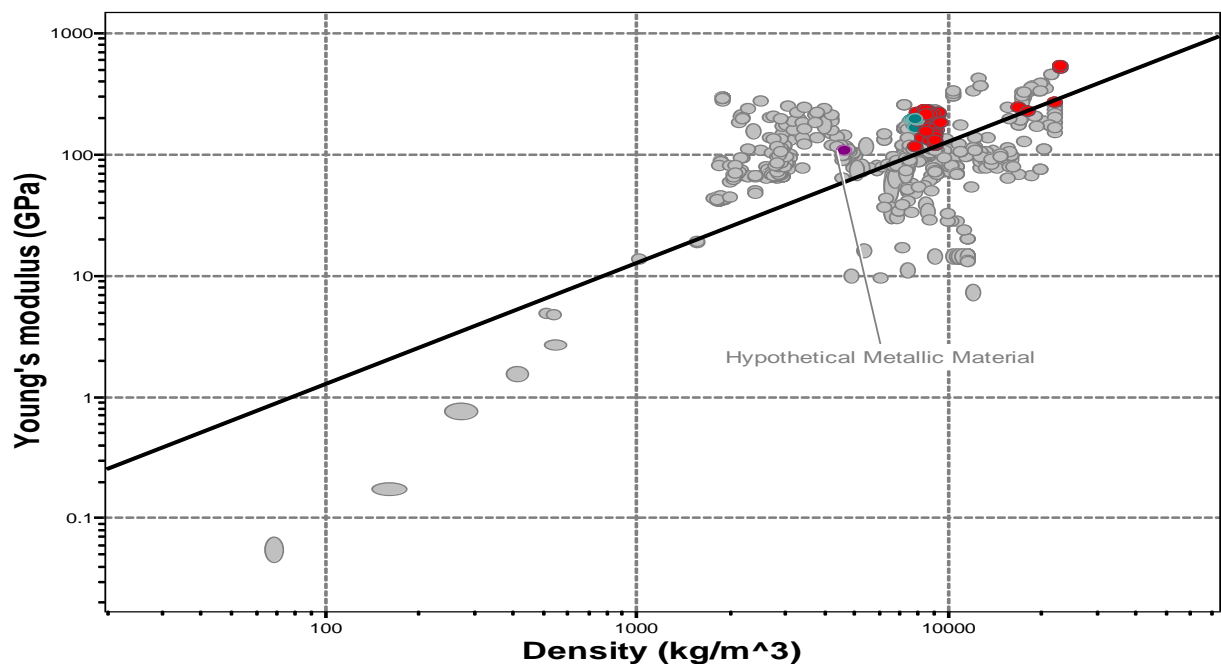


**Figure 3.3: Comparison of Specific Stiffness of Metals with reference to the Hypothetical Material.**

As stated in the problem definition, one of the main challenges with the existing solution deployed offshore is the high rate of crack propagation. Therefore, to mitigate against this identified challenge, metallic material with high fracture toughness property will be recommended as a candidate material for the FGM. To achieve this, the fracture toughness

of the 159 metallic materials that passed the initial test was compared with the cost per unit volume of each of the materials. This will guide in identifying materials with high fracture toughness as compared to the cost and benefit derived from the materials.

The chart below shows that only 111 of the 159 met the minimum criteria required for the fracture toughness ( $70\text{MPa}\cdot\text{m}^{0.5}$  minimum was used) and cost (Considered only cost below  $55\text{USD}/\text{Kg}$ ), they are broadly classified into the ranges of the following materials:

*Grades of Stainless Steel, Copper based alloys, Nickel based alloys, Chromium based alloys and Cobalts alloys.*

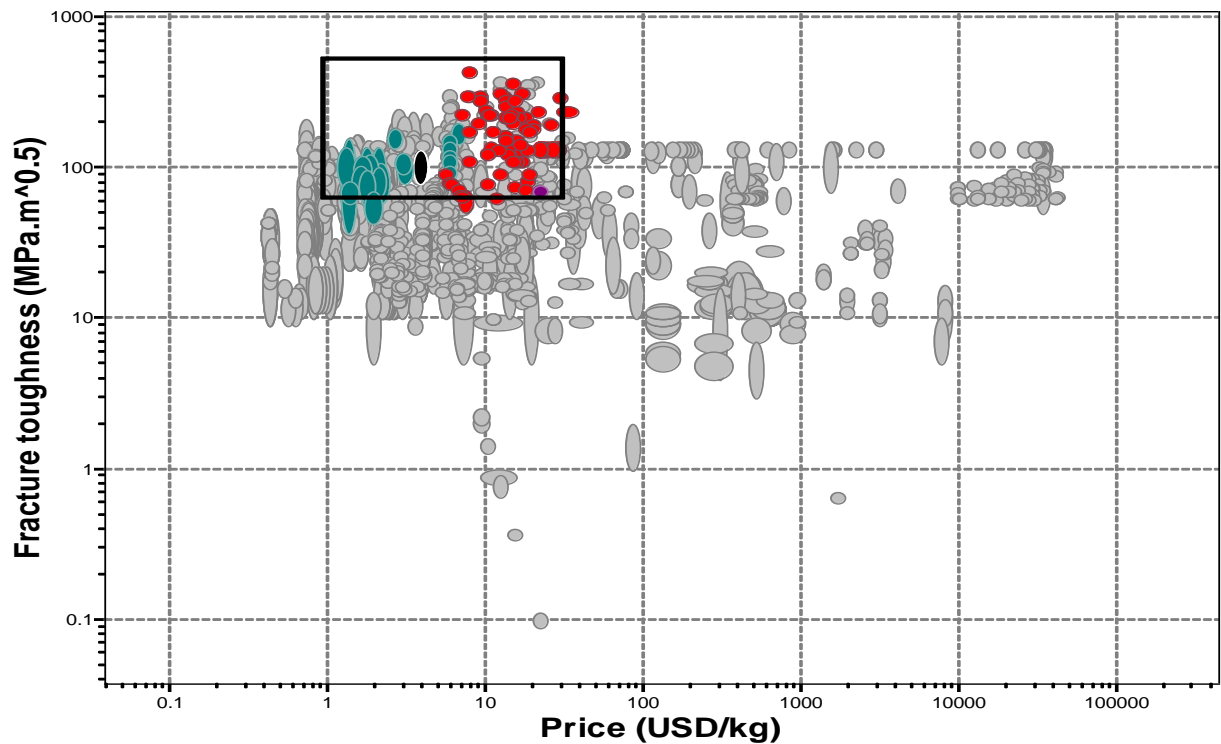


**Figure 3.4: Comparison of Fracture Toughness with Unit Price of identified Metals.**

The literatures review shows that the most widely deployed FGM production techniques are; *Centrifugal Casting, Hot Pressing, Powder Metallurgy, Sintering Process, Laser Based Direct Deposit, Combustion Synthesis and Colloidal Processing.* From the identified fabrication techniques, the sintering process of metal and ceramics was used as the basis for selecting the most appropriate metal to be used for the FGM considering the fact that the proposed FGM is a metal-ceramics FGM, the results from this evaluation reveals that only *Grades of Stainless Steel, Copper based alloys and Nickel based alloys* scaled through the test of identifying the possibility of being fabricated as through the conventional FGM fabrication process, that is the Sintering Process. Hence, the three identified metallic materials can potentially be used as candidate material for the proposed FGM.

The three identified possible candidate metallic materials have all been used as materials for FGM fabrication in the past, this is as proven from the review of available literatures. This gives comfort on material availability and availability of technology for fabricating the FGM using the materials; hence the three identified metallic materials will be ranked in terms of their suitability for the proposed service operation. This is as shown in the table below.

**Table 3.4: Detailed attributes of candidate Metals.**

	Price per unit volume (USD/Kg)	Fracture toughness (Mpa. m <sup>0.5</sup> )	Fatigue strength at 10 <sup>7</sup> Cycles (Mpa)	Tensile strength (Mpa)	Salt water application	Fresh water application	Density (Kg/m <sup>3</sup> )	Young Modulus (GPa)
Nickel-Fe-Cr alloy, INCOLOY 800, Annealed	7.72	434	212.5	620	3	3	195	7950
Stainless Steel, austenitic, ASTM CF-20 , cast, water quenched	2.655	158.5	274.5	530	2	2	195	7765
Copper C14200, Soft	5.46	92.75	105	220	1	1	122.5	8925

### 3.2.3 Ranking of Candidates Materials through MADM

The multiple attribute decision making (MADM) is a technique of problem solving that is specifically used to resolve complications in material selection from among a defined quantity of alternative materials. It provides details processes on the manner to which attribute of identified alternatives will be handled to give a desired choice of material. There are numerous techniques of MADM, this include, weighted product method(WPM), weighted sum method (WSM), analytic hierarchy process (AHP) technique for order preference by similarity to ideal solution (TOPSIS), ELECTRE, etc. The AHP and TOPSIS technique is the most widely applied for making decisions from wide ranges of alternatives. They are both decision making approaches that utilizes logic in arriving at a preferred choice from alternative sets of candidate materials that are defined in terms of their individual attributes (Victor & Larry, 2007).

AHP is used to arrive at the preferred candidate material and to equally rank the materials in terms of priorities. The AHP approach is an effective and malleable decision making technique that helps in setting priorities and make appropriate decision when considering both qualitative and quantitative features of a decision. It aids to reduce multifaceted choices to a sequences individual comparisons, AHP has the technique to provide strong justifications for all decisions made. This unique capability of AHP makes it the most regarded and extensively used decision-making technique (Rao & Davim, 2008).

### 3.2.3.1. Steps for the Proposed AHP Methodology.

The methodology to be utilized in ranking the candidate materials for the FGM, both Ceramics and Metals is based on the itemized attributes derived from the service condition the FGM will be deployed. The sequence of the Methodology is as shown below.

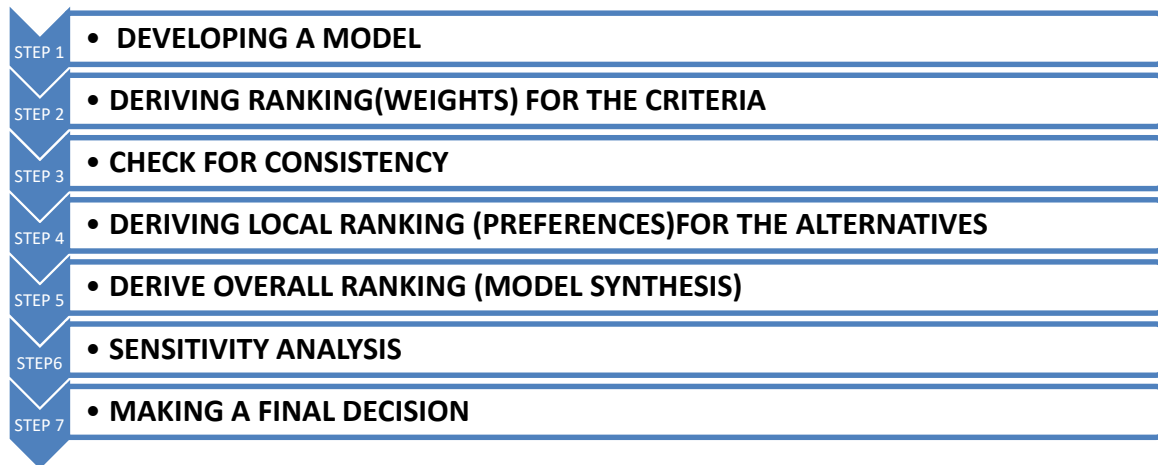


Fig. 3.5: AHP methodology for to be deployed for ranking all candidate materials (Mu & Pereyra-Rojas, 2017).

#### a) Model Development

This is the first step for an AHP analysis; it entails building of decision hierarchy which is also known as decision modeling. This simply involves the building of hierarchy to ease the analysis and decision making.

Analytic hierarchy process (AHP) technique is deployed when problem is structured as a hierarchy. Figure 3.6 demonstrates the hierarchy considered for the selection and ranking of candidate materials for the FGM. The first level in the hierarchy is our goal; this is to be able to select the most optimal metal and ceramics material for the FGM. The second level in the hierarchy constitutes our objective, these include the quantitative and qualitative requirements to be reviewed to enable the achievement of the goal as stated in the first hierarchy. The third level gives the classifications of the requirements as stated in level two, while the fourth level gives details of the criteria of all the classified requirements. These are the criteria to be used for comparing alternatives (Candidate Materials).

The AHP has the advantages hierarchical decomposition, this gives clearer and better understand of the problem and equally enables the precise achievement of decision based on the itemized criteria and the available alternatives to be evaluated.

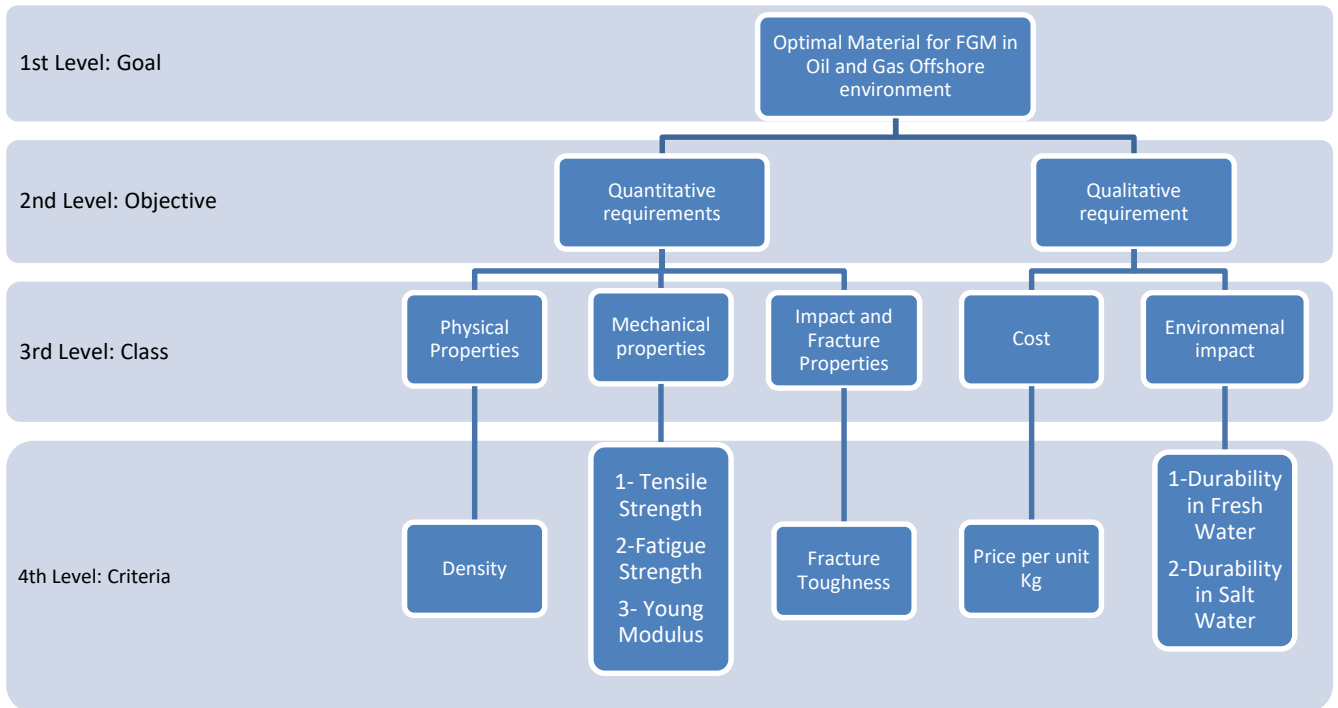


Fig 3.6: The hierarchy structure of performance criteria considered for the FGM materials selection problem.

### b) Deriving Ranking (Weights) for the Criteria

All itemized criteria in figure 3.6 will have different level of importance to the ultimate functionality of the materials selected for the FGM. Hence, a second step is required to guide in deriving the relative priorities (weights) for all the itemized criteria. It is term relative due to the fact that the criteria priorities obtained are measured against each other by means of comparison.

It can be assumed that when selecting materials for a particular service condition, all criteria to be considered in making the decision will not have equal importance. The subjectivity in assigning importance to the different criteria makes it necessary to first derive pairwise comparisons of the relative priority of each criterion with respect to each of the others (Mu & Pereyra-Rojas, 2017). The comparison was achieved using a numerical scale developed by Saaty (Saaty, 2012). This is as shown in Table 3.5

**Table 3.5: Saaty's pairwise comparison scale [101]**

Verbal Judgment	Numeric Value
	9
Extremely important	8
	7
Very Strongly more important	6
	5
Strongly more important	4
	3
Moderately more important	2
Equally important	1

To achieve this pairwise comparison, three tasks are involved:

- Developing a matrix for comparison at each level of the hierarchy starting from the second level and descending.
- Computing the relative weights of each element in the hierarchy.
- Checking the consistency of judgement through a continuous estimation of consistency ratio.

Elements are compared in sets with emphasis on their significance with each other on same level, this is further compared with an element in the preceding higher level. Starting with the top of the hierarchy and descending downward, these sets of comparisons at each level can be simplified to a number of square matrices  $A = [a_{ij}]_{n \times n}$  as shown in the subsequent equations (Navid, et. al. 2013):

$$\begin{bmatrix} a_{11} & a_{12} & \dots & a_{1n} \\ a_{21} & a_{22} & \dots & a_{2n} \\ \vdots & \vdots & \vdots & \vdots \\ a_{n1} & a_{n2} & \dots & a_{nn} \end{bmatrix} = \begin{bmatrix} a_{11} & a_{12} & \dots & a_{1n} \\ 1/a_{12} & 1/a_{22} & \dots & a_{1n} \\ \vdots & \vdots & \vdots & \vdots \\ 1/a_{1n} & 1/a_{2n} & \dots & a_{nn} \end{bmatrix} \quad 3.1$$

The reciprocal property of the matrix is represented as thus:

$$a_{ij} = \frac{1}{a_{ji}} \quad 3.2$$

As stated earlier, the Saaty's scale of relative importance of criteria from 1 to 9 is recommended for making subjective pair-wise comparisons (Table 3.8). After concluding with all sets of matrix comparison, Specific weights of vector  $w = (w_1, w_2, \dots, w_n)$  were computed (Victor & Larry, 2007). The weight computation involves two main steps. Firstly, the comparison of matrix sets,  $A = [a_{ij}]_{n \times n}$  this is normalized with Equation 3.3 and then secondly, the weights are computed using equation 3.4.

$$a_{ij}^* = \frac{a_{ij}}{\sum_{i=1}^n a_{ij}} \quad 3.3$$



For all  $j = 1, 2, \dots, n$

On the same note, weight is calculated as thus:

$$w_{ij} = \frac{\sum_{j=1}^n a_{ij}^*}{n} \quad 3.4$$

For all  $i = 1, 2, \dots, n$

Equation 3.5 gives the relationship between the weight of the vector  $w$ , and that of the comparison matrix set  $A$  that exists.

$$A \cdot w = \lambda_{max} \cdot w \quad 3.5$$

$\lambda_{max}$  Is an important parameter used for validation in AHP, it is equally used as referencing index to modify information by calculating the consistency ratio ( $CR$ ) of the vector estimate.

Calculating  $CR$  can be done by obtaining the consistency index ( $CI$ ) of each other  $n$  matrix from the equation 3.6 as shown:

$$CI = \frac{\lambda_{max} - n}{n - 1} \quad 3.6$$

Using equation 5,  $CR$  can be calculated as thus:

$$CR = \frac{CI}{RI} \quad 3.7$$

The random consistency index that can be obtained from a randomly generated pair-wise matrix comparison is called Random Inconsistency Index ( $RI$ ). This is as shown in table 3.9 below, the values of  $RI$  for 1 to 10 orders of matrices. The comparison is deemed acceptable if the values of  $CR < 0.1$ . However, if the values of  $CR \geq 0.1$ , it is an indication of judgement that is not consistent. Hence, the initially assumed values used for the pairwise comparison of the matrix  $A$  should be reevaluated and studied.

**Table 3.6: Random inconsistency indices (RI) for  $n = 10$ .**

N	1	2	3	4	5	6	7	8	9	10
RI	0	0	0.58	0.9	1.12	1.24	1.32	1.41	1.46	1.49

The total measure of all pair-wise comparisons of entities involve in the decision making by employing the geometric mean of each assessment as shown in equation 3.8:

$$a_{ij}^{hp} = \sqrt[Q]{\prod_{q=1}^Q a_{ij}^q} \quad 3.8$$

Given that  $a_{ij}^q$  is a constituent of matrix  $A$  with individual  $q(q = 1, 2, \dots, Q)$  and correspond to the geometric mean of all individuals  $a_{ij}^{hp}$ . The total  $CR$  for the group is computed with equations 3.6 and 3.7 [4].

Table 3.3 and 3.4 shows that all the itemized criteria have difference values, this can be inferred as different importance/priority to each contribution to the FGM in functioning appropriately as envisaged. To determine each criterion's priority, a pairwise comparison of all criteria was assessed by assigning value from the numeric scale as presented in Table 3.5. This portrays the relative preference (intensity judgement) from each of the compared pairs of criteria as informed by the basic requirements of the candidate material. This is as computed in table 3.7.

**Table 3.7: Pairwise comparison matrix with intensity judgments**

FGM Candidate Material Selection	Price per unit volume	Fracture toughness	Fatigue strength	Tensile strength	Salt /Fresh water application	Density	Young Modulus
Price per unit volume	1.00	0.25	2.00	2.00	0.20	3.00	0.50
Fracture toughness	5.00	1.00	7.00	4.00	0.20	6.00	2.00
Fatigue strength	0.25	0.14	1.00	0.50	0.11	0.50	0.20
Tensile strength	0.50	0.25	2.00	1.00	0.13	2.00	0.33
Salt/Fresh water application	5.00	2.00	9.00	8.00	1.00	8.00	4.00
Density	0.33	0.17	2.00	0.50	0.13	1.00	0.20
Young Modulus	2.00	0.50	5.00	3.00	0.25	4.00	1.00

Table 3.8 shows the results obtained when equations 1, 2, 3 and 4 are applied on the above matrix. The procedure followed as described earlier in this chapter is as follows; firstly, was to aggregate each of the cell in the matrix in table 3.7, this was followed with the normalization of the entire matrix. The normalized matrix was further weighted to arrive at the result is table 3.8.

From the results in Table 3.8, it is obvious that for the selection of FGM candidate material for offshore oil and gas service conditions as itemized in the criteria for the requirements, **durability** of material in Salt/Fresh Water application is the most important criterion (0.41) based on the intensity judgement made. This is followed by **fracture toughness** of the material (0.23), followed by **Young Modulus** (0.14), then material **Cost** (0.09), then subsequently **Tensile Strength** follows (0.06) and finally **Density** 0.04 , while **Fatigue Strength** had 0.03 in ranking.

The priorities of the criteria in Table 3.8 were not allocated arbitrarily but were established on empirical judgments guided by the basic attributes required from a material to function effectively in the proposed service condition. From Table 3.8, it can be interpreted that the criteria have the following priorities in descending order; 41%, 23%, 14%, 9%, 6%, 4% and 3% respectively..

**Table 3.8: Result presentation: original judgments and priorities**

FGM Candidate Material Selection	Price per unit volume	Fracture toughness	Fatigue strength	Tensile strength	Salt /Fresh water application	Density	Young Modulus	Priority
Price per unit volume	1.00	0.25	2.00	2.00	0.20	3.00	0.50	<b>0.09</b>
Fracture toughness	5.00	1.00	7.00	4.00	0.20	6.00	2.00	<b>0.23</b>
Fatigue strength	0.25	0.14	1.00	0.50	0.11	0.50	0.20	<b>0.03</b>
Tensile strength	0.50	0.25	2.00	1.00	0.13	2.00	0.33	<b>0.06</b>
Salt/Fresh water application	5.00	2.00	9.00	8.00	1.00	8.00	4.00	<b>0.41</b>
Density	0.33	0.17	2.00	0.50	0.13	1.00	0.20	<b>0.04</b>
Young Modulus	2.00	0.50	5.00	3.00	0.25	4.00	1.00	<b>0.14</b>

**c) Check for Consistency**

It is necessary to check that the decisions made in arriving at the priorities in section above are consistent. This is vital owing to the fact that the comparison made were pairwise, hence there will be need to ascertain the pairwise comparison results aligns with the results when a global comparison of all other criteria are perform with respect to each other. Some level of inconsistency is allowed in AHP since the assigned numeric values were derived from the individual’s judgement, this could sometimes be subjective.

From equation 5, 6 and 7, the consistency ratio (CR) which compares the consistency index (CI) of the matrix in Table 3.7 (the matrix based on our judgments) against the consistency index of a generic random matrix (RI) as represented in Table 3.6. The random matrix is the matrix with judgments made in a random manner, hence it is expected not to be consistent, it should be highly inconsistent. In specific terms, RI is the average consistency index of 500

matrices that are randomly filled. This is as provided in Table 3.6 for matrices of different sizes.

From equation 3.7, CR of 0.10 or less is deemed acceptable to continue the AHP evaluation. However, for greater than 0.10 consistency ration, it will be required to revise the judgments to be able to identify the major cause of the inconsistency.

Applying equations 3.3, 3.4, and 3.5 on Table 3.8, the value of  $\lambda_{max}$  can be determined. It is as shown in Table 3.9 below.

**Table 3.9: Calculation of  $\lambda$  max**

FGM Candidate Material Selection	Price per unit volume	Fracture toughness	Fatigue strength	Tensile strength	Salt /Fresh water application	Density	Young Modulus	Weighted Sum (A)	Priorities (B)	(A)/(B)
Price per unit volume	0.09	0.06	0.06	0.11	0.08	0.12	0.07	0.60	0.09	6.73
Fracture toughness	0.45	0.23	0.21	0.23	0.08	0.25	0.29	1.74	0.23	7.44
Fatigue strength	0.02	0.03	0.03	0.03	0.05	0.02	0.03	0.21	0.03	6.89
Tensile strength	0.04	0.06	0.06	0.06	0.05	0.08	0.05	0.40	0.06	7.01
Salt/Fresh water application	0.45	0.47	0.27	0.46	0.41	0.33	0.57	2.96	0.41	7.21
Density	0.03	0.04	0.06	0.03	0.05	0.04	0.03	0.28	0.04	6.80
Young Modulus	0.18	0.12	0.15	0.17	0.10	0.16	0.14	1.03	0.14	7.18
<b>Total</b>										<b>49.26</b>
<b><math>\lambda</math> max</b>										<b>7.04</b>

Recall equation 6 as thus:

$$CI = \frac{\lambda_{max} - n}{n - 1}$$

For this study, the numbers of criteria are 7, that means n=7. Applying this gives a Consistency Index of CI= 0.006. From Table 3.6, the Random Inconsistency Index for n=7, is 1.32 and recall equation 3.7,

$$CR = \frac{CI}{RI}$$

Having known the values for CI and RI, from the above equation CR was determined to be 0.0045, hence since proportion of inconsistency from original judgement CR 0.0045 determined is less than 0.10, it can be inferred that the original judgments for all the pairwise comparison of the matrix is reasonably consistent. Thus, the process of decision-making with AHP can be continued. However, if the value of the inconsistency proportion were to be greater than 0.1, the judgement from the pairwise matrices comparison will have to be reviewed. This is an iterative process that will be reviewed until all inconsistencies is minimized to the level stated above.

#### **d) Deriving Local Priorities (Preferences) for the Alternatives**

This step of AHP involves determining the preference for the relative priorities of all the identified candidate materials with respect to each the seven itemized criterion. In summary, this section tends to evaluate the ranking (priorities) of all candidate materials (Metal and Ceramics) in Tables 3.3 and 3.4 with respect to all the individual criterion as seen Tables 3.3 and 3.4. It is termed Local Priorities (Ranking) based on the fact that the comparison of the candidate materials is with each of the criterion and this is different from the overall ranking will be determined later.

To determine the local rankings, a pairwise comparison of candidate materials with each criterion is evaluated using the Saaty's numeric scale in Table 3.5. The pairwise comparison for metals will be done independently with that of ceramics; hence two models will be considered in this section. The Rule of Thumb is perform one comparison in a model with two candidate materials (alternatives) for each criterion (Material 1 with Material 2), and to perform three comparison in a model with three candidate materials (alternatives) for each criterion (Material 1 with Material 2, Material 2 with Material 3, and Material 1 with Material 3) and so on. From Tables 3.3 and 3.4 there are three (3) candidate materials for ceramics and four (4) candidate materials for ceramics, this means there will be three (3) comparison matrices for metals and six (6) comparisons matrices for ceramics with each of the criterion. This can be done with a sequence of questions as seen below. Recall from Tables 3.3 and 3.4, it means there will be twenty one (21) comparison matrices for metal and forty two (42) comparison matrices for ceramics that corresponds to the following statements:

- **Metals**

With respect to the Price, Fracture toughness, Fatigue strength, Tensile strength, Durability in Salt/Fresh water, Material Density and Young Modulus criteria:

- 1) Compare Nickel-Fe-Cr alloy with Stainless Steel, austenitic.
- 2) Compare Nickel-Fe-Cr alloy with Copper C14200, Soft
- 3) Compare Stainless Steel, austenitic alloy with Copper C14200, Soft

• **Ceramics**

With respect to the Price, Fracture toughness, Fatigue strength, Tensile strength, Durability in Salt/Fresh water, Material Density and Young Modulus criteria:

- 1) Compare Silicon Carbide (HIP) with Tungsten Carbide (Hot Press).
- 2) Compare Silicon Carbide (HIP) with Zirconia (Transformation toughened) L
- 3) Compare Silicon Carbide (HIP) with Alumina 94 (SGM)
- 4) Compare Tungsten Carbide (Hot Press) with Alumina 94 (SGM)
- 5) Compare Tungsten Carbide (Hot Press) with Zirconia (Transformation toughened) L
- 6) Compare Alumina 94 (SGM)with Zirconia (Transformation toughened) L

From the statement comparison for metals, the questions thus follow:

With respect to Price which of the candidate material is preferred; Nickel-Fe-Cr alloy or Stainless Steel, austenitic?

From the Saaty’s numeric scale for priorities and from Table 3.4, the preference between the two criteria can be determine with respect to price and adequately scaled numerically according to Saaty’s scale. Stainless Steel is preferred very strongly as compared to Nickel Alloy; hence a numerical value of 5 is assigned to Stainless Steel as compared with Nickel Alloy in the comparison Matrix. The same process is repeated for the remaining material comparison with respect to price, this is further normalized and prioritized as was done earlier in Section (b) above. The matrix in Table 3.10 shows the ranking of metals with respect to price in USD as provided in CES Edupack 2017 software.

**Table 3.10: Ranking of Metals with respect to Price**

	Nickel-Fe-Cr alloy, INCOLOY 800, Annealed	Stainless Steel, austenitic, ASTM CF-20 , cast, water quenched	Copper C14200, Soft	Ranking
Nickel-Fe-Cr alloy, INCOLOY 800, Annealed	1.00	0.17	0.33	0.09
Stainless Steel, austenitic, ASTM CF- 20 , cast, water quenched	6.00	1.00	5.00	0.71
Copper C14200, Soft	3.00	0.20	1.00	0.20

This is repeated for the remaining six (6) criteria, the results for the overall ranking for metals is as are as represented in table 3.11.

**Table 3.11: Local Ranking of the Metal Candidate Materials with respect to each criterion**

Candidate Materials	Price per unit volume (USD/Kg)	Fracture toughness (MPa. m <sup>0.5</sup> )	Fatigue strength at 10 <sup>7</sup> Cycles (MPa)	Tensile strength (MPa)	Durability in Salt/ Fresh water application	Density (Kg/m <sup>3</sup> )	Young Modulus (GPa)
Nickel-Fe-Cr alloy, INCOLOY 800, Annealed	0.09	0.76	0.28	0.64	0.33	0.20	0.23
Stainless Steel, austenitic, ASTM CF-20 , cast, water quenched	0.71	0.17	0.64	0.28	0.33	0.20	0.12
Copper C14200, Soft	0.20	0.06	0.08	0.07	0.33	0.60	0.65

Similar, a comparison of the identified ceramics material with respect to price was made to understand the ceramics material to be preferred when price is considered (e.g. Silicon Carbide (HIP) or Tungsten Carbide (Hot Press))

Also refer to the Saaty’s numeric scale for priorities and Table 3.4, the preference between the two criteria can be determine with respect to price and adequately scaled numerically in alignment to Saaty’s scale. Silicon Carbide Steel is preferred strongly as compared to Tungsten Carbide in respect to price; hence a numerical value of 4 is assigned to Silicon Carbide as compared with Tungsten Carbide. Same is repeated for the remaining material comparison with respect to price; this is further normalized and prioritized (Ranked) as was done earlier. The matrix in Table 3.12 shows the ranking of metals with respect to price.

**Table 3.12: Ranking of Ceramics with respect to Price.**

	Silicon Carbide (HIP)	Tungsten Carbide (Hot Press)	Alumina 94 (SGM)	Zirconia (Transformation toughened) L	Ranking
Silicon Carbide (HIP)	0.12	0.25	0.10	0.22	0.17
Tungsten Carbide (Hot Press)	0.03	0.06	0.08	0.04	0.05
Alumina 94 (SGM)	0.82	0.56	0.73	0.67	0.69
Zirconia (Transformation toughened) L	0.04	0.13	0.08	0.07	0.08

This is repeated for the remaining six (6) criteria, the results for the overall local ranking for Ceramics is as represented in table 3.13.

**Table 3.13: Local Ranking of the Ceramics Candidate Materials with respect to each criterion**

Candidate Materials	Price per unit volume (USD/Kg)	Fracture toughness (MPa. m <sup>0.5</sup> )	Fatigue strength at 10 <sup>7</sup> Cycles (MPa)	Tensile strength (MPa)	Durability with Fresh/Salt water application	Density Kg/m <sup>3</sup> )	Young Modulus (GPa)
Silicon Carbide (HIP)	0.17	0.04	0.54	0.50	0.25	0.48	0.22
Tungsten Carbide (Hot Press)	0.05	0.24	0.16	0.16	0.25	0.04	0.57
Alumina 94 (SGM)	0.69	0.12	0.08	0.08	0.25	0.30	0.13
Zirconia (Transformation toughened) L	0.08	0.59	0.23	0.26	0.25	0.18	0.08

**e) Derive Overall Priorities (Model Synthesis)**

So far, the local rankings (priorities) that give indication of the preferred candidate materials for both metals and ceramics based on their individual standing as compared with each criterion has have been obtained. This further calculates the overall ranking for each of the itemized candidate material; this overall ranking takes cognizance of the weight of each criterion that was used in the earlier comparison. Being the fact that all values provided in this model are used in this section, hence the section is termed Model Synthesis. The overall ranking is calculated by first considering the local rankings as presented in Tables 3.11 and 3.13.

Tables 3.11 and 3.13 were further re-evaluated to consider the weights of each criterion, the various weighted rankings for the candidate material is as shown in Table 3.14 and 3.15 for both metals and ceramics.

**Table3.14: Weighted Ranking of Metals Candidate Materials**

	Price per unit volume (USD/Kg)	Fracture toughness (MPa. m <sup>0.5</sup> )	Fatigue strength at 10 <sup>7</sup> Cycles (MPa)	Tensile strength (MPa)	Durability with Salt/Fresh water application	Density (Kg/m <sup>3</sup> )	Young Modulus (GPa)
<b>Criteria Weights</b>	<b>0.0892</b>	<b>0.2336</b>	<b>0.0304</b>	<b>0.0574</b>	<b>0.4102</b>	<b>0.0411</b>	<b>0.1434</b>
Nickel-Fe-Cr alloy, INCOLOY 800, Annealed	0.0082	0.1782	0.0086	0.0369	0.1354	0.0082	0.0330
Stainless Steel, austenitic, ASTM CF-20 , cast, water quenched	0.0630	0.0405	0.0195	0.0162	0.1354	0.0082	0.0175
Copper C14200, Soft	0.0180	0.0148	0.0024	0.0042	0.1354	0.0246	0.0929

**Table3.15: Weighted Ranking of Ceramics Candidate Materials**



	Price per unit volume (USD/Kg)	Fracture toughness (MPa. m <sup>0.5</sup> )	Fatigue strength at 10 <sup>7</sup> Cycles (MPa)	Tensile strength (MPa)	Durability with Fresh/Salt water application	Density (Kg/m <sup>3</sup> )	Young Modulus (GPa)
<b>Criteria Weights</b>	<b>0.0892</b>	<b>0.2336</b>	<b>0.0304</b>	<b>0.0574</b>	<b>0.4102</b>	<b>0.0411</b>	<b>0.1434</b>
Silicon Carbide (HIP)	0.0154	0.0104	0.0163	0.0287	0.1025	0.0198	0.0318
Tungsten Carbide (Hot Press)	0.0047	0.0564	0.0048	0.0093	0.1025	0.0017	0.0823
Alumina 94 (SGM)	0.0619	0.0290	0.0023	0.0045	0.1025	0.0122	0.0181
Zirconia (Transformation toughened) L	0.0071	0.1377	0.0070	0.0149	0.1025	0.0074	0.0111

In conclusion, the overall candidate materials ranking is obtained by adding all the candidate materials weighted ranking for each of the criterion in the rows in tables 3.14 and 3.15. This is as shown in Tables 3.16 and 3.17 according, the rankings in the tables are arranged in descending order.

**Table 3.16: Overall Ranking for Metals**

FGM's Candidate Materials for Metals	Overall Ranking
<b>1. Nickel-Fe-Cr alloy, INCOLOY 800, Annealed</b>	<b>0.408</b>
2. Stainless Steel, austenitic, ASTM CF-20 , cast, water quenched	0.300
3. Copper C14200, Soft	0.292

**Table 3.17: Overall Ranking for Ceramics**

FGM's Candidate Materials for Ceramics	Overall Ranking
<b>1. Zirconia (Transformation toughened) L</b>	<b>0.288</b>
2. Tungsten Carbide (Hot Press)	0.262
3. Alumina 94 (SGM)	0.231
4. Silicon Carbide (HIP)	0.225

From the tables above, it means given the various importance (Weight) of all the identified criteria for the FGM Material Selection (Price, Fracture Toughness, Fatigue Strength, Tensile Strength, Durability in Fresh and Sea Water Application, Density and Young Modulus), Annealed Nickel-Fe-Cr alloy (INCOLOY 800) is the preferable Metal for the FGM tailored service conditions (overall ranking = 0.408), while Zirconia (Transformation toughened L) is the preferable ceramics for the same service conditions (overall ranking = 0.288).

#### **f) Sensitivity Analysis**

From the overall ranking of all candidate materials, it can be deduced that the overall ranking is highly dependent on the weight assigned to each criterion, it is worthwhile to perform sensitivity analysis to be able to appreciate the deviation that could arise in the final results if

some of the assumptions made to arrive at the initial weighting of the criteria changes. This process is vital, as it gives an appreciation on robustness of the original decision and the drivers (criteria that drastically alter the original results). Hence, this process must be concluded before making final decision.

Recall that in Table 3.8, Price was assigned lower priority as compared to other criteria due to the fact that in Selecting possible candidate materials as shown in Figures 3.2 and 3.4 price limits were used, hence this was assumption for the lower priority assigned Price in Table 3.8. On the same Density was assigned lower priority in Table 3.8 due to the assumption that weight will not be a concern on the Offshore Facilities were the FGM will be deployed. Based on the foregoing, the real question is what will be the best alternative candidate materials if the assumptions made as stated above becomes unrealistic. Sensitivity analysis with the following scenarios was performed to provide for uncertainties in weight, price and density:

1. All criteria having the same weight.
2. Increasing the weight assigned to price and maintaining the weightings proportion of other criteria in Table 3.8.
3. Increasing the weight assigned to density and maintaining the weighting proportion of other criteria as in “b” above.

**Table 3.18a: Scenario 1 for Metals**

	Price per unit Weight	Fracture toughness	Fatigue strength	Tensile strength	Salt/Fresh water application	Density	Young Modulus	Ranking
<b>Criteria Weights</b>	<b>0.1429</b>	<b>0.1429</b>	<b>0.1429</b>	<b>0.1429</b>	<b>0.1429</b>	<b>0.1429</b>	<b>0.1429</b>	
Nickel-Fe-Cr alloy, INCOLOY 800, Annealed	0.0132	0.1090	0.0403	0.0919	0.0471	0.0286	0.0328	<b>0.3629</b>
Stainless Steel, austenitic, ASTM CF-20 , cast, water quenched	0.1010	0.0248	0.0915	0.0404	0.0471	0.0286	0.0175	<b>0.3509</b>
Copper C14200, Soft	0.0288	0.0091	0.0111	0.0105	0.0471	0.0857	0.0926	<b>0.2849</b>

**Table 3.18b: Scenario 2 for Metals**

	Price per unit Weight	Fracture toughness	Fatigue strength	Tensile strength	Salt/Fresh water application	Density (Kg/m3)	Young Modulus (GPa)	Ranking
<b>Criteria Weights</b>	<b>0.2000</b>	<b>0.2032</b>	<b>0.0265</b>	<b>0.0499</b>	<b>0.3569</b>	<b>0.0357</b>	<b>0.1247</b>	
Nickel-Fe-Cr alloy, INCOLOY 800, Annealed	0.0184	0.1550	0.0075	0.0321	0.1178	0.0071	0.0287	0.3666
Stainless Steel, austenitic, ASTM CF-20 , cast, water quenched	0.1414	0.0353	0.0169	0.0141	0.1178	0.0071	0.0152	0.3479
Copper C14200, Soft	0.0403	0.0129	0.0021	0.0037	0.1178	0.0214	0.0808	0.2789

**Tables 3.18c: Scenario 3 for Metals**

	Price per unit weight	Fracture toughness	Fatigue strength	Tensile strength	Salt/Fresh water application	Density (Kg/m3)	Young Modulus (GPa)	Ranking
Criteria Weights	0.2000	0.1775	0.0231	0.0436	0.3117	0.1400	0.1090	
Nickel-Fe-Cr alloy, INCOLOY 800, Annealed	0.0184	0.1354	0.0065	0.0281	0.1029	0.0280	0.0250	0.3444
Stainless Steel, austenitic, ASTM CF-20 , cast, water quenched	0.1414	0.0308	0.0148	0.0123	0.1029	0.0280	0.0133	0.3436
Copper C14200, Soft	0.0403	0.0113	0.0018	0.0032	0.1029	0.0840	0.0706	0.3140

**Table 3.19 a: Scenario 1 for Ceramics**

	Price per unit weight	Fracture toughness	Fatigue Strength	Tensile strength	Fresh/Salt water application	Density	Young Modulus	Ranking
<b>Criteria Weights</b>	<b>0.1429</b>	<b>0.1429</b>	<b>0.1429</b>	<b>0.1429</b>	<b>0.1429</b>	<b>0.1429</b>	<b>0.1429</b>	
Silicon Carbide (HIP)	0.0247	0.0064	0.0766	0.0713	0.0357	0.0688	0.0317	0.3151
Zirconia (Transformation toughened) L	0.0114	0.0842	0.0327	0.0371	0.0357	0.0257	0.0111	0.2379
Alumina 94 (SGM)	0.0992	0.0177	0.0110	0.0113	0.0357	0.0425	0.0181	0.2355
Tungsten Carbide (Hot Press)	0.0075	0.0345	0.0225	0.0230	0.0357	0.0058	0.0820	0.2110

**Table 3.19b: Scenario 2 for Ceramics**

	Price per unit Weight	Fracture toughness)	Fatigue strength	Tensile strength	Fresh/Salt water application	Density	Young Modulus	Ranking
<b>Criteria Weights</b>	<b>0.2000</b>	<b>0.2055</b>	<b>0.0268</b>	<b>0.0505</b>	<b>0.3610</b>	<b>0.0361</b>	<b>0.1262</b>	
Alumina 94 (SGM)	0.1389	0.0255	0.0021	0.0040	0.0902	0.0108	0.0159	0.2874
Zirconia (Transformation toughened) L	0.0159	0.1212	0.0061	0.0131	0.0902	0.0065	0.0098	0.2629
Tungsten Carbide (Hot Press)	0.0105	0.0496	0.0042	0.0081	0.0902	0.0015	0.0725	0.2366
Silicon Carbide (HIP)	0.0346	0.0092	0.0143	0.0252	0.0902	0.0174	0.0280	0.2189

**Tables 3.19c: Scenario 3 for Ceramics**

	Price per unit Weight	Fracture toughness	Fatigue strength	Tensile strength	Fresh/Salt water application	Density	Young Modulus	Ranking
Criteria Weights	0.2000	0.1775	0.0231	0.0436	0.3117	0.1400	0.1090	
Alumina 94 (SGM)	0.1389	0.0220	0.0018	0.0035	0.0779	0.0417	0.0138	0.2995
Silicon Carbide (HIP)	0.0346	0.0079	0.0124	0.0218	0.0779	0.0675	0.0241	0.2462
Zirconia (Transformation toughened) L	0.0159	0.1047	0.0053	0.0113	0.0779	0.0252	0.0085	0.2488
Tungsten Carbide (Hot Press)	0.0105	0.0429	0.0036	0.0070	0.0779	0.0057	0.0626	0.2102

### g) Making a Final Decision

This is the final step required to make an informed decision on the Candidate Material for the FGM. To achieve this, it will be required to compare overall ranking as represented in Tables 3.16 and 3.17 with the priorities from the sensitivity analysis in Table 3.18 and 3.19. This is to give an appreciable if the differences from the sensitivity analysis are large enough to tweak the decisions (Ranking) in tables 3.16 and 3.20.

The Chart below gives a fair comparison of the three Scenarios with that of the overall ranking for both Metals and Ceramics Candidate Materials.

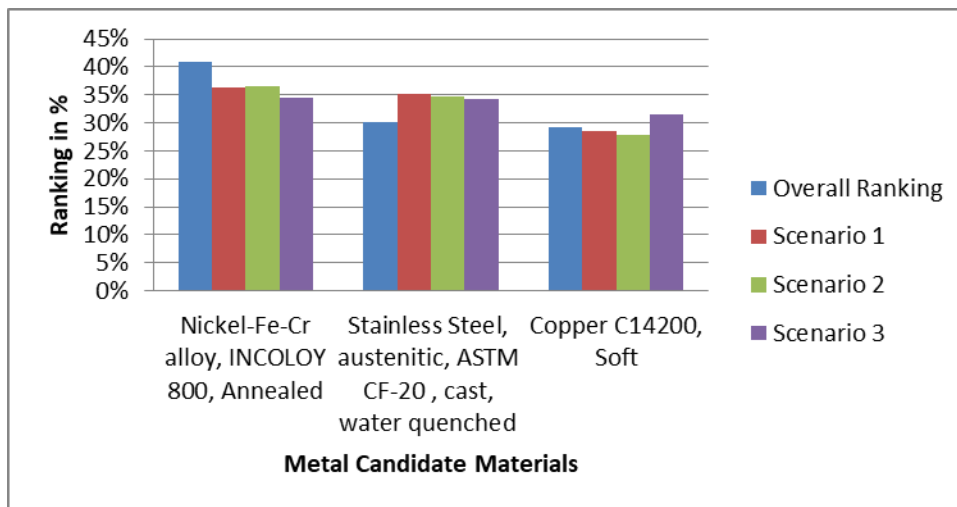


**Fig. 3.7: Representation of all analyzed results for the Metallic Candidate material.**

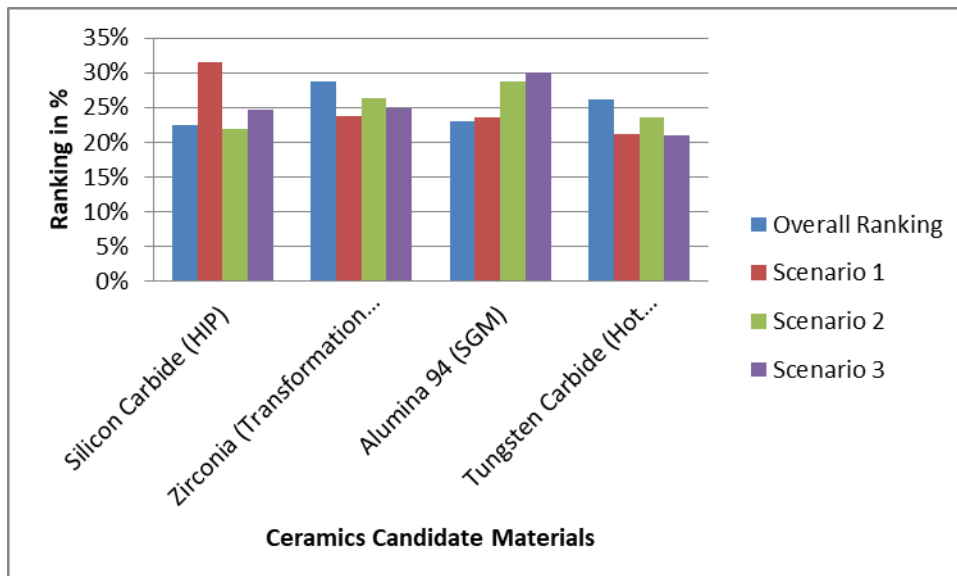


**Fig 3.8: Representation of all analyzed results for the Ceramics Candidate material**

### 3.3. CONCLUDING REMARKS

Having evaluated all existing metals and ceramics based on the predefined operational range as required for the oil and gas operations and based on all the analysis and sensitivities carried out as summarized in Fig. 3.7 and 3.8. The ranking of the best material for both metal and ceramics is as detailed in in Table 3.20.

**Table 3.20: Final Results Presentation.**

	E (GPa)	Coefficient of thermal expansion CTE (/K)	Poisson's ratio	Thermal conductivity k (W/m.K)	Specific Heat Capacity Cv (J/g.K)	Density (kg/m3)	Tensile Strength (MPa)	Ranking
<b>Ranking for Metal</b>								
Nickel-Fe-Cr alloy, INCOLOY 800, Annealed	195	14.25	0.34	11.5	502.5	7950	620	1
Stainless Steel, austenitic, ASTM CF-20 , cast, water quenched	195	17.5	0.27	15.5	500	7765	530	2
Copper C14200, Soft	122.5	17.5	0.345	165.5	380.5	8925	220	3
<b>Ranking for Ceramics</b>								
Zirconia (Transformation toughened) L	246.5	9.8	0.3	2	450	5740	414	1
Alumina 94 (SGM)	330	7.55	0.24	21	880	3650	250.5	2
Silicon Carbide (HIP)	400	5	0.15	80.05	802	3145	500.5	3
Tungsten Carbide (Hot Press)	669	5.8	0.21	29	180	15700	352.5	4

## **CHAPTER 4: DEVELOPMENT OF NUMERICAL MODEL FOR FGM PIPES**

### **4.1. INTRODUCTORY REMARKS**

A numerical modelling approach was used in this chapter to evaluate properties and behaviour of FGM against a prescribed defined number of criteria; this same approach was applied to assess different pipeline configurations; straight pipe, pipe bend (elbow) and tee-piece. The results from the extensive analysis conducted will be addressed in subsequent chapters.

However, in the present chapter a methodology has been developed to demonstrate the use of finite element method on application of a straight FGM pipe. This methodology was used to develop the straight FGM pipe model on Abaqus Software with loading condition to replicate the actual conditions of the referenced offshore piping systems. The usage of FGM for piping in oil and gas industry is still evolving as a result, little or no information exist that could be used as benchmarks to the present research. Apart from the corrosion concern, thermal and mechanical loading is the next consideration of the referenced offshore oil and gas piping system, this led to a focused review of the literature on studies of FGM pipes subjected to transient thermo-mechanical loading. It is noted that the available literature on this subject were limited, the closest was the study by Ghannad *et al.* [102] who presented a 2D thermo-elastic model of an axisymmetric FGM hollow cylinder. Compared to other studies, Ghannad provided a more realist behaviour of the FGM pipe as the work considers the edge effects for finite-length pipe.

The adopted methodology makes an attempt to examine the problem of an axisymmetric cylindrical FGM pipe subjected to thermal and pressure loading. To achieve this, the developed model is validated with published work by Ghannad et al, 2019. The result from this present research was compared with a classical analytical approach and a numerical approach using the ANSYS finite element code.

### **4.2. FGM MODEL DEVELOPMENT FOR A STRAIGHT PIPE**

#### **4.2.1 Problem Formulation**

The focus herein is on an axisymmetric plane-strain problem as shown in the schematic in Fig.4.1. A 20 Layers axisymmetric plan was considered so as to explore the benefit of the FGM properties gradation and it was assumed that the properties of FGM material varies along the thickness direction only. The inner surface  $Z = -h/2$ , towards the inner diameter of the cylinder is ceramic rich (Zirconia), while the outer surface  $Z = h/2$ , towards the outer

diameter of the cylinder is metal rich (Titanium). Same FGM material was used by Ghannad, hence the choice of the material was ensure effective result benchmark and validation.

The effective material properties at any given point within the axisymmetric plane, such as like Young's modulus  $E$ , mass density  $\rho$ , thermal expansion coefficient  $\alpha$ , of the functionally graded plane can be determined by power law as stated in equations 4.1, 4.2, & 4.3.

The volume fraction variation  $V_f$ , of ceramic throughout the plain thickness gives an indication of the volumetric fraction of ceramic at a given location along the thickness. The fraction is established on the combination of metal and ceramic and gives an indication of the material composition in terms of volume at any given location along the thickness. Assuming the volume fraction for Ceramics is defined as  $V_f$ , therefore the volume fraction of metal will be the balance of the material and this can be defined as  $1 - V_f$ . As stated earlier  $E, \rho, k$  and  $\alpha$  varies in accordance to power law and their correspondence values are determined and entered into ABAQUS/CAE 6.14 Software accordingly.

It is a known fact that Young's modulus  $E$  and thermal expansion coefficient  $\alpha$  are temperature dependent. On the other hand, mass density  $\rho$  and the thermal conductivity  $k$  are independent of the temperature. The Poisson's ratio  $\nu$  is assumed to be constant as it is not so temperature dependent. ABAQUS/CAE 6.14 Standard Model Software was used to simulate the axisymmetric 20-layered FGM model subjected to both Thermal and Mechanical loading. As stated, the model was based on an axisymmetric shell deformable structure clamped at both ends. The details of the model development are described in the following subsection.

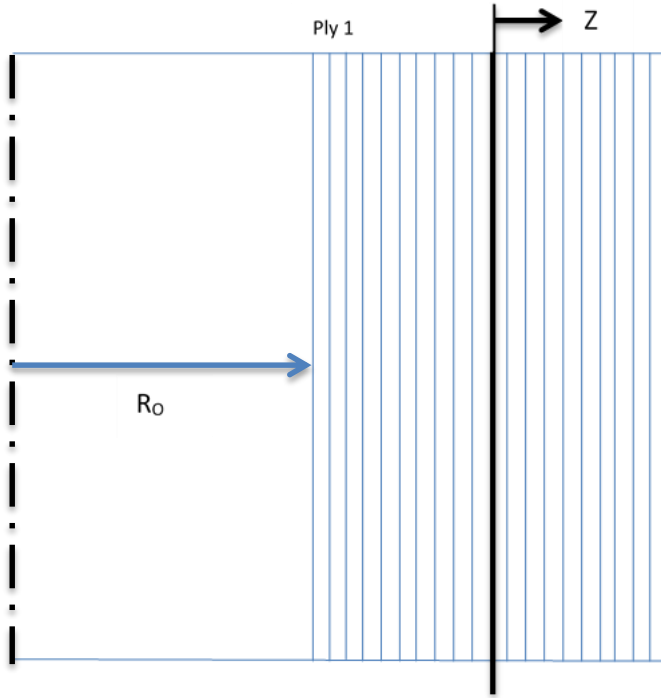


Figure 4.1: Figure depicting the origin of Z

#### 4.2.2 Model Focus and Developments

The methodology utilised to model the axisymmetric pipe with FGMs using a finite element approach was established by defining the coordinate systems, theoretical formulation and boundary conditions. Units used were as follows: length [ $m$ ], pressure [ $N/m^2$ ], temperature [ $^{\circ}K$ ], expansion [ $1/^{\circ}K$ ], density [ $kg/m^3$ ], conductivity [ $W/m \cdot ^{\circ}K$ ]. Due to the nature of FGM material properties that changes throughout the thickness of the cylinder, the numerical model was separated into numerous distinct sections so as to properly capture the changes in properties. The models were treated like isotropic materials. Material properties were calculated at the mid-plane of each section using the power law equations as outlined below:

$$E(z) = (E_o - E_i) \left( \frac{1}{2} + \frac{z}{h} \right)^n + E_i \quad (4.1)$$

$$\alpha(z) = (\alpha_o - \alpha_i) \left( \frac{1}{2} + \frac{z}{h} \right)^n + \alpha_i \quad (4.2)$$

$$k(z) = (k_o - k_i) \left( \frac{1}{2} + \frac{z}{h} \right)^n + k_i \quad (4.3)$$

The sections and the corresponding properties are then crusted together to create the through-the-thickness variation of material properties. Although the gradual change in material properties is not reflected in the layered sections, the material gradation can be obvious when a sufficient number of sections is been considered. Fig. 4.1 depicts an axisymmetric section of a cylinder with its thickness discretized into twenty layers, Ply 1 in Fig. 4.1 is at the inner



diameter of the cylinder, and the origin of the  $z$  axis is at the mid-plane of the cylinder thickness with  $+z$  in the direction towards the outer diameter.

The FGM model developed has its inner section to be ceramic rich, while the outer section is metal rich. The mixture of the two materials makes up the thickness characteristics. This material variation is determined by a parameter, “ $n$ ” (non-homogeneity factor). At  $n = 0$  the plate is a fully metal plate while at  $n = \infty$  the plate is fully ceramic. Material properties depends on the  $n$  value and the position of “ $z$ ” along the thickness of the cylinder. Material properties vary according to a power law as shown in equation 4.1, 4.2, & 4.3. Typically, the properties therefore vary through the cylinder thickness according to power law.

The model is made of a moderately thick-walled cylindrical shell with an outer radius  $r_o$  and inner radius  $r_i$ ; and length  $L$ ; which is subjected to axisymmetric conditions of pressure  $P$ , external heat flux  $H_i$  at inner surface, the outer surface of the cylinder is considered to be interacting with the ambient temperature. From Fig. 4.2, the position of a distinctive point  $m$ , ( $r$ ) within the cylindrical shell element can be identified by two parameters,  $R$  and  $z$ , as  $r = R + z$ .

$R$  represents the distance from the center line of the cylinder in the axial direction,  $z$  is the distance, typically from a point in the middle of the cylinder thickness. It is worth noting that,  $z$  and  $x$  must be within the range of  $-h/2 \leq Z \leq h/2$ ,  $0 \leq x \leq L$  respectively, where  $h$  is the thickness of the cylinder.

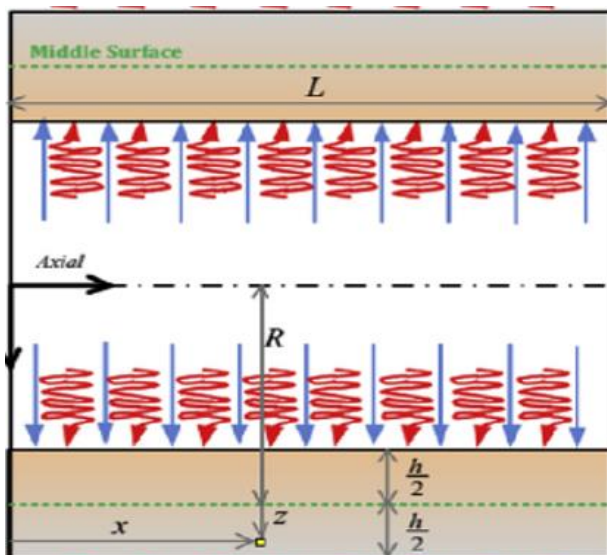


Figure 4.2: Cross-section of cylinder under Thermo-Mechanical Loading [102]

### 4.2.3 Geometry and material properties

The candidate pipe can be represented as an axisymmetric construction with a cylindrical shape. It was dimensioned with an inner radius  $r_i = 40\text{mm}$ , an outer radius  $r_o = 60\text{mm}$  and a length  $L = 800\text{mm}$ . The parts were then partitioned into 20 layers with the same thickness using datum planes as shown in Fig 4.3a and 4.3b

The axisymmetric cylindrical shell structure is Zirconia rich from the inside and Titanium rich from the outside, the material properties of the inner and outer surface is as listed below:

Inner surface (Zirconia):

$$E = 117.0 \text{ (GPa)}; \nu = 0.3; \rho = 5890 \text{ Kg/m}^3; \alpha = 7.11 \times 10^{-6} \text{ (1/K)}$$

$$k = 204 \text{ (W/m} \cdot \text{K)}$$

Outer surface (Titanium):

$$E = 66.2 \text{ (GPa)}; \nu = 0.3; \rho = 4430 \text{ Kg/m}^3; \alpha = 10.3 \times 10^{-6} \text{ (1/K)}$$

$$k = 18.1 \text{ (W/m} \cdot \text{K)}$$

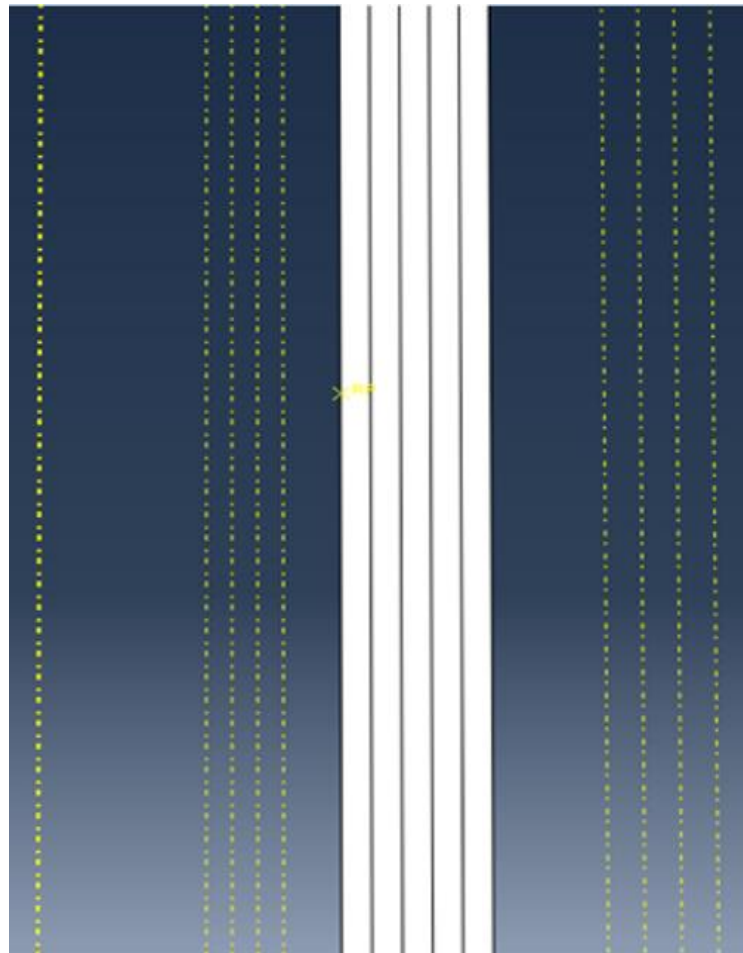
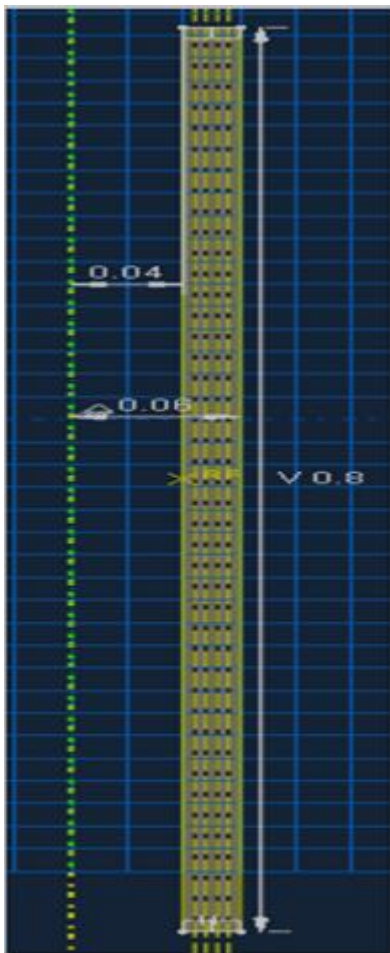


Figure 4.3a: Cylinder Part Sketch

Figure 4.3b: of the and partitioned part of the cylinder with datum planes in Abaqus

#### 4.2.4 Element type and mesh sensitivity

Fig 4.4 shows details of a typical finite element mesh of the axisymmetric pipe section. The behaviour of different element sizes in the cross-section of the axisymmetric section was examined to provide both accurate results and reduced computation time.

Mesh Convergence study was carried out and the result converges satisfactorily with 270 number of elements. The axisymmetric pipe was meshed with CAX4T elements which has three degrees of freedoms for each node: temperature, and two translations in radial and axial directions. A Standard Element with linear geometric order was utilised, the sections were modelled using the 4-node axisymmetric thermally coupled quadrilateral, bilinear displacement and temperature (CAX4T).

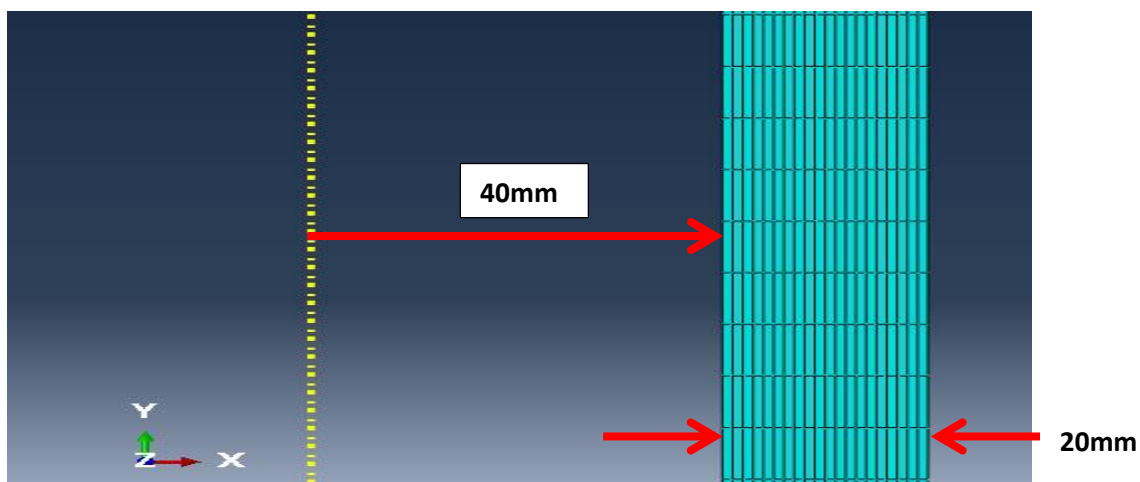


Figure 4.4: Meshed axisymmetric cylindrical shell

#### 4.2.1 Loading and boundary conditions

The nodes at the end of the cylinder were restrained at both ends with two types of boundary conditions as defined below:

- An encastrement for the mechanical boundary condition
- A fixed temperature of 50 °C was used so as to replicate the model been validated.
- The loading conditions applied to the inner wall of the cylinder is as stated below:
- A receding surface heat flux of 150 W.m<sup>-2</sup>
- An internal pressure of 80 MPa

A predefined temperature of 25°C was also applied at the initial step of the model. These are as shown in Fig. 4.5.

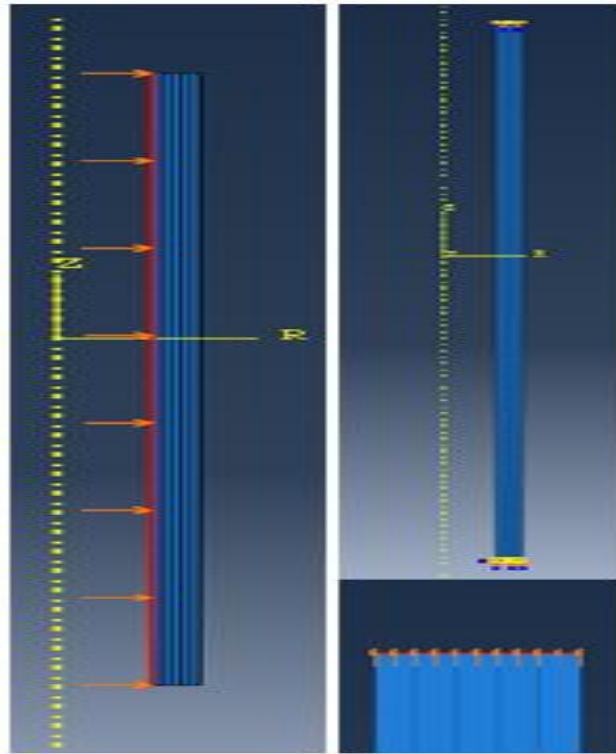


Fig. 4.5: Thermal boundary conditions (left), mechanical boundary conditions (top right), and zoom on the surface of mechanical boundary conditions (bottom right)

### 4.3. RESULTS VALIDATION

To ensure validation of the finite element models that were modelled using Abaqus, the numerical FEM analysis results for temperature distribution, radial/axial displacements, radial/axial/circumferential stresses were compared against that of Analytical and FEM (Using commercial FE Code ANSYS) of similar study conducted by Ghannad et al., 2017.

The main aim of the comparison was to verify and validate the accuracy of the finite element model. The comparison of the FEA results for the temperature distribution, radial displacement, axial displacement, axial stress, circumferential stress and Von-mises stress along the middle surface of the cylinder length is as shown from Fig 4.6a, 4.6b, 4.6c, 4.6d, 4.6e & 4.6f. Table 4.1 also give a detailed comparison between the stresses from the research conducted by Ghannad et.al 2017 and that of the current research using ABAQUS/CAE 6.14 Software. The comparison of results obtained with that from Ghannad's Paper shows good agreement with above 95% accuracy with most of the variables used for the comparison. However, for the axial stress with  $n=1$ , there was slight divergence in the outcome when compared with the referenced literature (about 30%). But the axial stress for  $n=5$  shows good agreement with that of the referenced literature, with deviation within 5% when compared with both the numerical and analytical results from the literature. This is as shown in Table 4.1.

The First-order shear deformation theory (FSDT) and FEM values for the stresses at  $x = L/2$  &  $z = 0$  from Ghannad et. al outcome was compared with that of the current study. The result reveals that circumferential stress, axial stress and Von-mises stress for the model using  $n=5$  had less than 5% deviation, while the circumferential stress and Von-mises stress for the model using  $n=1$  shows similar excellent outcome.

Table 4.1: Comparison of the results for FSDT and FEM calculations for stresses at  $x = L/2$  &  $z = 0$  by Ghannad et. al. 2017 and that of the current study with Abaqus

	Method	n=1	n=5
<b>Circumferential Stress</b>	Analytical Ghannad et. al	147.72	173.85
	FEM (ANSYS) Ghannad et. al	150.67	170.47
	FEM (Abaqus)	160.13	172.4
<b>Axial Stress</b>	Analytical Ghannad et. al	-10.59	-26.84
	FEM (ANSYS) Ghannad et. al	-8.35	-31.12
	FEM (Abaqus)	-5.99	-32.79
<b>Von Mises</b>	Analytical Ghannad et. al	167.03	194.49
	FEM (ANSYS) Ghannad et. al	166.43	198.23
	FEM (Abaqus)	175.24	201.23

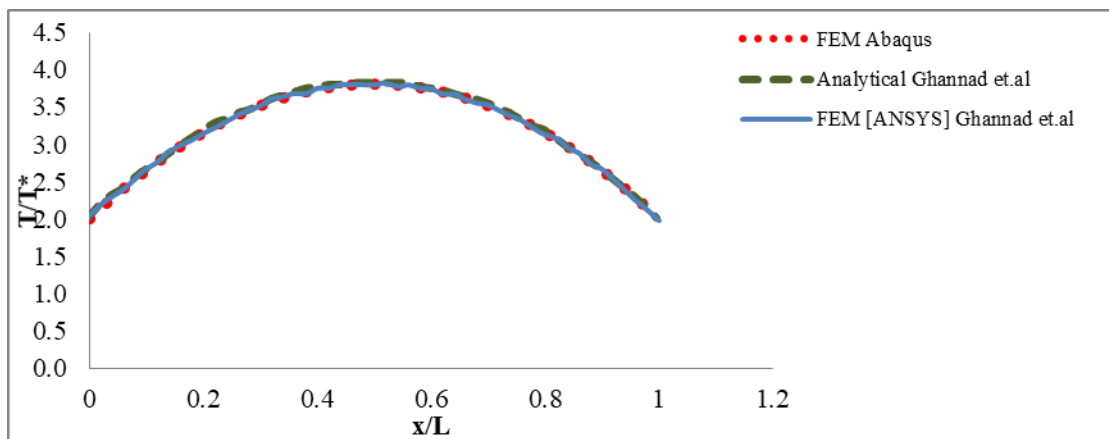


Figure 4.6a: Distribution of temperature along the middle surface in FGM cylinder

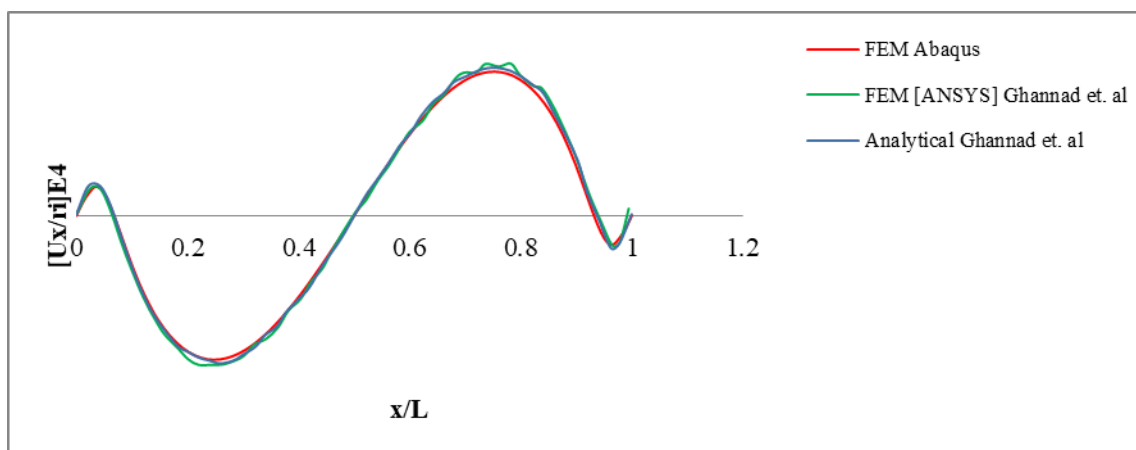


Figure 4.6b: Distribution of axial displacement along the middle surface in FGM cylinder

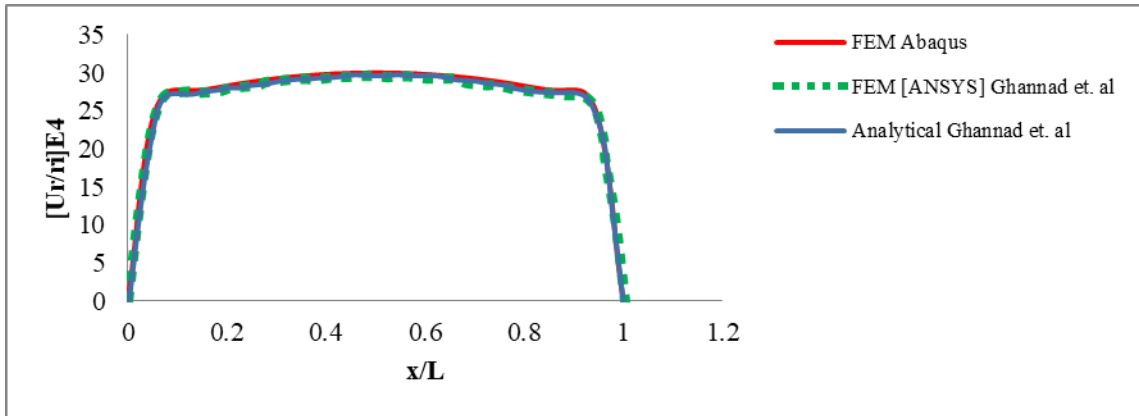


Figure 4.6c: Distribution of radial displacement along the middle surface in FGM cylinder

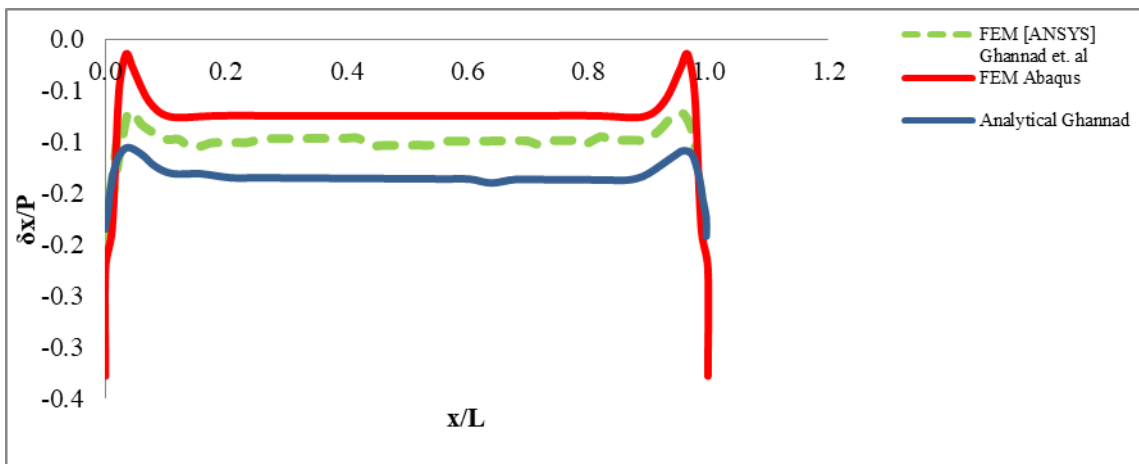


Figure 4.6d: Distribution of axial stress along the middle surface in FGM cylinder

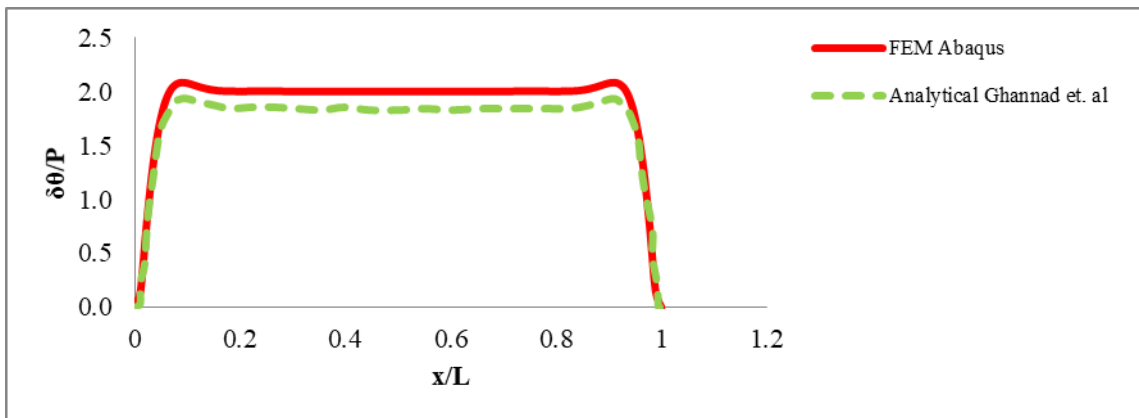


Figure 4.6e: Distribution of circumferential stress along the middle surface in FGM cylinder

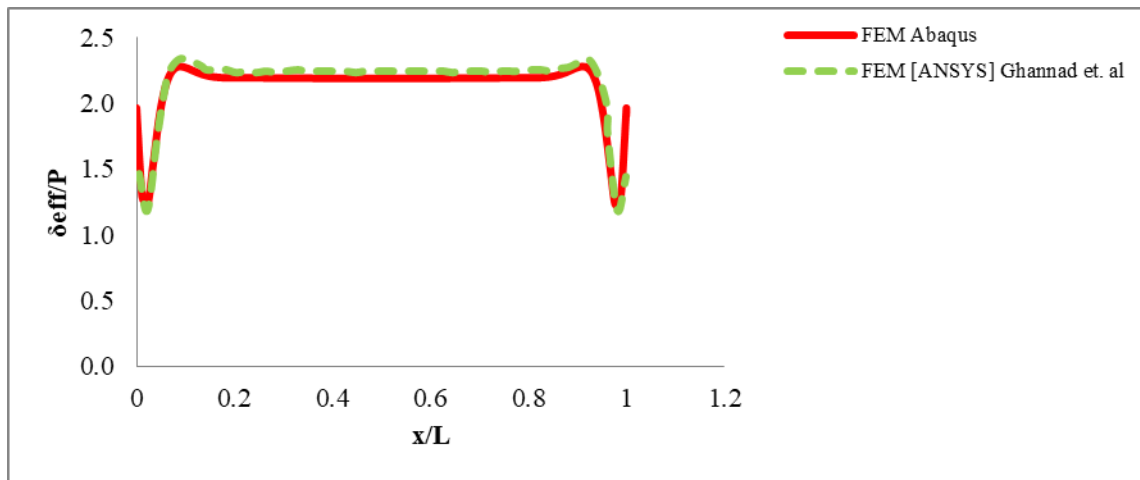


Figure 4.6f: Distribution of Von mises effective stress along the middle surface in FGM cylinder

#### 4.4. PARAMETRIC STUDY

The developed finite element model predicts the behaviour of the axisymmetric cylinder subjected to both thermal and mechanical loading. Using this model, parametric studies were carried out to understand the effect of number of layers and “n” (non-homogeneity factor) on the FGM behaviour.

##### 4.4.1 The effect of number of layers

A study of the effect of number of layers was examined, the layer configurations were 5, 10 and 20 layer systems. This study intends to help understand the behaviour and variation in strength, stiffness and load carry capability of the FGM pipe when designed with different number of layers. The parameters considered for the study were temperature distribution, radial displacement, axial displacement and Von-mises stress, all considered along the middle of the cylinder. While the loading conditions, boundary conditions and ambient condition were same for the various scenarios considered. Fig.4.7a, 4.7b, 4.7c & 4.7d depict the performance of the different layered FGM model considered under the various parameters. From Fig 4.7 (a) it can be seen that the number of layers of FGM has no significant effect on the axial displacement, although shows slight changes; with less than 1% changes in the axial displacement as the number of layers. This view is further affirmed in table 4.2 in which the axial displacement remain unchanged for both 5 and 10 layers.

From Fig. 4.7 (b), it can be depicted that number of layers of FGM has no effect on the radial displacement of the FGM. While from Fig. 4.7 (c), shows same trend with no significant changes in the temperature distribution along the length of the FGM Pipe as the number layer increases, hence increase in number of layers has no significant effect on the temperature

distribution along the length of the FGM pipe. This trend is similar to the effect of number of layers on the axial displacement; with less than 3% increase in temperature distribution as shown in table 4.2.

From Fig 4.7 (d), it can be seen that increase in number of layers of FGMs has little influence on the Von-mises, it slightly increases with the increase in number of layer and slightly decreases with a further increase in the number of layers. However the difference between maximum Von-mises between the three scenarios considered is less than 3%. Hence the effect of number of layers on the considered properties of an FGM in minimal and can be negligible.

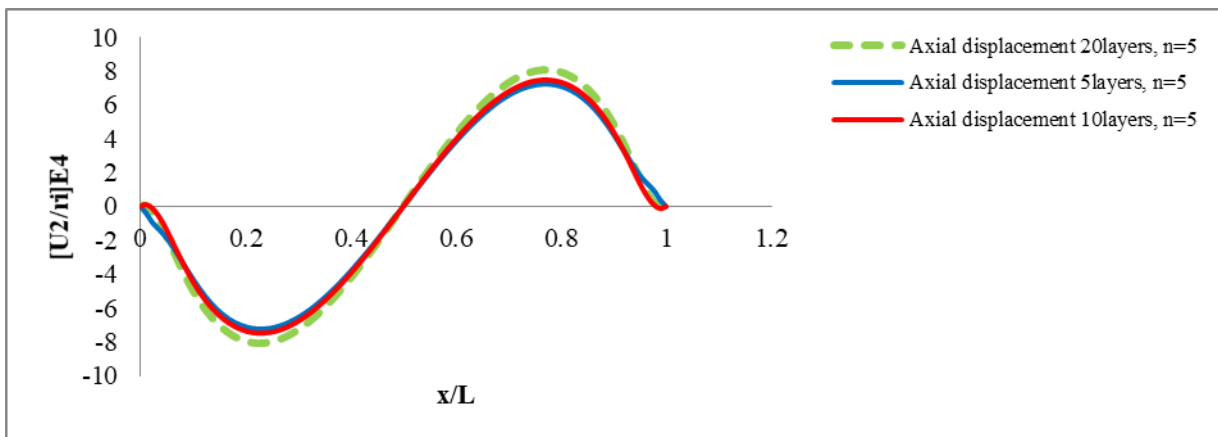


Figure 4.7a: Comparison of distribution of axial displacement along the middle surface in FGM cylinder for FGM of different number of layers.

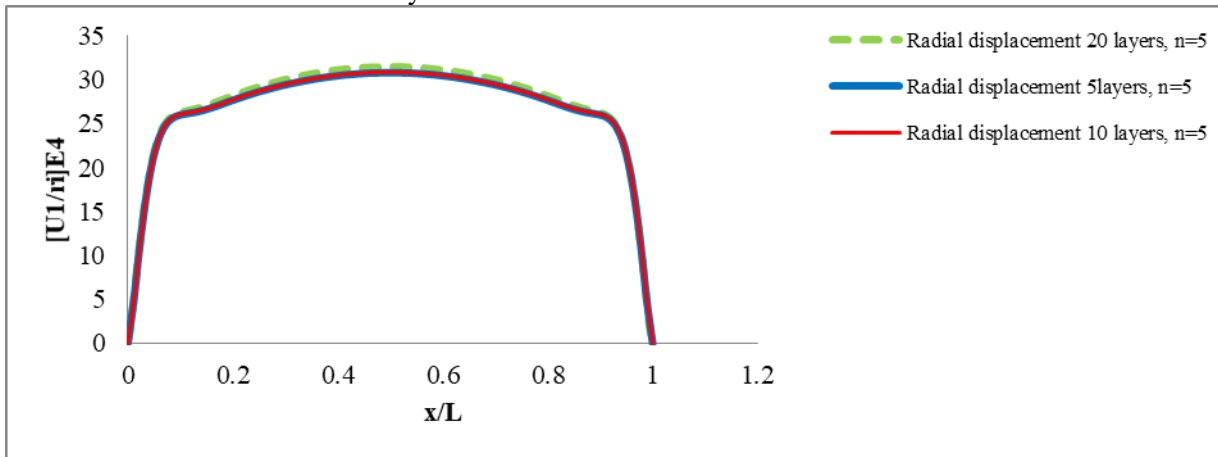


Figure 4.7b: Comparison of distribution of radial displacement along the middle surface in FGM cylinder for FGM of different number of layers



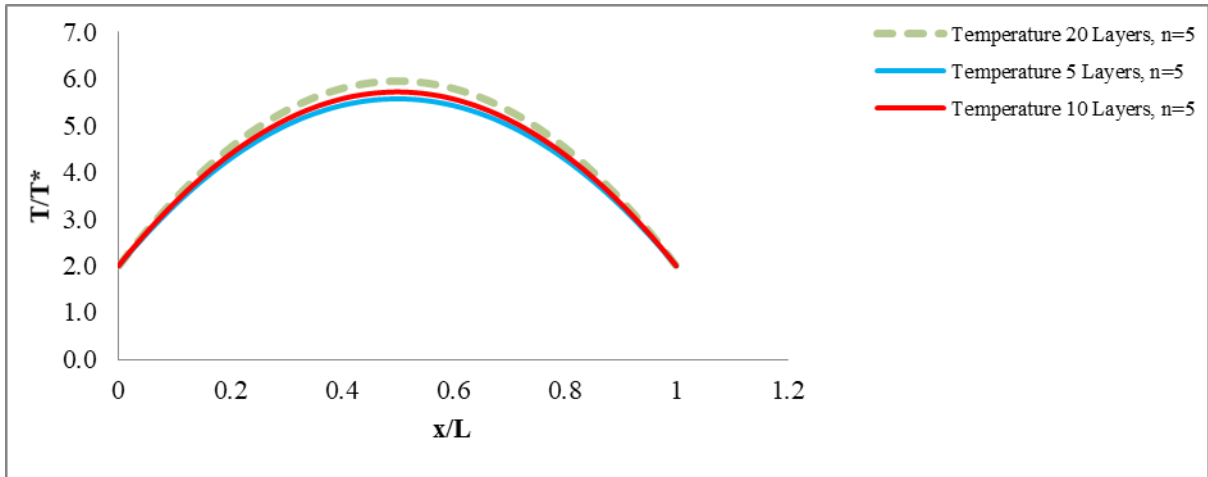


Figure 4.7c: Comparison of distribution of temperature along the middle surface in FGM cylinder for FGM of different number of layers .

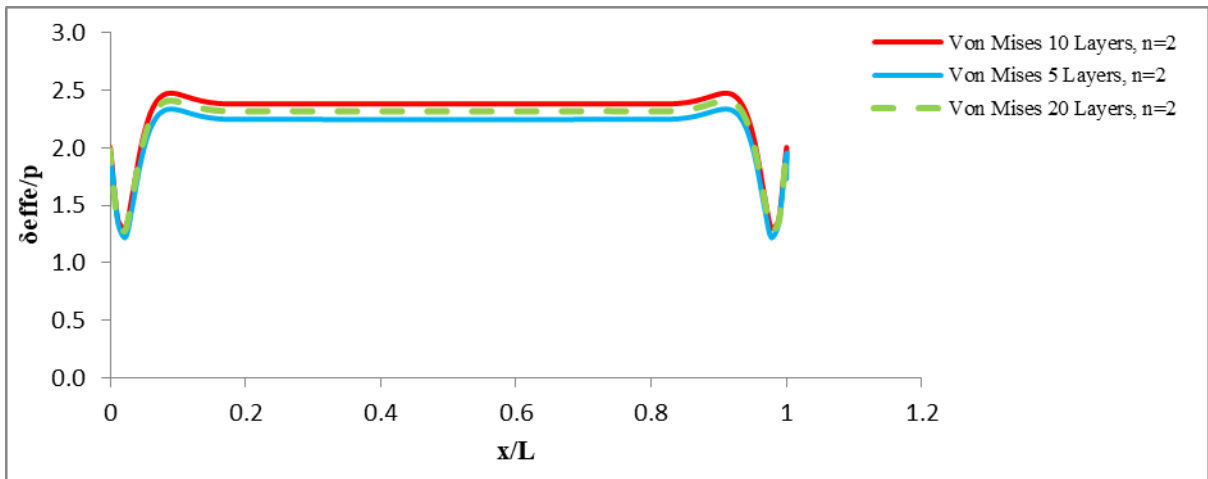


Figure 4.7d: Comparison of distribution of Von mises along the middle surface in FGM cylinder for FGM of different number of layers

#### 4.4.2 The effect of non-homogeneity factor (n)

A further study on the effect of non-homogeneity factor (n) was also considered, the n-factors considered for this study were n=1, 2, and 5. Similarly, parameters considered were temperature distribution, radial displacement, axial displacement and Von-mises stress, all considered along the middle of the cylinder. The loading conditions, boundary conditions and ambient condition were constant for the various studies. Fig. 4.8a, 4.8b, 4.8c & 4.8d depict the performances of the FGM models with different n-factors considered under the various parameters. From these figures, it can be seen that non-homogeneity (n) factor of Zirconia/Titanium FGM has a significant effect on the FGM's performance when subjected to loading conditions. It clearly shows that as non-homogeneity factor increases, temperature distribution, radial displacement and Von-mises stress significantly increases proportionately,

the only exception is the axial displacement that shows slight discrepancy in the proportionate increase. This is as shown in Table 4.2.

Table 4.2: Summary table for comparison of the results for different layers and n-factors for the four parameters at  $x = L/2$  &  $z = 0$ .

		n=1	n=2	n=5
<b>Radial displacement (mm) (U1)</b>	10 Layers	0.0001179	0.0001163	0.0001234
	5 Layers	0.000118	0.0001166	0.0001233
<b>Axial displacement (mm) (U2)</b>	10 Layers	0	0	0
	5 Layers	0	0	0
<b>Von Mises (Pa) (<math>\delta_{eff}</math>)</b>	10 Layers	1.78E+08	1.91E+08	2.05E+08
	5 Layers	1.67E+08	1.80E+08	1.97E+08
<b>Temperature (T) (<math>^{\circ}</math>C)</b>	10 Layers	95.2912	110.412	143.009
	5 Layers	95.3427	109.892	139.346

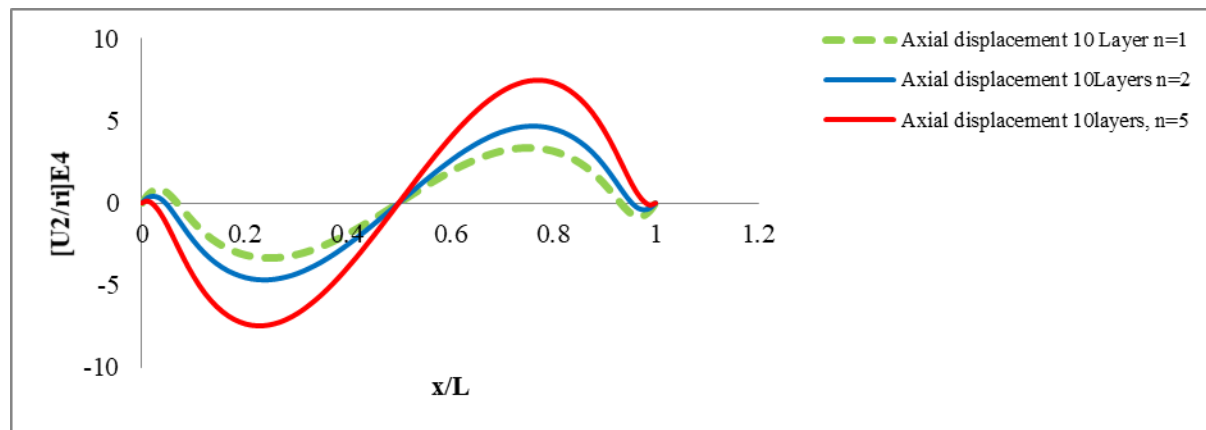


Figure 4.8a: Comparison of distribution of axial displacement along the middle surface in FGM cylinder for FGM of different n-factors (non-homogeneity factor)

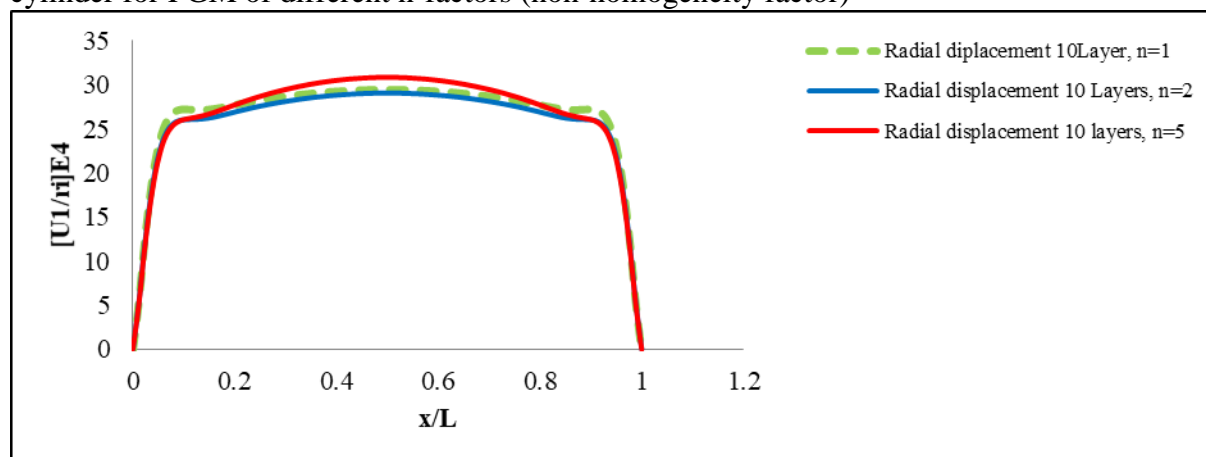


Figure 4.8b: Comparison of distribution of radial displacement along the middle surface in FGM cylinder for FGM of different n-factors (non-homogeneity factor)

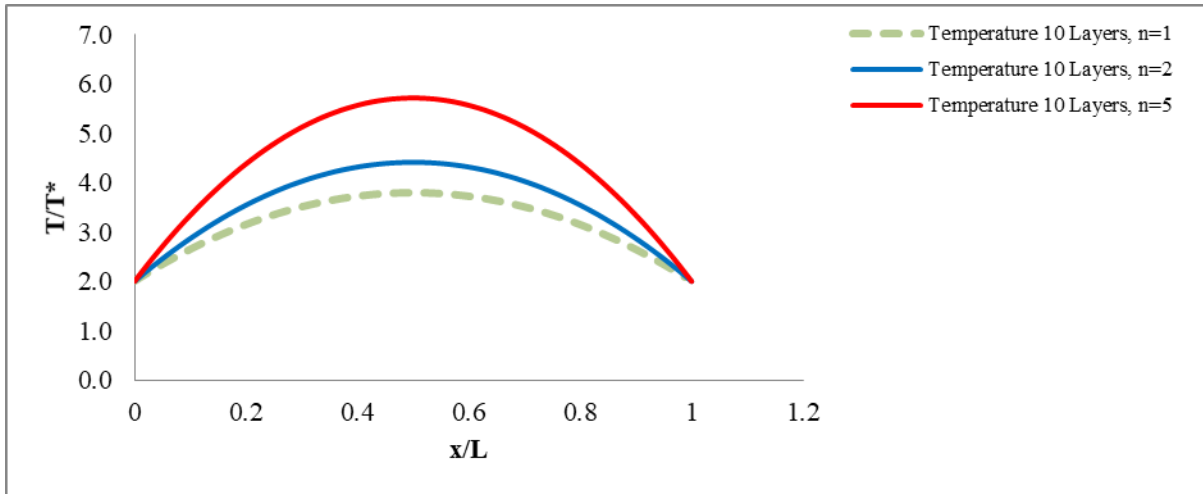


Figure 4.8c: Comparison of distribution of temperature along the middle surface in FGM cylinder for FGM of different n-factors (non-homogeneity factor)

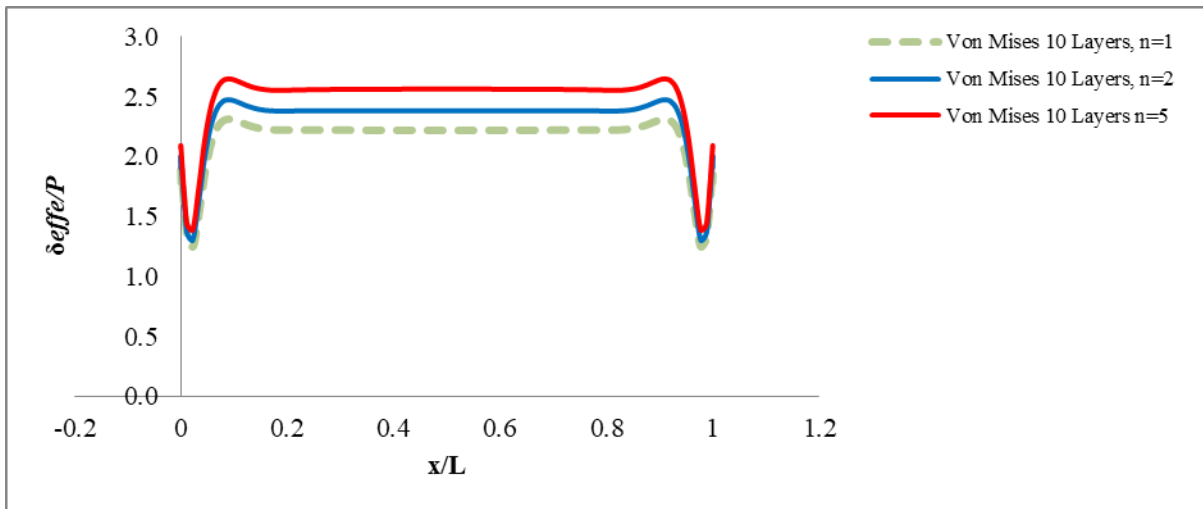


Figure 4.8d: Comparison of distribution of Von-mises along the middle surface in FGM cylinder for FGM of different n-factors (non-homogeneity factor)

#### 4.5. CONCLUDING REMARKS

The numerical investigation of an axisymmetric cylindrical pipe constructed with Zirconia and Titanium FGM with variable number of layers subjected to thermal and mechanical loading was considered using the Abaqus software. A series of results validation was also undertaken on the model to ascertain the validity of the FGM Models.

The FGM finite element models developed were validated against already published results with ANSYS and first order-shear deformation theory (FSDT) from Ghannad et. al 2017 and it shows good agreement. The FGM finite element models were able to closely depict the behaviour of the Zirconia/Titanium axisymmetric cylindrical model subjected to mechanical and thermal loading. Hence, a parametric study was conducted to understand further the effect of number of layers and non-homogeneity factor (n) on the FGM Model.

It was also seen that the number of layers of FGM has no effect on the radial displacement, but shows slight effect on axial displacement, temperature and Von-mises; as they increase slightly with increase in number of layers with the exception of Von-mises the slightly decreases with further increase in number of layers. However, the study shows that the non-homogeneity (n) factor of the FGM has significant effect on the FGM's performance under loading. It clearly shows that as non-homogeneity factor increases, the radial displacement, temperature distribution and Von-mises equally increase significantly with similar proportion, the only exception is the axial displacement that shows slight discrepancy in its proportionate increase as the n-factor increases.

The validation of the developed methodology in this chapter becomes the basis and reference point for all other models to be developed in subsequent chapters. It is worth of note that the FGM material combination and loading conditions applied for the validated model was informed by the material and loading conditions of the referenced journal by Ghannad.

The subsequent chapters will utilize the same validated approach to determine the design limits for all the piping configuration considered. However, the loading condition, FGM material combination and piping configuration will be based on actual line list data for the referenced offshore oil and gas piping system and candidate material selection from Chapter 3.

## CHAPTER 5 DESIGN LIMIT PREDICTION FOR FGM

### 5.1. DETERMINATION OF EFFECTIVE YIELD STRENGTH OF FGM

To adequately predict the design limit for an FGM component, it is necessary to define some sort of appropriate failure criterion. For an isotropic material, a common industrial approach is to use the Von-mises criterion for three dimensional systems as found in many international pressure vessel codes. With an FGM component, the concept of yield across a section is null and void and therefore an alternative approach is required to provide an equivalent failure criterion. As such, it is necessary to determine the effective yield strength of the entire FGM through the wall thickness of the component. This is challenging, as, to date, there is no known and proven approach of determining an FGM's effective yield strength. The present work has been able to offer an approach to determining the effective yield strength of FGM's.

It is a known fact that the yield strength of each layer of the FGM is unique to that layer, these are dependent on the yield strength of ceramic and metal that made up the FGM. Thus, the volume fractions of ceramic and metallic components that represent the amount of each material in the pipe is used to infer the effective yield strength.

$$V_{ceramic} = \left(\frac{1}{2} - \frac{z}{h}\right)^n \quad [5.1]$$

To determine the volume fractions of ceramics, the pipe thickness (h), the position of ceramics in the entire FGM thickness (z) and non-homogeneity factor must be known.

$$V_{metal} = 1 - V_{ceramic} \quad [5.2]$$

On the same note, the volume fraction of metal was derived by subtracting the ceramic's volume fraction from the entire FGM's volume.

So, the effective yield strength can be written as:

$$\sigma_{y,eff} = \sigma_{y,c} \cdot V_c + \sigma_{y,m} \cdot V_m \quad [5.3]$$

$$\sigma_{y,eff} = \sigma_{y,c} \cdot \left(\frac{1}{2} - \frac{z}{h}\right)^n + \sigma_{y,m} \left(1 - \left(\frac{1}{2} - \frac{z}{h}\right)^n\right) \quad [5.4]$$

with  $\sigma_{y,c}$  and  $\sigma_{y,m}$  as the ceramic and metal yield strength respectively.

From equation 5.4 above it can be seen that the effective yield strength is dependent on the parameter z. The objective is to determine an equation that is only dependent on non-homogeneity parameter "n", as it is the only parameter that will influence the variation of yield strength.

From the known mathematical principles:

For  $n=1$ , there is an equally concentration of ceramic and metal in the FGM. Hence, effective yield strength  $\sigma_{y,eff}$  is the average between  $\sigma_{y,c}$  and  $\sigma_{y,m}$ .

For  $n > 1$ , there is much ceramic than metal in the FGM. Hence, effective yield strength  $\sigma_{y,eff}$  will be closer to the value of  $\sigma_{y,c}$  than  $\sigma_{y,m}$ .

For  $n < 1$ , there is much metal than ceramic in the FGM. Hence, effective yield strength  $\sigma_{y,eff}$  will be closer to the value of  $\sigma_{y,m}$  than  $\sigma_{y,c}$ .

From equation 5.4, in order to eliminate the parameter  $z$  from the equation, it is replaced by a factor “A” represented as thus,

$$A = \left( \frac{1}{2} - \frac{z}{h} \right)^n \quad [5.5]$$

Thus, equation 5.4 is presented as thus:

$$\sigma_{y,eff} = \sigma_{y,c} \cdot A + \sigma_{y,m} \cdot (1 - A) \quad [5.6]$$

The next step is to find the expression of A that is dependent of the n parameter.

From equation 5.5, we know that,

$$\left\{ \begin{array}{l} A = \frac{1}{2} \text{ when } n = 1 \text{ (half metal/half ceramic)} \\ A = 0 \text{ when } n = 0 \text{ (full metal)} \\ A = 1 \text{ when } n \rightarrow \infty \text{ (full ceramic)} \end{array} \right.$$

The above scenarios was represented graphically, consequently, the function A (n) evolves as stated in Figure 5.1 below:

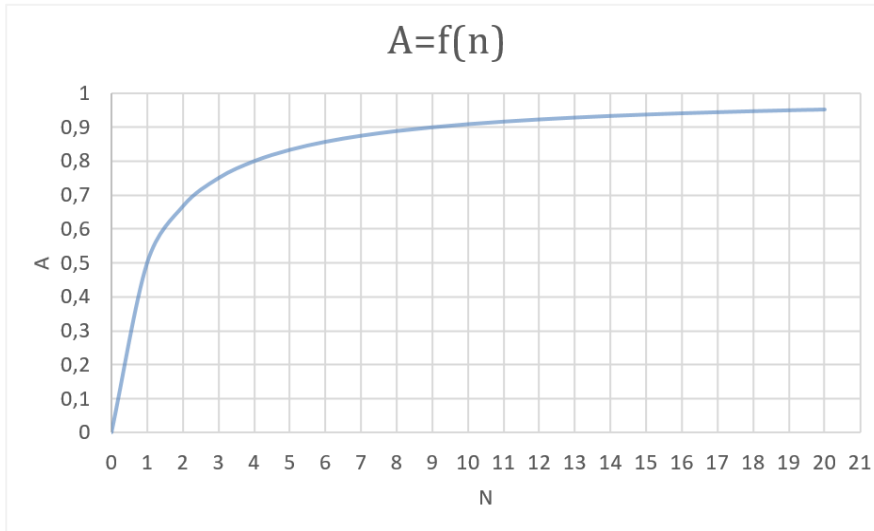


Fig. 5.1: Curve representing “A” as a function A (n)

This function has the following equation,

$$A(n) = \frac{n}{n+1} \quad [5.7]$$

Indeed,

$$\begin{cases} A(1) = \frac{1}{2} \\ A(0) = 0 \\ \lim_{n \rightarrow \infty} A(n) = 1 \end{cases}$$

From Equation 5.7 and 5.6, the effective yield strength as a function of non-homogeneity parameter “n” is determined in equation 5.8.

$$\sigma_{y,eff} = \sigma_{y,c} \cdot \left(\frac{n}{n+1}\right) + \sigma_{y,m} \cdot \left(\frac{1}{n+1}\right) \quad [5.8]$$

Equation 5.8 gives the effective yield strength of the pipe depending only on the non-homogeneity parameter n. The properties of the identified candidate material used is as shown in table 5.1.

Table 5.1: Properties of a typical identified candidate material

	Material properties	E (GPa)	CTE (/K)	Poisson's ratio	k (W/m.K)	Cv (J/kg.K)	Density (kg/m3)	Tensile Strength (MPa)	N	YS (MPa)
Ceramic (inside)	Zirconia (toughened)	246.5	0.0000098	0.3	2	450	5740	414	4	414
Metal (outside)	INCOLOY 800 (annealed)	195	0.00001425	0.34	11.5	502.5	7950	620		310

Applying the ceramic and metal yield strength from table 5.1 in equation 5.8 for different values of n. The respective effective yield strength is presented in the table 5.2 below.

Table 5.2: Effective yield strength of the FGM 1 pipe with different non-homogeneity parameter values.

Non-homogeneity parameter (n)	Effective yield strength ( $\sigma_y, \text{eff}$ )
0.5	344.6 MPa
1	362 MPa
2	379.3 MPa
5	396.6MPa

To further verify the accuracy of this developed equation for the effective yield strength, the results in table 5.2 was compared with results derived from the traditional averaging of the yield strength calculated by an average of the layers' yield strength. The average yield strength has the following equation:

$$\sigma_{y,average} = \frac{\sum_{i=1}^l \sigma_{y,i}}{l} \quad [5.9]$$

with,

$l$ , the number of layers

$\sigma_{y,i}$  , the yield strength of the layer number  $i$

A comparison of the results for the effective yield strength using the averaging approach and the developed technique for different number of layers and non-homogeneity factor is as presented below.

Table 5.3: Comparison for n=0.5

Number of layers	$\sigma_{y, \text{average}}$ (MPa)	$\sigma_{y, \text{eff}}$ (MPa)	Relative error (%)
5	343.5	344.6	0.32
10	345.3	344.6	0.2
20	344.9	344.6	0.09

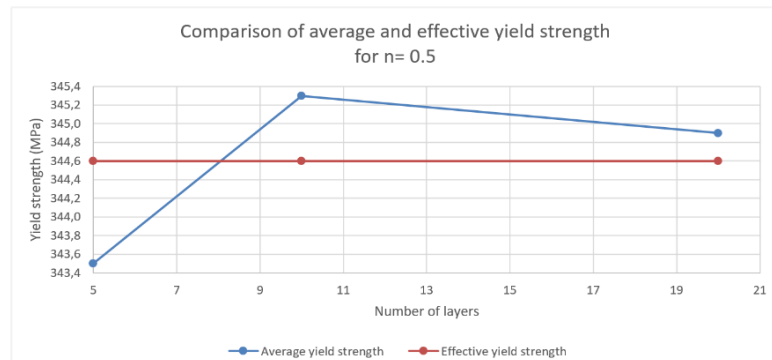




Table 5.4: Comparison with n=1

Number of layers	$\sigma_{y, \text{ average}}$ (MPa)	$\sigma_{y, \text{ eff}}$ (MPa)	Relative error (%)
5	360.9	362	0.77
10	362	362	0
20	362	362	0

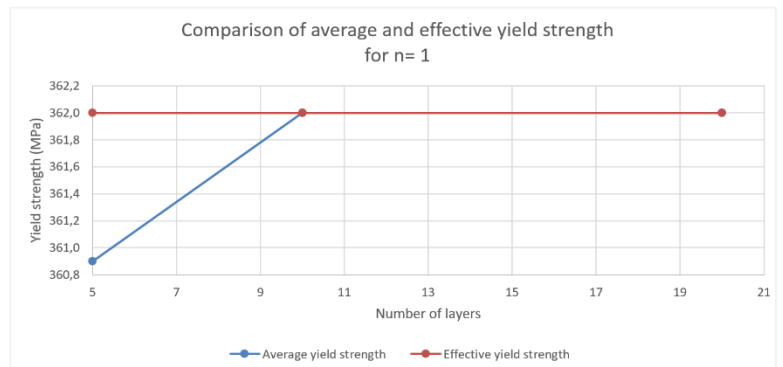


Table 5.5: Comparison with n=2

Number of layers	$\sigma_{y, \text{ average}}$ (MPa)	$\sigma_{y, \text{ eff}}$ (MPa)	Relative error (%)
5	378.4	379.3	0.24
10	379.1	379.3	0.05
20	379.3	379.3	0

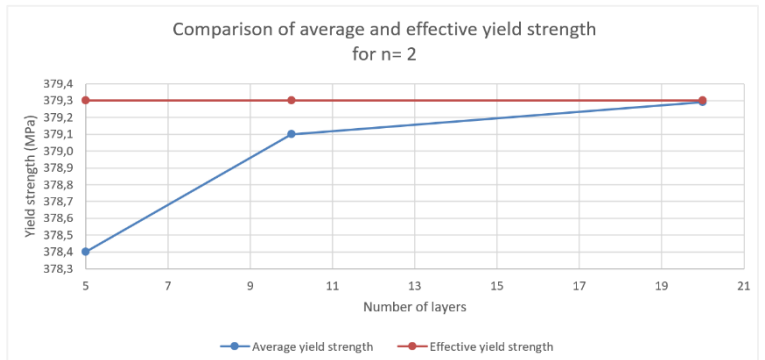
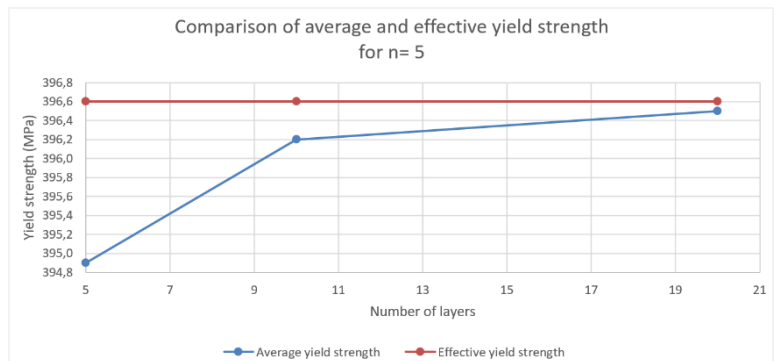


Table 5.6: Comparison with n=5

Number of layers	$\sigma_{y, \text{ average}}$ (MPa)	$\sigma_{y, \text{ eff}}$ (MPa)	Relative error (%)
5	394.9	396.6	0.43
10	396.2	396.6	0.10
20	396.5	396.6	0.03



The outcome of the effective yield strength utilizing the two approaches as detailed above (traditional averaging and novel approach), show less than 0.5% deviation in outcome for all the number of layers considered and for all the non-homogeneity factor considered.

It was also observed that the accuracy of the outcome from the develop technique increases with increase in number of layers, this validates the appropriateness of the novel approach in determining the effective yield strength of FGM traditional approach will be cumbersome for FGM's with layer number of layers.

## 5.2. FEA OF THE IDENTIFIED CANDIDATE MATERIALS-USING STRAIGHT PIPE CONFIGURATION AS CASE STUDY

### 5.2.1 Description of the model

Having identified the candidate materials and a suitable approach to determine the effective yield strength the analysis in the preceding sections focused on how to determine the design limits for each of the candidate materials identified in Chapter 3 for all pipe configurations considered. The subsequent sections detailed all numerical analysis and models developed and was used to determine the design limits for each of the candidate material for the straight pipe configuration. A 12 inches Schedule 80 straight pipe was considered for the analysis; this is to replicate the referenced piping system.

### 5.2.2 Part Module

The part used was an axisymmetric part along the Y- axis, thus, the cross-section of the pipe along its thickness was created.

The axisymmetric part was modelled different layers consideration; it is a 12'' schedule 80 straight pipe, which means that the inner radius is 144.47 mm and the wall thickness is 17.48 mm. The length does not play a role in the modelling, 800mm was used for the pipe length.

- $L = 800$  mm
- $r_i = 144.47$  mm
- $r_o = 161.95$  mm
- $t = 17.48$  mm

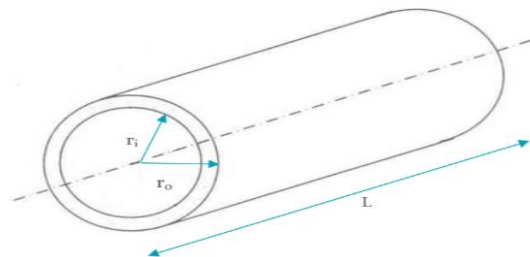


Fig 5.2: A typical representation of the axisymmetric modelled pipe in 3D.

### 5.2.3 Property Module

The property module is a tool on Abaqus that guides and enable the user to select and assign specific material properties to any identified section of the modelled part on Abaqus. This tool was used to assign material properties to the modelled axisymmetric FGM pipe modelled.

From the detailed material selection process done in the chapter three that was driven by the requirement of the Deep Water Oil and Gas operations. Based on these requirements and economics four (4) distinct FGM combinations (Metal and Ceramics) were developed to be able to meet the need of the operations.

The metals and ceramics used for the Four (4) distinct FGMs are as detailed below:

Metal 1: Ni-Fe-Cr alloy, INCOLOY 800, annealed  
Metal 2: Stainless steel, austenitic, ASTM CF-20, cast, water quenched  
Metal 3: Copper, C14200, soft

Ceramic 1: Zirconia, transformation toughened, L  
Ceramic 2: Alumina 94, SGM  
Ceramic 3: Silicon carbide, HIP  
Ceramic 4: Tungsten carbide, hot press

The combination of these materials (Metal and Ceramic) was used for Four (4) FGM's is as stated below:

Table 5.7: Composition of the four different FGMs.

FGM 1	FGM2	FGM3	FGM4
Metal1-Ceramic1	Metal2-Ceramic2	Metal3-Ceramic3	Metal3-Ceramic4

As stated above, Seven (7) materials were considered in this study for the FGM combinations. All the properties of these materials were found from CES Edupack and are as presented in details in the table 5.8 below:

Table 5.8: Mechanical and thermal properties of the metal and ceramic materials.

	E (GPa)	Coefficient of thermal expansion CTE( /K)	Poisson's ratio	Thermal conductivity k (W/m.K)	Specific HeatCapacity Cv (J/kg.K)	Density (kg/m3)	Tensile Strength (MPa)	Ranking	Yield Strength (Mpa)
<b>Ranking for Metal</b>									
Nickel-Fe-Cr alloy, INCOLOY 800, Annealed	195	14,25	0,34	11,5	502,5	7950	620	1	310
Stainless Steel, austenitic, ASTM CF-20 , cast, water quenched	195	17,5	0,27	15,5	500	7765	530	2	250
Copper C14200, Soft	122,5	17,5	0,345	165,5	380,5	8925	220	3	55
<b>Ranking for Ceramics</b>									
Zirconia (Transformation toughened) L	246,5	9,8	0,3	2	450	5740	414	1	414
Alumina 94 (SGM)	330	7,55	0,24	21	880	3650	250,5	2	250
Silicon Carbide (HIP)	400	5	0,15	80,05	802	3145	500,5	3	500
Tungsten Carbide (Hot Press)	669	5,8	0,21	29	180	15700	352,5	4	352

To be able to determine the FGM properties at a specified position, the volume fractions of both the metal and ceramic was used. This is as shown in the equation 5.9 and 5.10 below:

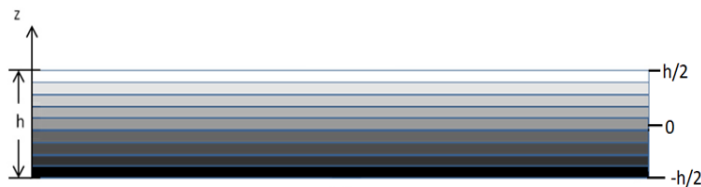


Figure 5.3: Picture depicting position of Metal/Ceramics in the FGM

$$V_{ceramic} = \left(\frac{1}{2} - \frac{z}{h}\right)^n \quad [5.9]$$

$$V_{metal} = 1 - V_{ceramic} \quad [5.10]$$

with,

- $h$  the thickness of the pipeline
- $z$  the position in the thickness ( $-h/2 < z < h/2$ )
- $n$  the non-homogeneity parameter

From the above figure, it should be noted that for  $z=h/2$ ,  $V_{\text{ceramic}} = 0$  and  $V_{\text{metal}} = 1$ , conversely for  $z=-h/2$ . Hence, it is logical that at  $z=h/2$  the FGM is fully metal and at  $z=-h/2$  it is fully ceramic. From the equations above, a new parameter, the non-homogeneity parameter ( $n$ ) has been introduced. This parameter represents how the variation of the properties progresses along the thickness.

Having known the effect of non-homogeneity factor and volume fraction as stated in chapter four, the properties of the FGM at any point could be determined with the power law equations 4.1, 4.2 and 4.3 as stated in chapter four (4).

These equations are used to calculate all the different properties along the thickness of the axisymmetric pipe, an example is shown in the preceding tables for FGM 1, Five (5) Layers and  $n=1$ .

Table 5.9: Development of the properties along the thickness with  $n=1$  for the FGM 1.

Material properties	E (GPa)	CTE(/K)	Poisson's ratio	k (W/m.K)	Cv (J/kg.K)	Density (kg/m3)	Tensile Strength (MPa)	N	YS (Mpa)
Zirconia (toughened)	246.5	0.0000098	0.3	2	450	5740	414	1	414
INCOLOY 800 (annealed)	195	0.00001425	0.34	11.5	502.5	7950	620		310
Position [-h/2 ; h/2]	E	CTE	k	k (W/m.K)	Cv	d	Tensile Strength (MPa)	Yield strength	
-1.00E-02	246.5	9.80E-06	0.30	2.0	450.0	5740	414	414	
-9.00E-03	243.9	1.00E-05	0.30	2.5	452.6	5851	424	409	
-8.00E-03	241.4	1.02E-05	0.30	3.0	455.3	5961	435	404	
-7.00E-03	238.8	1.05E-05	0.31	3.4	457.9	6072	445	398	
-6.00E-03	236.2	1.07E-05	0.31	3.9	460.5	6182	455	393	
-5.00E-03	233.6	1.09E-05	0.31	4.4	463.1	6293	466	388	
-4.00E-03	231.1	1.11E-05	0.31	4.9	465.8	6403	476	383	
-3.00E-03	228.5	1.14E-05	0.31	5.3	468.4	6514	486	378	
-2.00E-03	225.9	1.16E-05	0.32	5.8	471.0	6624	496	372	
-1.00E-03	223.3	1.18E-05	0.32	6.3	473.6	6735	507	367	
0	220.8	1.20E-05	0.32	6.8	476.3	6845	517	362	
1.00E-03	218.2	1.22E-05	0.32	7.2	478.9	6956	527	357	
2.00E-03	215.6	1.25E-05	0.32	7.7	481.5	7066	538	352	
3.00E-03	213.0	1.27E-05	0.33	8.2	484.1	7177	548	346	
4.00E-03	210.5	1.29E-05	0.33	8.7	486.8	7287	558	341	
5.00E-03	207.9	1.31E-05	0.33	9.1	489.4	7398	569	336	
6.00E-03	205.3	1.34E-05	0.33	9.6	492.0	7508	579	331	
7.00E-03	202.7	1.36E-05	0.33	10.1	494.6	7619	589	326	
8.00E-03	200.2	1.38E-05	0.34	10.6	497.3	7729	599	320	
9.00E-03	197.6	1.40E-05	0.34	11.0	499.9	7840	610	315	
1.00E-02	195.0	1.43E-05	0.34	11.5	502.5	7950	620	310	

Table 5.101: Example of properties in each layer for  $l = 5$  (FGM 1,  $n=1$ ).

Layer number	E (GPa)	Coefficient of thermal expansion CTE( /K)	Poisson's ratio	Thermal conductivity k (W/m.K)	Specific HeatCapacity Cv (J/kg.K)	Density (kg/m3)	Tensile Strength (MPa)	Yield strength
Layer 1	241.35	1.02E-05	0.30	3.0	455.3	5961	434.6	398.4
Layer 2	231.05	1.11E-05	0.31	4.9	465.8	6403	475.8	382.8
Layer 3	220.75	1.20E-05	0.32	6.8	476.3	6845	517	362.0
Layer 4	210.45	1.29E-05	0.33	8.7	486.8	7287	558.2	341.2
Layer 5	200.15	1.38E-05	0.34	10.6	497.3	7729	599.4	320.4

This is repeated for the entire non-homogeneity factor being considered and for all the FGM also. Generally four (4) models were developed based on FGM combination stated above and

for each of these four FGM's, another five models were developed based on the non-homogeneity factor value.

#### 5.2.4 Step Module

The model deployed a coupled temperature-displacement analysis, this is premised on the fact that temperature will create some stress in the pipe. The time period of step is 1800 seconds with an automatic increment was used.

#### 5.2.5 Load Module

In this module, both boundary conditions with mechanical and thermal loadings were implemented. It is vital to note that the loadings are not yet known as it will be determined based on the design limits for each FGM. However, to arrive at the design limits the initial loading with thermal loading of 427 K and a pressure of 3.2 MPa both on the inner surface were applied. These values were changed in order to be as close as possible of the design limit. It is vital to note that the pressure was applied as loading on Abaqus, while the temperature was applied as a boundary condition. The other boundary condition implemented is a Y symmetry on the top and bottom of the pipe. This boundary condition prevents the pipe from moving along the Y axis and rotating around the X and Z axis and an ambient temperature of 298K was implemented in the whole pipe through the predefined field on Abaqus. This is represented in figure 5.4 below.

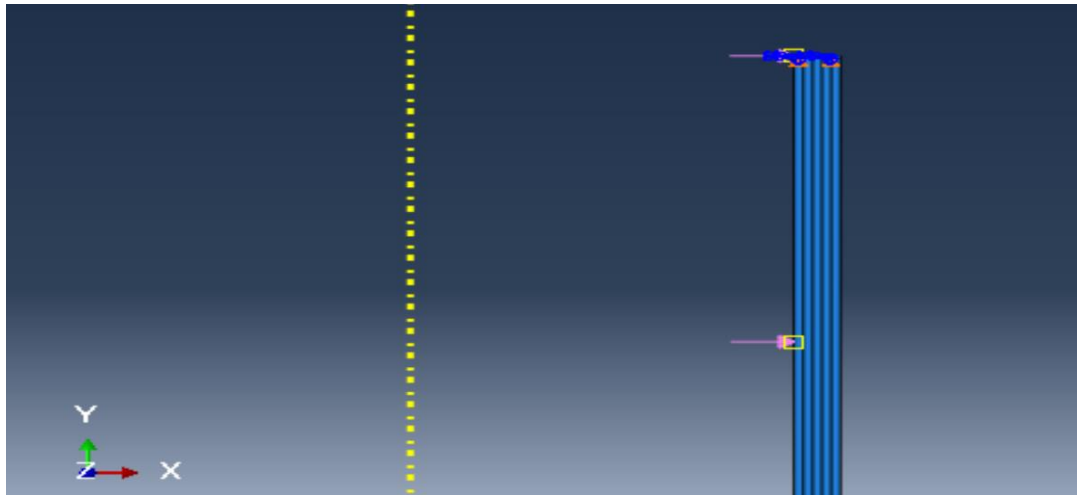


Fig. 5.4: Loading and boundary conditions on the axisymmetric pipe

#### 5.2.6 Mesh Module

The mesh used divides the part in 100 linear quadrilateral elements of type CAX4T. This type of element is a 4-node axisymmetric thermally coupled quadrilateral, bilinear displacement and temperature elements. It enables Abaqus to calculate the coupled thermal-mechanical stress at each node. In addition, a linear interpolation between the values at each node was used.

### 5.3. ESTABLISHING THE DESIGN LIMIT FOR THE FGM'S

In this section, the steps taken to determine the design limit for the first FGM that is composed of the Ni-Fe-Cr alloy (INCOLOY 800) for the metal and the Zirconia (transformation toughened) for the ceramic is described. This same approach is applicable to the remaining three FGM's.

The first approach was the model of an FGM with 5-layered part and non-homogeneity factor,  $n=1$ . The yield strength for FGM 1 and  $n=1$  is 362 MPa (calculated with the effective yield strength equation 5.8).

The pressure was kept constant at 3.2 MPa initially and the temperature was varied starting from 427K. The iterative method deployed for the temperature design limit determination is represented in figure 5.5a below. In a similar manner, the temperature was kept constant at determined temperature design limit and the pressure was varied starting from 3.2MPa. Same iterative method was deployed for the pressure design limit determination as represented in figure 5.5b below. In summary if Von-mises stress is higher than the yield strength, the temperature is reduced. Conversely, if the Von-mises stress is lower than the yield strength, the temperature is increased. This is repeated until a point is achieved when the yield strength is almost same with the Von-mises stress; that means the normalized stress in equation 5.14 is almost equal to 1.

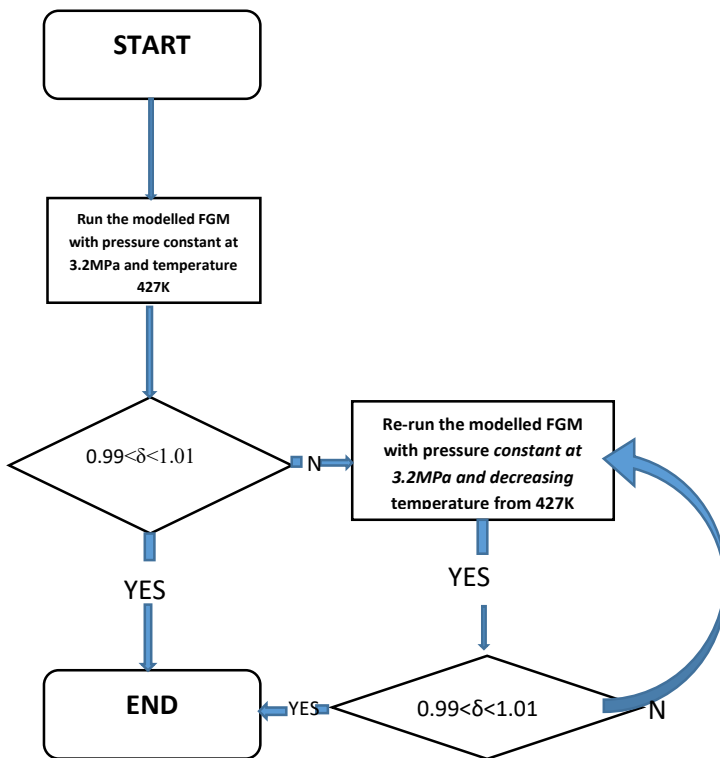


Figure 5.5a2: Approach adopted for the temperature loading.

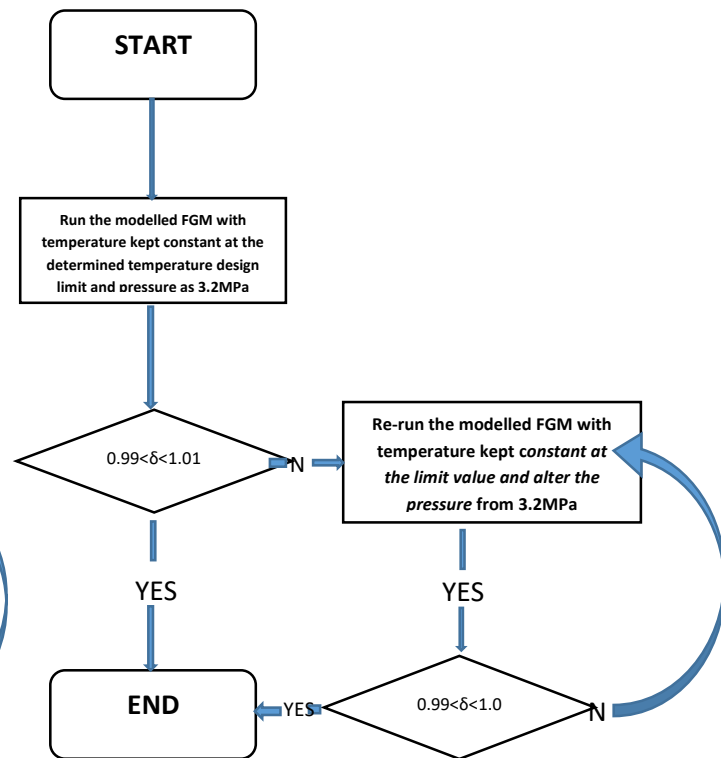


Figure 5.5b3: Approach adopted for the pressure loading

The check for failure criterion is to know if the Von-mises stress induced in the material is equal to or exceeds the material yield strength (for ductile material). This can be simplified as detailed in equation 5.14 below:

$$\delta_{VM} \geq \delta_y \quad [5.14]$$

Where  $\delta_{VM}$  is the maximum Von-mises stress and  $\delta_y$  is the yield stress.

Table 5.6 was used to determine the yield strength in each of the elbow pipe layer and the result from the Abaqus software can be used to determine the Von-mises stress localized to each layer of the FGM for a given Pressure and Thermal Loading. To enable the adequate comparison of the values of equation 5.14 in all the FGM layers and predicts the possibility of failure (yielding) in any of the layers, a normalized stress approach was adopted based on the principle of equation 5.15 as thus:

$$\sigma_{norm} = \frac{\sigma_{VM,max}}{\sigma_{y,eff}} \quad [5.15]$$

Equation 5.15 was used to determine the risk of failure through yielding if the normalized stress is greater than one (1); that means the material has exceeded the elastic limit. However, if the normalized stress is less than one (1), then there is no risk of failure due to yielding. It is vital to note that the FGM design limit is reached when any of the FGM's layer normalized stress is closest to one (1), above this limit the material will begin to yield (Fail). For the purpose of this research the normalized stress is between  $0.99 < \text{normalized stress} < 1.01$ .

Thus, for FGM 1 and non-homogeneity factor of 1, applying a thermal loading of 419K the Von-mises from Abaqus software is as presented in the figure below.

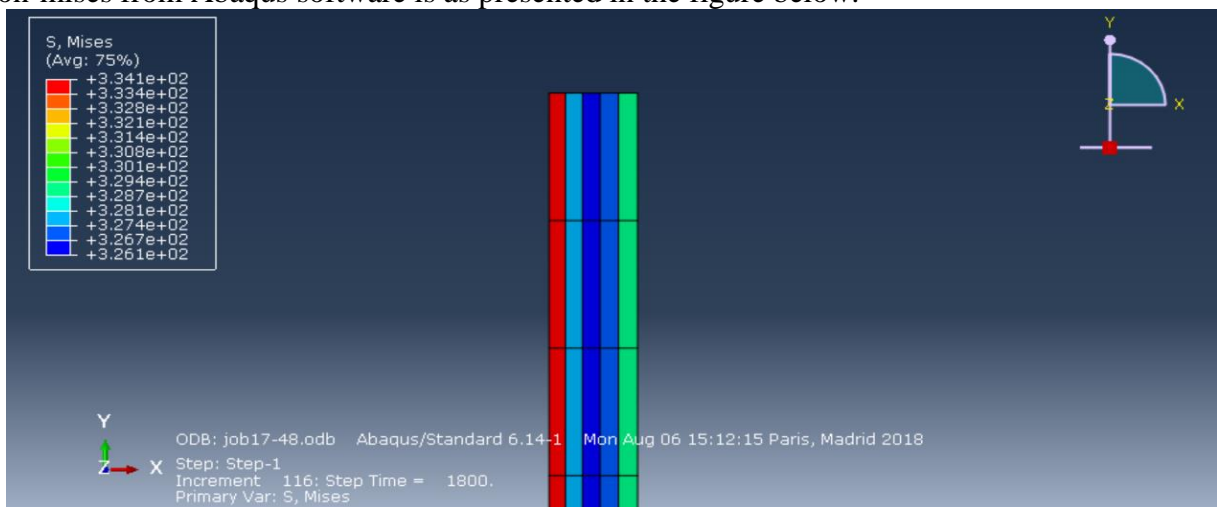


Fig. 5.6 : Von-mises stress in the pipe for FGM 1 and n=1.

Applying equation 5.15, 5.8 and the value of the yield strength for each of the layer, table 5.11 and figure 5.7 was developed.

Table. 5.11 : Normalised stress in 5-layer pipe with FGM 1, n=1 and T=419K

	Maximum Von Mises stress (MPa)	Yield strength (MPa)	Normalised stress
Layer 1	334	398	0.8392
Layer 2	328	382	0.8586
Layer 3	326	362	0.9005
Layer 4	327	341	0.9589
Layer 5	329	320	1.0281

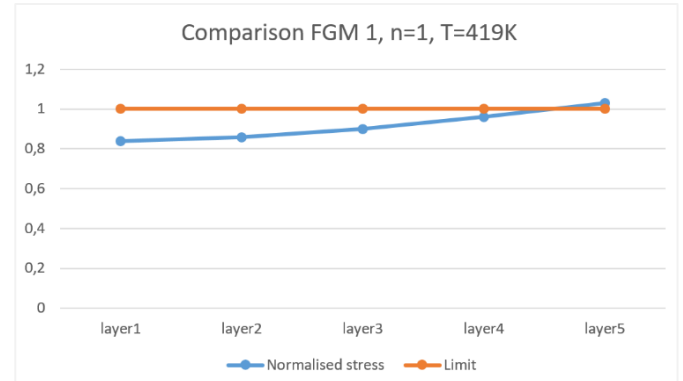


Fig. 5.7: Representation of the normalised stress in the layers of the FGM 1, n=1 pipeline for T=419K.

From the above figures, layer 5 will yield due to the fact that the Von mises stress is greater than the yield strength in the Material, hence the thermal loading is decreased to 415K so as to achieve a reduced Von mises stress. This will ensure that the normalized stress is between  $0.99 < \text{normalized stress} < 1.01$ .

Table 5.12: Normalised stress in 5-layer pipe with FGM1, n=1 and T=415K.

	Maximum Von Mises stress (MPa)	Yield strength (MPa)	Normalised stress
Layer 1	324	398	0.8141
Layer 2	318	382	0.8324
Layer 3	316	362	0.8729
Layer 4	317	341	0.9296
Layer 5	319	320	0.9969

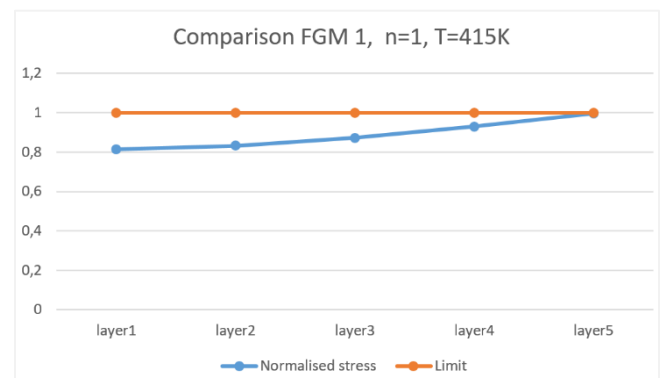


Fig. 5.84: Representation of the normalised stress in the layers of the FGM 1, n=1 pipeline for T=415K.

From the above figures, it is clear that the condition for design limit is achieved at a maximum temperature is 415K for FGM=1, n=1. This same approach was replicated as detailed in table 5.5b was used for Pressure loading and the other FGM's with the corresponding non homogeneity factors (n). The results for all the design limits obtain for the straight pipe axisymmetric FGM pipes is as detailed in tables 5.13 and 5.14.



Table 5.13: Straight Pipe Temperature Design Limits

Straight Pipe Temperature Design Limit				
	FGM1	FGM2	FGM3	FGM4
n=1	415	366	323.5	315.5
n=2	419	375	331.5	318
n=3	423	373	338	326.6
n=4	425	372	344	322
n=5	427	373	353	324.5

Table 5.14: Straight Pipe Pressure Design Limits

Straight Pipe Pressure Design Limit				
	FGM1	FGM2	FGM3	FGM4
n=1	10	3.3	13	15
n=2	13	3.5	23	21
n=3	12	6.5	27	24
n=4	12	8	33	26
n=5	16	9	36	27

A further comparison of the design limits for the FGM's was performed, this was to give better insight on the FGM's design limits when the non-homogeneity factor is altered. This is as presented in figures 5.9 and 5.10

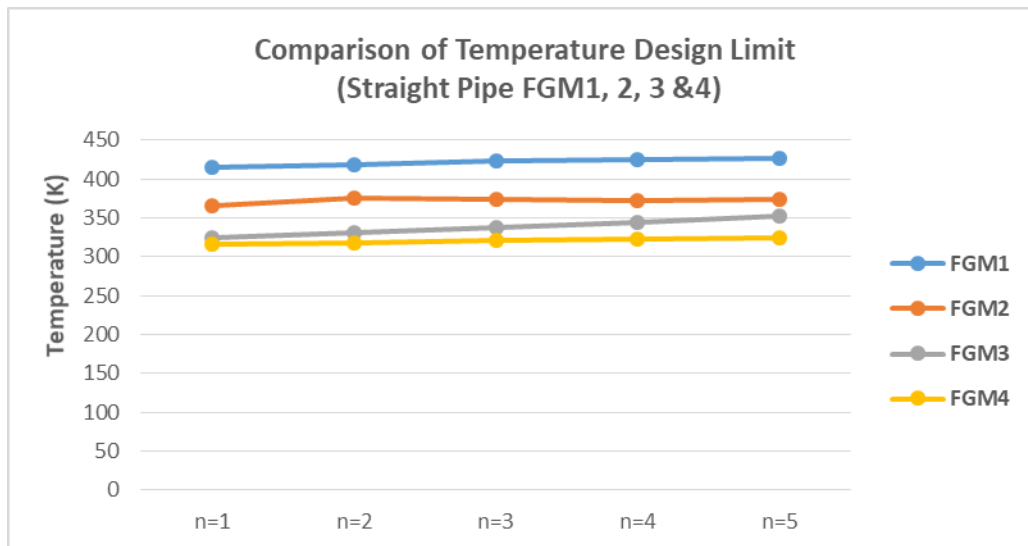


Fig. 5.9: Temperature Design Limit comparison for the FGM's

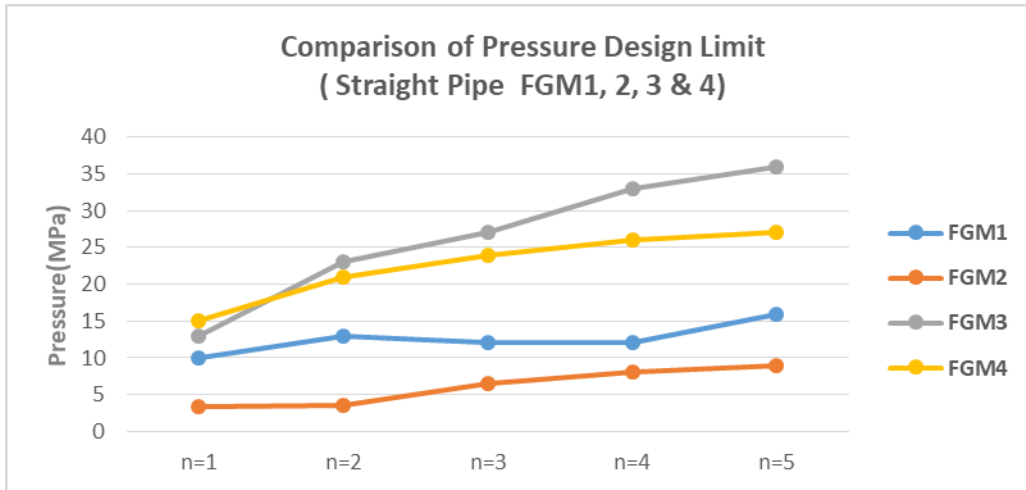


Fig. 5.10: Temperature Design Limit comparison for the FGM's

#### 5.4. CONCLUDING REMARKS

The results from table and figure 5.9 revealed the temperature design limits for the four FGM configurations and the influence of non-homogeneity factor on these limits. It shows that the FGM material combination and non-homogeneity factor has significant influence on temperature design limits of FGM, it shows direct proportionality with increase in non-homogeneity factor.

On the same note, the results from table and figure 5.10 revealed that pressure design limit is equally influenced by both non-homogeneity factor and material combination, with pressure design limit increasing proportionately with non-homogeneity in most cases.

Furthermore, the research proffered an approach to determine the effective yield strength of multiple layered FGM's. The developed approach was benchmarked with the convention averaging approach for limited layered FGM, and it showed good agreement as the result converges with higher number of layers. In addition, the temperature and pressure design limits for 20 distinct FGM's with different material combinations and non-homogeneity factor under thermal and pressure loading was determined. This limits for all the FGM's as a function of temperature and pressure are represented in Figure 5.11.

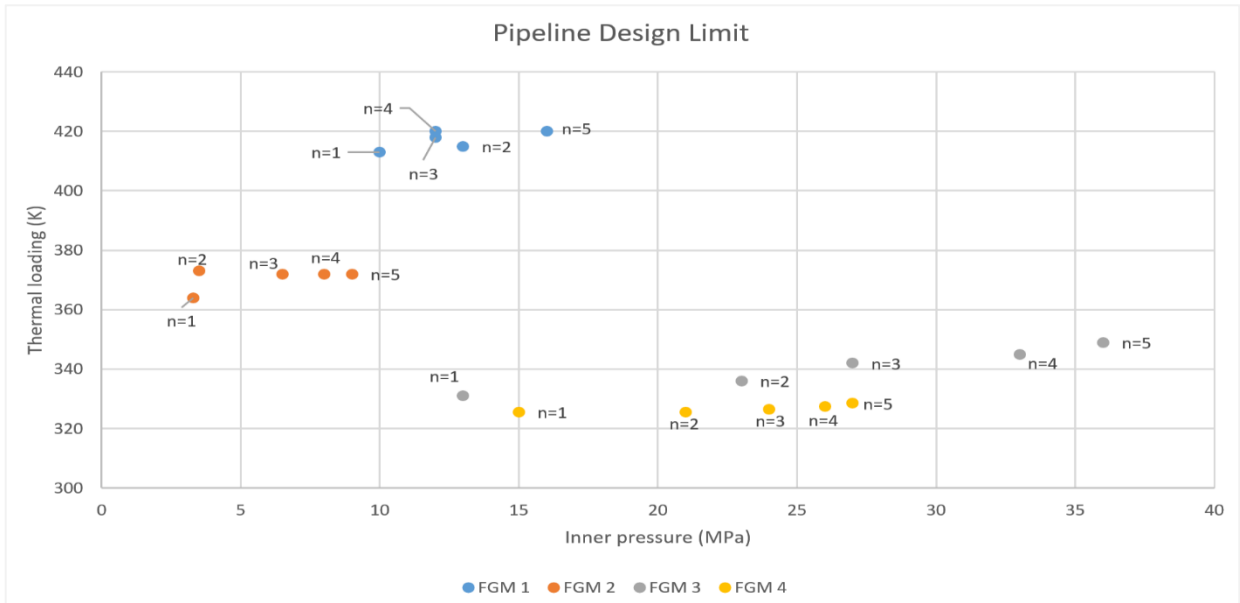


Fig. 5: Design limit for the FGM pipeline depending on the inner pressure and thermal loading.

## **CHAPTER 6: ELBOW PIPE CONFIGURATION FGM DESIGN LIMITS AND ITS IMPACT ON THE FGM BEHAVIOUR**

### **6.1. INTRODUCTION**

Pipelines and piping are increasingly used in oil and gas activities due to the increasing rate of oil and gas exploration and utilization of petroleum product, these pipes are often exposed to high rate of corrosion due to the terrain and environment to which they are deployed. The major protection deployed against corrosion is often coating of the pipeline, however this research has explored the use of Functional Graded Material (FGM) made from the most suitable material to mitigate against the effect of corrosion in oil and gas operations. Models of straight FGM pipes were developed and analysis to help in the determination of the design limits to which these FGM pipe could be deployed in oil and gas operations. The usage of pipe in oil and gas operation is not limited to straight pipes, and it is noted that pipe bends and elbows are also crucial to form parts of the piping system that is widely utilised in oil and gas operations (Jian et. al. 2014).

Elbow pipes normally change the direction of fluid flow in pipelines and piping, hence are exposed to unique type of loading, which includes temperature, internal pressure, torsion, bending moment and sometime a combination of these loading because of thermal expansion (Jian et. al. 2014). On this premise, it is vital to maintain the operational integrity of elbow pipes in the entire piping structure. Furthermore, if this elbow integrity is neglected, it could lead to accidents in the oil or gas facility due to the unique loading system in elbow pipes; this could lead to a great loss. Hence, it is vital to equally determine design limits of elbow pipe under combine loading condition.

In this chapter, the behaviour of an FGM pipe elbow is examined with the aim of predicting its elastic design limit when subjected to numerous loading conditions. Finite Element Analysis of four (4) elbow FGM pipes made of different material combinations is modelled and analysed using the ABAQUS software package, and the resulting allowable pressure and temperature limits are compared with the limits obtained from FGM straight pipes. Further parametric studies are also conducted to determine the influence of non-homogeneity factor on the design limits for the elbow FGM pipes.

### **6.2. MODELLING OF ELBOW PIPES**

The uniqueness of the elbow pipe is its capability to deform (ovalize) when subjected to closing bending moment and internal pressure loading, whilst at the same time, the internal pressure

opposes the pipe's ovalization and try to maintain the pipe cross section to be circular. This is resulted from the Flexibility Factor that enables the pipe to exhibit additional rotation when subjected to Bending Moment as compared to straight pipes (Gaurav & Tembhare, 2013). The FEA of the elbow pipe was guided by the ASME B31.1 codes, but with slight variation from the norm being that the material used was not conventional and the design parameters such as internal pressure and temperature were to be determined for a predefined elbow pipe.

At the time of writing, there is little available in the literature on the design and analysis of FGM piping components, however, Ghannad et. al 2017 has presented the 2D thermo-elastic behaviour of an FG cylinder under thermo-mechanical loads using a first order shear theory, which can be used to validate the approach.

In the present research, the loading on the elbow FGM pipe is therefore limited to internal pressure and temperature loading only, and the outcome was used to determine the design limits of the identified candidate materials. Further parametric studies were performed on the elbow FGM Pipes to provide insight on elbow FGM behavior when certain properties are varied. The preceding sections focused on the elbow FGM geometry development, material selection, loading, boundary conditions and results.

### 6.2.1 Model Geometry

The elbow FGM Pipe was modelled using the same generic pipe dimensions and schedule as the straight pipe, which is 12 inch nominal bore and Schedule 80 thickness. This was intentionally chosen to be able to benchmark with the straight pipe and the solution being considered for the oil and gas operations. The geometry is as shown in figure 6.2, below.

The elbow model has inner diameter as 288.9mm (i.e.  $r_i = 144.45\text{mm}$ ) and the wall thickness is 17.48mm. The bend angle of the elbow Pipe considered was  $90^\circ$ , also the length of the attached straight pipe is long enough ( $L > 3r$ ) to discount the effect of the end boundary conditions on limit loads of the Elbow FGM giving sufficient die-out distance from any external effects. These dimensions are as shown in Table 6.6 below:

Table 6.6: Elbow Pipe Dimensions

$t(\text{mm})$	$R(\text{mm})$	$r=r_i + t / 2 (\text{mm})$	$L (\text{mm})$	$r_i (\text{mm})$	$\lambda= Rt/r^2$
17.5	200	153.25	1000	144.45	0.149

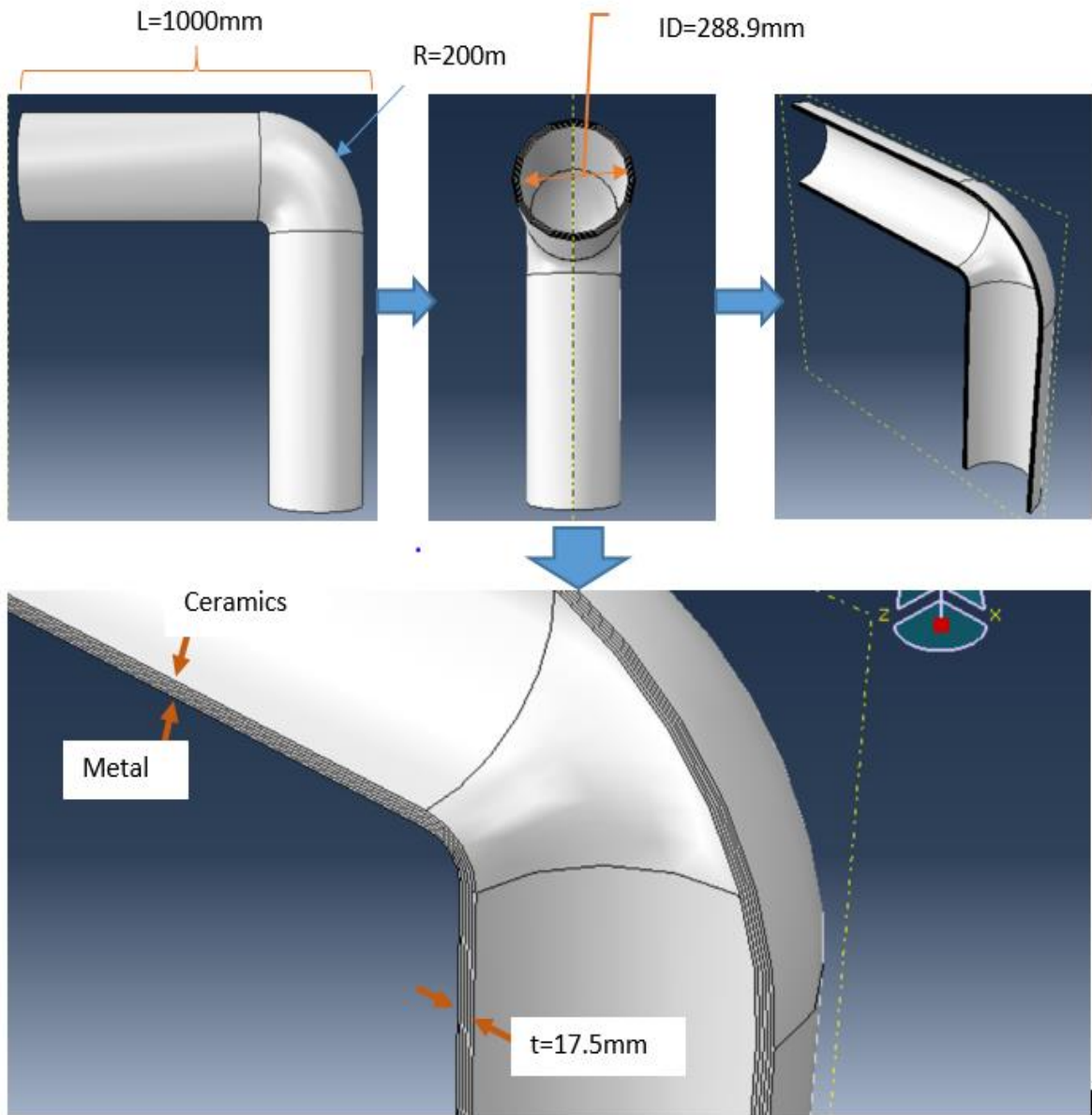


Figure 6.2: Schematic of the Modelled Elbow FGM Pipe

## 6.2.2 Materials

### 6.2.1.1.FGM Material Composition

The detailed material selection process was done in an earlier chapter with the aid of the CES Edupack Software, the choice of the material was driven by the requirement of the Deep Water Oil and Gas operations. Based on these requirements and economics four (4) distinct FGM combinations (Metal and Ceramics) were developed to be able to meet the need of the Operations as stated above. The model deployed the use of ceramics at the inner surface of the Elbow Pipe while metal at the outer surface. This choice was premised on the material properties like high toughness and thermal resistance, high strength and excellent corrosion

resistance. These properties will progressively change from that of ceramic to the metal gradually in the thickness of the pipe.

The metals and ceramics used for the four (4) distinct FGMs are as detailed below:

Metal 1: Ni-Fe-Cr alloy, INCOLOY 800, annealed

Metal 2: Stainless steel, austenitic, ASTM CF-20, cast, water quenched

Metal 3: Copper, C14200, soft

Ceramic 1: Zirconia, transformation toughened, L

Ceramic 2: Alumina 94, SGM

Ceramic 3: Silicon carbide, HIP

Ceramic 4: Tungsten carbide, hot press

The combination of these materials (Metal and Ceramic) was used for Four (4) FGM's is as stated below:

Table 6.2: Composition of the 4 different FGMs.

FGM 1	FGM2	FGM3	FGM4
Metal1-Ceramic1	Metal2-Ceramic2	Metal3-Ceramic3	Metal3-Ceramic4

### 6.2.1.2.FGM Materials Properties

As stated above, seven (7) materials were considered in this study for the FGM combinations. All the properties of these materials were found from CES Edupack and are as presented in details in the table 6.3 below:

Table 6.3: Mechanical and thermal properties of the metal and ceramic materials.

	E (GPa)	Coefficient of thermal expansion CTE( /K)	Poisson's ratio	Thermal conductivity k (W/m.K)	Specific HeatCapacity Cv (J/kg.K)	Density (kg/m3)	Tensile Strength (MPa)	Ranking	Yield Strength (Mpa)
<b>Ranking for Metal</b>									
Nickel-Fe-Cr alloy, INCOLOY 800, Annealed	195	14,25	0,34	11,5	502,5	7950	620	1	310
Stainless Steel, austenitic, ASTM CF-20 , cast, water quenched	195	17,5	0,27	15,5	500	7765	530	2	250
Copper C14200, Soft	122,5	17,5	0,345	165,5	380,5	8925	220	3	55
<b>Ranking for Ceramics</b>									
Zirconia (Transformation toughened) L	246,5	9,8	0,3	2	450	5740	414	1	414
Alumina 94 (SGM)	330	7,55	0,24	21	880	3650	250,5	2	250
Silicon Carbide (HIP)	400	5	0,15	80,05	802	3145	500,5	3	500
Tungsten Carbide (Hot Press)	669	5,8	0,21	29	180	15700	352,5	4	352

To be able to determine the elbow FGM properties at a specified position, the volume fractions equation for both the metal and ceramic was used as detailed in equation 5.9 and 5.10 of chapter 5.

From equations 5.9 and 5.10, for  $z=h/2$ ,  $V_{ceramic} = 0$  and  $V_{metal} = 1$ , conversely for  $z=-h/2$ . Hence, it is logical that at  $z=h/2$ , the FGM is fully metal and at  $z=-h/2$ , it is fully ceramic. The equations

introduced a new parameter known as the non-homogeneity parameter (n). This parameter represents how the variation of the properties progresses through the elbow FGM pipe thickness.

Having known the effect of non-homogeneity factor and volume fraction as stated in the above, the properties of the FGM at any point can be determined with the power law equations as stated in equations 4.1, 4.2 and 4.3 in chapter 4.

These equations are used to calculate all the different properties in the thickness of the elbow pipe, an example is shown in the preceding tables for FGM 1, five (5) layers and n=1.

Table 6.4: Development of the properties along the thickness with n=1 for the FGM 1.

Material properties	E (GPa)	CTE(/K)	Poisson's ratio	k (W/m.K)	Cv (J/kg.K)	Density (kg/m3)	Tensile Strength (MPa)	N	YS (Mpa)
Zirconia (toughened)	246.5	0.0000098	0.3	2	450	5740	414	1	414
INCOLOY 800 (annealed)	195	0.0001425	0.34	11.5	502.5	7950	620		310
Position [-h/2 ; h/2]	E	CTE	k	k (W/m.K)	Cv	d	Tensile Strength (MPa)	Yield strength	
-1.00E-02	246.5	9.80E-06	0.30	2.0	450.0	5740	414	414	
-9.00E-03	243.9	1.00E-05	0.30	2.5	452.6	5851	424	409	
-8.00E-03	241.4	1.02E-05	0.30	3.0	455.3	5961	435	404	
-7.00E-03	238.8	1.05E-05	0.31	3.4	457.9	6072	445	398	
-6.00E-03	236.2	1.07E-05	0.31	3.9	460.5	6182	455	393	
-5.00E-03	233.6	1.09E-05	0.31	4.4	463.1	6293	466	388	
-4.00E-03	231.1	1.11E-05	0.31	4.9	465.8	6403	476	383	
-3.00E-03	228.5	1.14E-05	0.31	5.3	468.4	6514	486	378	
-2.00E-03	225.9	1.16E-05	0.32	5.8	471.0	6624	496	372	
-1.00E-03	223.3	1.18E-05	0.32	6.3	473.6	6735	507	367	
0	220.8	1.20E-05	0.32	6.8	476.3	6845	517	362	
1.00E-03	218.2	1.22E-05	0.32	7.2	478.9	6956	527	357	
2.00E-03	215.6	1.25E-05	0.32	7.7	481.5	7066	538	352	
3.00E-03	213.0	1.27E-05	0.33	8.2	484.1	7177	548	346	
4.00E-03	210.5	1.29E-05	0.33	8.7	486.8	7287	558	341	
5.00E-03	207.9	1.31E-05	0.33	9.1	489.4	7398	569	336	
6.00E-03	205.3	1.34E-05	0.33	9.6	492.0	7508	579	331	
7.00E-03	202.7	1.36E-05	0.33	10.1	494.6	7619	589	326	
8.00E-03	200.2	1.38E-05	0.34	10.6	497.3	7729	599	320	
9.00E-03	197.6	1.40E-05	0.34	11.0	499.9	7840	610	315	
1.00E-02	195.0	1.43E-05	0.34	11.5	502.5	7950	620	310	

Table 6 56: Example of properties in each layer for l = 5 (FGM 1, n=1).

Layer number	E (GPa)	Coefficient of thermalexpansion CTE( /K)	Poisson's ratio	Thermal conductivity k (W/m.K)	Specific HeatCapacity Cv (J/kg.k)	Density (kg/m3)	Tensile Strength (MPa)	Yield strength
Layer 1	241.35	1.02E-05	0.30	3.0	455.3	5961	434.6	398.4
Layer 2	231.05	1.11E-05	0.31	4.9	465.8	6403	475.8	382.8
Layer 3	220.75	1.20E-05	0.32	6.8	476.3	6845	517	362.0
Layer 4	210.45	1.29E-05	0.33	8.7	486.8	7287	558.2	341.2
Layer 5	200.15	1.38E-05	0.34	10.6	497.3	7729	599.4	320.4

This is repeated for the entire non-homogeneity factor being considered and for all the FGM's.

### 6.2.3 Step Module

The elbow pipeline was subjected to a thermal load and an internal pressure, a fully coupled temperature-displacement procedure was used for the analysis. The time period of step is 3600 seconds with an automatic increment was used.

### 6.2.4 Load Module

The boundary conditions, mechanical and thermal loadings were applied to the elbow FGM pipe in this module on the Abaqus software. The approach used for the load application on the elbow pipe is similar to that of the straight pipe. It is vital to note that unlike the conventional



modelling where the loads are known, in the present research, the loads are not yet known. Hence, a thermal loading of 481 K and a pressure of 3.2 MPa were initially applied on the inner surface of the elbow FGM with a predefined temperature of 298K used as the ambient temperature, with an iterative approach then deployed to determine the thermal and load design limit by comparing the effective FGM yield stress with the Von-mises stress for the combined thermal and mechanical (pressure loading). A similar approach was used to determine the pressure design limits; the determined design temperature for each FGM model was kept constant while the pressure was been varied from the 3.2MPa in an iterative manner to be able to determine the pressure design limits for all the FGM models considered. The approach used for both the thermal and pressure design limits is as represented in Fig. 5.5 a & b.

The pressure and temperature were both applied at the elbow pipe inner surface. The pressure is applied as a load while the temperature is applied as boundary condition for the first step. It is important to state that in Abaqus the pressure is applied as a load, while but the temperature is applied as boundary condition as shown in figure 6.3 below.

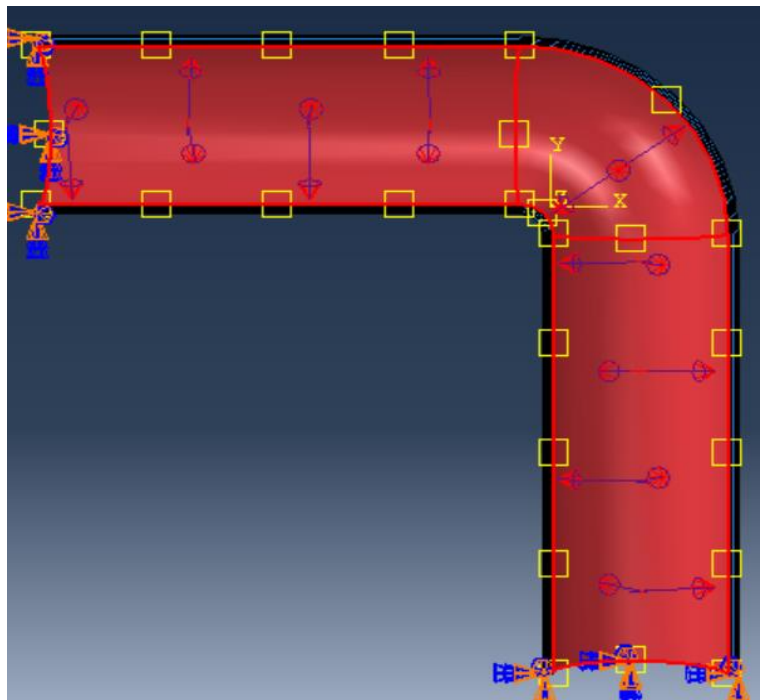


Figure 6.3: Loading and boundary conditions on the elbow pipe.

### 6.2.5 Mesh Module

The mesh is used by Abaqus software to discretize the part in numerous elements of the modelled part. This enables the software to calculate the stresses at each node.

A mesh convergence study was carried out and 5120 elements were used for the elbow pipe model. The part of the modelled elbow FGM pipe was meshed by assigning seeds of 0.03mm global size along the edges. The element type assigned was: hexagonal, 8-node thermally couple brick, trilinear displacement and temperature with C3D8T elements.

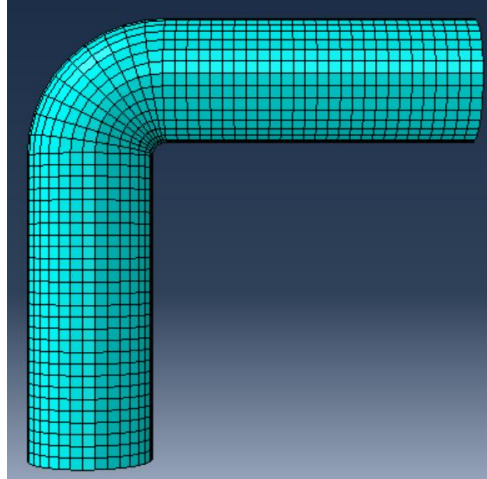


Figure 6.4: The meshed elbow pipe

### 6.2.6 Results: Establishing the Design Limits for the Elbow FGM's

The results for the temperature and pressure design limit of an elbow FGM pipe was determined when the elbow pipe was subjected to both thermal and mechanical loading at a standard predefined temperature of 298K. The analysis focused on five (5) layers elbow FGM Pipe, this was as a result of the learning from the straight pipe design limit determination in which the five (5) layered models resulted in higher pressure and thermal limits as desired.

The presented results also revealed the effect of the non-homogeneity factor ( $n$ ) on the determined limits. It equally compares the results from the limits obtained from both straight and elbow pipe for the four (4) identified FGM's for the candidate materials determined in earlier chapter.

The determination of the design limit for this research was based on the Distortion Energy Theory; in which two types of energy is being compared. The distortion energy in reality scenario and the distortion energy as at the failure time, according to this theory failure occur when the distortion energy real case exceeds the energy as at the time of failure (ASME Handbook).

The distortion energy needed per ( $U_d$ ) is expressed in terms of the principal stress as shown in equation 10.

$$U_d = \frac{1+\nu}{3E} \left[ \frac{(\sigma_1 - \sigma_2)^2 + (\sigma_2 - \sigma_3)^2 + (\sigma_3 - \sigma_1)^2}{2} \right]$$

[6.6]

$U_d$  is normally written in terms of Von-Mises the equivalent stress ( $\delta_{VM}$ ), this is as express in equation 11.

$$U_d = \frac{1+\nu}{3E} \delta_{VM}^2$$

[6.7]

On the same note, the distortion energy at the time of failure is express as thus:

$$u_{d,sim} = \frac{1+\nu}{3E} \sigma_y^2$$

[6.8]

Hence, equation 6.8 is limit value of the distortional energy density for any given material (ASME Handbook). Based on Von-mises failure criterion, any material subjected to multi-axial loading will undergo yielding when the distortional energy is equal or have greater value than the limit value of the material as stated in equation 6.8.

$$\frac{1+\nu}{3E} \delta_{VM}^2 \geq \frac{1+\nu}{3E} \delta_y^2 \quad [6.9]$$

From equation 6.9, the check for failure criterion is to know if the Von mises stress induced in the material is equal to or exceeds the material yield strength (for ductile material). This can be simplified as detailed in equation 6.10 below:

$$\delta_{VM} \geq \delta_y \quad [6.10]$$

Table 6.4 was used to determine the yield strength in each of the elbow pipe layer and the result from the Abaqus software was used to determine the Von-mises stress localized to each layer of the FGM for a given Pressure and Thermal Loading. To enable the adequate comparison of the values of equation 6.10 in all the FGM layers and predicts the possibility of failure (yielding) in any of the layers, a normalized stress approach was adopted based on the principle of equation 6.10. It is as thus:

$$\sigma_{norm} = \frac{\sigma_{VM,max}}{\sigma_{y,eff}} \quad [6.11]$$

Equation 6.11 was used to determine the risk of failure through yielding if the normalized stress is greater than one (1); that means the material has exceed the elastic limit. However, if the normalized stress is less than one (1), then there is no risk of failure due to yielding. It is vital to note that the FGM design limit is reached when any of the FGM's layers normalized stress is closest to one (1), above this limit the material will begin to yield (Fail). For the purpose of

this research the normalized stress is between  $0.99 < \text{normalized stress} < 1.01$ . The adopted approach in determining the design limit for the elbow pipe is same with that of the straight pipe illustrated in figure 5.5 of chapter 5.

Applying the above approach, figure 6.5 revealed the maximum Von-mises stress for the limiting temperature of 474K from the Abaqus model for the FGM 1 (Metal 1: Ni-Fe-Cr alloy, INCOLOY 800, annealed and Ceramic 1: Zirconia, transformation toughened, L), with non-homogeneity factor (n) as 1. This was achieved by varying the temperature while the pressure was kept constant and applying equation 6.11 the limiting temperature of 474K was determined. The results of the stress component considered were those close to the elbow bend of the FGM pipe, this was done so as to eliminate the influence of stress concentration at boundary conditions of the pipe end edges. On the same note, the maximum Von-mises for the limiting pressure for the same FGM 1 as presented in figure 6.6 was achieved by varying the pressure while the temperature was kept constant and also applying equation 6.11 the limiting pressure of 2.5MPa was determined.

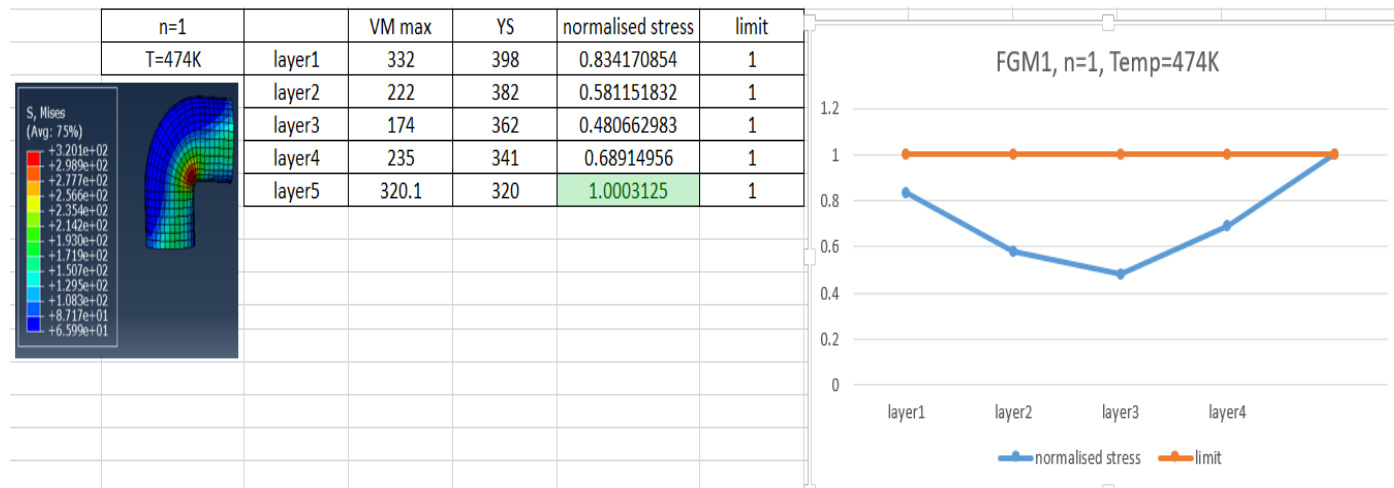


Figure 6.5: Temperature design limit for FGM 1 and n=1

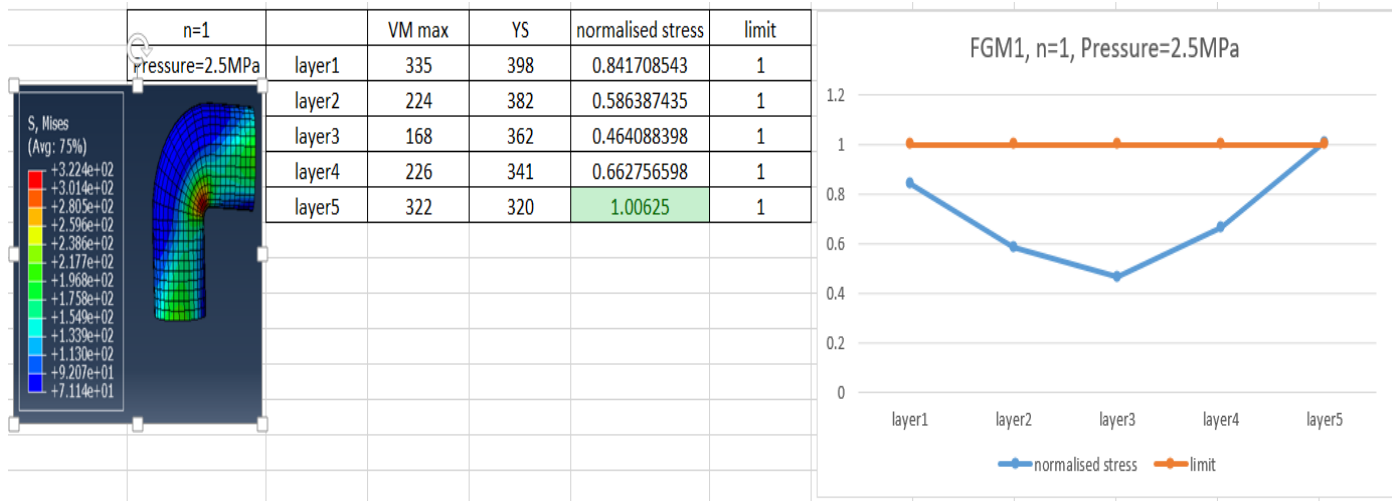


Figure 6.6: Pressure design limit for FGM 1 and n=1

The same approach was used to determine the pressure and temperature design limits for all the other considered FGM combinations with their distinct non-homogeneity factors as considered. The comprehensive results for all the design limits obtained for the elbow FGM Pipes is as detailed in Appendix A, and summary of the temperature and pressure design limits for the four (4) FGM combination considered and their distinct non-homogeneity factors (n) are as detailed in tables 6.8 and 6.9.

Table 6.8: Elbow FGM Temperature Design Limits

Elbow Pipe Temperature Design Limit				
	FGM1	FGM2	FGM3	FGM4
n=1	474	381	320	313
n=2	476	387	334	318
n=3	477	383	343	321
n=4	480	381	351	323
n=5	481	379	357	325

Table 6.9: Elbow FGM Pressure Design Limits

Elbow Pipe Pressure Design Limit				
	FGM1	FGM2	FGM3	FGM4
n=1	2.2	2.26	0.82	0.8
n=2	2.4	2.28	0.82	0.85
n=3	2.3	2.28	0.83	0.87
n=4	2.4	2.3	0.84	0.9

n=5	2.42	2.3	0.86	0.93
-----	------	-----	------	------

A further comparison of the design limits for the FGM's was performed; this was designed to give better insight on the FGM's design limits when the non-homogeneity factor is altered. This is as presented in figures 6.7 and 6.8.

The summarized results for the temperature and pressure design limits as presented in tables 6.8/6.9 above and figure 6.7/6.8 below revealed that non-homogeneity factor (n) influences the temperature design limits of elbow pipes more significantly than its effect on the pressure design limit the pipe. In addition, FGM material combination has significant effect on both temperature and pressure design limits of elbow FGM pipes. In summary, for thermal consideration of elbow FGM pipes, emphasis should be on both FGM material combination and the non-homogeneity factor, while for pressure considerations, emphasis should be more on FGM material combination than on non-homogeneity factor.

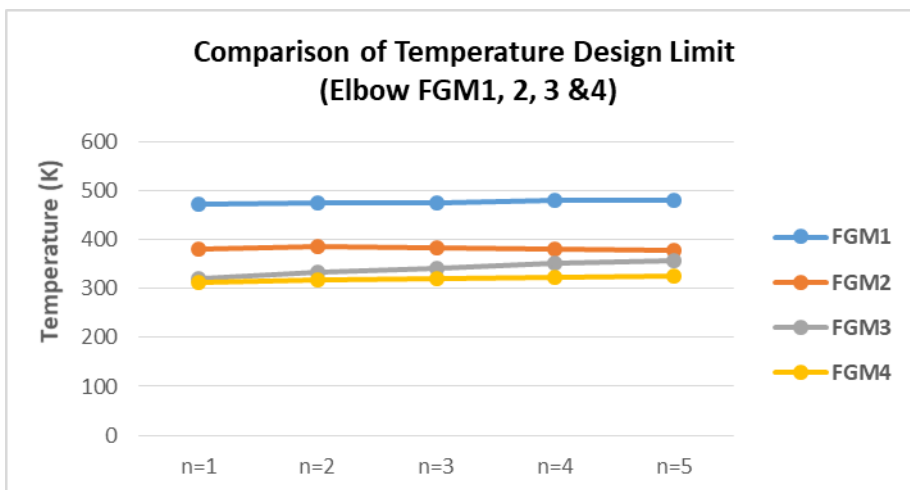


Figure 6.7: Temperature Design Limit comparison for the FGM's

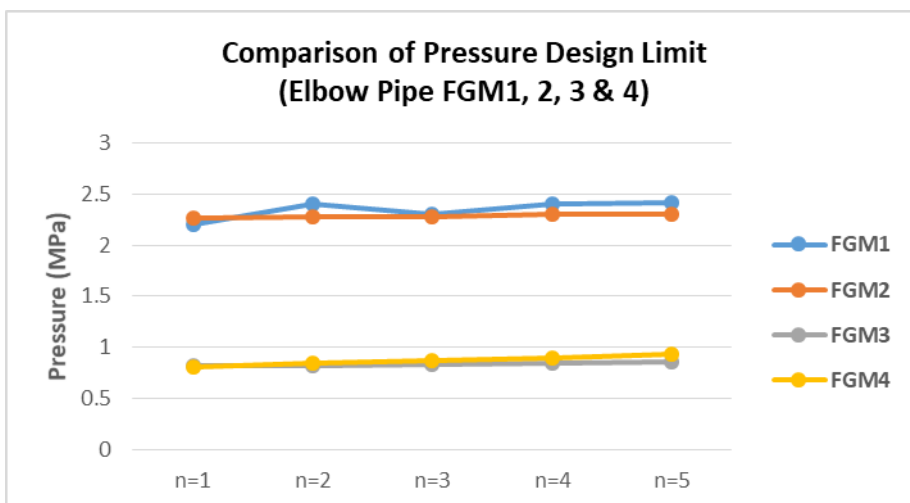


Figure 6.8: Pressure Design Limit comparison for the FGM's

### 6.2.7 Detailed Result Comparison for Straight and Elbow FGM Pipe

The determined design limits for both the straight and elbow Pipe were further compared, this was intended to give good understanding of the limits for all the configurations. This is as detailed in figures 6.9 and 6.10.

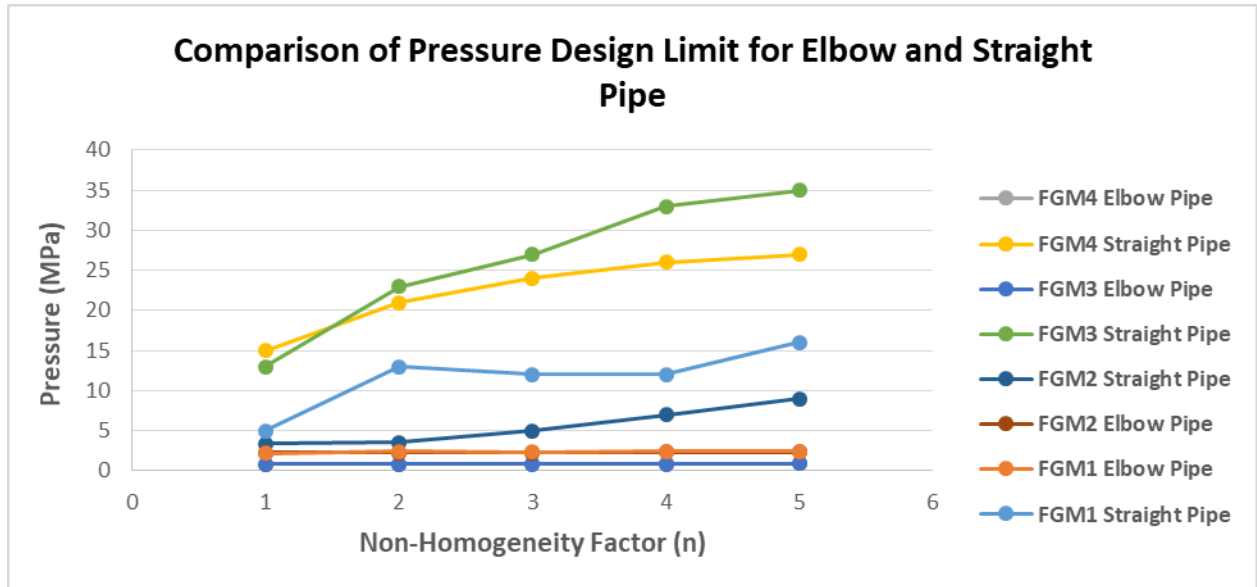


Figure 6.9: Pressure Design Limit comparison for Straight and Elbow Pipe.

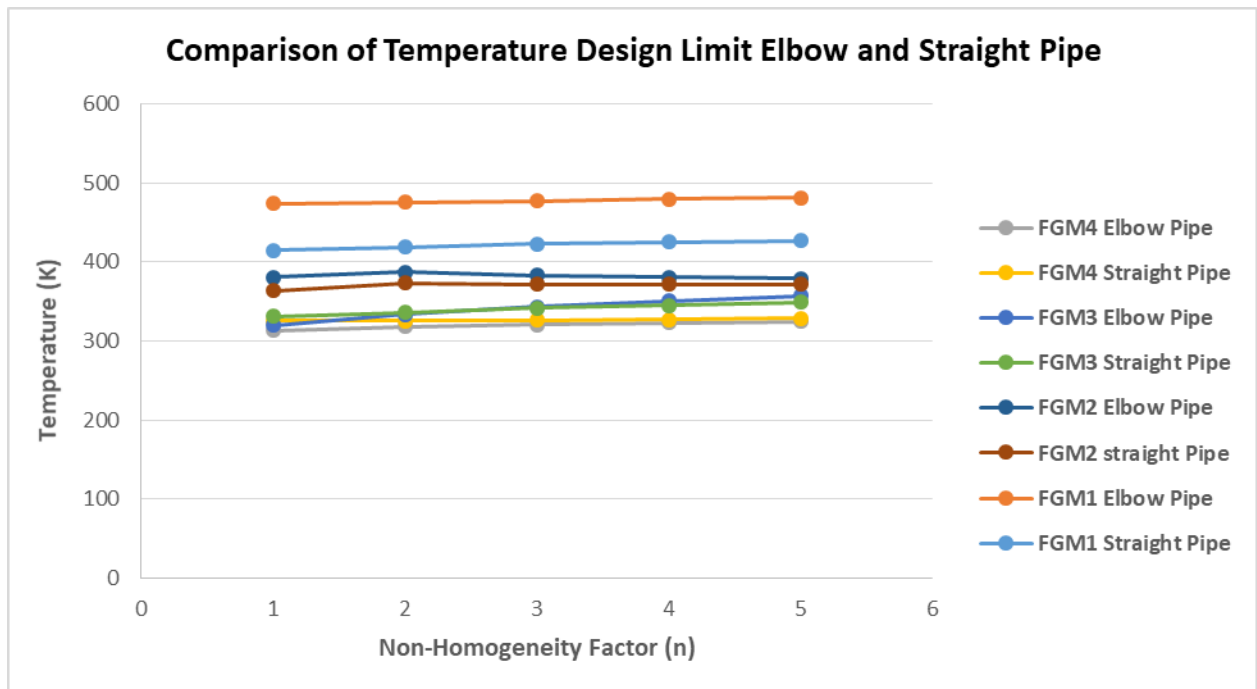


Figure 6.10: Temperature Design Limit comparison for Straight and Elbow Pipe.

The comparison of the temperature and pressure design limits between straight and elbow FGM pipe as displayed in figure 6.9/6.10 and tables 5.9, 5.10, 6.8 & 6.9 revealed quite close temperature limits between the two configurations. The difference in the temperature limits ranges from 0.15-14% at maximum, it equally showed similar trend in the temperature limits variation; it increases with increase in non-homogeneity factor for both configuration.

However, the comparison of the pressure design limit between the two configurations shows huge disparity in the limits, but the trend for the pressure limit variation for the both configuration is somewhat similar, as they both showed minimal incremental variation in the limits with increase in non-homogeneity factor.

### 6.3. CONCLUDING REMARKS

In this chapter, the design limits for 20 different elbow FGM pipelines were determined, this comprises of 4 FGMs with 5 different non-homogeneity factor with each of the modelled pipe having different temperature and pressure ratings. The results from table 6.8/6.9 and figure 6.7/6.8 revealed the temperature and pressure design limits for the four elbow FGM pipes and the influence of non-homogeneity factor on these limits.

The results revealed the significance of non-homogeneity factor (n) on temperature design limits of elbow pipes as compared to its significance on pressure design limit of the pipe. On the same note, it revealed that FGM material combination has significance on both temperature and pressure design limits of elbow FGM pipes.

A further comparison of the value and significance of the both limits for straight and elbow FGM pipe reveals that, both configurations have relatively close temperature design limits. On the contrary, the pressure design limits for the both configurations have huge disparity.

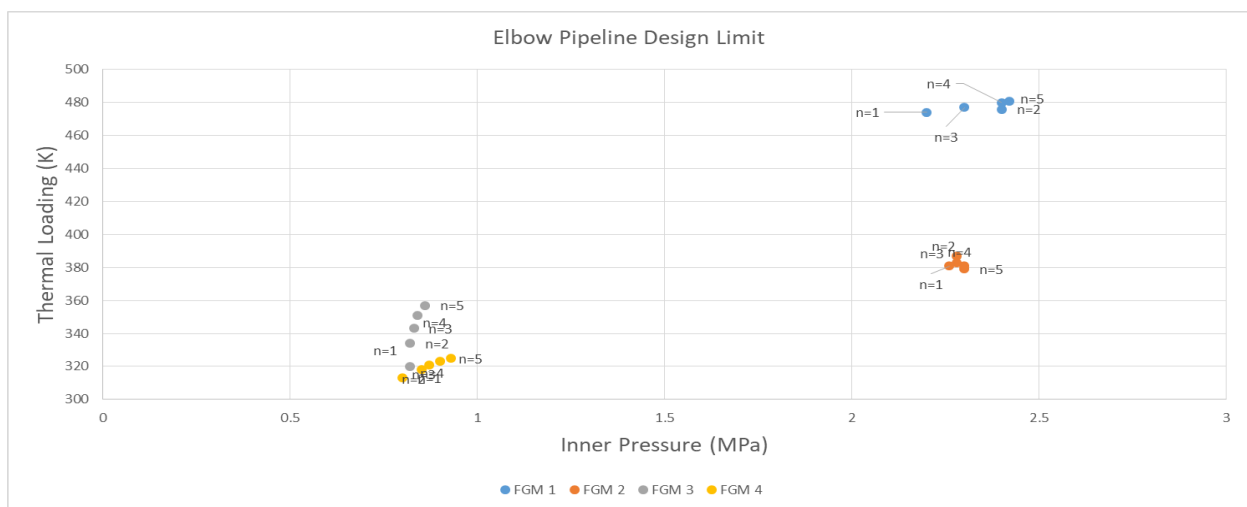


Figure 6.11: Temperature Design Limit comparison for Straight and Elbow Pipe



Figure 6.11 give a detailed representation of the design limits for all the 20 different elbow FGM pipe considered. It revealed that FGM1 and FGM2 gives higher pressure and thermal design limits. Hence, could be deployed in areas with high pressure and thermal considerations. Figure 6.11 could therefore serve as guide in the choice of the FGM to deploy based on the operational requirements and rating (Pressure and Temperature).

# **CHAPTER 7: T-PIECE PIPE CONFIGURATION FGM DESIGN LIMITS AND ITS IMPACT ON FGM BEHAVIOUR**

## **7.1. INTRODUCTORY REMARKS**

Different configurations of pipelines and piping are increasingly used in oil and gas activities due to the increasing rate of oil and gas exploration and utilization of petroleum product, these pipes are often exposed to high rate of corrosion due to the terrain to which they are deployed. The use of Functional Graded Material (FGM) as a mitigation against the effect of corrosion in oil and gas operations has been explored in previous chapters for the Straight and Elbow Pipe. This present chapter focuses on the behaviour of a typical T-Piece Functional Graded Materials operating within the oil and gas operation parameters.

The behaviour of the T-Piece FGM pipe is examined with the aim of predicting its elastic design limits when subjected to both thermal and mechanical loading conditions. Finite Element Analysis of four (4) T-Piece FGM pipes made of different material combinations was modelled with ABAQUS software package, this limits was compared with the limits obtained from FGM straight and Elbow pipes. Further parametric studies were performed to determine the influence of non-homogeneity factor on the design limits of the T-Piece FGM pipes.

## **7.2. MODELLING OF T-PIECE PIPE**

In a piping system, a branched piece is used to change the flow direction of fluid to a desired location, branch piece comes in form of either Y, T or crossed configurations. The usual configuration is to cut a hole and insert a branch or pull through a transition in the main pipe so as to fix the branch pipe into the main pipe, which enables the flow directional change. This concept leads to the generation of internal pressure deformations that could further degenerate to longitudinal and hoop stresses which flattens the pipe and leads to localized buckling (Arash, 2000). This will eventually lead to the collapse and failure of the T-piece pipe.

The loading of the T-Piece pipe as presented in this chapter is limited to internal pressure and temperature actions only and the outcome of the analysis was used to determine the design limits of the identified candidate materials. Parametric studies were performed on the T-Piece FGM Pipes to have good understanding of T-Piece FGM pipe when certain properties are varied. The following sections expand on the T-Piece model geometry development, FGM model validation, material selection, loading, boundary conditions and subsequent results.

### 7.3. MODEL GEOMETRY

The main section of the T-Piece FGM Pipe was model using the same pipe schedule as has been used for the straight pipe and elbow pipe components, which 12in nominal bore and Schedule 80 pipe wall thickness. This was intentionally chosen to be able to benchmark with the straight pipe and the solution being considered for the oil and gas operations. The channel (nozzle) used for the T-Piece was two-third of the main pipe that is 8 inches. The geometry is as shown in figure 7.1, below.

The T-Piece main pipe model has inner diameter as 288.9mm (i.e.  $r_i = 144.45\text{mm}$ ) and the wall thickness is 17.48mm. The nozzle (channel) of T-piece has inner diameter of 192.6mm (i.e.  $r_i = 90.47\text{mm}$ ) and the wall thickness remain the same as that of the main pipe. These dimensions are as shown in Table 7.1 below:

Table 7.1: T-Piece Pipe Dimensions

t (mm)	$r_i$ pipe(mm)	$r_o=r_i + t$ (mm)	L (mm)	$r_i$ nozzle (mm)	$r_o=r_i + t$ (mm)
17.48	144.45	161.96	1700	90.47	107.95

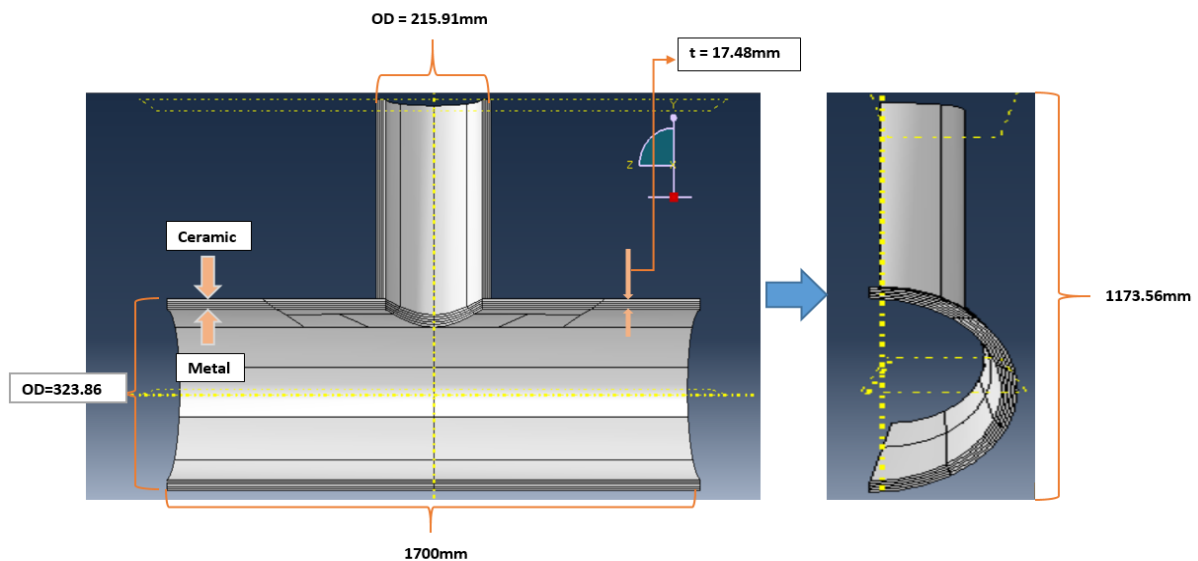


Figure 7.1: Schematic of the Modelled T-Piece FGM Pipe

### 7.4. T-PIECE NUMERICAL RESULT VALIDATION

The modelled T-Piece FGM result was validated with the analytical approach developed by Decock that provided a solution for the determination of the Stress Concentration Factor of the T-Piece component. The solution by Decock was proposed at ICPVT-2. Conf. on Pressure Vessel Tech, Part II, ASME, San Antonio, Texas, Oct 1973 (ASME Handbook).

The solution by Decock was based upon the fact that the maximum stress occurs at the crotch corner. This gives the equation for the stress concentration (SCF) as thus:

$$SCF = \frac{2 + \frac{2d}{D} \sqrt{\frac{d}{D} \frac{t}{T}} + \frac{1.25d}{D} \sqrt{\frac{D}{T}}}{1 + \frac{t}{T} \sqrt{\frac{d}{D} \frac{t}{T}}} \quad [7.1]$$

The Parameters for the T-Piece component been validated, is as thus:

Pressure applied, $p$	=	2MPa
Design temperature	=	25°C
Thickness of the Cylinder ( $T$ )	=	17.48mm
Inside diameter of Cylinder ( $D_i$ )	=	288.9mm
Mean Diameter of Cylinder ( $D=D_i + T$ )	=	306.38mm
Thickness of nozzle ( $t$ )	=	11.65mm
Inside Diameter of the nozzle ( $d_i$ )	=	192.6mm
Mean Diameter of the nozzle ( $d=d_i + t$ )	=	204.25mm

Applying the above data with the Decock equation gives an SCF of 4.416

The circumferential membrane stress range in a cylindrical shell can be calculated from the classical stress/pressure relationship for a cylinder, as follows:-

$$\sigma_{\theta} = \frac{PD}{2T} \quad [7.2]$$

$$\sigma_{\theta} = \frac{2 \cdot 306.38}{2 \cdot 17.48} = 17.53 \text{MPa}$$

The maximum stress range for the T-Piece is derived from multiplying SCF and the circumferential membrane stress. This is as detailed below.

$$4.416 * 17.53 \text{ MPa} = 77.4 \text{ MPa}$$

The same parameters above was used to develop a model on Abaqus using a homogenous material with properties as shown in table 7.2 below, this is to replicate the solution derived with the Decock equation.

Table 7.2: Properties of materials used for the result validation

Material properties	E (GPa)	CTE(/K)	Poisson's ratio	k (W/m.K)	Cv (J/g.K)	Density (kg/m3)	Tensile Strength (MPa)
ASTM CF-20 (stainless steel)	195	0.000175	0.27	15.5	500	7765	530

The result from the FEA analysis performed on Abaqus using the above material properties with the dimensions as stated above for the T-Piece is as represented in figure 7.2; this reveals the principal stresses for the T-Piece Model.

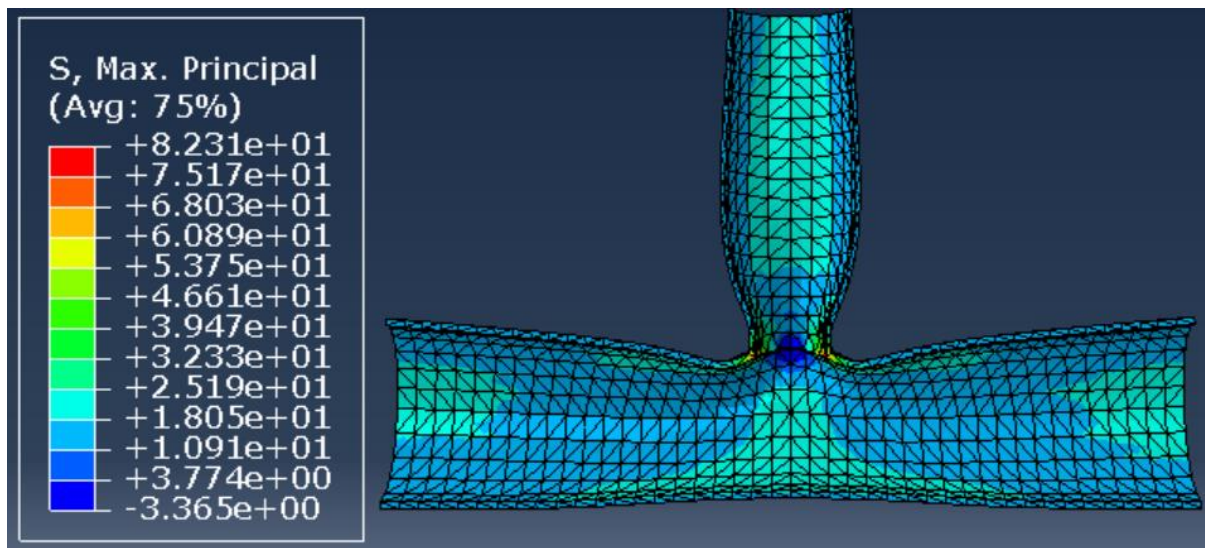


Fig. 7.2: Principal Stresses for the replicated T-Piece Model

From the results of the FEA, the Maximum Principal Stress for the T-Piece is 82.3MPa, when compared with the maximum stress of 77.4MPa derived from the SCF applying the Decock equation on the T-Piece with the same dimensions. The comparison shows good agreement (94.1%) with the FEA results from Abaqus with only 5.9% deviation in the maximum stress value.

## 7.5. MATERIALS

### 7.5.1. FGM Material Composition

In furtherance to the development and validation of the T-Piece pipe model in the above section, the preceding sections considered the development and application of the FGM materials selected in chapter 3 with the aid of the CES Edupack Software. As reiterated in previous chapters, the choice of the material was driven by the requirement of the Deep Water Oil and Gas operations. Four (4) distinct FGM combinations (Metal and Ceramics) were developed to be able to meet the need of the Operations as stated above. The model deployed the use of ceramics at the inner surface of the T-Piece Pipe while metal at the outer surface. This choice was premised on the material properties like high toughness and thermal resistance, high strength and excellent corrosion resistance. These properties will progressively change from that of ceramic to the metal gradually through the thickness of the T-piece pipe.

The metals and ceramics used for the Four (4) distinct FGMs are as detailed below:

Metal 1: Ni-Fe-Cr alloy, INCOLOY 800, annealed

Metal 2: Stainless steel, austenitic, ASTM CF-20, cast, water quenched

Metal 3: Copper, C14200, soft

Ceramic 1: Zirconia, transformation toughened, L

Ceramic 2: Alumina 94, SGM

Ceramic 3: Silicon carbide, HIP

Ceramic 4: Tungsten carbide, hot press

The combination of these materials (Metal and Ceramic) was used for four (4) FGM's is as stated below:

Table 7.3: Composition of the 4 different FGMs.

FGM 1	FGM2	FGM3	FGM4
Metal1-Ceramic1	Metal2-Ceramic2	Metal3-Ceramic3	Metal3-Ceramic4

### 7.5.2. FGM Materials Properties

As stated above, Seven (7) materials were considered in this study for the FGM combinations. All the properties of these materials were found from CES Edupack and are as presented in details in the table 7.4 below:

Table 7.4: Mechanical and thermal properties of the metal and ceramic materials.

	E (GPa)	Coefficient of thermalexpansion CTE( /K)	Poisson's ratio	Thermal conductivity k (W/m.K)	Specific HeatCapacity Cv (J/kg.K)	Density (kg/m3)	Tensile Strength (MPa)	Ranking	Yield Strength (Mpa)
<b>Ranking for Metal</b>									
Nickel-Fe-Cr alloy, INCOLOY 800, Annealed	195	14,25	0,34	11,5	502,5	7950	620	1	310
Stainless Steel, austenitic, ASTM CF-20 , cast, water quenched	195	17,5	0,27	15,5	500	7765	530	2	250
Copper C14200, Soft	122,5	17,5	0,345	165,5	380,5	8925	220	3	55
<b>Ranking for Ceramics</b>									
Zirconia (Transformation toughened) L	246,5	9,8	0,3	2	450	5740	414	1	414
Alumina 94 (SGM)	330	7,55	0,24	21	880	3650	250,5	2	250
Silicon Carbide (HIP)	400	5	0,15	80,05	802	3145	500,5	3	500
Tungsten Carbide (Hot Press)	669	5,8	0,21	29	180	15700	352,5	4	352

To be able to determine the T-Piece FGM properties at a specified position, the volume fractions equation for both the metal and ceramic was used as detailed in equation 5.9 and 5.10 of chapter 5.

From equations 5.9 and 5.10, for  $z=h/2$ ,  $V_{ceramic} = 0$  and  $V_{metal} = 1$ , conversely for  $z=-h/2$ . Hence, it is logical that at  $z=h/2$  the FGM is fully metal and at  $z=-h/2$  it is fully ceramic. These equations introduced a new parameter known as the non-homogeneity parameter (n), this parameter represents how the variation of the properties progresses along the T-Piece FGM pipe thickness.

Having known the effect of non-homogeneity factor and volume fraction as stated in the above, the properties of the FGM at any point was determined with the power law equations as stated in equations 4.1, 4.2 and 4.3 in chapter 4.

These equations are used to calculate all the different properties in the thickness of the T-Piece pipe, an example is shown in the preceding tables for FGM 1, Five (5) Layers and  $n=1$ .

Table 7.5: Development of the properties along the thickness with n=1 for the FGM 1.

Material properties	E (GPa)	CTE( /K)	Poisson's ratio	k (W/m.K)	Cv (J/kg.K)	Density (kg/m3)	Tensile Strength (MPa)	N	YS (Mpa)
Zirconia (toughened)	246.5	0.0000098	0.3	2	450	5740	414	1	414
INCOLOY 800 (annealed)	195	0.00001425	0.34	11.5	502.5	7950	620		310

Position [-h/2 ; h/2]	E	CTE	k	k (W/m.K)	Cv	d	Tensile Strength (MPa)	Yield strength
-1.00E-02	246.5	9.80E-06	0.30	2.0	450.0	5740	414	414
-9.00E-03	243.9	1.00E-05	0.30	2.5	452.6	5851	424	409
-8.00E-03	241.4	1.02E-05	0.30	3.0	455.3	5961	435	404
-7.00E-03	238.8	1.05E-05	0.31	3.4	457.9	6072	445	398
-6.00E-03	236.2	1.07E-05	0.31	3.9	460.5	6182	455	393
-5.00E-03	233.6	1.09E-05	0.31	4.4	463.1	6293	466	388
-4.00E-03	231.1	1.11E-05	0.31	4.9	465.8	6403	476	383
-3.00E-03	228.5	1.14E-05	0.31	5.3	468.4	6514	486	378
-2.00E-03	225.9	1.16E-05	0.32	5.8	471.0	6624	496	372
-1.00E-03	223.3	1.18E-05	0.32	6.3	473.6	6735	507	367
0	220.8	1.20E-05	0.32	6.8	476.3	6845	517	362
1.00E-03	218.2	1.22E-05	0.32	7.2	478.9	6956	527	357
2.00E-03	215.6	1.25E-05	0.32	7.7	481.5	7066	538	352
3.00E-03	213.0	1.27E-05	0.33	8.2	484.1	7177	548	346
4.00E-03	210.5	1.29E-05	0.33	8.7	486.8	7287	558	341
5.00E-03	207.9	1.31E-05	0.33	9.1	489.4	7398	569	336
6.00E-03	205.3	1.34E-05	0.33	9.6	492.0	7508	579	331
7.00E-03	202.7	1.36E-05	0.33	10.1	494.6	7619	589	326
8.00E-03	200.2	1.38E-05	0.34	10.6	497.3	7729	599	320
9.00E-03	197.6	1.40E-05	0.34	11.0	499.9	7840	610	315
1.00E-02	195.0	1.43E-05	0.34	11.5	502.5	7950	620	310

Table 7 67: Example of properties in each layer for l = 5 (FGM 1, n=1).

Layer number	E (GPa)	Coefficient of thermalexpansion CTE( /K)	Poisson's ratio	Thermal conductivity k (W/m.K)	Specific HeatCapacity Cv (J/kg.K)	Density (kg/m3)	Tensile Strength (MPa)	Yield strength
Layer 1	241.35	1.02E-05	0.30	3.0	455.3	5961	434.6	398.4
Layer 2	231.05	1.11E-05	0.31	4.9	465.8	6403	475.8	382.8
Layer 3	220.75	1.20E-05	0.32	6.8	476.3	6845	517	362.0
Layer 4	210.45	1.29E-05	0.33	8.7	486.8	7287	558.2	341.2
Layer 5	200.15	1.38E-05	0.34	10.6	497.3	7729	599.4	320.4

Tables 7.5 and 7.6 summarized the properties used for FGM 1 with non-homogeneity factor (n) as 1, this same procedure is repeated for the entire FGM's considered for the T-Piece model with their respective non-homogeneity factor.

## 7.6. STEP MODULE

The T-piece pipeline was subjected to a thermal load and an internal pressure, a fully coupled temperature-displacement procedure was used for the analysis. The time period of step is 3600 seconds with an automatic increment was used.

## 7.7. LOAD MODULE

The boundary conditions, mechanical and thermal loadings were implemented to the T-piece FGM pipe in this module on the Abaqus software. The approach used for the load application on the T-piece pipe is similar to that of the straight and elbow pipe. It is vital to note that unlike the conventional modelling were the loads are known. In this research, the loads are not yet known. Hence thermal loading of 565 K and a pressure of 3.2 MPa were initially applied on the inner surface of the T-piece FGM with a predefined temperature of 298K used as the ambient temperature. Thereafter, the determined limit for temperature was kept constant and the 3.2MPa pressure was been varied. Iterative approach was then deployed to determine the



thermal and load design limit by comparing the effective FGM yield stress with the Von-mises stress for the combined thermal and mechanical (pressure loading).

The pressure and temperature were both applied at the T-piece pipe inner surface. The pressure is applied as a load while the temperature is applied as boundary condition for the first step. It is important to state that in Abaqus the pressure is applied as a load, while the temperature is applied as boundary condition as shown in figure 7.3 below.

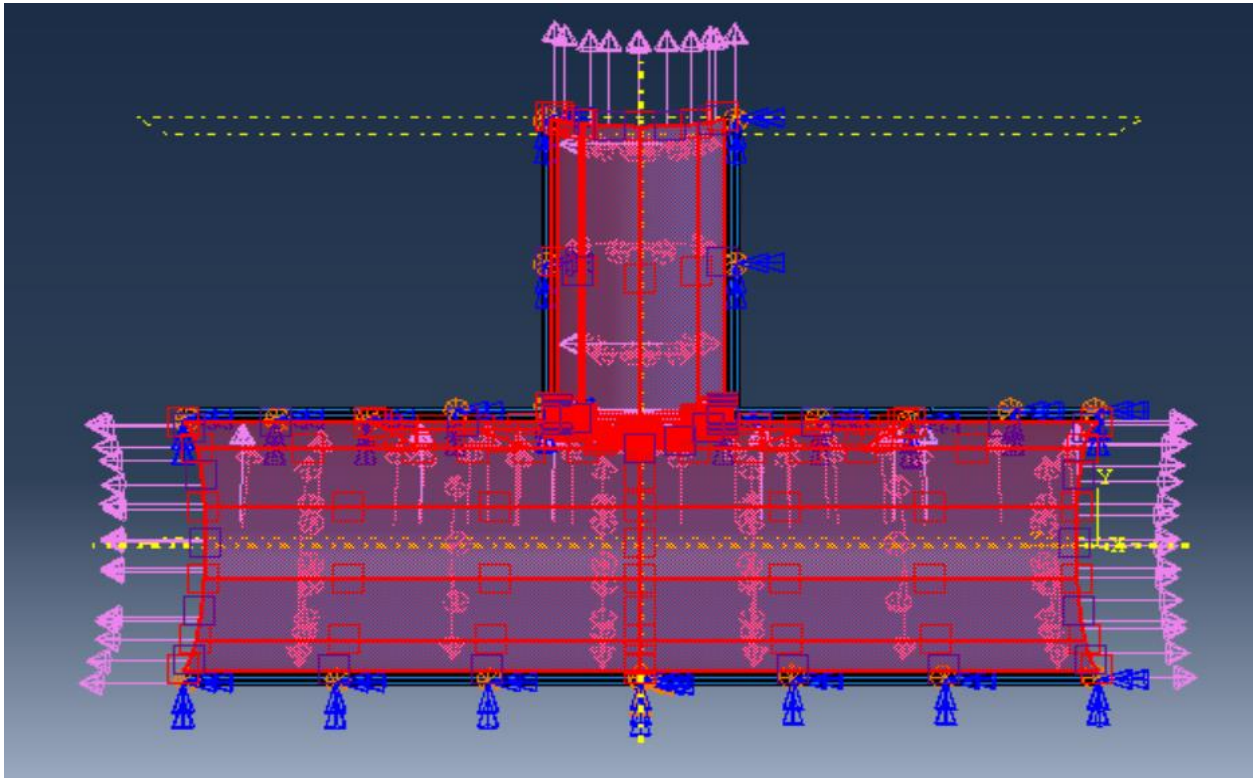


Figure 7.3: Loading and boundary conditions on the T-Piece pipe.

## 7.8. MESH MODULE

The mesh is used on Abaqus software to discretize the part in numerous elements so that Abaqus software can calculate the stresses at each node.

A mesh convergence study was carried out and 30,000 elements was used for the T-Piece pipe model; seeds were defined by assigning a global size as 0.025 mm along the edges. Then the element type was assigned: 4-node thermally couple tetrahedron, linear displacement and temperature with C3D4T elements. This is as presented in figure 7.4 below.

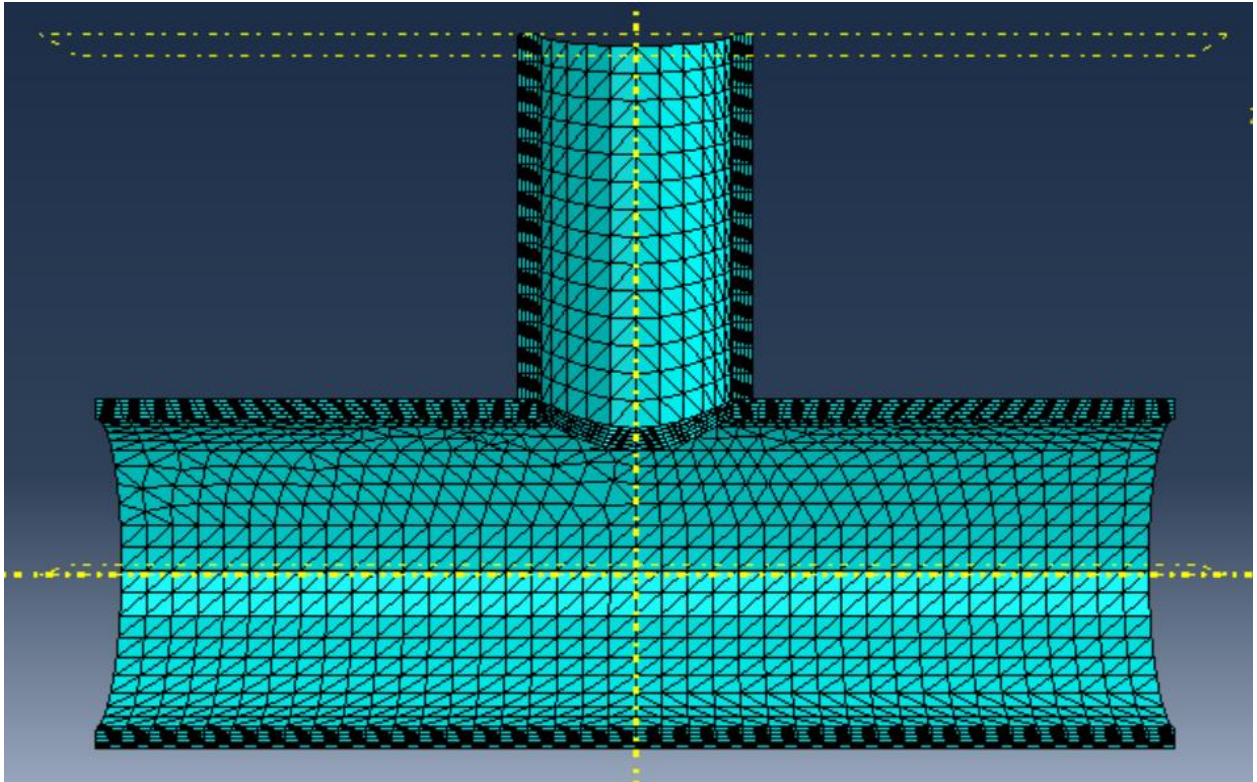


Figure 7.4: The Meshed T-Piece pipe.

## 7.9. RESULTS

The results for the temperature and pressure design limit of the T-piece FGM pipe was determined when the T-Piece pipe was subjected to both thermal and mechanical loading at a standard predefined temperature of 298K. The analysis focused on five (5) Layers T-piece FGM pipe, this was resulted from the learning with the straight and elbow pipe design limit determination in which the five (5) layered models resulted in higher pressure and temperature limits as desired.

The presented result revealed the effect of the non-homogeneity factor ( $n$ ) on the determined limits. A further comparison of the results obtained from the limits for both straight, elbow and T-Piece pipe was considered for the four (4) identified FGM's with reference to the candidate materials determined in earlier chapters.

Design limits determination was premised on the Distortion Energy Theory as detailed in chapter 6 and considering equations 6.6, 6.7, 6.8 and 6.9, the material is subjected to multi-axial loading will undergo yielding when the distortional energy is equal or have greater value than the limit value of the material as stated in equation 6.8.

Hence, the check for failure criterion is to know if the Von-mises stress induced in the material is equal to or exceeds the material yield strength. This can be simplified as stated in equation 7.6 below:

$$\delta_{VM} \geq \delta_y \quad [7.6]$$

Table 7.4 was used to determine the yield strength in each of the T-Piece pipe layer and the result from the Abaqus software was used to determine the Von-mises stress localized to each layer of the FGM for a given Pressure and Thermal Loading. To enable the adequate comparison of the values of equation 7.6 in all the FGM layers and predicts the possibility of failure (yielding) in any of the layers, a normalized stress approach was adopted based on the principle of equation 7.6. It is as thus:

$$\sigma_{norm} = \frac{\sigma_{VM,max}}{\sigma_{y,eff}} \quad [7.7]$$

Equation 7.7 was used to determine the risk of failure through yielding if the normalized stress is greater than one (1); that means the material has exceed the elastic limit. However, if the normalized stress is less than one (1), then there is no risk of failure due to yielding. It is vital to note that the FGM design limit is reached when any of the FGM's layers normalized stress is closest to one (1), above this limit the material will begin to yield (Fail). For the purpose of this research the normalized stress is between  $0.99 < \text{normalized stress} < 1.01$ . The adopted approach in determining the design limit for the T-piece pipe is same with that of the straight and elbow pipe illustrated in figure 5.5 of chapter 5.

Applying the above approach, figure 7.5 revealed the maximum Von-mises stress for the limiting temperature of 565K from the Abaqus model for the FGM 1 (Metal 1: Ni-Fe-Cr alloy, INCOLOY 800, annealed and Ceramic 1: Zirconia, transformation toughened, L), with non-homogeneity factor (n) as 1. This was achieved by varying the temperature while the pressure was kept constant and applying equation 7.7 the limiting temperature of 565K was determined. On the same note, the maximum Von-mises for the limiting pressure for the same FGM 1 as presented in figure 7.6 was achieved by varying the pressure while the temperature was kept constant and also applying equation 7.7 the limiting pressure of 6.6 MPa was determined

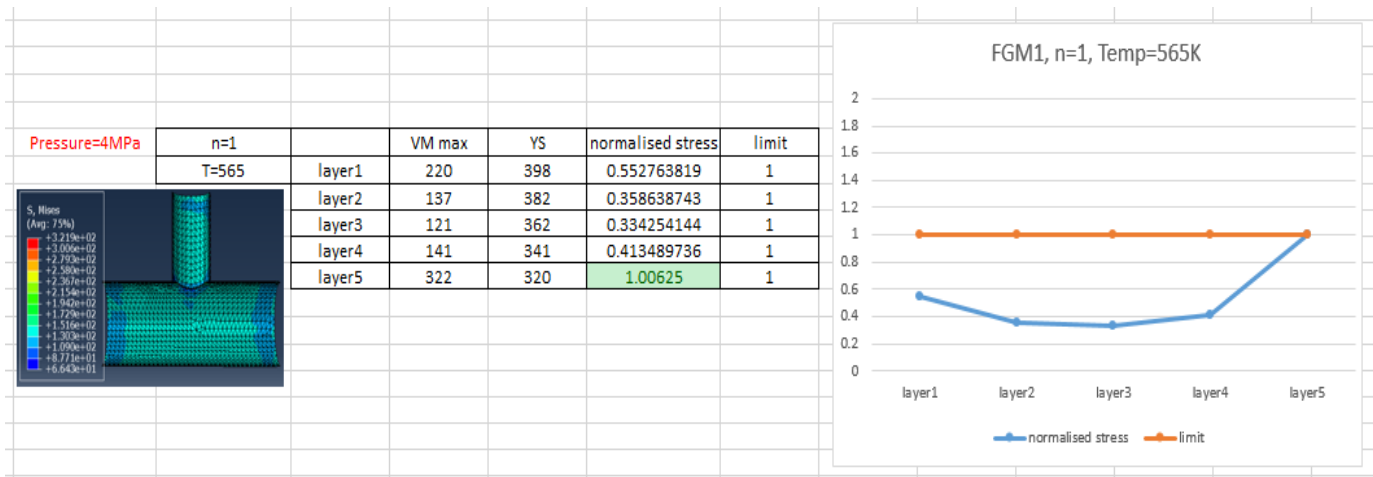


Figure 7.5: Temperature design limit for FGM 1 and n=1

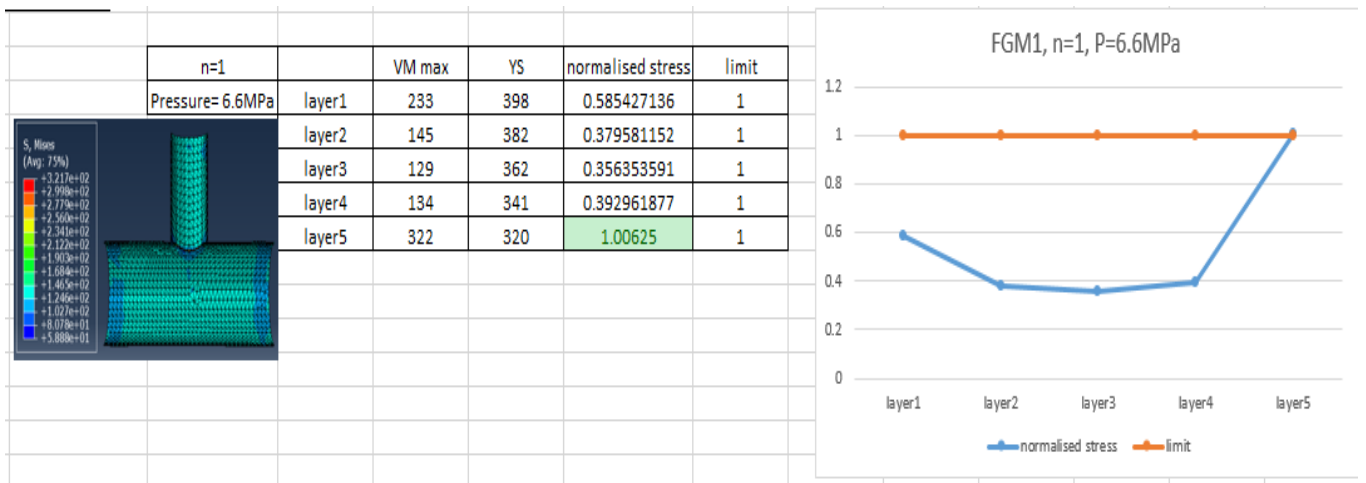


Figure 7.6: Pressure design limit for FGM 1 and n=1

The same approach was used to determine the pressure and temperature design limits for all the other considered FGM combinations with their distinct non-homogeneity factors considered. The comprehensive results for all the design limits obtain for the T-Piece FGM Pipes is as detailed in Appendix B, and the summary of the temperature and pressure design limits for the four (4) FGM combination considered and their distinct non-homogeneity factors (n) are as detailed in tables 7.8 and 7.9.

Table 7.8: T-Piece FGM Temperature Design Limits

<b>T-Piece Pipe Temperature Design Limit</b>				
	<b>FGM1</b>	<b>FGM2</b>	<b>FGM3</b>	<b>FGM4</b>
<b>n=1</b>	<b>565</b>	<b>397</b>	<b>319.5</b>	<b>312.5</b>
<b>n=2</b>	<b>510</b>	<b>371</b>	<b>320</b>	<b>311</b>
<b>n=3</b>	<b>487</b>	<b>363.5</b>	<b>322.5</b>	<b>311.6</b>
<b>n=4</b>	<b>489</b>	<b>360.5</b>	<b>325.5</b>	<b>312.3</b>
<b>n=5</b>	<b>484</b>	<b>359.5</b>	<b>328</b>	<b>313.3</b>

Table 7.9: T-Piece FGM Pressure Design Limits

<b>Elbow Pipe Pressure Design Limit</b>				
	<b>FGM1</b>	<b>FGM2</b>	<b>FGM3</b>	<b>FGM4</b>
<b>n=1</b>	<b>6.6</b>	<b>4.9</b>	<b>8.2</b>	<b>7.8</b>
<b>n=2</b>	<b>20</b>	<b>12.2</b>	<b>10.4</b>	<b>9.4</b>
<b>n=3</b>	<b>24.2</b>	<b>13.6</b>	<b>6.2</b>	<b>10.4</b>
<b>n=4</b>	<b>26</b>	<b>14.4</b>	<b>12.78</b>	<b>11.1</b>
<b>n=5</b>	<b>24.8</b>	<b>15</b>	<b>13.8</b>	<b>11.7</b>

A further comparison of the design limits for the FGM's was performed; this was to give better insight on the T-Piece FGM's design limits when the non-homogeneity factor is altered. This is as presented in figures 7.7 and 7.8.

The results from the table 7.8/7.9 and figure 7.5/7.6 revealed that for most cases, as the non-homogeneity factor (n) increases, the temperature and pressure design limits of T-piece pipes increases. In addition, it also revealed that FGM material combination has significant effect on both temperature and pressure design limits of elbow FGM pipes. In summary, for thermal and pressure consideration of T-Piece FGM pipes, the emphasis should be on both FGM material combination and the non-homogeneity factor.

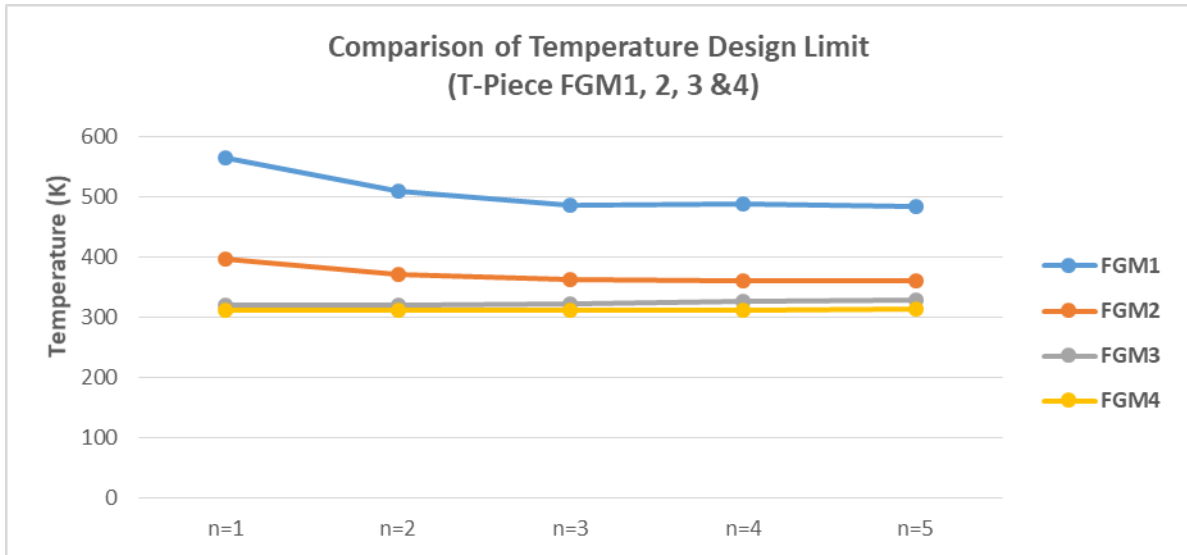


Figure 7.7: Temperature Design Limit comparison for the FGM's

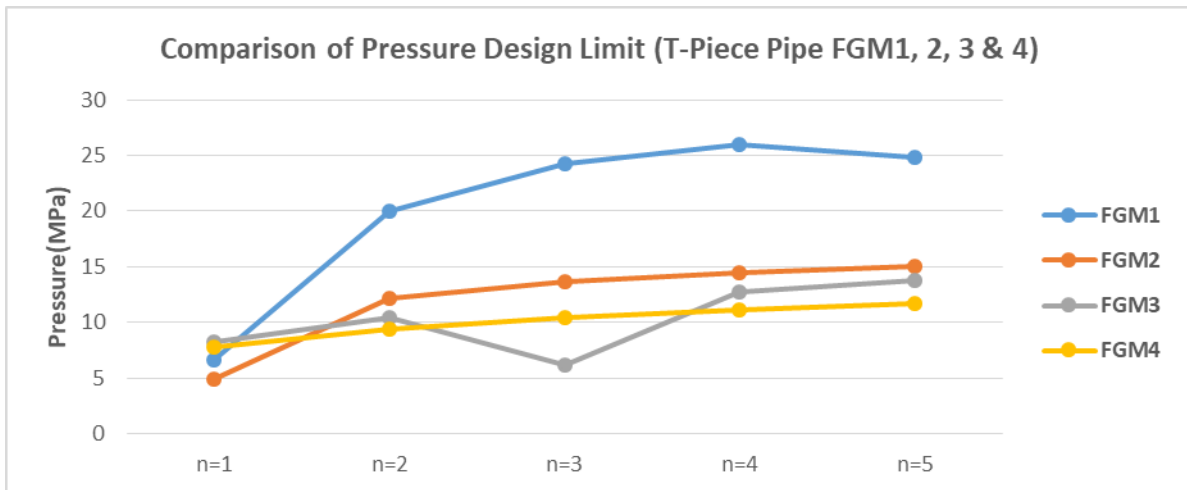


Figure 7.8: Pressure Design Limit comparison for the FGM's

## 7.10. CONCLUDING REMARKS

In this chapter, similar to the preceding chapters, the design limits for 20 different T-Piece FGM pipelines were determined, this comprises of four FGMs with five different non-homogeneity factors with each of the modelled pipe having different temperature and pressure ratings. The results from table 7.8/7.9 and figure 7.7/7.8 revealed the temperature and pressure design limits for the four T-Piece FGM pipes and the influence of non-homogeneity factor on these limits.

The results revealed the significance of non-homogeneity factor (n) on temperature design limits of T-Piece FGM pipes as compared to its significance on pressure design limit of the pipe. On the same note, it revealed that FGM material combination has significance on both temperature and pressure design limits of T-Piece FGM pipes.

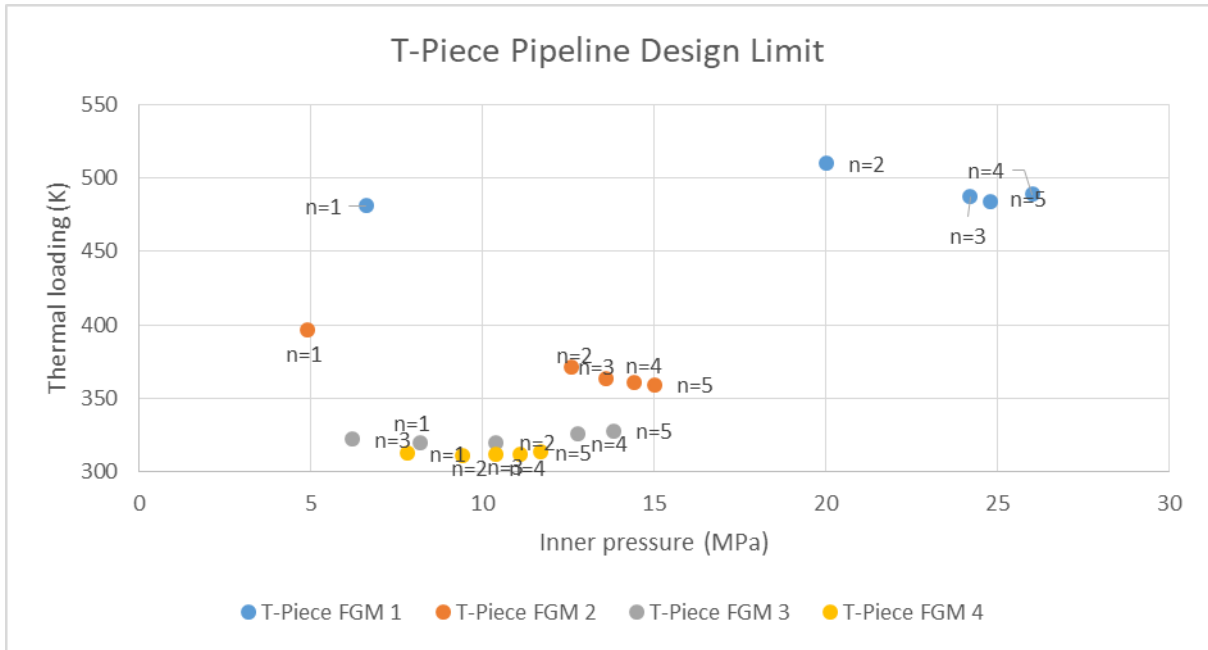


Figure 7.11: Temperature Design Limit comparison for T-Piece Pipe

Figure 7.11 give a detailed representation of the design limits for all the 20 different T-Piece FGM Pipelines considered. It was revealed that FGM1 and FGM2 gives higher thermal design limits, while only FGM 1 provides a distinct pressure design limit. Figure 7.11 could serve as guide in the choice of the particular T-Piece FGM to deploy based on operational needs in terms of the required rating (Pressure and Temperature). The non-homogeneity factor for the various T-Piece FGM considered in figure 7.11 can be obtained by referring to tables 7.8 and 7.9.

## **CHAPTER EIGHT: DESIGN RECOMMENDATIONS**

### **8.1. INTRODUCTORY REMARKS**

This chapter proposed the design recommendations for FGM's behaviours when subjected to thermal and mechanical loading. The recommendations focus on FGM's material selection, effective yield strength and the design limits for FGM configurations based on oil and gas operational window.

### **8.2. IDEAL FGM MATERIALS FOR DEEP OFFSHORE OIL AND GAS OPERATIONS**

The material parameters used to determine the ideal FGM Metal/Ceramics for oil and gas operations were; cost per unit volume, fracture toughness, fatigue strength, tensile strength, salt and fresh water application, density and Young's modulus of the materials. Identifying each of these properties for each of the recommended materials was vital due to the uniqueness of deep-water operations of oil and gas. CES Edupark 2017 software was used as a check to identify all materials with the appreciable properties highlighted above. The analytic hierarchy process (AHP) technique was further used to determine the ideal FGM material combination and to perform sensitivity analysis. The results from the detailed study therefore recommends the following FGM materials Metal/ceramics as suitable for offshore oil and gas operations.

#### Metals

Metal 1: Ni-Fe-Cr alloy, INCOLOY 800, annealed

Metal 2: Stainless steel, austenitic, ASTM CF-20, cast, water quenched

Metal 3: Copper, C14200, soft

#### Ceramics

Ceramic 1: Zirconia, transformation toughened, L

Ceramic 2: Alumina 94, SGM

Ceramic 3: Silicon carbide, HIP

Ceramic 4: Tungsten carbide, hot press

### **8.3. FGM BEHAVIOURAL DEPENDENCE NUMBER OF LAYERS AND NON-HOMOGENEITY FACTOR (n)**

FGM Pipe made from metals and ceramics with 20 number of layers subjected to thermal and mechanical loading was modelled on the Abaqus software to determine the effect of number of layers and non-homogeneity factor (n) on the FGM behaviour. As stated in chapter 4, this model was validated against an already published result with ANSYS and first order-shear deformation theory (FSDT) from Ghannad et. al [2017] and it showed good agreement.



The results from the detailed FEA as stated above recommends that the number of layers of FGM has no significant effect on the radial displacement, axial displacement, temperature and Von-mises, This is as shown in figure 8a-8d below. On the contrary, the non-homogeneity (n) factor of FGM has significant effect on FGM's performance under thermal and mechanical loading. Increase in non-homogeneity factor of the FGM, leads to proportionate increase in the radial displacement, axial displacement, temperature distribution and von-mises. This is as shown in figure 8e-8h below.

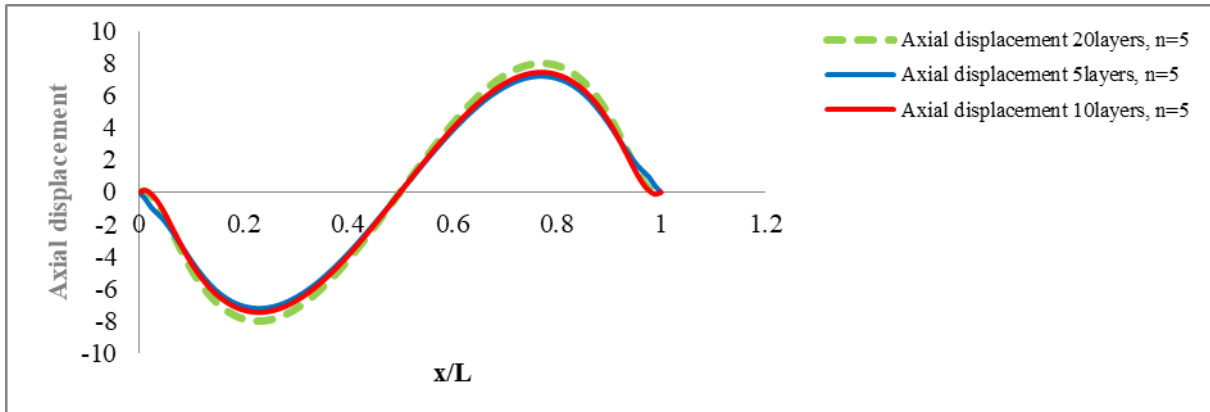


Figure 8a: Axial displacement comparison.

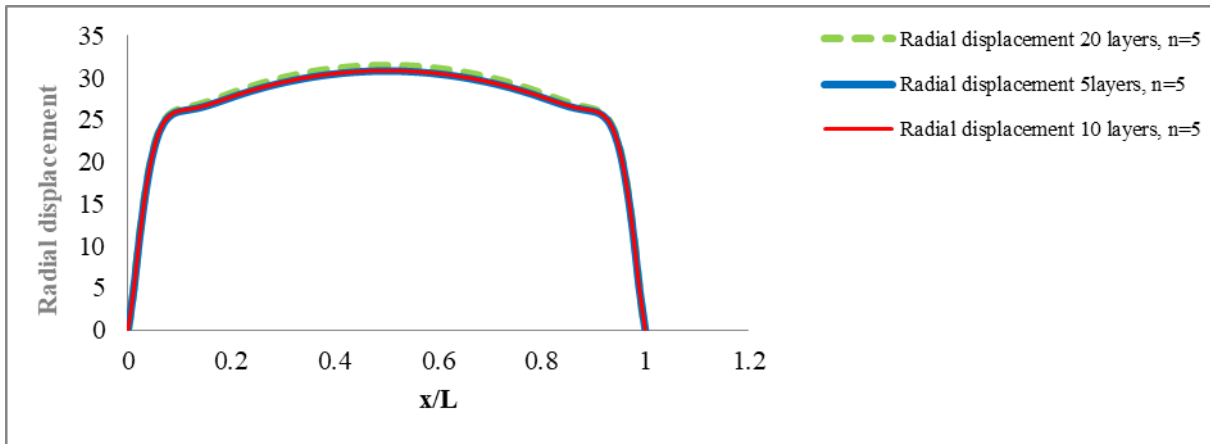


Figure 8b: Radial displacement comparison

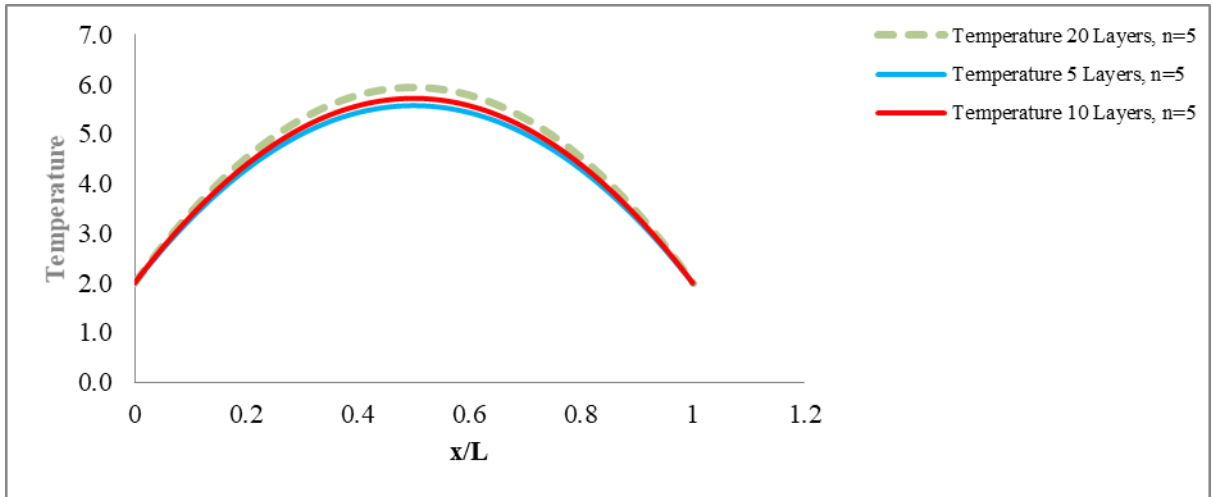


Figure 8c: Temperature distribution comparison

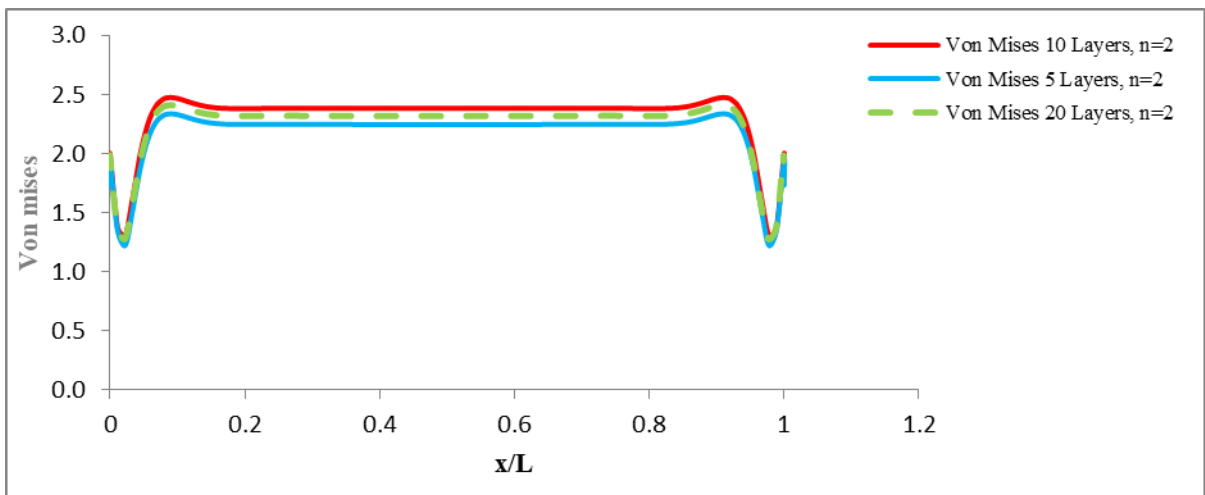


Figure 8d: Von-mises comparison

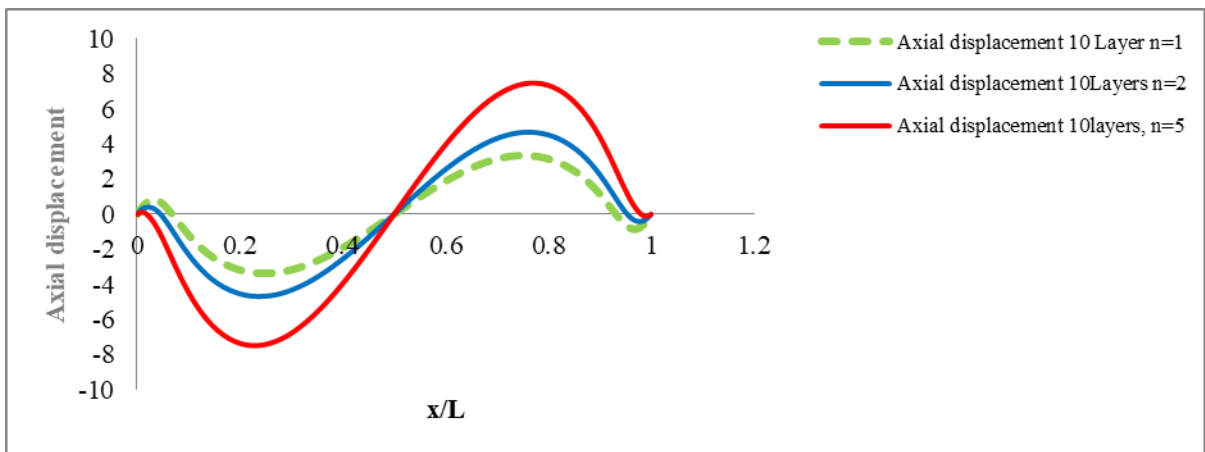


Figure 8e: Axial displacement comparison

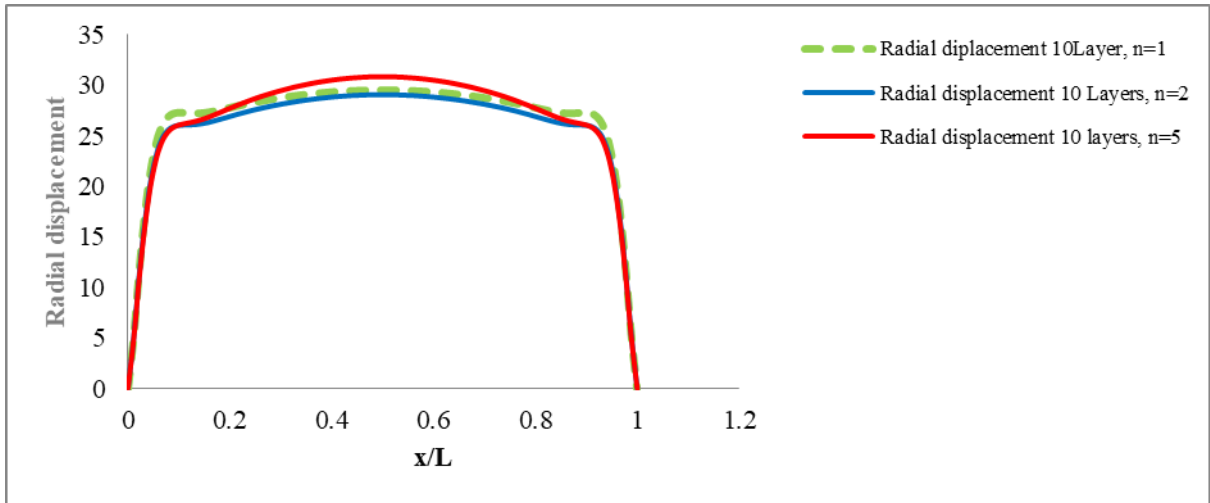


Figure 8f: Radial displacement comparison

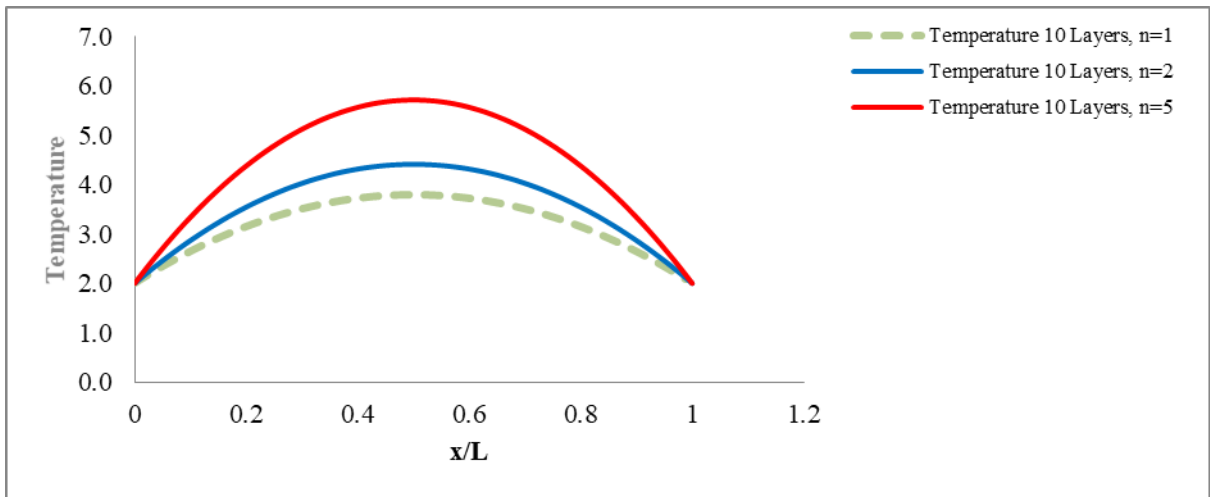


Figure 8g: Temperature distribution comparison

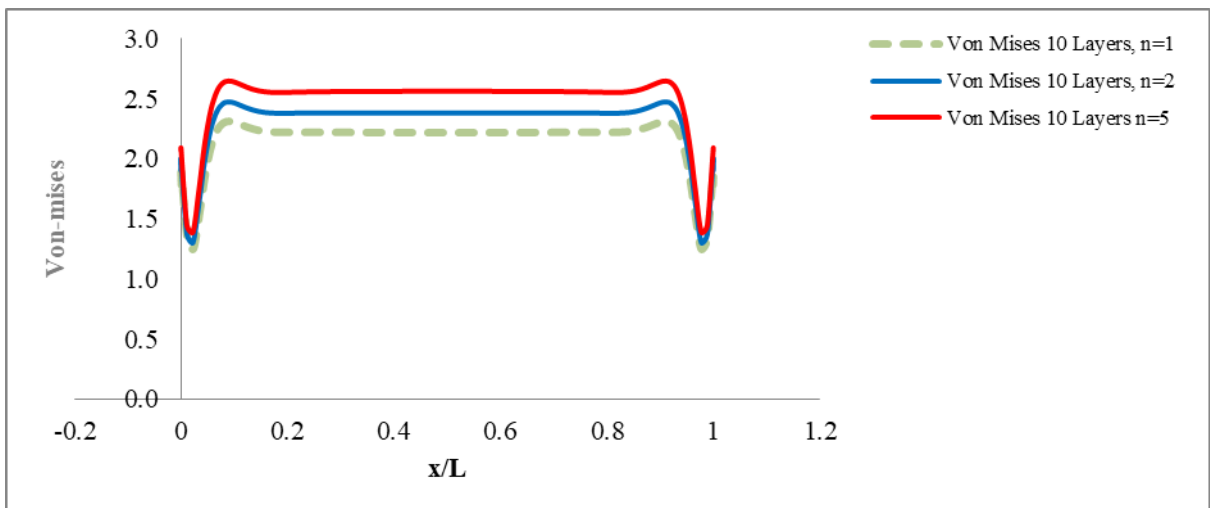


Figure 8h: Von-mises comparison

#### 8.4. EFFECTIVE YIELD STRENGTH OF FGM COMPONENTS

The determination of the total yield strength of the constituent layers of the FGM is a precursor to determining the design limit of the FGM when Von-mises failure criteria is been considered. The traditional approach of achieving the effective yield strength will be to determine the net average of each of the yield strength in the entire FGM. This approach becomes cumbersome when the number of layers in the FGM increases. The proposed novel approach as stated in equation 8.1 can be used for the determination of effective yield strength of FGM's that depends only on the non-homogeneity factor (n). This approach was bench marked against the traditional averaging methods and it showed excellent agreement with deviation reducing minimally to about zero as the number of layers increases.

$$\sigma_{y,eff} = \sigma_{y,c} \cdot \left(\frac{n}{n+1}\right) + \sigma_{y,m} \cdot \left(\frac{1}{n+1}\right)$$

[8.1]

The equation was premised on the Power Law equation and was compared and validated with analytical approach of summing up all averages for the individual FGM constituent. The details of the equation development and all assumptions/validations used are as presented in chapter 5 of this research.

#### 8.5. DESIGN LIMIT FOR STRAIGHT FGM PIPE

It is vital to know all design limits of all the recommended FGM material constituents as this will give insight on the suitability of any specific FGM constituent to the deep offshore oil and gas operations in Gulf of Guinea. The Von-mises failure criteria was used to determine the design limit (failure condition;  $\delta v \geq \delta y$ ) for all the four (4) straight pipe FGM that was modelled. They are as thus:

FGM 1: Ni-Fe-Cr alloy, INCOLOY 800, annealed/ Zirconia, transformation toughened, L

FGM 2: Stainless steel, austenitic, ASTM CF-20, cast, water quenched/ Alumina 94, SGM

FGM 3: Copper, C14200, soft/ Silicon carbide, HIP

FGM 4: Copper, C14200, soft/ Tungsten carbide, hot press

From the referenced line listing of the seawater processing line that formed the basis for this study, the operating temperature and pressure range is 318K and 2.1MPa respectively. The comparison of the derived design limits for the all the modelled straight pipe FGM's and the required operating conditions is represented in Figure 8i below:

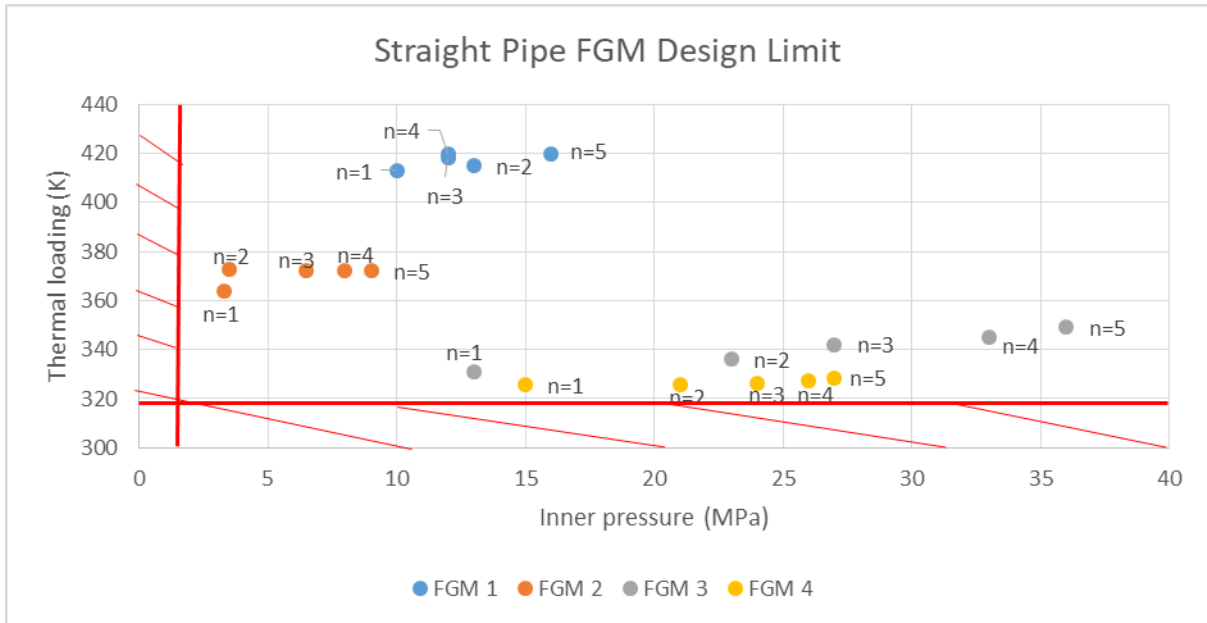


Figure 8i: Pressure and Temperature Design Limits for Straight FGM Pipes

Based on the foregoing, this research recommends as thus for straight pipe FGM operations in deep offshore oil and gas operations in Gulf of Guinea:

- All the 20-modelled FGM's are adequate and could be perfectly deployed on the sea water injection line based on the present operating conditions.
- For thermal loading preferences and considerations, the FGM's are to be considered in the following descending order FGM 1>FGM 2>FGM 3>FGM 4.
- For Pressure loading preferences and considerations, the FGM's are to be considered in the following descending order FGM 3>FGM 4>FGM 1>FGM 2
- The matrix developed in figure 8i could be used for FGM selection based on oil and gas service conditions similar to that in Gulf of Guinea.

### 8.6. DETERMINATION OF DESIGN LIMIT FOR ELBOW FGM PIPE

The Von-mises failure criteria was equally used to determine the design limit (failure condition;  $\delta_v \geq \delta_y$ ) for all the elbow FGM's. The Four (4) Metal/Ceramics FGM considered are as thus:

FGM 1: Ni-Fe-Cr alloy, INCOLOY 800, annealed/ Zirconia, transformation toughened, L

FGM 2: Stainless steel, austenitic, ASTM CF-20, cast, water quenched/ Alumina 94, SGM

FGM 3: Copper, C14200, soft/ Silicon carbide, HIP

FGM 4: Copper, C14200, soft/ Tungsten carbide, hot press

As stated in the section above, the referenced line listing of the seawater processing line that formed the basis for this study, the operating temperature and pressure range is 318K and

2.1MPa respectively. The comparison of the derived design limits for the all the modelled elbow pipe FGM's and the required operating conditions is represented in Figure 8j below:

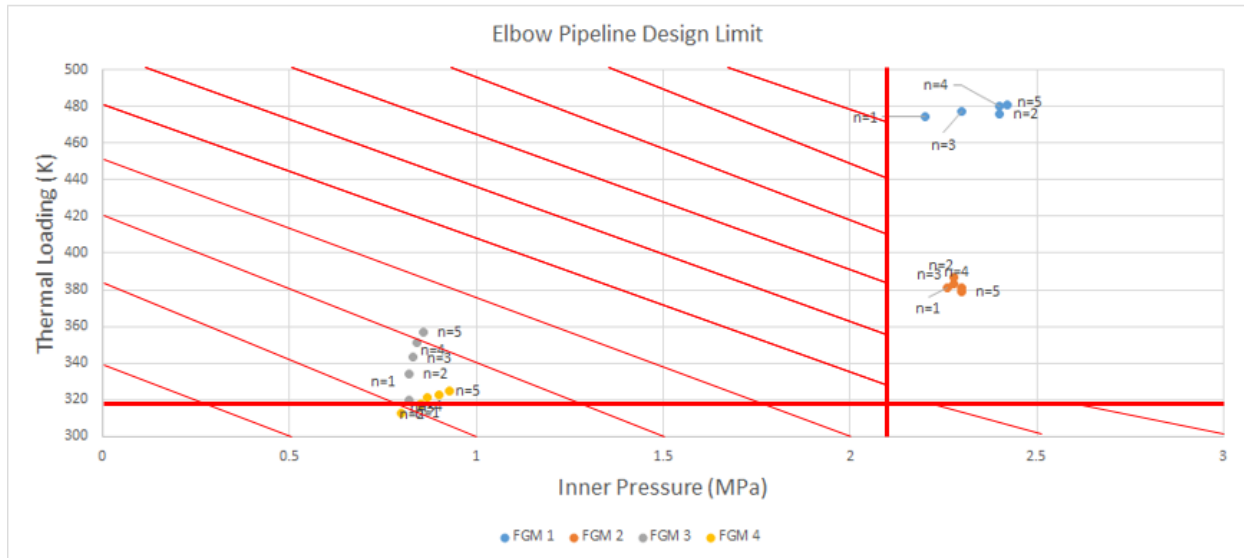


Figure 8.j: Pressure and Thermal Design Limits for Elbow FGM Pipes

Based on the foregoing, this research recommends as thus for the elbow pipe operations in deep offshore oil and gas operations in Gulf of Guinea:

- Only 10-modelled FGM's are adequate and could be perfectly deployed for the sea water injection line based on the present operating conditions. These are Elbow Pipes made from FGM's 1 and 2.
- For thermal loading preferences and considerations, the FGM's are to be considered in the following descending order FGM 1>FGM 2>FGM 3>FGM 4
- For pressure loading preferences and considerations, the FGM's are to be considered in the following descending order FGM 3>FGM 4>FGM 1>FGM 2
- The matrix developed in figure 8j could be used for elbow pipe configuration FGM selection based on oil and gas service conditions similar to that in Gulf of Guinea.

### 8.7. DETERMINATION OF DESIGN LIMIT FOR T-PIECE FGM PIPE

Similar approach was used for the T-Piece, the Von-mises failure criteria was used to determine the design limit (failure condition;  $\delta_v \geq \delta_y$ ) for all the T-Piece FGM's. Four (4) Metal/Ceramics FGM were as thus:

FGM 1: Ni-Fe-Cr alloy, INCOLOY 800, annealed/ Zirconia, transformation toughened, L

FGM 2: Stainless steel, austenitic, ASTM CF-20, cast, water quenched/ Alumina 94, SGM

FGM 3: Copper, C14200, soft/ Silicon carbide, HIP

FGM 4: Copper, C14200, soft/ Tungsten carbide, hot press

Still maintaining the same principle, the referenced line listing of the seawater processing line that formed the basis for this study, the operating temperature and pressure range is 318K and 2.1MPa respectively. The comparison of the derived design limits for the all the modelled T-Piece pipe FGM's and the required operating conditions is represented in Figure 8k below:

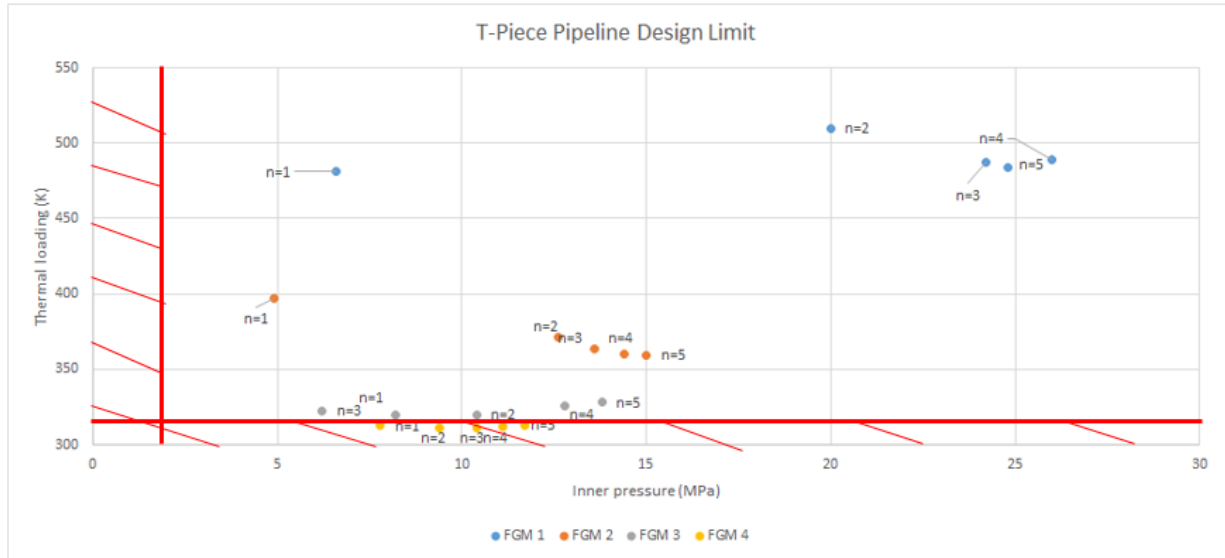


Figure 8.k: Pressure and Thermal Design Limits for Elbow FGM Pipe

Based on the foregoing, this research recommends as thus for the T-Piece pipe:

- Most of the modelled FGM's are adequate and could be perfectly deployed on the seawater injection line based on the present operating conditions, with the exception of the T-Piece FGM pipe made from FGM 4.
- For thermal loading preferences and considerations, the FGM's are to be considered in the following descending order FGM 1>FGM 2>FGM 3>FGM 4.
- Pressure loading limits for the considered T-Piece FGM's have no direct correlation with the FGM material combination. Hence for pressure loading preference and considerations, the FGM will be considered on individual basis depending on their non-homogeneity factors.
- The matrix developed in figure 8k could be used for T-Piece pipe configuration FGM selection based on Oil and Gas service conditions similar to that in Gulf of Guinea.

## **8.8. CONCLUDING REMARKS**

The dependence of FGM unique behaviours (radial displacement, axial displacement, temperature and Von-mises) on number of layers and non-homogeneity factor (n) when subjected to thermal and pressure loading was recommended in this study.

Furthermore, a novel approach to determine the effective yield strength of the FGM material combination was recommended in this research. In addition, the study recommended the pressure and temperature regime/limits all the considered FGMs could be effectively deployed based on configurations and materials combinations.

The recommendations from the research was premised on numerical analysis approach deployed for the entire study, this could be further improved if the modelled FGM's are further validated in future studies.



## **CHAPTER NINE: CONCLUSIONS AND FURTHER WORK**

### **9.1. INTRODUCTION**

The focus of this research was to explore the potential of using Functionally Graded Pipe (FGM) for the Sea Water Processing Line on most FPSO in deep offshore operations in Gulf of Guinea. To achieve this, representative Functionally Graded Pipeline components were modelled, analyzed and validated numerically on Abaqus by subjecting it to both thermal and mechanical loading.

The material constituent of the FGM used was modelled with the aid of CES Edupack Software and was ranked based on the materials ability to withstand the real-time operation conditions on the referenced Sea Water Processing Line. In addition, the design limits of all the modelled FGM pipes were predicted based on Von-mises failure criteria.

Lastly, parametric studies of the FGM pipe configurations (Straight FGM pipe, Elbow FGM pipe and T-Piece FGM pipe configuration) and a variety of material combinations was performed. This gave insight on the most optimal configuration and material combination for the service conditions.

### **9.2. MATERIAL SELECTION AND RANKING**

Engineering materials available as at 2017 on CES Edupack was assessed to determine the most suitable metal/ceramics material to be deployed for the FGM pipe that will meet the unique operating requirements. In tandem, the Analytic Hierarchy Process (AHP) technique was used to rank the materials identified on CES Edupark. A sensitivity analysis was carried on the identified materials based on weight, price and density variations in the final ranking of the materials. The study revealed the most ranked Metal/Ceramic combinations are as detailed below:

Metal 1: Ni-Fe-Cr alloy, INCOLOY 800, annealed

Metal 2: Stainless steel, austenitic, ASTM CF-20, cast, water quenched

Metal 3: Copper, C14200, soft

Ceramic 1: Zirconia, transformation toughened, L

Ceramic 2: Alumina 94, SGM

Ceramic 3: Silicon carbide, HIP

Ceramic 4: Tungsten carbide, hot press

### **9.3. NUMERICAL INVESTIGATION OF FGM AND DESIGN LIMIT PREDICTION**

Sixty (60) FGM pipes were modelled for the three FGM configurations considered, finite element analysis (FEA) using the Abaqus Finite Element system was used to reasonably mimic the physical behaviour of a series of offshore piping systems configurations. The three piping

configurations considered were Straight, Elbow and T- Piece pipe components; all these were modelled for a range of pressure and temperature conditions. From the reviewed literature, only a few benchmarks were available to validate the computational models, this was because of the evolving nature of the usage of FGM for piping in the oil and gas industry. Using the research by Ghannad *et al.* on “2D thermo-elastic model of an axisymmetric FGM hollow cylinder”, the developed FGM was validated using the following parameters; axial stress, circumferential stress and von-mises stress. The validation result comparison showed excellent agreement with the referenced journal with deviations of 5% at the maximum with both the numerical and analytical results from the journal.

As an FGM cannot have a single yield point by definition, an equation for the determination of effective yield strength for FGM's was developed which depends on the yield strength of the FGM constituents and the non-homogeneity factor of the FGM. This equation was validated using the conventional averaging approach of the FGM yield strengths determination and it showed excellent agreement with less than 1% for FGM's with higher numbers of layers.

The normalized stress approach was used for the determination of the design limit; this approach compared the effective yield strength of the FGM to the effective Von-mises stress for each of the configurations to determine the FGM failure tendencies due to yielding. The FGM design limit was determined when any of the layers in the FGM normalized stress was closest to one (1), above this limit the material begins to yield (Fail). The design limit was determined using the normalized stress between the ranges of  $0.99 < \text{normalized stress} < 1.01$ . The FEA of the FGM's considered was limited to thermal and pressure loading, hence only thermal and pressure design limits were determined for all the FGM's.

This study compared the design limits for Straight, Elbow and T-Piece Pipe to provide appreciable understanding of the limits for all the configurations as detailed in figures 7.9 and 7.10.

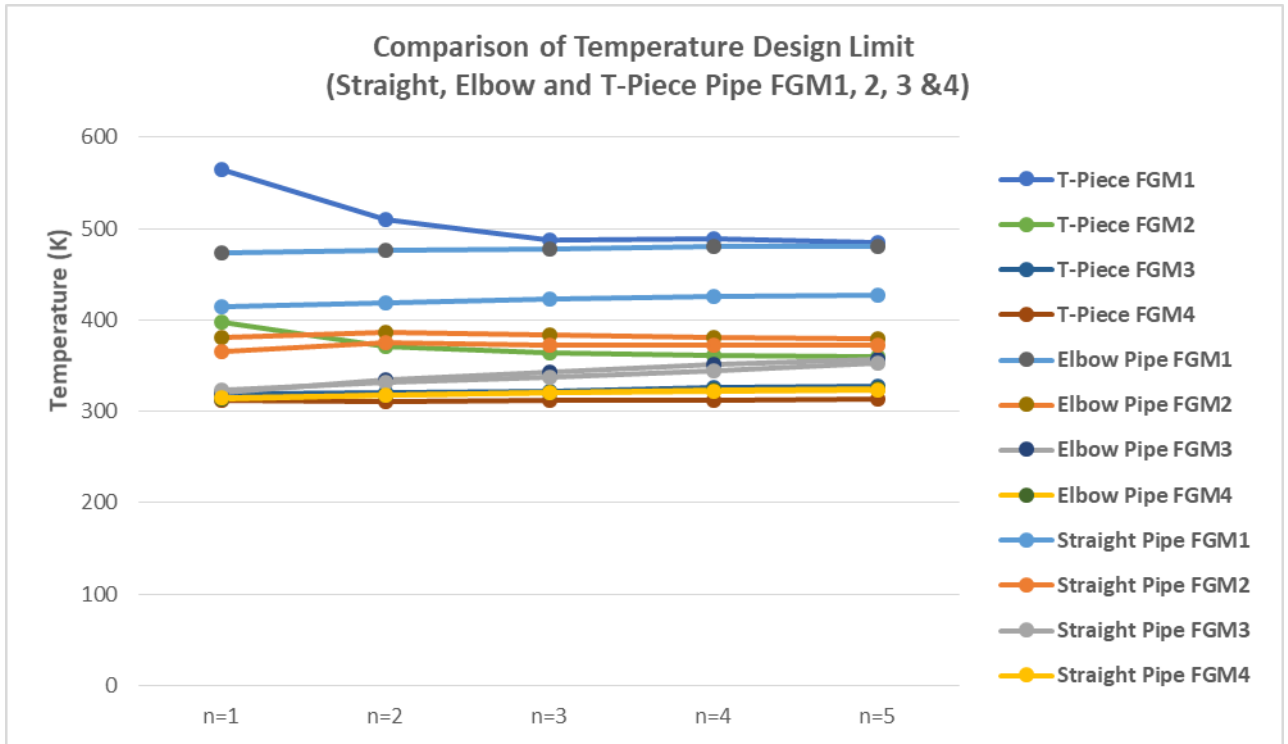


Figure 7.9: Pressure Design Limit comparison for Straight, Elbow and T-Piece Pipe.

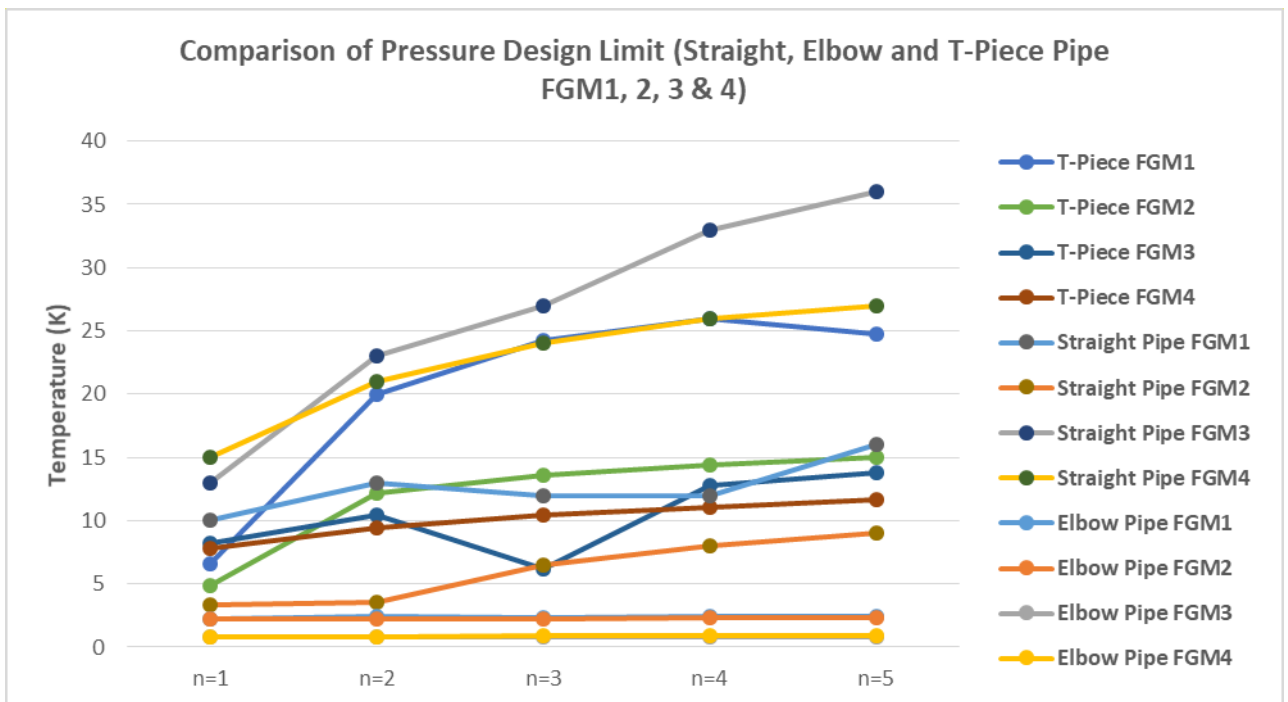


Figure 7.10: Temperature Design Limit comparison for Straight, Elbow and T-Piece Pipe.

The comparison of the temperature and pressure design limits between straight, elbow and T-Piece FGM pipe as displayed in figure 7.9/7.10 and tables 5.9, 5.10, 6.8, 6.9, 7.8 & 7.9 revealed that the temperature design limits between the three configurations were within a close range with a maximum of 8% variation for most the FGM material combination considered.

However, the FGM 1 material combination was an outlier with the temperature design limit variation of up to 27% between the three configurations. In addition, Straight and Elbow FGM pipe exhibited similar trend in the temperature limits variation; it increases with increase in non-homogeneity factor for both configurations. This is contrary for the T-Piece FGM pipe, the temperature design limit mostly reduces with increase in non-homogeneity factor.

In addition, the comparison of the pressure design limit between the three configurations shows huge disparity in the limits, but the trend for the pressure limit variation for the three configurations were somewhat similar, as they both showed minimal incremental variation in the limits with increase in non-homogeneity factor.

From the typical oil and gas operating envelop considered in Gulf of Guinea as depicted in figures 8i, 8j and 8k, the design limit results for the **Straight pipes** revealed that all the 20 FGM's could be deployed for the operations being considered. In addition, the design limit results for the **T-Pieces Pipes** also revealed that most of the FGM's modelled could be adequately deployed for the operations being considered. But on the contrary, the design limit results for the **Elbow Pipes** revealed that only 10 FGM's from the 20 modelled FGM's could be adequately deployed for the operations being considered.

Considering the FGM's material constituent, the study revealed that only FGM 1 and FGM 2 could be deployed for higher temperature and pressure design consideration. Hence, it could be inferred that FGM's made from the material combination below are more adequate for higher temperature/pressure operation irrespective of the configuration (i.e., straight pipe, elbow pipe and T-piece pipe).

- Ni-Fe-Cr alloy, INCOLOY 800, annealed and Zirconia, transformation toughened, L
- Stainless steel, austenitic, ASTM CF-20, cast, water quenched and Alumina 94, SGM

On the contrary, the study revealed that FGM 3 and FGM 4 could only be deployed to minimally high temperature and pressure for straight pipe FGM configuration only. Hence, material combination for FGM 3 and 4 as detailed below are more adequate for lower pressure and temperature when considering other FGM configurations like elbow and T-piece pipes.

- Copper, C14200, soft and Silicon carbide, HIP
- Copper, C14200, soft and Tungsten carbide, hot press

The design limits of all the considered FGM's for the different configurations revealed that FGMs are more suitable for straight pipe configuration, although could be used for Elbow and T-Piece but not as good as straight pipe.

Finally, it is worth noting that the work undertaken herein developed matrices (8i, 8j and 8k) dependent on internal pressure and thermal loading for Straight, Elbow and T-Piece FGM Pipe configurations, this could serve as guide in material selection for FGM's in oil and gas service conditions similar to that in Gulf of Guinea.

#### **9.4. SUGGESTION FOR FURTHER WORK**

The recommendations from the research was premised on the limitation of adopting only numerical analysis approach through the entire study, this could be further improved if the modelled FGM's are further validated through other approaches in future studies, to this end the following future researches are suggested.

- Present research considered mainly numerical analysis to deduce all the findings, hence further study can be performed premised on experimental approach. This will help to bridge all gaps and assumption between the numerical and experimental results.
- The present study considered only thermal and pressure loading conditions, a further research could be perform that will consider other loading conditions like bending, fatigue life of the FGM, cracks on FGM etc. this will provide a broader understanding of FGM pipes.
- The present research focused on few of the possible metal/ceramics material combinations for the FGM models. The identified candidate materials were 3 metals and 4 ceramics materials. From this materials combination variables, about 24 different metal/ceramic FGM could be developed each exhibiting there unique properties. However, the present study considered only 4 of these possibilities. Hence, further studies is recommended on the other aspect of material combination yet to be explored.

## REFERENCES

- Afshar, R., Bayat, M., Lalwani, R.K. & Yau, Y.H. (2015). Elastic *behavior of glass-like functionally graded infinite hollow cylinder under hydrostatic loads using finite element method*. Materials and Design, vol. 32, pp. 781–787.
- Alibeigloo, A. (2010). Exact solution for thermo-elastic response of functionally graded rectangular plates. Composite Structures, vol. 92, pp. 113–121.
- Alireza, B. (2014). Corrosion and Materials Selection A Guide for the Chemical and Petroleum Industries
- Andrew, R., Hongjun, L. & Donald, M. (2005). Plastic collapse of pipe bends under combined internal pressure and in-plane bending. International Journal of Pressure Vessels and Piping, vol. 82, pp. 407–416.
- Arash, H. D. (2000). Finite element analysis of thermally induced residual stress in Functionally Graded Materials.
- Batani, M, et. al (2013). A comprehensive study on stability of FGM plates. International Journal of Mechanical Sciences, vol. 75, pp. 134–144.
- Belytschko, T., Lu, Y.Y. & Gu, L. (1994). Element Free Galerkin Methods. International Journal for Numerical Methods in Engineering, vol. 37, pp. 229-256
- Bergmann, W.: Werkstofftechnik, Teil 1: Grundlagen. Hanser Verlag, 3rd edition, 2000.
- Bhattacharya, S., Singh, I. V. & Mishra, B. K. (2013). Fatigue life simulation of functionally graded materials under cyclic thermal load using XFEM. International Journal of Mechanical Sciences, 82, pp. 41–59
- Christo M. T., Veerappan, A. R., & Shanmugam, S. (2012). Comparison of plastic limit and collapse loads in pipe bends with shape imperfections under in-plane bending and an internal pressure. International Journal of Pressure Vessels and Piping, vol. 99-100, PP. 23-33.
- Clémentine, M., Sophie, L., Bruno, S., Nicolas, G. & Frédéric, B., (2018). Alumina-titanium functionally graded composites produced by spark plasma sintering. Journal of Materials Processing Tech, vol. 254 pp. 277–282. Accessed: 12/05/2018
- Da-Guang, Z., (2013). Modeling and Analysis of FGM rectangular plates based on physical neutral surface and high order shear deformation theory. International Journal of Mechanical Sciences, vol. 68, pp. 92–104
- Decock, J. (1973). Determination of stress concentration factors and fatigue assessment of flush and extruded nozzles in welded pressure vessels, 2nd Int. Conf. on Pressure Vessel Technology, Part II, Material. Fabrication and Inspection, pp. 821-34.

- Douglas, E. B. & John, J. M. (2007). Microstructure and kinetics of a functionally graded NiTi–TiC<sub>x</sub> composite produced by combustion synthesis, *Journal of Alloys and Compounds*, vol. 430, pp. 274–281. Accessed: 10/08/17
- El-Galy, I. M, Ahmed, M. H. & Bassiouny, B. I. (2017). Characterization of functionally graded Aluminium (Al) and Silicon Carbide Particles (SiCp) metal matrix composites manufactured by centrifugal casting. *Alexandria Engineering Journal*, Accessed 02/06/2017.
- Encyclopedia of Materials Science and Technology, Functionally Graded Materials, vol. 1-11, pp. 3408.
- Escribano, J. A., García, J. L., Alvaredo, P., Ferrari, B., Gordo, E., & Sanchez-Herencia, A.J. (2015). FGM stainless steel-Ti(C, N) cermet through colloidal processing [14]. *Int. Journal of Refractory Metals and Hard Materials*, vol. 49, 143–152. Accessed: 13/05/2018
- Faisal, N.H., Anil Prathuru, K., Saurav, G., Ahmed, Droubi, R.M. G., Beake, B.D. & Fu, Y.Q. (2017). Cyclic Nanoindentation and Nano-Impact Fatigue Mechanisms of Functionally Graded TiN/TiNi Film. *Shap. Mem. Superelasticity*, vol. 3, pp. 149–167. Accessed: 10/08/17
- Fatih, E., Canakci, A., Temel V. & Serdar O. (2015). Corrosion and wear behavior of functionally graded Al<sub>2024</sub>/SiC composites produced by hot pressing and consolidation. *Journal of Alloys and Compounds*, vol. 644, pp. 589–596. Accessed 10/08/2017
- Fallah, F. & Nosier, A. (2012). Nonlinear behavior of functionally graded circular plates with various boundary supports under asymmetric thermo-mechanical loading. *Composite Structures*, vol. 94, pp. 2834–2850.
- Finot, M. & Suresh, S. (1996). Small and large deformation of thick and thin-film multi- layers: Effect of layer geometry, plasticity and compositional gradients. *Journal of the Mechanics and Physics of Solids*, vol. 44, pp. 683-721.
- Gagandeep, B., Singh, I. V, Mishra, B. K. & Bui, T. Q. (2015). Numerical simulation of functionally graded cracked plates using NURBS based XIGA under different loads and boundary conditions. *Composite Structures*, vol. 126, pp. 347–359.
- Gaurav Bhende and Girish Tembhare (2013). Stress Intensification & Flexibility in Pipe Stress Analysis. *International Journal of Modern Engineering Research (IJMER)* Vol.3, Issue.3, May-June. 2013 pp-1324-1329.

- Ghannad, M. & Parhizkar Y. M. (2017). 2D Thermo elastic behaviour of a FG cylinder under thermomechanical loads using a first shear order theory. *International Journal of Pressure Vessels and Piping*, vol. 149, pp. 75-92.
- Golmakani, M. E. & Kadkhodayan, M. (2011). Large deflection analysis of circular and annular FGM plates under thermo-mechanical loadings with temperature-dependent properties. *Composites: Part B*, vol. 42, pp. 614–625.
- Guoqiang, L., Yang, D., Shulong, L., Kan, Y., Qiang, S. & Lianmeng, Z. (2014). Fabrication and properties of W-Cu functionally graded material by tape-casting. *Key Engineering Materials Online*: 2014-06-18 ISSN: 1662-9795, Vol. 616, pp 66-71. Accessed 10/08/2017.
- Handbook, *Metals Engineering –Design*, American Society of Mechanical Engineers (ASME), Working Stress, p. 527.
- Haizhu, P., Tianshu, S. & Zhihai, W. (2015). An analytical model for collinear cracks in functionally graded materials with general mechanical properties. *Composite Structures*, vol. 132, pp. 359–371.
- Hiroyuki, M., (2009). Stress analysis of functionally graded plates subjected to thermal and mechanical loadings. *Composite Structures*, vol. 87, pp. 344–357.
- Hoang, V. T. & Nguyen, D. D. (2010). Nonlinear analysis of stability for functionally graded plates under mechanical and thermal loads. *Composite Structures*, vol. 92, pp. 1184–1191.
- Hoffman, M., Mai, W. Y., Wakayama, S., Kawahara, M. & Kishi, T. (1995). Crack-tip degradation processes observed during in situ cyclic fatigue of partially stabilized zirconia. *Journal of the American Ceramic Society*, vol. 78, pp. 2801–2810.
- Horibe, S. & Hirahara, R.(1991) Cyclic fatigue of ceramic materials: Influence of crack path and fatigue mechanisms. *Acta metallurgica et materialia*, vol.39, pp.1309– 1317.
- Hornbogen, E. & Werkstoffe (1994). Springer-Verlag, 6th edition Berlin.
- Hosseini, S. S., Bayesteh, H. & Mohammad, S. (2013). Thermo-mechanical XFEM crack propagation analysis of functionally graded materials. *Materials Science & Engineering*, vol.561, pp. 285–302.
- Huu-Tai, T. & Seung-Eock, K. (2015). A review of theories for the modeling and analysis of functionally graded plates and shells. *Composite Structures*, vol. 128, pp. 70–86.
- Huu-Tai, T. & Seung-Eock, K. (2015). A review of theories for the modeling and analysis of functionally graded plates and shells. *Composite Structures*, vol. 128, pp. 70–86.
- In-Jin, S. & Zuhair, A. M. (2005). Synthesis of TiC, TiC–Cu Composites, and TiC–Cu Functionally Graded Materials by Electrothermal Combustion.



- Ismail, M., Belaid, M. & Samir, B. (2013). Static and dynamic analysis of functionally graded plates using Four-variable refined plate theory by the new function. *Composites: Part B*, vol. 45, pp. 748–757. Accessed: 05/04/16
- Jacob, L. P. (2003). *Thermoplastic analysis and optimization of Functionally Graded Plates and Shells*.
- Jastrzebski, Z. D. (1976). *The Nature and Properties of Engineering Materials*. John Wiley & Sons
- Jacob, Rajan T.P.D, Joseph M.A., and B.C. Pai (2016). *Processing and Characterization of Functionally Graded Aluminum (A319)—SiCp Metallic Composites by Centrifugal Casting Technique*. The Minerals, Metals & Materials Society and ASM International. Accessed 14/08/2017.
- Jian, L., Chang-Yu Zhou, Ji-Lin Xue, & Xiao-Hua He, (2014). Limit loads for pipe bends under combined pressure and out-of-plane bending moment based on finite element analysis. *International Journal of Mechanical Sciences*, vol. 88, pp. 100–109.
- [94] Jian, L., Chang-Yu, Z., Peng, C., Xiao-Hua H. (2015). Plastic limit loads for pipe bends under combined bending and torsion moment. *International Journal of Mechanical Sciences*, vol. 92, pp. 133–145.
- Jing-Hua Z., Guang-Ze L., & Shi-Rong L. (2015). Analysis of transient displacements for a ceramic–metal functionally graded cylindrical shell under dynamic thermal loading. *Ceramics International*, vol. 41, pp. 12378–12385.
- Jiri M., Hanna, B., Vlastimil, B., Pavel, S., Tomás, C., & Zdenek, P. (2015). W–steel and W–WC–steel composites and FGMs produced by hot pressing [15]. *Fusion Engineering and Design*, vol. 100, pp. 364–370.
- Joachim, R., Harders, H. & Bäkeret, M., *Mechanical Behavior of Engineering Materials; Metals, Ceramics, Polymers and Composite*. Springer-Verlag Berlin Heidelberg.
- John J. M. (2006). *Combustion Synthesis of a Functionally Graded Nickel Titanium alloy (Nitinol, NiTi) and Titanium Carbide (TiC<sub>x</sub>) Composite*
- Justyna, Z., Paulina, W., Aleksandra, M., Katarzyna, K. & Waldemar, K. (2016). Al<sub>2</sub>O<sub>3</sub>/Ni functionally graded materials (FGM) obtained by centrifugal-slip casting method. Open access at Springerlink.com. Accessed: 10/08/17
- Kamran, A. (2013). Three dimensional static analysis of two dimensional Functionally Graded Plates. *International journal of recent advances in Mechanical Engineering*, vol. 2, No. 2.

- Kamran, A., Manouchehr, S. & Mehdi, A. (2014). Transient thermal stresses in functionally graded thick truncated cones by graded finite element method. *International Journal of Pressure Vessels and Piping*, vol. 119, pp. 52-61
- Lange, G. (editor): *Systematic Analysis of Technical Failures*. Ir Publications, 1985.
- Liping, W., Junyan, Z., Zhixiang, Z., Yiming, L., Litian, H. & Qunji, X. (2006). Fabrication of a nanocrystalline Nickel-Cobalt alloy (Ni-Co) and Cobalt-oxide (Wurtzite, CoO) functionally graded layer with excellent electrochemical corrosion and tribological performance [19]. *INSTITUTE OF PHYSICS PUBLISHING, Nanotechnology*, vol. 17, 4614–4623 doi:10.1088/0957-4484/17/18/014.
- Loc, V. T., Ferreira, A. J. M. & Nguyen-Xuan, (2013). Isogeometric analysis of functionally graded plates using higher-order shear deformation theory. *Composites: Part B*, vol. 51, pp. 368–383. Accessed: 04/40/1
- Lourdes, D. B., Brandon, B., Richard, O., John, P. B., Dillon, R. P., Andrew, A. S., Bryan, M., Zi-Kui, L. & Allison, M. B. (2018). Characterization of a functionally graded material of Ti-6Al-4V to 304L stainless steel with an intermediate V section. *Journal of Alloys and Compounds*, vol., 742 pp. 1031-1036. Accessed: 13/04/18
- Malekzadeh, P. & Monajjemzadeh S.M. (2013). Dynamic response of functionally graded plates in thermal environment under moving load. *Composites: Part B* vol. 45, pp. 1521–1533.
- Malekzadeh, P. & Shojaee, S.A. (2013). Dynamic response of functionally graded plates under moving heat source. *Composites: Part B*, vol. 44, pp. 295–303.
- McCrum, N. G., Buckley, C. P. & Bucknall, C. B. (1988). *Principles of Polymer Engineering*. Oxford University Press
- Mine, U. U. (2013). Investigation of thermal and Mechanical loading on Functionally Graded Material Plates. *Journal of Mechanical, Aerospace. Industrial and Mechanical Engineering*, Vol. 7, pp. 11.
- Miyamoto Y., Kaysser W.A., Rabin B.H., Kawasaki A. & Ford, R.G. (1999). *Functionally Graded Materials: Design, Processing and Applications*. Chapman 43 Hall
- Muhammad, A. F., Ahmad, K. & Muhammad, A. H., (2015). Interfacial diffusion reaction and mechanical characterization of 316L stainless steel-hydroxyapatite functionally graded materials for joint prostheses. *Ceramics International*, vol. 41, pp. 14458–14467. Accessed: 13/04/18
- Muhammad, I. A. L., Siti, N. S. J., Shahnor, B., Ahmad, H., Dheya, S. A., Faizal, M., Dewan, M. N., Noor, M. I. & Izwan, I. (2014). Effect of Sintering Temperature on Functionally

Graded Nickel/Alumina Plate [18]. *Applied Mechanics and Materials*, ISSN: 1662-7482, Vol.629, pp.437-443, doi:10.4028/www.scientific.net/AMM.629.437

- Mu, E. & Pereyra-Rojas, M. (2017). *Practical Decision Making*. Springer Briefs in Operations Research, Accessed 19/06/2018
- Mustafa, U., Erhan, B., Bertan, S., Kemal, O. M., Necip, C., Orhan, R. Y., & Omer, K. (2014). Ballistic performance of Silicon Carbide (SiC)–AA7075 functionally graded composite produced by powder metallurgy. *Materials and Design*, vol. 56, pp. 31–36. Accessed 09/08/2017.
- Nakamura, T. (2000). *Determination of properties of Graded Materials by Inverse Analysis and Instrumented Indentation*. Acta Metallurgica Inc., Published by Elsevier Science.
- Navid, V., Sundararajan, N., Octavio, A., Gonzalez-Estrada, T. R., Tinh, Q. B. & Stéphane, .A.B. (2013). NURBS-based finite element analysis of functionally graded plates: Static bending, vibration buckling and flutter. *Composite Structures*, vol. 99, pp. 309–326.
- Nguyen-Xuan, L. V. T., Chien, H. T., Kulasegaram, S. & Bordas, S. P. A. (2014). Isogeometric analysis of functionally graded plates using a refined plate theory. *Composites: Part B*, vol. 64, pp. 222–234. Accessed: 04/04/16
- Pan, E. (2003). Exact solution for functionally graded anisotropic elastic composite laminates. *Journal of Composite Materials*, vol. 37, (21) pp. 1903-1920
- Praveen, G, N & Reddy, J. N. (1998). Nonlinear transient thermos-elastic analysis of functionally graded ceramic-metal plates. *Int. J. Solids Structure*, vol. 35. (33) pp. 4457 - 4476.
- Rao, R. V. & Davim, J. P. (2008). A decision-making framework model for material selection using a combined multiple attribute decision-making method. *International Journal for Advance Manufacturing Technology*, vol.35, pp.751–760. Accessed 16/06/2018.
- Rodriguez-Castro, R., Wetherhold, R.C., & Kelestemur, M.H. (2002), Microstructure and mechanical behavior of functionally graded Al-A359/SiCp composite. *Materials Science and Engineering*, vol. A323, pp. 445–456. Accessed 21/8/2017
- Rogers, T.G., Watson, P. & Spencer, A. J. M. (1995). Exact three-dimensional elastic solutions for bending of moderately thick inhomogeneous and laminated strips under normal pressure. *International Journal of Solids and Structures*, vol. 32, (12) pp. 1659-1673.
- Saaty, T. L. (2012). *Decision Making for Leaders: The Analytic Hierarchy Process for Decisions in a Complex World*. Third Revised Edition, Pittsburgh: RWS Publications.
- Sabine, D. & Lutz, K. (2017). Mechanical properties of a High-alloy metastable austenitic steels (CrMnNi steel) and Magnesia Partially Stabilized Zirconia (Mg-PSZ) Functionally

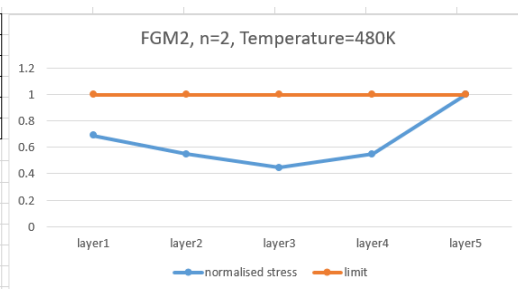
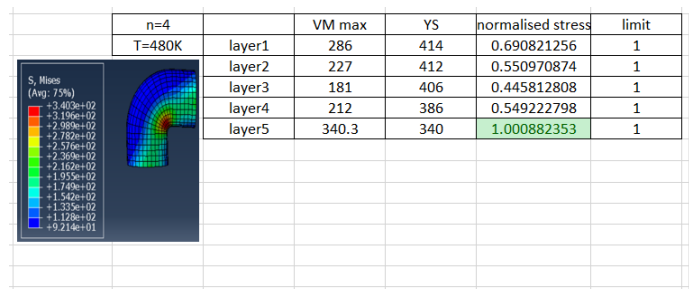
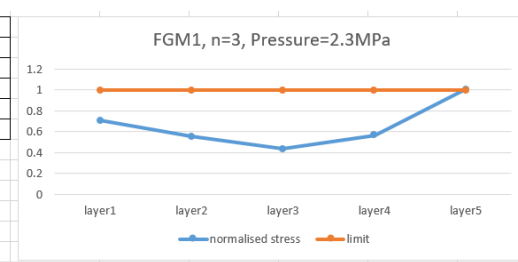
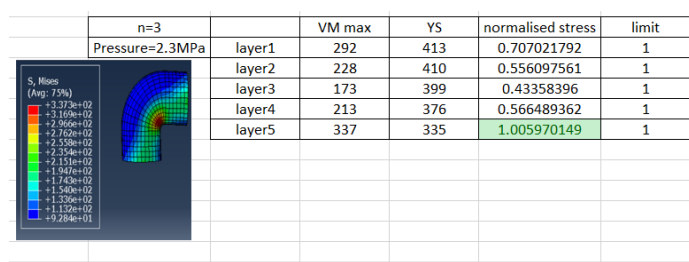
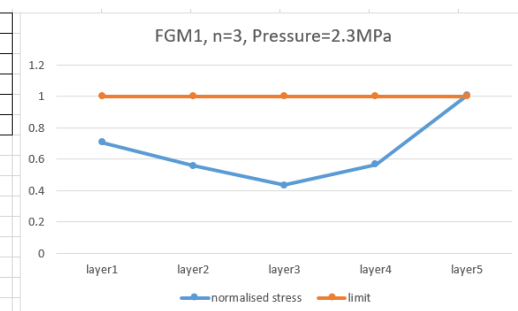
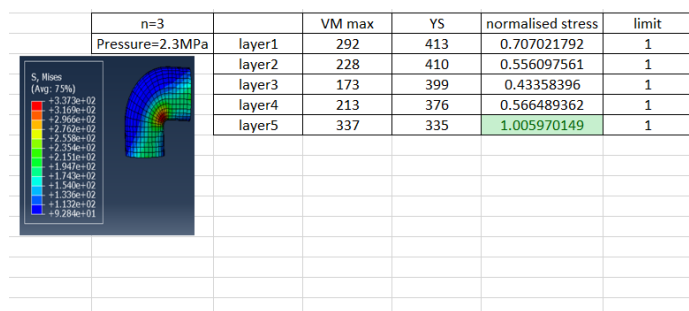
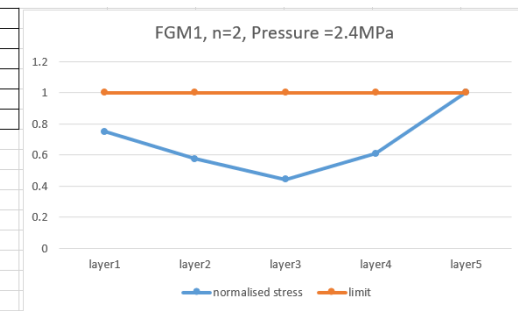
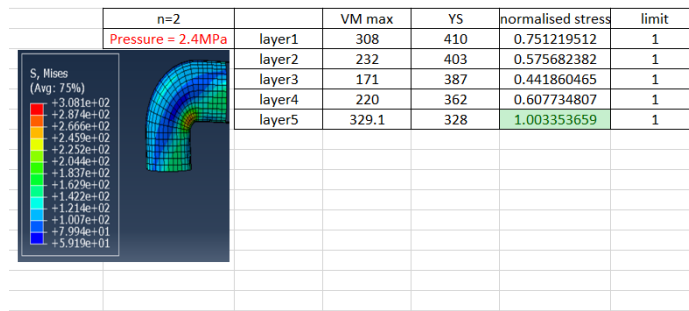
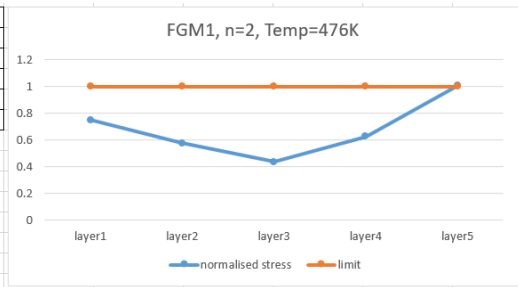
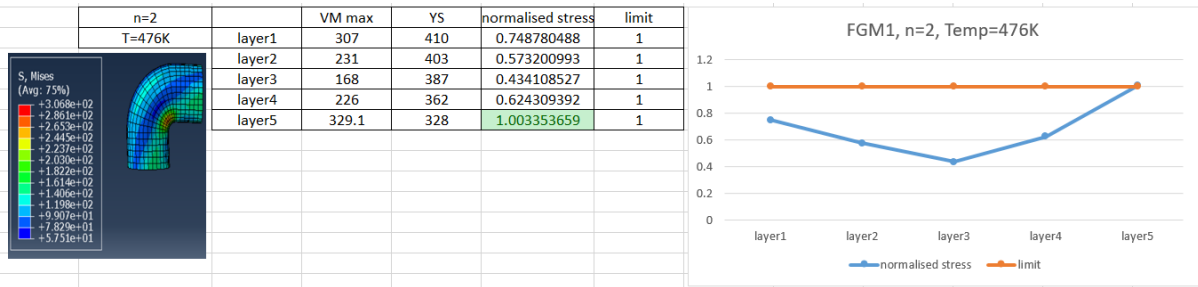
- Graded Material processed by asymmetric Spark Plasma Sintering (SPS). *Materials and Design*, vol. 115, pp. 8–16. Accessed: 12/04/18
- Salehi, M. A. V., Naderi, M. R. M., Varmaziar, A. (2013). Fatigue behavior of functionally graded steel produced by electro-slag remelting. *Materials Science & Engineering*, vol. A 584, pp. 143–149.
- Sandeep, A., Addis, K., Vijaya, B. C. & Arun, S. (2012). Researched on dynamic curving cracks in functionally graded materials under thermo-mechanical loading. *International Journal of Solids and Structures*, vol. 49, pp. 1637–1655
- Sator, L. S., Sladek, J. V. & Young, D. L. (2016). Elastodynamics of FGM plates by mesh-free method. *Composite Structures*, vol. 140, pp. 309–322.
- Schott, D. (editor): *Werkstoffermüdung – Ermüdungsfestigkeit*. Deutscher Verlag für Grundstoffindustrie, Stuttgart, 4th edition, 1997
- Setoodeh, A. R. & Afrahim, S. (2014). Non-linear dynamic analysis of FG micro-pipes conveying fluid based on strain gradient theory. *Composite Structures*, vol. 116, pp. 128–135.
- Shariyat, M., Jafari R. (2013). Nonlinear low-velocity impact response analysis of a radially preloaded two-directional-functionally graded circular plate: A refined contact stiffness approach. *Composites: Part B*, vol. 45, pp. 981–994
- Shun-Jie Li, C. Z., Jian, L., Xiang-Ming, P. & Xiao-Hua, H. (2017). Effect of bend angle on plastic limit loads of pipe bends under different load conditions. *International Journal of Mechanical Sciences*, pp. 131–132 (2017) 572–585.
- Singha, M. K., Prakash, T. & Ganapathi, M. (2011). Finite element analysis of functionally graded plates under transverse load. *Finite Elements in Analysis and Design*, vol. 47, pp. 453–460
- Sumesh, S. V., Shanmugam, S. AR. (2017). Structural Deformations on Critical Cracked Pressurised Pipe Bends: Implication on the Von Mises Stresses. *Materials Today: Proceedings*, vol. 4, pp. 10163–10168.
- Suphi, Y. (2006). Buckling driven delamination of orthotropic Functionally Graded Material.
- Swaminathan, K., Naveenkumar, D. T. & Zenkour, A. M. (2015). Stress vibration and buckling analyses of FGM plates—A state-of-the-art Review. *Composite Structures*, vol. 120, pp.10–31. Accessed: 04/04/16
- Takahiro, K., Masafumi, S., Hisashi, S. & Yoshimi, W. (2015). Fabrication of copper/diamond functionally graded materials for grinding wheels by centrifugal sintered-casting. *Journal of Materials Processing Technology*, vol. 217, pp. 294–301. Accessed 01/05/2018.

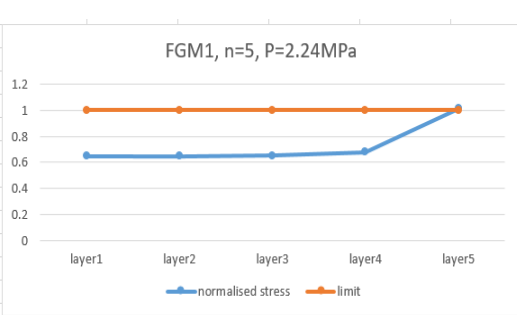
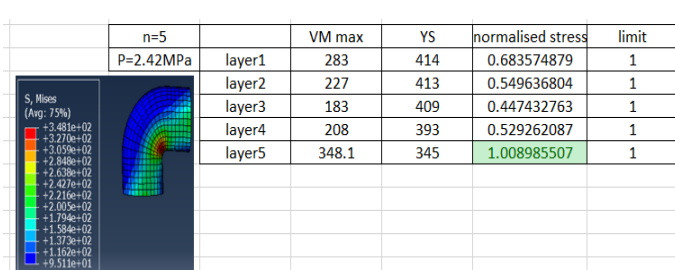
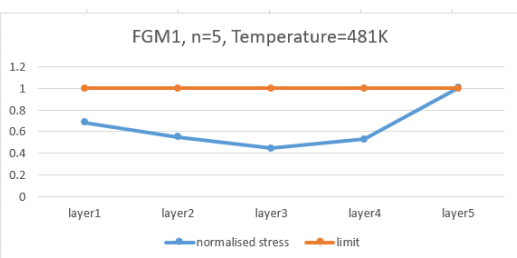
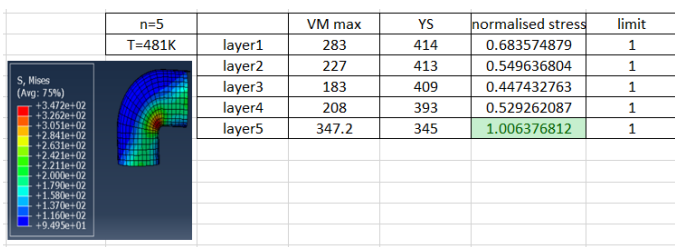
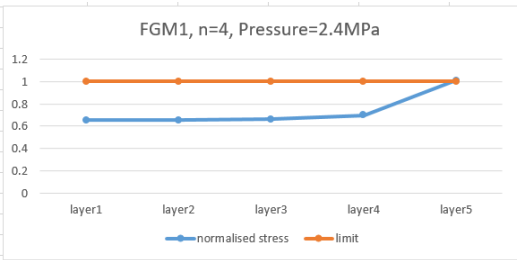
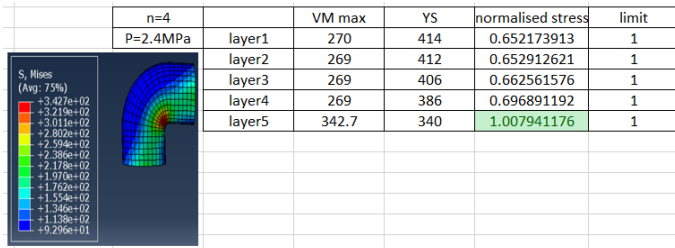
- Tieliang, Y., Weiguang, Z., Qibai, H. & Shande, L. (2016). Sound radiation of functionally graded materials plates in thermal environment. *Composite Structures*, vol. 144, pp. 165–176. Accessed: 19/03/16
- Todd, R. J. (2000). Analysis of Functionally Graded Material objects representation material.
- Ueda, S. & Gasik, M. (2000). Thermo-elastoplastic analysis of W-Cu functionally graded materials subjected to a uniform heat flow by micromechanical model. *Journal of Thermal Stresses*, vol. 23, pp. 395-409
- Vel, S. & Batra, R.C. (1999). Analytical solutions for rectangular thick laminated plates subjected to arbitrary boundary conditions. *AIAA Journal*, vol. 37, (11) pp. 1464-1473
- Victor, B. & Larry, W. B. (2007). *Modelling and Analysis of Functionally Materials and Structures*.
- Wilfredo, M. R., Glaucio, H. P., Emilio, C. & Nelli, S. (2012) Analysis, manufacture and characterization of Ni/Cu functionally graded structures. *Materials and Design*, vol. 41, pp. 255–265. Accessed 01/05/2018
- Won-Hong, L., Sung-Cheon, H. & Weon-Tae, P. (2015). A refined higher order shear and normal deformation theory for E-, P-, and S-FGM plates on Pasternak elastic foundation. *Composite Structures*, vol. 122, pp. 330–342.
- Woo-Young, J. & Sung-Cheon, H. (2014). Transient analysis of FGM and laminated composite structures using a refined 8-node ANS shell element. *Composites: Part B*, vol. 56, pp. 372–383.
- XinXing, M., Bin Xiao, S. C., BingHuang, C. & Huan, X. (2018). A novel approach to fabricate W/Cu functionally gradient materials (FGM). *International Journal of Refractory Metals & Hard Materials*, vol. 72, pp. 183–193. Accessed 01/05/2018.
- Xing-Hong, Z., Han, Du, S.-Y., Wood, J. V. (2000). Microstructure and mechanical properties of TiC-Ni functionally graded materials by simultaneous combustion synthesis and compaction. *Mater. Sci.*, vol. 35, pp. 1925–1930.
- Yarraparredy, E., Zekovic, S. H., Kovacevic, S. R. (2006), Development of Nickel and Tungsten Carbide based FGM's by a Laser Based Direct Metal Deposition (LBDMD) Process for industrial slurry erosion application [20]. *Proceedings of the Institution of Mechanical Engineers*, B.12, pp. 220. Accessed: 10/08/17
- YongjinWang, R. S. & Yaping, L. (2015). Flow mechanism of 9Cr18 steel during thixoforging and its properties for functionally graded material. *Materials and Design*, vol. 86, pp. 41–48. Accessed: 13/04/18

- Yoshimi Watanabe, Y. I., Hisashi, S. & Eri, M.-F. (2009). A Novel Fabrication Method for Functionally Graded Materials under Centrifugal Force: The Centrifugal Mixed-Powder Method. [www.mdpi.com/journal/materials](http://www.mdpi.com/journal/materials). Accessed: 12/04/2018
- Yun-Han, L., Jiang-Tao, L., Chang-Chun, G. & Xin-De, B. (2002). Fabrication and evaluation of SiC/Cu functionally graded material used for plasma facing components in fusion reactor. *Journal of Nuclear Materials*, vol. 303, pp. 188–195. Accessed 10/08/2017.
- Yun-Jae, K. & Chang-Sik, O. (2007). Effects of attached straight pipes on finite element limit analysis for pipe bends. *International Journal of Pressure Vessels and Piping*, vol. 84, pp. 177–184.
- Zhanqi, C., Guanfeng, Z., Yenan, W. & Florin, B. (2015). A peridynamic model for dynamic fracture in functionally graded materials. *Composite Structures*, vol. 133, pp. 529–546
- Zhaohui, Z., Xiangbo, S., Chao, Z., Sai, W., Shukui, L., Fuchi, W. (2013). A new rapid route to in-situ synthesizes TiB–Ti system functionally graded materials using spark plasma sintering method. *Materials Science & Engineering*, vol. A 565, pp. 326–332. Accessed: 12/04/18
- Zhong-Min, W. & Yan-Zhuang, L. (2016). Transverse vibration of pipe conveying fluid made of functionally graded materials using a symplectic method. *Nuclear Engineering and Design*, vol. 298, pp. 149–159.

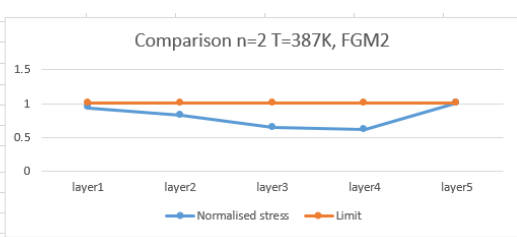
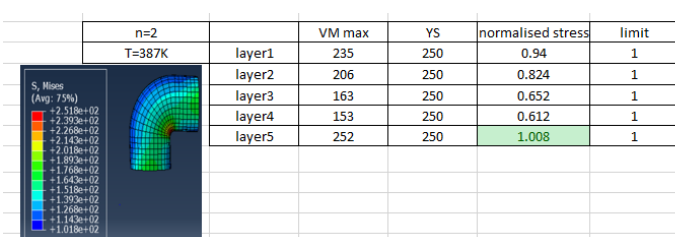
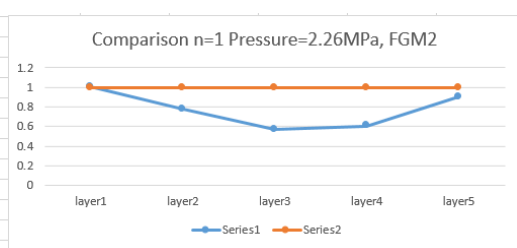
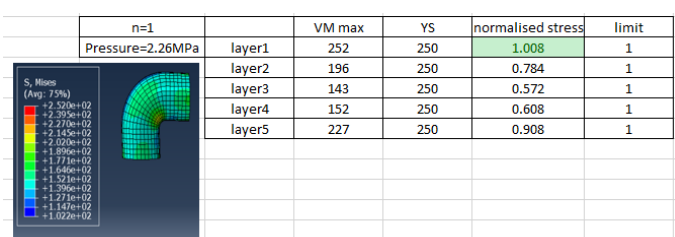
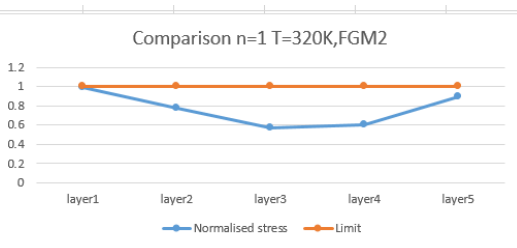
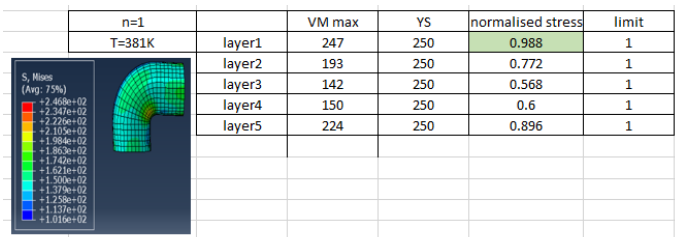
# APPENDIX A: TEMPERATURE AND PRESSURE DESIGN LIMIT FOR ELBOW PIPES

## DESIGN LIMITS FOR FGM 1

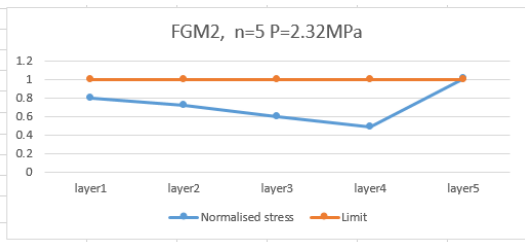
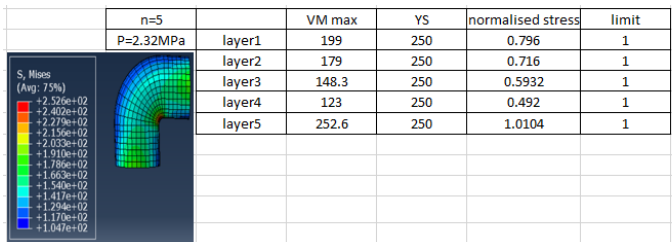
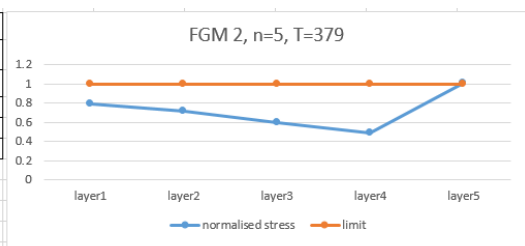
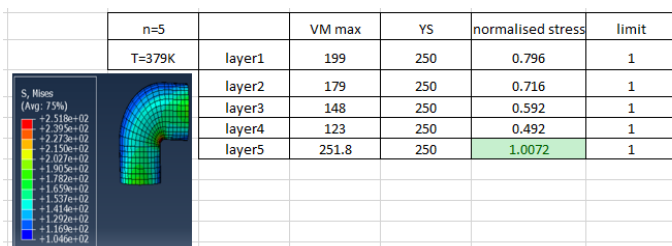
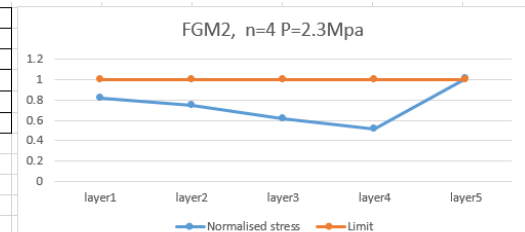
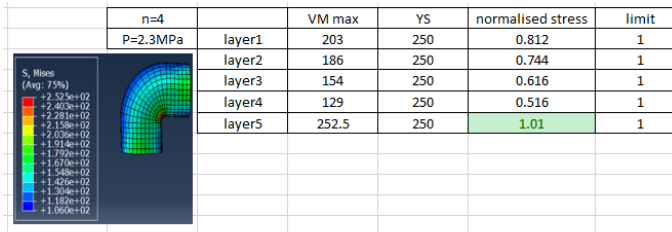
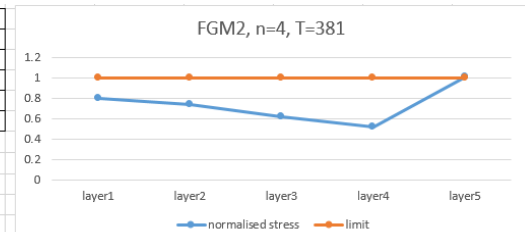
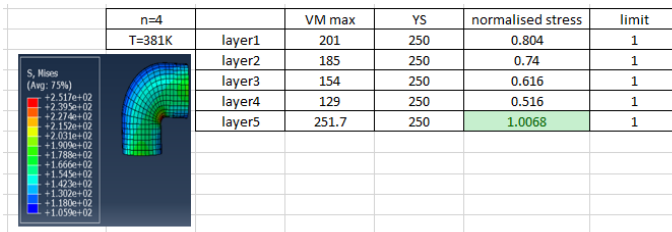
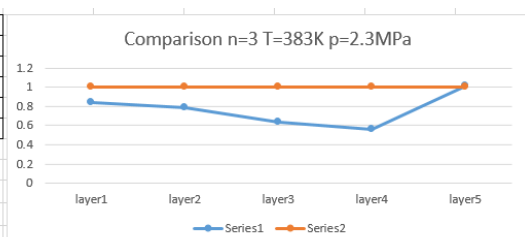
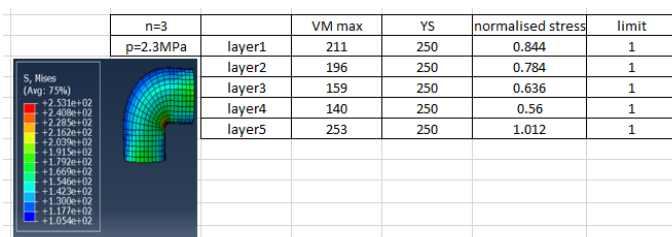
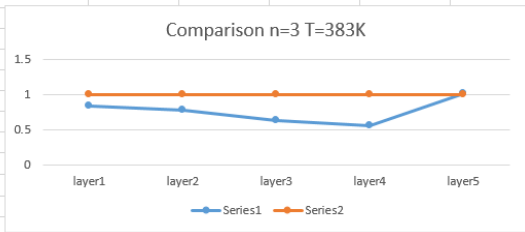
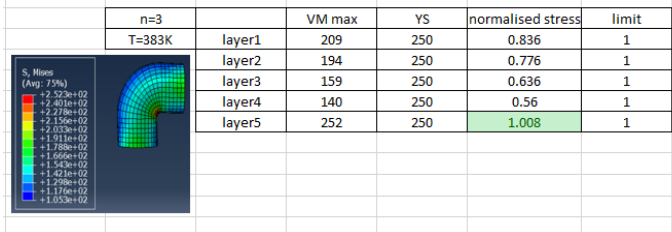
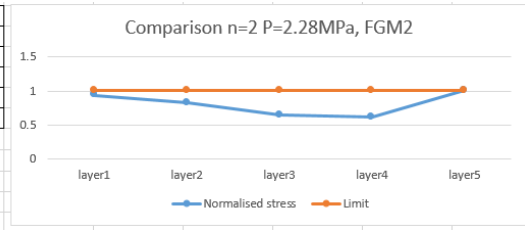
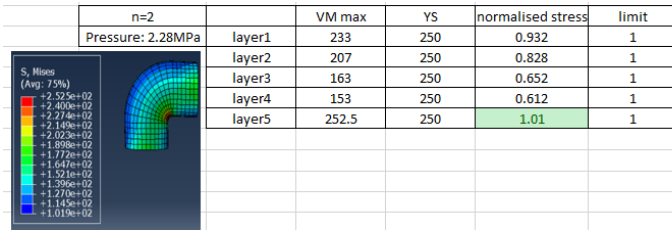




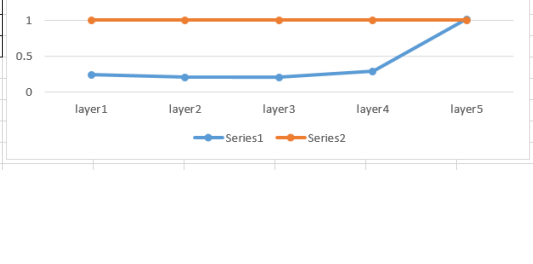
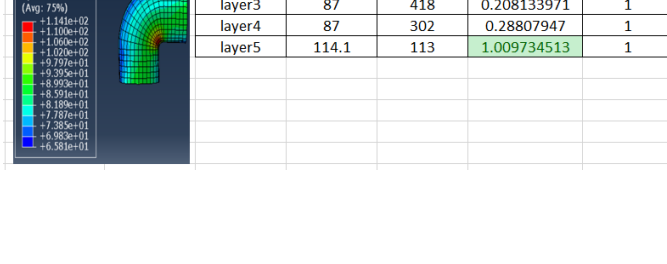
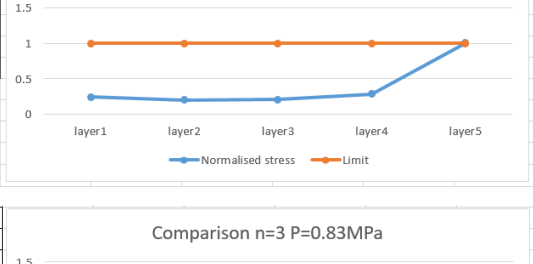
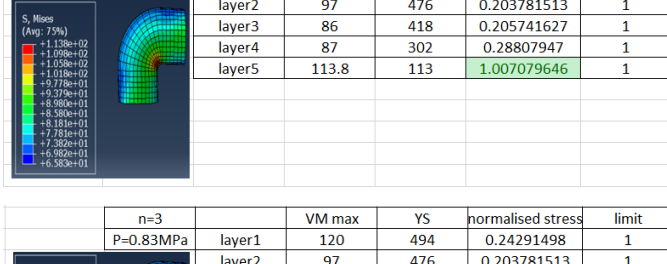
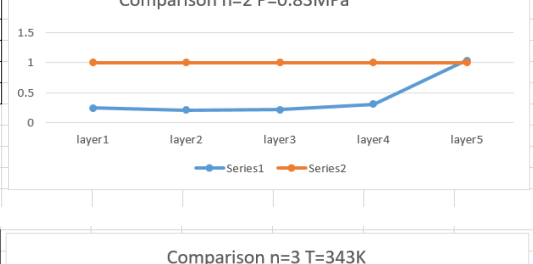
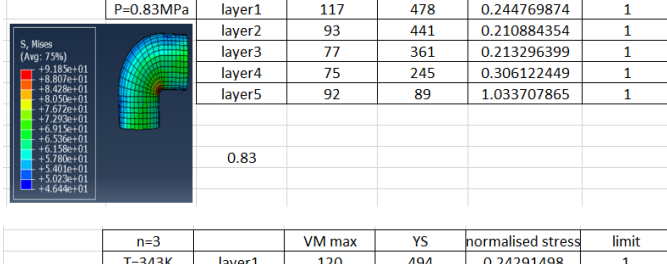
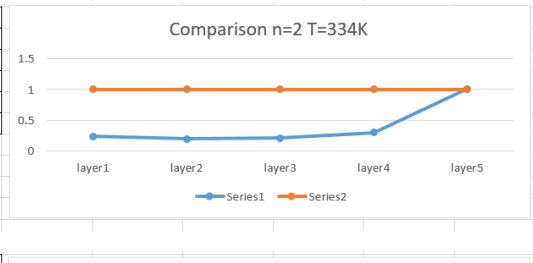
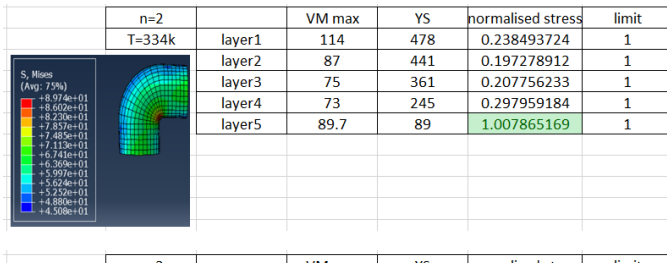
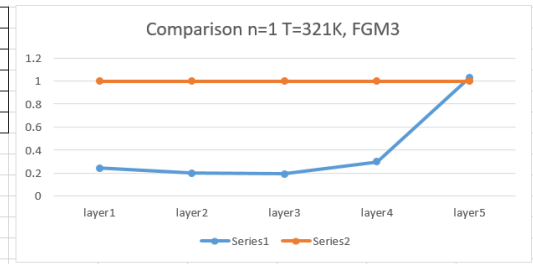
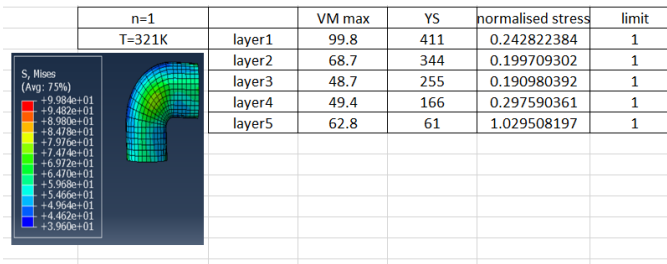
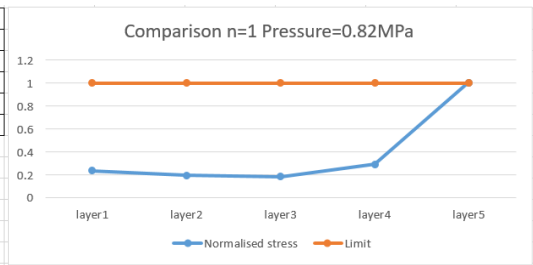
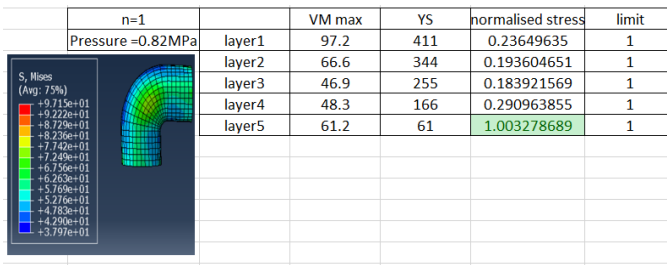
## DESIGN LIMITS FOR FGM 2

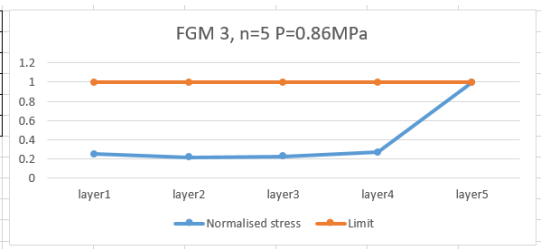
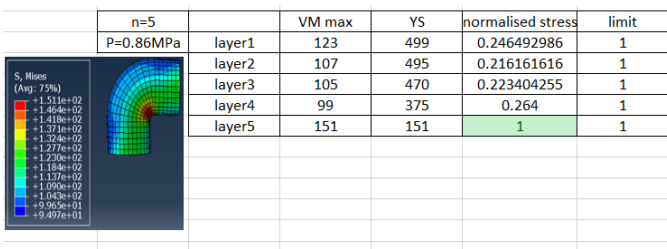
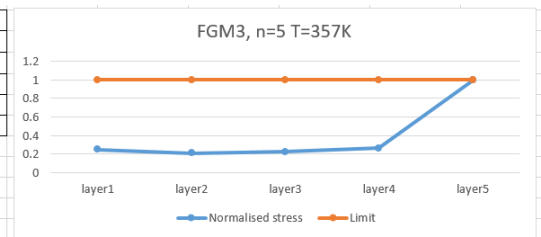
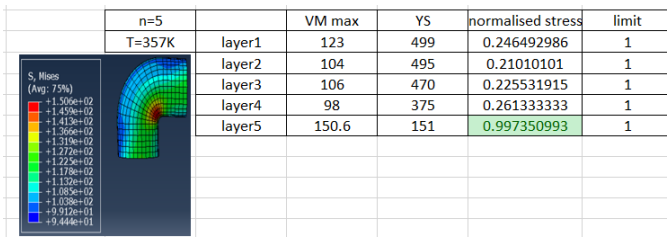
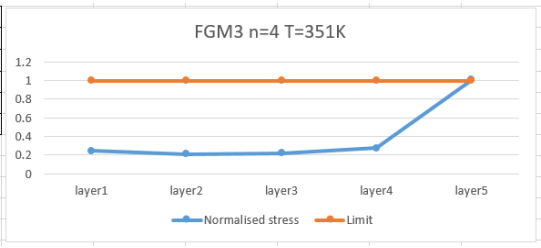
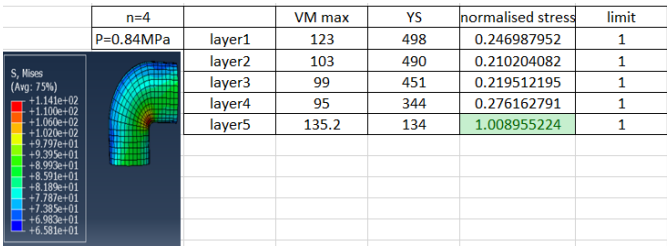
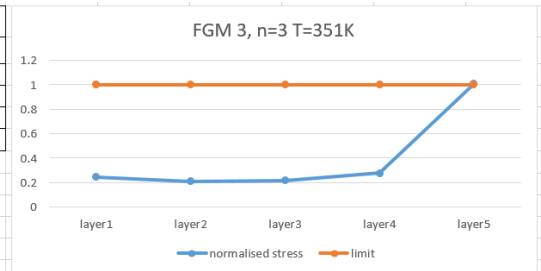
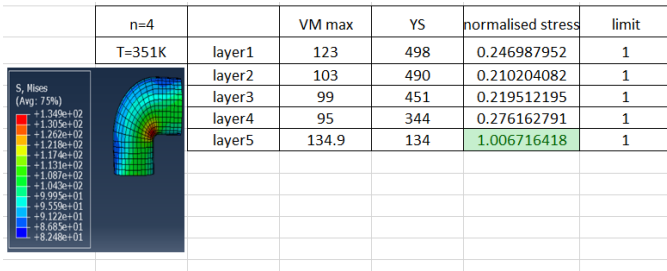




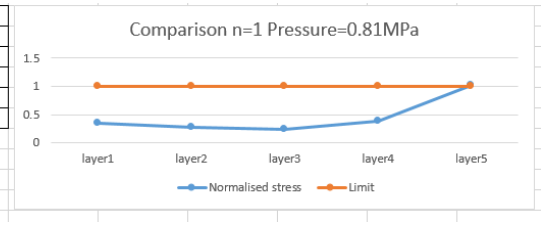
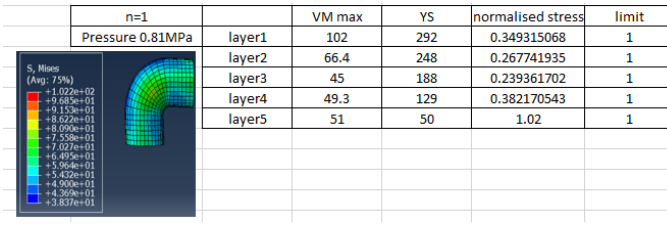
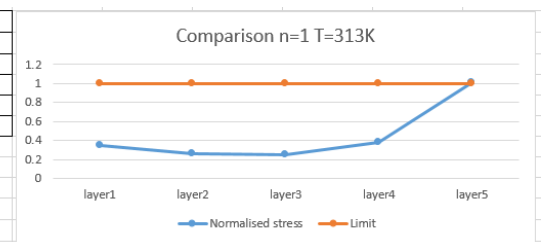
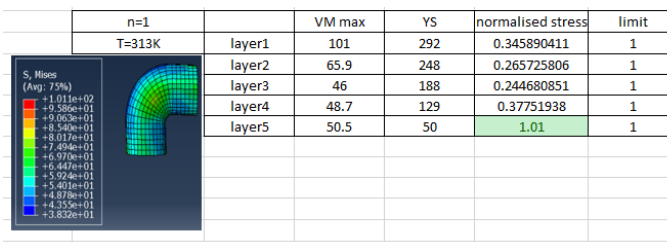


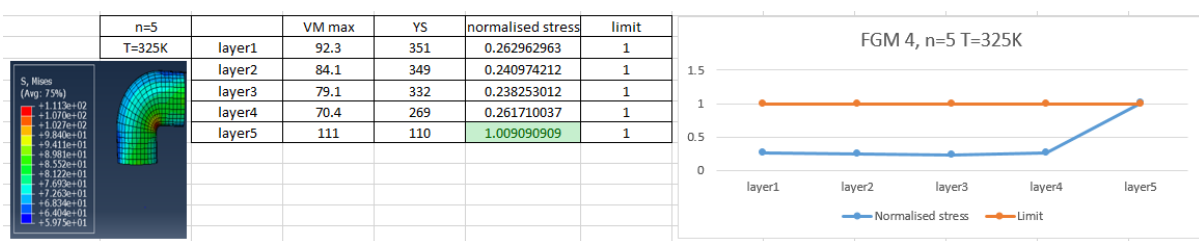
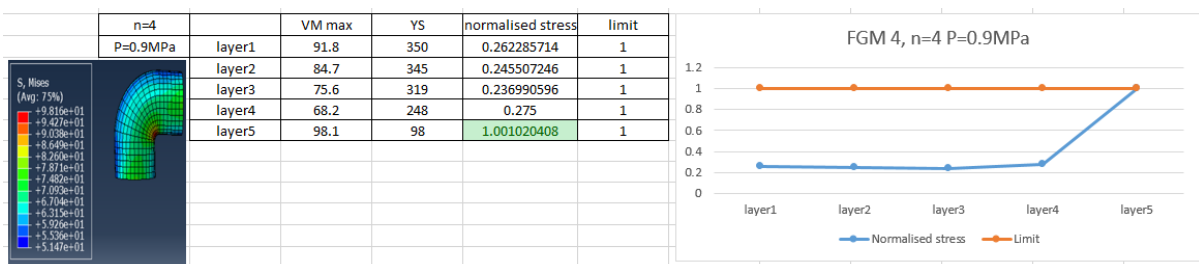
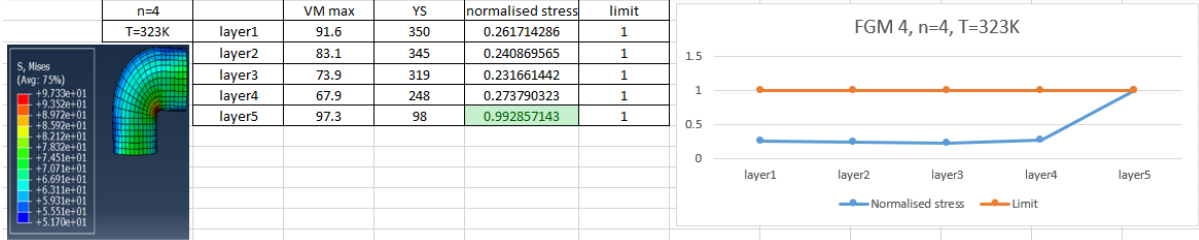
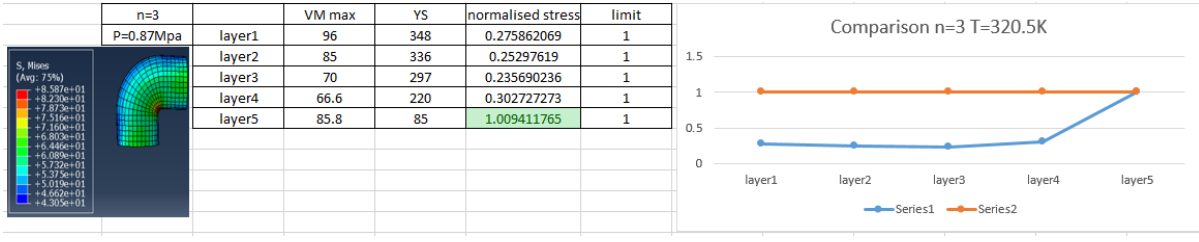
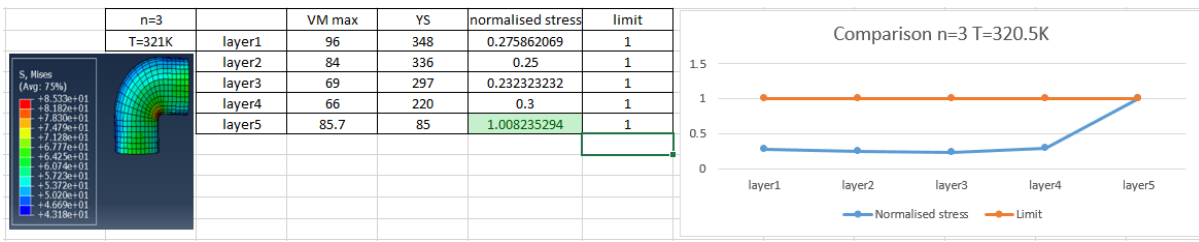
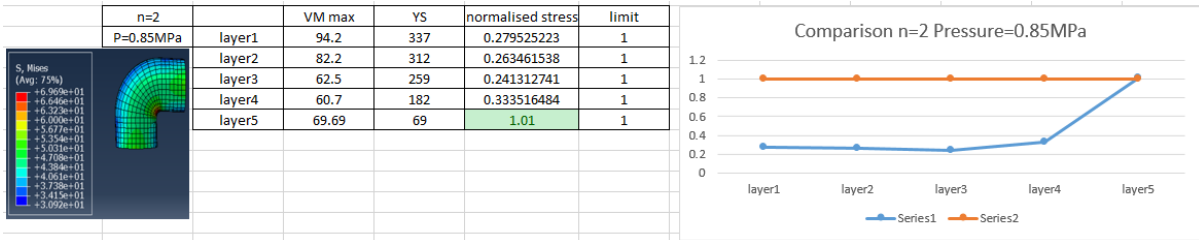
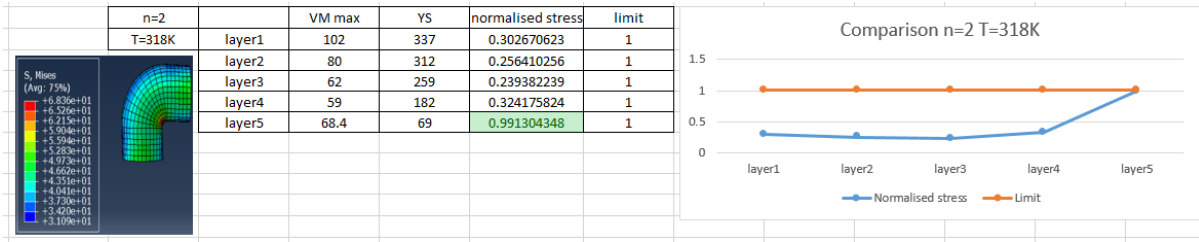
# DESIGN LIMITS FOR FGM 3



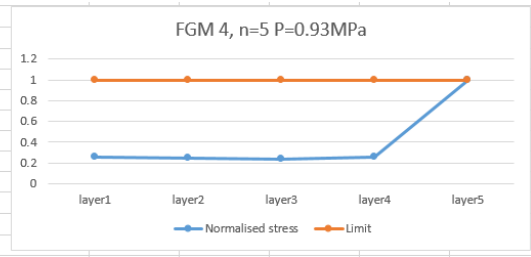
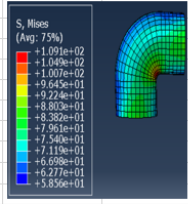


## DESIGN LIMITS FOR FGM 4





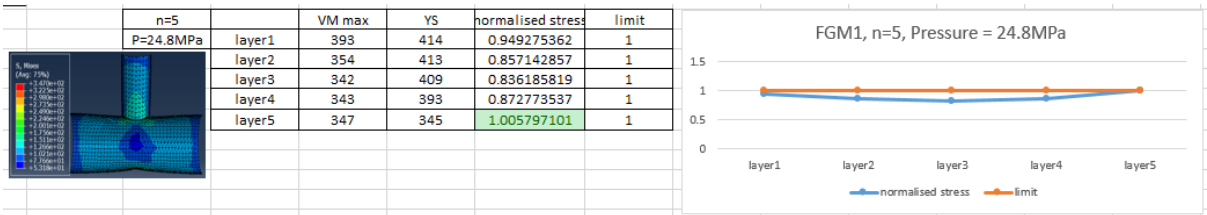
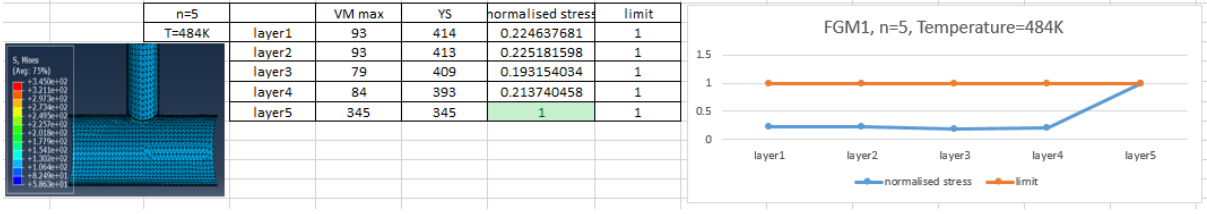
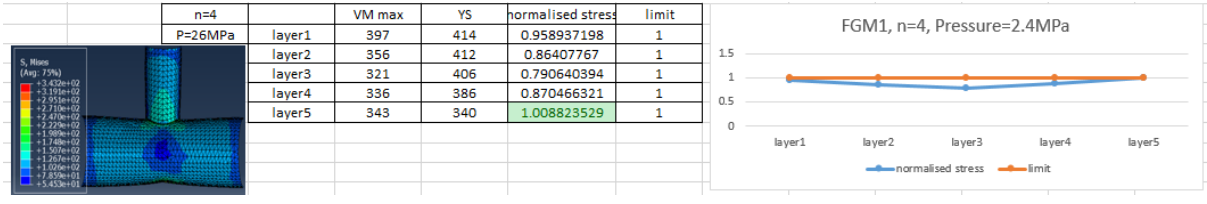
n=5		VM max	YS	normalised stress	limit
P=0.93MPa					
layer1	89.3	351	0.254415954	1	
layer2	84.5	349	0.242120344	1	
layer3	77.5	332	0.233433735	1	
layer4	68.5	269	0.25464684	1	
layer5	109.1	110	0.991818182	1	



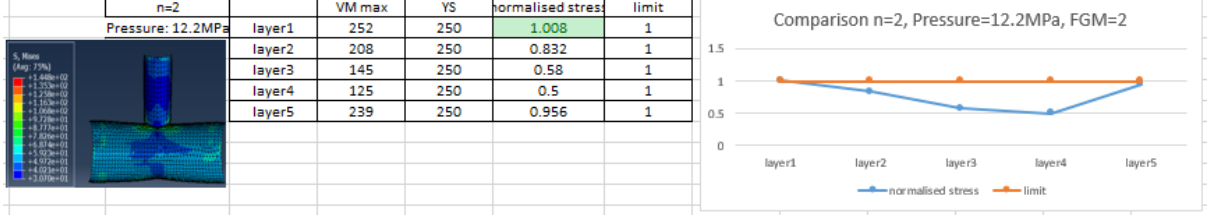
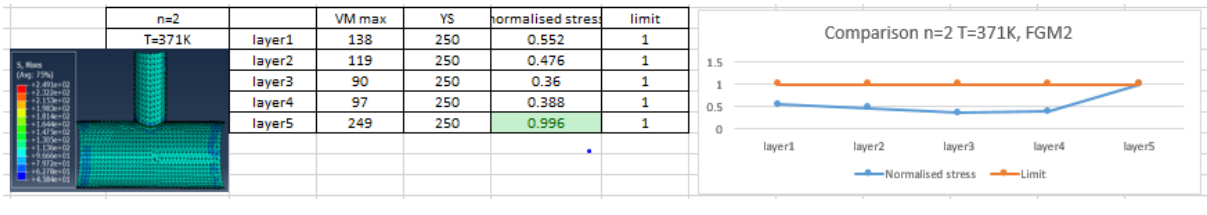
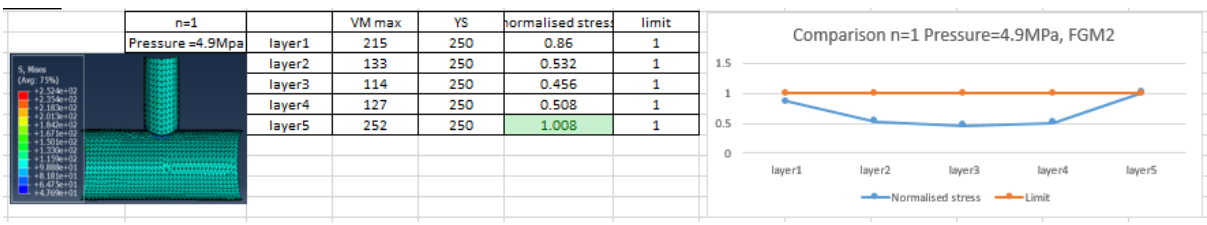
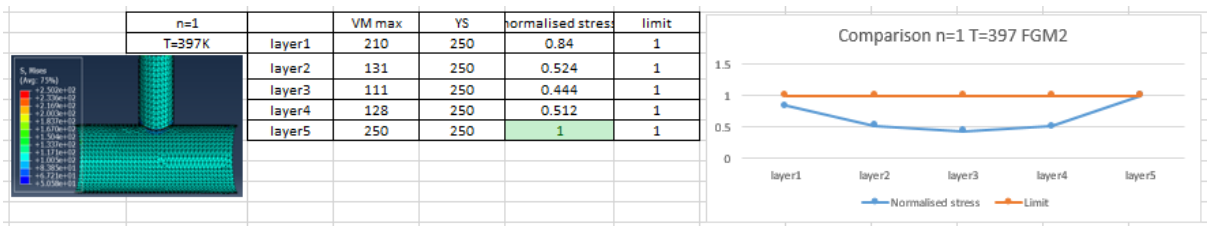
# APPENDIX A: TEMPERATURE AND PRESSURE DESIGN LIMIT FOR T-PIECE FGM PIPES

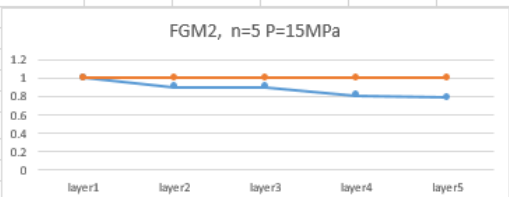
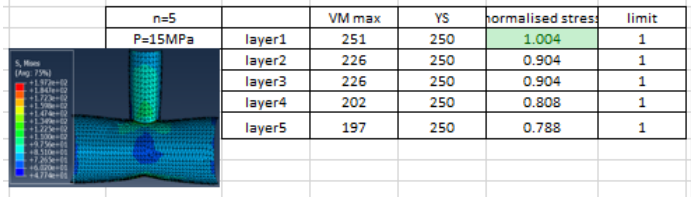
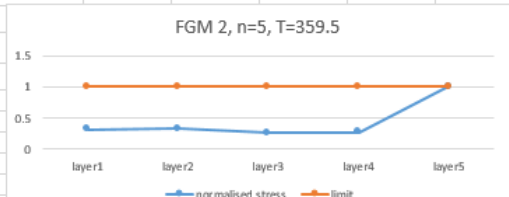
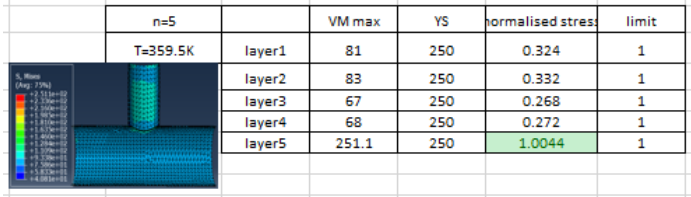
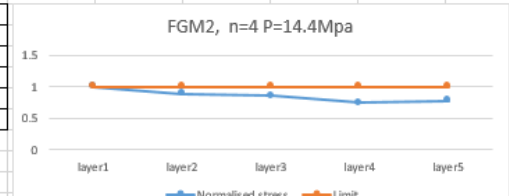
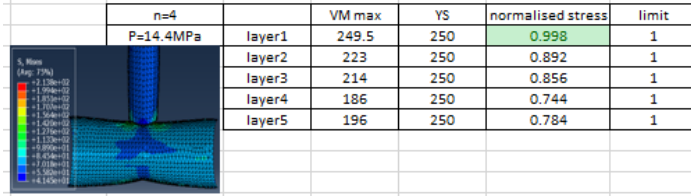
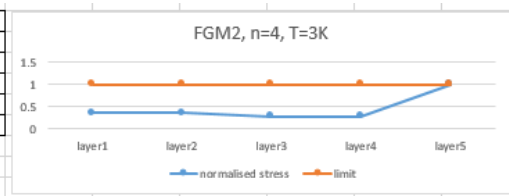
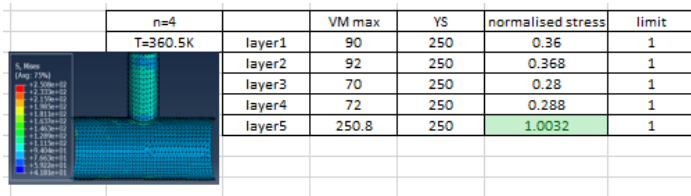
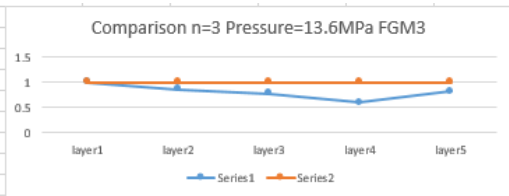
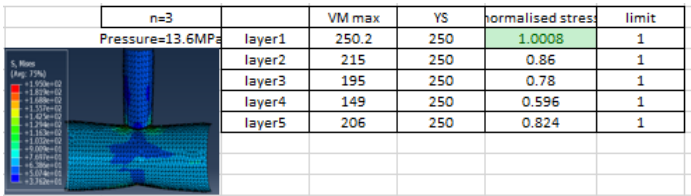
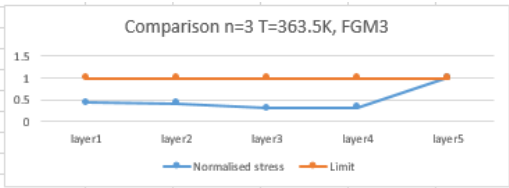
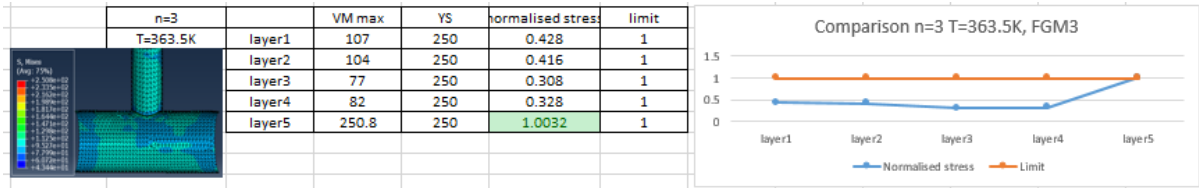
## DESIGN LIMITS FOR FGM 1



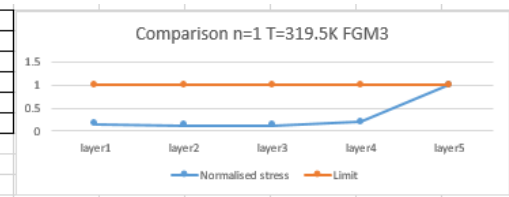
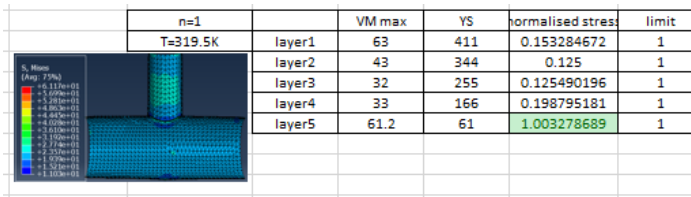


## DESIGN LIMITS FOR FGM 2

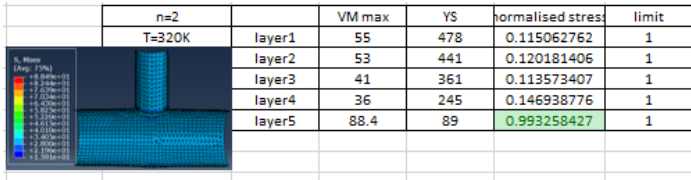




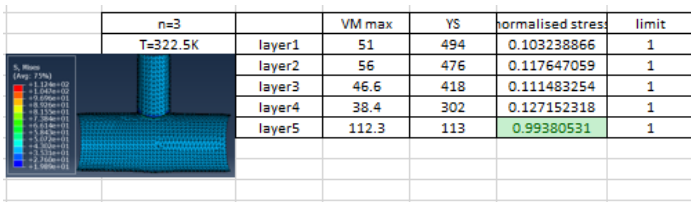
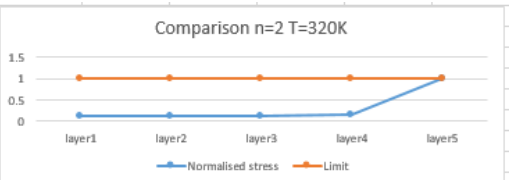
## DESIGN LIMITS FOR FGM 3



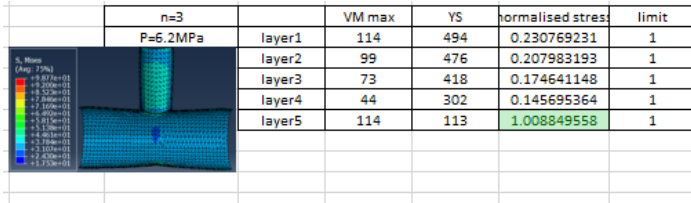
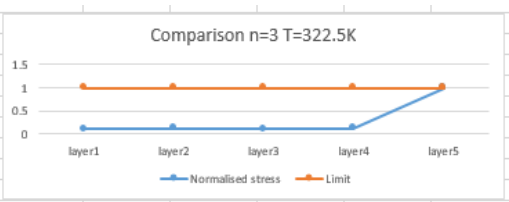




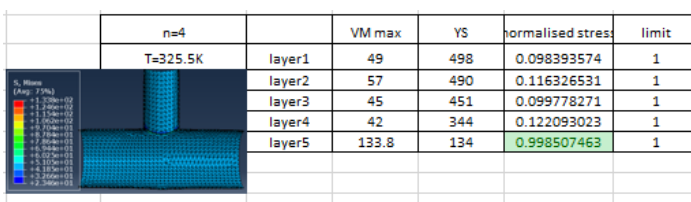
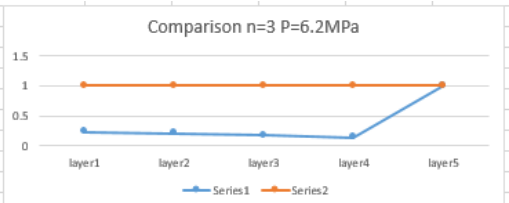
	n=2	VM max	YS	normalised stress	limit
	T=320K				
layer1		55	478	0.115062762	1
layer2		53	441	0.120181406	1
layer3		41	361	0.113573407	1
layer4		36	245	0.146938776	1
layer5		88.4	89	0.993258427	1



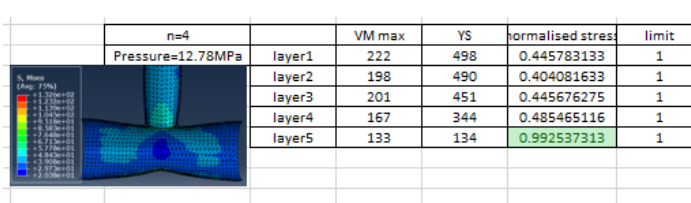
	n=3	VM max	YS	normalised stress	limit
	T=322.5K				
layer1		51	494	0.103238866	1
layer2		56	476	0.117647059	1
layer3		46.6	418	0.111483254	1
layer4		38.4	302	0.127152318	1
layer5		112.3	113	0.99380531	1



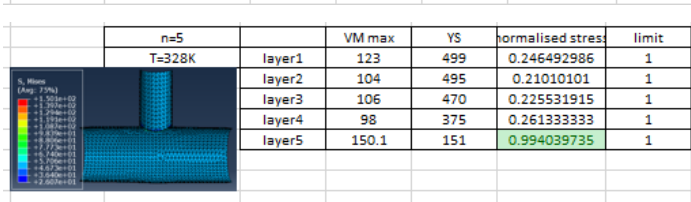
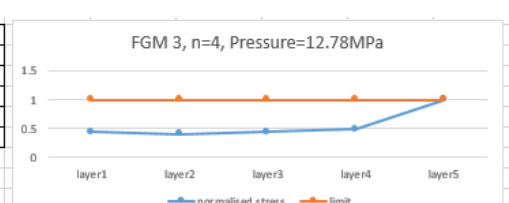
	n=3	VM max	YS	normalised stress	limit
	P=6.2MPa				
layer1		114	494	0.230769231	1
layer2		99	476	0.207983193	1
layer3		73	418	0.174641148	1
layer4		44	302	0.145695364	1
layer5		114	113	1.008849558	1



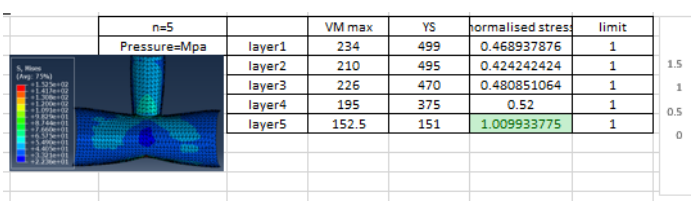
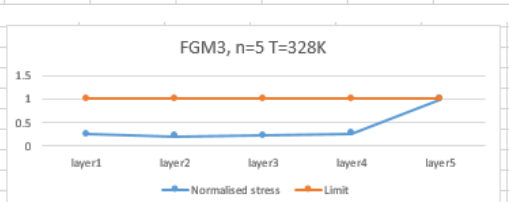
	n=4	VM max	YS	normalised stress	limit
	T=325.5K				
layer1		49	498	0.098393574	1
layer2		57	490	0.116326531	1
layer3		45	451	0.099778271	1
layer4		42	344	0.122093023	1
layer5		133.8	134	0.998507463	1



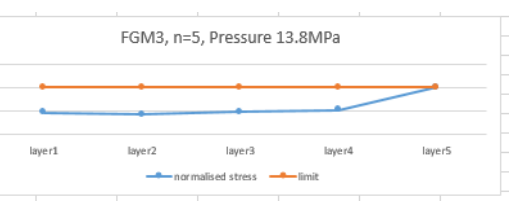
	n=4	VM max	YS	normalised stress	limit
	Pressure=12.78MPa				
layer1		222	498	0.445783133	1
layer2		198	490	0.404081633	1
layer3		201	451	0.445676275	1
layer4		167	344	0.485465116	1
layer5		133	134	0.992537313	1



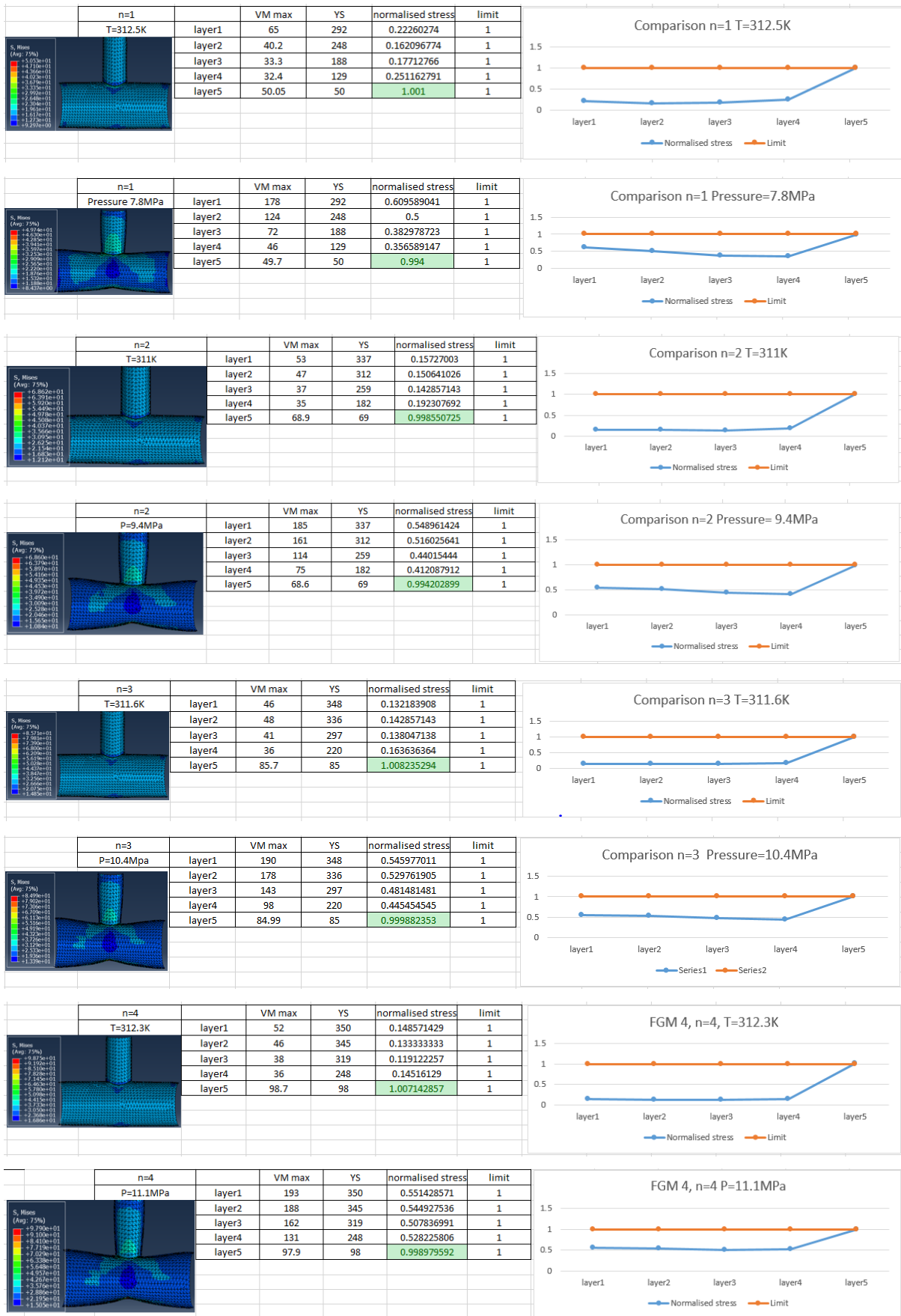
	n=5	VM max	YS	normalised stress	limit
	T=328K				
layer1		123	499	0.246492986	1
layer2		104	495	0.21010101	1
layer3		106	470	0.225531915	1
layer4		98	375	0.261333333	1
layer5		150.1	151	0.994039735	1

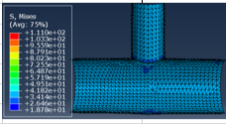


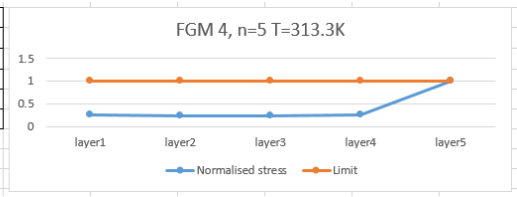
	n=5	VM max	YS	normalised stress	limit
	Pressure=Mpa				
layer1		234	499	0.468937876	1
layer2		210	495	0.424242424	1
layer3		226	470	0.480851064	1
layer4		195	375	0.52	1
layer5		152.5	151	1.009933775	1

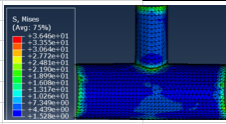


# DESIGN LIMITS FOR FGM 4



		n=5	VM max	YS	normalised stress	limit
		T=313.3K				
		layer1	92.3	351	0.262962963	1
		layer2	84.1	349	0.240974212	1
		layer3	79.1	332	0.238253012	1
		layer4	70.4	269	0.261710037	1
	layer5	111	110	1.009090909	1	



		n=5	VM max	YS	normalised stress	limit
		P=11.7MPa				
		layer1	197	351	0.561253561	1
		layer2	177	349	0.507163324	1
		layer3	176	332	0.530120482	1
		layer4	149	269	0.553903346	1
	layer5	109.4	110	0.994545455	1	

